

THE UNIVERSITY OF HULL

**AQUEOUS FOAMS AND AERATED OIL-IN-WATER
EMULSIONS PARTLY STABILISED BY EDIBLE PARTICLES**

being a Thesis submitted for the Degree of Doctor of Philosophy
in the University of Hull

by

Saeed Mashinchi
MChem (University of Hull)
BSc (Tehran Azad University)

June 2014

ACKNOWLEDGEMENTS

First and foremost, I would like to thank my academic supervisor, Prof. Bernard P. Binks, for his consistently excellent supervision and guidance. I am sincerely grateful to have worked with you.

I thank Rich Products Corporation (Buffalo, U.S.A.) for financial support in sponsoring this research project. My industrial supervisors, Mr. Shawn Campbell and Mr. Mike Piatko, have always offered great encouragement and support, and for this I thank them.

I am grateful to Prof. Paul D.I. Fletcher and Prof. Vesselin N. Paunov for sparking my interest in colloid science and to all members of the Surfactant & Colloid Group, both past and present, for their support and friendship.

I also thank, Tony Sinclair for all the SEM and Cryo-SEM images and to Yousillya Bunga for some of the experimental data collected in the course of her final year MChem project with my help and guidance.

Finally, but most importantly, I would like to thank my family and friends for being supportive throughout this section of my life. I will never forget the support. Particular thanks go to my parents and grandmother for instilling in me the attitude to continue my education. I truly feel failure is not possible with you all by my side. Included in this is my wife Anna without her this would have been a lot harder – thank you.

SCIENTIFIC PRODUCTION

Some of the findings obtained from this project have given rise to the following patent, publications and presentations:

1. Patent: 'Edible Foamable Compositions Comprising Calcium Carbonate'
M. P. Piatko, D.Falkov, I. Ilyin, P. Koblents, S. Campbell, M. Toerne, B. P. Binks, and S. Mashinchi
U.S. Application No. 14/132,706; filed December 18, 2013.
PCT Application No. PCT/US2013/076066; filed December 18, 2013.
2. Publication: 'Synergy in stabilising aqueous foams using a mixture of food-grade surfactant and edible nanoparticles' *submitted to Soft Matter.*
B. P. Binks, S. Campbell, S. Mashinchi, M. P. Piatko
3. Publication: 'Aerated palm kernel oil-in-water emulsions partly stabilised by calcium carbonate particles' *in preparation.*
B. P. Binks, S. Campbell, S. Mashinchi, M. P. Piatko
4. Publication: 'Stability and aeration properties of oil-in-water emulsions stabilised by sodium stearyl lactylate' *in preparation.*
B. P. Binks, S. Campbell, S. Mashinchi, M. P. Piatko
5. Publication: 'Gelling properties of palm kernel oil-in-water emulsions' *in preparation.*
B. P. Binks, S. Campbell, S. Mashinchi, M. P. Piatko
6. Oral Presentation: 'Aqueous foams and aerated emulsions partly stabilised by calcium carbonate particles'
27th Conference of the European Colloid and Interface Society, Sofia, Bulgaria, 2013.
7. Oral Presentation: 'Model whipped cream foams stabilised by calcium carbonate particles'
The University of Hull Chemistry postgraduate colloquium, Hull, UK 2013.
8. Oral Presentation: 'Interfacial and foaming properties of a popular food-grade surfactant'
The 6th International Symposium on Food Rheology and Structure, Zurich, Switzerland, 2012.

ABSTRACT

The objectives of this thesis are to enhance the understanding of edible solid particle behaviour at oil-water and at air-water interfaces, and how their adsorption at these interfaces affects the emulsion and foam stability. Materials stabilised solely by solid particles are of great interest due to long-term stability, lower emulsifier content and also in order to replace surfactants and oils, which are often used in food and pharmaceutical products. The project is funded by Rich Products, a leading manufacturer of non-dairy icings and toppings. The interest of Rich Products in this research is in application of calcium carbonate nanoparticles in whipped cream formulations. Air bubbles in whipped cream are coated and stabilised by adsorption of fat droplets during aeration. Particular interest of the company was to see whether calcium carbonate particles could fulfil all or part of the role played by fat droplets in stabilising air bubbles in whipped cream. In addition, this may decrease the fat content of such whipped cream products, desirable for certain consumers.

Aeration properties of aqueous dispersions of particles and an anionic food-grade surfactant, sodium stearyl lactylate, are studied. It is shown that the hydrophilic nature of the particles prevented their adsorption at air-water interfaces. Oppositely charged surfactant molecules were used to modify the surface properties of the particles. The *in situ* surface modification of the particles upon adsorption of the surfactant molecules is shown to promote the adsorption of particles at air-water interfaces. The particles were observed to form a rigid barrier around air bubbles and provide long-term stability to aqueous foams. The effect of surfactant concentration, particle addition and aeration method are all presented. The progress in preparation of model whipping cream emulsions and aerated emulsions was then continued by preparation of palm kernel oil-in-water emulsions. It is shown how aeration of palm kernel oil-in-water emulsions in the presence of surface modified calcium carbonate particles provides long-term stability to aerated emulsions. The results from characterisation of the model whipped cream foams are presented and discussed in relation to foams stability. It is shown that adsorption of calcium carbonate particles together with palm kernel oil droplets around air bubbles prevents foam collapse and enhances the foam life-time. The effect of particle concentration, oil volume fraction and whipping duration on several properties of the model whipped creams are presented. Together with preparation and characterisation of model samples, aeration properties of Vanilla Bettercreme[®], a commercial non-dairy

ready-to- whip cream manufactured by the sponsor of the project are also presented. This product has been used as a reference in different stages of this project.

Palm kernel oil-in-water emulsions stabilised by calcium carbonate particles or by sodium stearyl lactylate are then compared in terms of their stability towards coalescence. It is observed that in the emulsions stabilised by surfactants, oil droplets joined together and resulted in emulsion destabilisation. On the other hand, in particle-stabilised emulsions adsorption of the particles around oil droplets creates a rigid barrier around them and prevents the droplets joining together. The effect of emulsifier concentration and oil volume fraction are studied in detail.

Finally, preparation of oil-in-water emulsions and aerated oil-in-water emulsions containing non-crystallisable oils are investigated. The aim was to understand the interactions of fluid oil droplets with an air-water interface. Both the emulsions and aerated emulsions were stabilised by sodium stearyl lactylate. It is shown that the oil type, surfactant concentration and the oil volume fraction affect the stability of the emulsions and aerated emulsions prepared. The size of oil droplets in aerated oil-in-water emulsions is shown to be the determining factor for their stability.

TABLE OF CONTENTS

CHAPTER 1	INTRODUCTION.....	1
1.1	Industrial relevance of current research	1
1.2	Colloids	1
1.3	Emulsions.....	3
1.3.1	<i>Emulsion stabilisers</i>	4
1.3.2	<i>Solid particles at fluid-fluid interfaces</i>	6
1.3.3	<i>Emulsion stability</i>	10
1.4	Foams and aerated emulsions.....	12
1.4.1	<i>Foam formation and stability</i>	13
1.4.2	<i>Particle-stabilised foams</i>	14
1.4.3	<i>Whipped cream</i>	16
1.5	Presentation of thesis.....	19
1.6	References	21
CHAPTER 2	EXPERIMENTAL	25
2.1	Materials.....	25
2.1.1	<i>Water</i>	25
2.1.2	<i>Oils</i>	25
2.1.2.1	Palm kernel oil	25
2.1.2.2	High oleic sunflower oil	25
2.1.2.3	Dodecane	26
2.1.3	<i>Surfactants</i>	26
2.1.3.1	Sodium stearyl lactylate.....	26
2.1.3.2	Sodium dodecylsulphate	27
2.1.4	<i>Particles</i>	27
2.1.4.1	Precipitated calcium carbonate	27

2.1.5	<i>Vanilla Bettercreme[®] commercial whipping cream</i>	28
2.1.6	<i>Xanthan gum</i>	28
2.1.7	<i>Other chemicals</i>	28
2.2	<i>Methods</i>	29
2.2.1	<i>Characterisation of sodium stearoyl lactylate powder</i>	29
2.2.1.1	Differential scanning calorimetry	29
2.2.2	<i>Preparation of sodium stearoyl lactylate aqueous dispersions</i>	29
2.2.2.1	Heat treated and non-heat treated	29
2.2.3	<i>Characterisation of sodium stearoyl lactylate aqueous dispersions</i>	30
2.2.3.1	Optical microscopy	30
2.2.3.2	Cryo-scanning electron microscopy	30
2.2.3.3	Surface tension.....	30
2.2.4	<i>Characterisation of particles</i>	31
2.2.4.1	Scanning electron microscopy	31
2.2.4.2	Surface area.....	31
2.2.4.3	Contact angle	31
2.2.5	<i>Preparation of particle dispersions in water and in surfactant aqueous dispersions</i>	32
2.2.6	<i>Characterisation of particle dispersions in water and in surfactant aqueous dispersions</i>	33
2.2.6.1	Particle size distribution.....	33
2.2.6.2	Conductivity.....	34
2.2.6.3	Zeta potential	34
2.2.6.4	Adsorption isotherm	34
2.2.7	<i>Preparation of aqueous foams from particles alone, surfactant alone and surfactant-particle mixture dispersions</i>	35
2.2.7.1	Hand shaking	35
2.2.7.2	Hand mixer	35

2.2.8	<i>Characterisation of aqueous foams from particles alone, surfactant alone and surfactant-particle mixtures</i>	36
2.2.8.1	Particle association with foam	36
2.2.9	<i>Characterisation of bulk palm kernel oil</i>	37
2.2.9.1	Solid fat content determination via Differential Scanning Calorimetry	37
2.2.10	<i>Preparation of model whipping cream emulsions</i>	37
2.2.10.1	High pressure homogeniser	37
2.2.10.1.1	Laboratory table top homogeniser	37
2.2.10.1.2	Pilot laboratory homogeniser.....	39
2.2.11	<i>Characterisation of model whipping cream emulsions</i>	39
2.2.11.1	Droplet size distribution.....	39
2.2.11.2	Stability.....	39
2.2.12	<i>Aeration of model whipping cream emulsions and Vanilla Bettercreme®</i>	40
2.2.13	<i>Characterisation of model whipped emulsions and whipped Vanilla Bettercreme®</i>	41
2.2.13.1	Overrun	41
2.2.13.2	Cryo-scanning electron microscopy	42
2.2.13.3	Quiescent foam stability	42
2.2.13.4	Rheology	42
2.2.13.5	Peaking assessment.....	43
2.2.13.6	Pastry bag evaluation	44
2.2.14	<i>Preparation of palm kernel oil-in-water emulsions</i>	44
2.2.15	<i>Preparation of oil-in-water emulsions containing non-crystallisable oils</i>	45
2.2.16	<i>Aeration of oil-in-water emulsions containing non-crystallisable oils</i> ...	45
2.2.17	<i>Characterisation of oil-in-water emulsions and aerated emulsions</i>	45

2.2.17.1	Optical microscopy	45
2.2.17.2	Stability	46
2.2.17.3	Droplet size distribution.....	47
2.2.17.4	Surface and interfacial tension.....	47
2.2.17.5	Life-time of single oil droplets at the air-surfactant solution interface	47
2.3	References	49
CHAPTER 3 AQUEOUS DISPERSIONS AND FOAMS OF PRECIPITATED CALCIUM CARBONATE, SODIUM STEAROYL LACTYLATE AND THEIR MIXTURES.....		50
3.1	Introduction	50
3.2	Characterisation of precipitated calcium carbonate particles.....	53
3.2.1	<i>Scanning Electron Microscopy</i>	53
3.2.2	<i>Surface area</i>	53
3.3	Aqueous dispersions of precipitated calcium carbonate particles.....	55
3.4	Foaming properties of aqueous dispersions of particles	59
3.5	Characterisation of sodium stearyl lactylate	59
3.5.1	<i>Melting point determination by thermal analysis</i>	59
3.5.2	<i>Bilayer and multilayer vesicle formation in water</i>	61
3.5.3	<i>Surface activity of the surfactant at air-water surface</i>	63
3.6	Aqueous foams of sodium stearyl lactylate	65
3.6.1	<i>Foamability</i>	65
3.6.2	<i>Foam stability</i>	70
3.7	Aqueous dispersions of precipitated calcium carbonate and sodium stearyl lactylate mixtures	74
3.7.1	<i>Dispersion stability</i>	74
3.7.2	<i>Particle size distribution evolution upon surfactant adsorption</i>	75

3.7.3	<i>Zeta potential of particles and contact angle of aqueous surfactant on particle disks</i>	77
3.7.3.1	Adsorption isotherm of surfactant on particles	79
3.8	Aqueous foams of sodium stearoyl lactylate – precipitated calcium carbonate mixtures	81
3.8.1	<i>Foamability</i>	81
3.8.2	<i>Foam stability</i>	85
3.9	Conclusions	91
3.10	References	93
CHAPTER 4 MODEL WHIPPING CREAM EMULSIONS AND AERATED EMULSIONS		95
4.1	Introduction	95
4.2	Melting behaviour of bulk palm kernel oil <i>via</i> thermal analysis	97
4.3	Model whipping cream emulsions	99
4.4	Model whipped cream foams	105
4.4.1	<i>Influence of particle concentration on whipping properties</i>	105
4.4.1.1	Overrun	105
4.4.1.2	Structural properties and stability	107
4.4.1.3	Stability to liquid drainage	117
4.4.2	<i>Effect of oil volume fraction</i>	118
4.4.2.1	Flow behaviour of emulsions before aeration	118
4.4.2.2	Overrun	121
4.4.2.3	Structural properties of foams	123
4.4.2.4	Stability of foam towards serum drainage	129
4.4.3	<i>Effect of whipping duration</i>	130
4.4.3.1	Overrun and bubble size evolution	130
4.4.3.2	Structural properties of foam	134
4.4.3.3	Stability of foams towards serum drainage	138

4.4.3.4	PKO droplet size evolution upon whipping.....	139
4.5	Homogenisation method	141
4.5.1	<i>Pilot laboratory homogeniser</i>	141
4.6	Effect of temperature on whipping properties of VBC	144
4.7	Conclusions	148
4.8	References	150
CHAPTER 5 COMPARATIVE STUDY OF PALM KERNEL		
OIL-IN-WATER EMULSIONS STABILISED BY EITHER		
PARTICLES OR SURFACTANTS		
152		
5.1	Introduction	152
5.2	Effect of stabiliser concentration	154
5.3	Gelling of emulsions	159
5.4	Effect of oil volume fraction	163
5.5	Conclusions	165
5.6	References	166
CHAPTER 6 OIL-IN-WATER EMULSIONS AND AERATED EMULSIONS		
CONTAINING NON-CRYSTALLISABLE OIL		
168		
6.1	Introduction	168
6.2	Oil-in-water emulsions	171
6.2.1	<i>Surfactant concentration scan at fixed oil volume fraction</i>	171
6.2.2	<i>Effect of oil volume fraction</i>	181
6.3	Aerated oil-in-water emulsions	187
6.3.1	<i>Effect of surfactant concentration</i>	187
6.3.2	<i>Foamability-experimental vs. calculated</i>	192
6.3.3	<i>Stability of the foams</i>	195
6.3.4	<i>Effect of oil volume fraction</i>	203
6.4	Entering and spreading coefficients <i>via</i> surface and interfacial tensions ...	206
6.5	Conclusions	208

6.6	References	210
CHAPTER 7	FINAL CONCLUSIONS AND FUTURE WORK.....	213
7.1	Conclusions	213
7.2	Future work	215
7.3	References	217

CHAPTER 1 INTRODUCTION

1.1 Industrial relevance of current research

Food is an important part of our life as it provides us with the necessary nutrients to sustain our bodies and live healthy life styles. However, over the years there has been an increase in demand from customers for the development of fast-food products which also contain healthy nutritional values. Therefore, food companies are investing on a better understanding of the science behind the development of such products via the possible restructuring of food products.

This research is funded by Rich Products Corporation in Buffalo, U.S.A. Rich is the founder of the non-dairy segment of the frozen-food industry. The company is a leading supplier and solutions provider to the foodservice, in-store bakery and retail marketplaces. The company is the world leader in non-dairy toppings and icings.¹ The interest of the company in this Ph.D. project is to investigate the application of food-grade Ramsden agents (solid particles) as stabilisers of gas bubbles by enhancing or replacing the function of fat globules in dessert toppings and non-dairy icings. This will aim to increase the stability of air cells by decreasing coalescence and drainage in whipped toppings.

1.2 Colloids

A colloid is typically defined as a system, where one phase (the dispersed phase) is finely divided and dispersed in the second phase (the continuous phase).² The two substances, or phases, in a colloidal dispersion could be any combination of solids, liquids and gases resulting in the varied categories of colloidal systems as detailed in Table 1.1. In dispersed systems, the material inside the dispersed phase retains some of its bulk properties and can have a large variety of shapes and structures. Due to the size of the dispersed phases, typically 1-10000 nm, they are characterised by having a large interfacial area. Associated with the large interfacial area is a considerable amount of interfacial energy, causing the fragments of the dispersed phases to combine and form larger aggregates in order to reduce the total free energy of the system.³

Table 1.1. Classification of colloidal systems based on dispersed and continuous phases.⁴

Dispersed phase	Continuous phase	Name of dispersion	Examples
gas	liquid	foam	whipped cream
	solid	solid foam	filters
liquid	gas	liquid aerosol	spray
	liquid	emulsion	salad dressing
solid	gas	solid aerosol	smoke
	liquid	suspension	paint
	solid	solid suspension	metal alloys

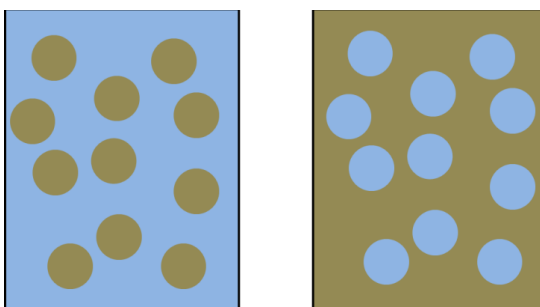
In a dispersion of solid particle in a liquid, known as a dispersion or suspension depending on the particle size, aggregation affects the flow behaviour of the dispersion, which is of importance for many of their applications. The structure of colloidal dispersions and the dynamical complexity present in them, gives rise to a diversity of rheological phenomena in such systems. Some examples of these rheological phenomena are shear thickening, shear thinning and viscoelasticity.

The random movement of colloidal particles driven by their thermal energy in a liquid medium, known as Brownian motion, may cause collision between particles and their aggregation. Aggregation is a form of colloidal instability and can be either weak or strong depending on the interactions in between species. However, this process may be controlled by engineering the surface properties of the colloidal particles and the forces acting between them. There are two main mechanisms to prevent aggregation of solid particles and stabilise the colloidal dispersion. One way is by varying the charge on the particles, for example by modifying pH, known as charge stabilisation. Secondly, the surface properties of colloidal particles can be modified by adsorption of other molecules, such as polymer chains, which eventually increases the repulsion between particles and is known as steric stabilisation.³ Chapter 3 will discuss in detail the stabilisation of calcium carbonate aqueous dispersions by adsorption of surface-active molecules on the surface of these particles. The dispersions are then used to stabilise aqueous foams by adsorption of surface modified particles at air-water interfaces.

1.3 Emulsions

Emulsions are an important type of colloidal system, containing at least one immiscible liquid dispersed in another in the form of small droplets. Simple emulsions are of the oil-in-water (e.g. cream, milk and mayonnaise) or water-in-oil (e.g. butter and margarine) types, as shown schematically in Figure 1.1. The first phase in the nomenclature used above corresponds to the dispersed phase, usually existing in the form of small droplets. The second represents the continuous phase. The diameter of the dispersed droplets in most emulsions is typically less than 10 μm .⁵ Multiple emulsions are more complex than simple emulsions in that droplets of dispersed phase also contain droplets. Multiple emulsions can be either oil-in-water-in-oil or water-in-oil-in-water.⁶

Figure 1.1. Schematic representation of oil-in-water (left) and water-in-oil (right) emulsions.



The contact between water and oil molecules is energetically unfavourable in emulsions, which implies that emulsions are thermodynamically unstable. Emulsions formed by homogenisation of pure oil and pure water are not stable and separate into their individual bulk phases rapidly, that is a system of lower density phase on top of a layer of higher density phase.⁷ In order to prepare emulsions that are kinetically stable (metastable) they need an extra component called an emulsifier.⁸ Adsorption of emulsifier molecules at an interface decreases the interfacial tension associated with that interface. The interface between two phases becomes more deformable as the interfacial tension decreases and results in the formation of small droplets. An emulsifier can provide kinetic stability for an emulsion for a period of time. This timescale can vary from seconds to years⁵ and strongly depends on the properties of the interface between the dispersed and the continuous phase.⁹

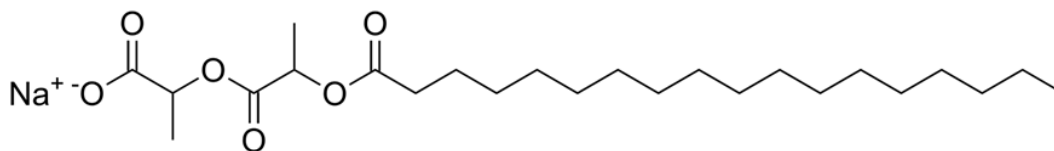
Various natural and produced food products consist either fully or partially as emulsions or have been in an emulsified condition at some stage during their processing. Examples include milk, whipped cream, mayonnaise, margarine, ice-cream, desserts, etc.^{5, 10} Food emulsions are typically of the oil-in-water type; however water-in-oil emulsions also exist such as butter, margarines and spreads. As with emulsions in general, food emulsions are thermodynamically unstable and they require stabilising components to achieve kinetic stability. Kinetic stability in food emulsions and foams can be achieved by adding surfactants such as Sodium Stearoyl Lactylate (SSL) and/or proteins like sodium caseinate and/or thickening agents such as xanthan gum.¹¹ A typical food emulsion contains triglycerides, water, surfactants, polysaccharides, proteins, salts, preservatives, flavours and colours. Each ingredient plays a different role in a food emulsion and structural complexity arises from interactions between the ingredients. The ingredients in food emulsions can exist in various shapes, sizes, structures and molecular weights. In addition, the ingredients can be isolated dispersed species, or they may assemble together to form aggregates of different shapes and sizes.¹² The diversity of ingredients and their various structures results in a wide variety of different physico-chemical characteristics such as appearance, texture, taste and shelf-life in food emulsions.⁵ The study of food emulsions is, then, a physico-chemical study of a system viewed as a dispersion of macromolecules and particles in different states of organisation.¹²

1.3.1 Emulsion stabilisers

There has been much research dealing with improving the kinetic stability of food emulsions using emulsifiers and stabilisers.¹³ Emulsifiers are single or mixed chemical species that promote emulsification and provide kinetic stability by interfacial action.¹⁴ Surfactants are the most widely used emulsifiers in emulsification. Some of the important surfactant molecules applied in the food industry are mono- and di-glycerides (glycerol monostearate), polysorbates (Tweens), phospholipids (lecithin) and sucrose esters.¹⁵ Emulsifier molecules possess both polar and non-polar regions in their structure; hence have amphiphilic character. Their structure consists of a hydrophilic head group, and one or more hydrophobic tails due to the presence of the hydrocarbon chains. Figure 1.2 represents the chemical structure of an SSL molecule, a popular surfactant in

food manufacturing, which consists of a negatively charged head group and a C18 hydrocarbon tail group.

Figure 1.2. Chemical structure of SSL molecule.



According to the charge on the head group of surfactant molecules they can be classified into non-ionic and ionic with either a positive or negative charge. Another classification of surfactants is based on their ability to dissolve in an oil or water phase, respectively. Bancroft's rule states that the continuous phase of an emulsion is the liquid in which the surfactant is more soluble.¹⁶ However Binks¹⁷ showed that this is only applicable to systems at surfactant concentrations in excess of their cmc and stated that continuous phase is the phase in which the micelles are preferably formed. The first quantitative way to relate the quality of an emulsion (behaviour or stability) to the structure of the surfactant was introduced by Griffin.¹⁸ He assigned numerical values to surfactants to manage a system of classification to correlate the solubility of surfactants in water to their properties. The system of classification is called HLB (Hydrophile-Lipophile Balance), and is based on the fact that all surfactant molecules possess both hydrophilic and hydrophobic functional groups. The relative proportion of hydrophilic and hydrophobic functional groups signifies the emulsification properties of that surfactant.¹⁹ The amphiphilic nature of the surfactant molecules enables them to either bind at various interfaces as monomers (water-oil, air-oil and air-water) or form other structures (such as multi-layer vesicles or micelles).

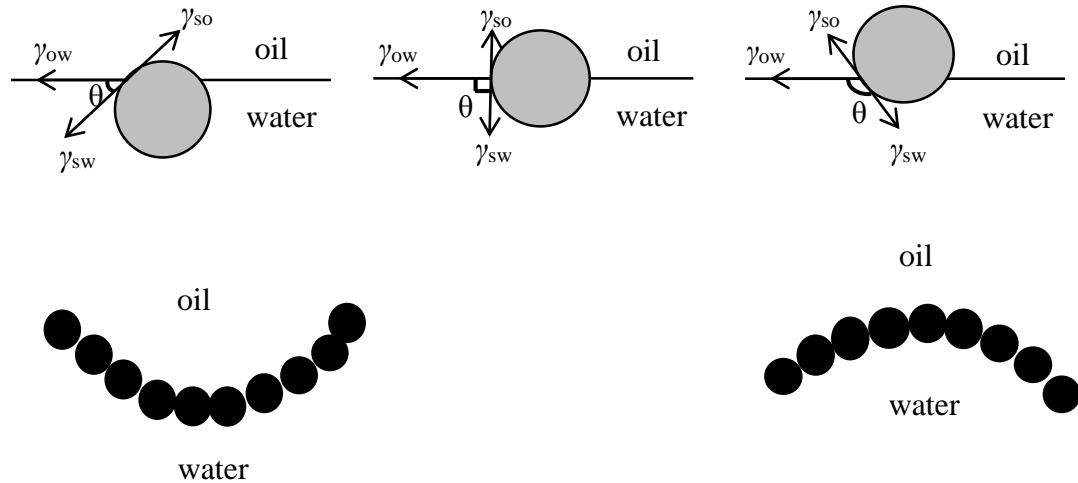
Protein molecules are another type of stabiliser in food emulsions and foams.²⁰ Similarly to surfactants, proteins are amphiphilic molecules and they possess both hydrophilic and hydrophobic groups in their structure. Once adsorbed at the interface, their structure rearranges itself depending on the properties of the dispersed and continuous phase and in accordance with their interactions. This structural rearrangement and interaction leads to the stabilisation of emulsions through the formation of viscoelastic layers around droplets of the dispersed phase in emulsions and air bubbles in foams.^{21, 22}

Solid particles are another class of stabilisers. The presence of solid species in food emulsions and food foams has been known for many years. Examples include solid fat crystals in whipped cream, egg yolk particles in mayonnaise and ice crystals in ice-cream. It should be mentioned that unambiguous role of such particles is difficult to ascertain in complex food formulations. More details about the roles of solid particles in emulsions have been discovered in recent years.^{11, 12, 23, 24} Adsorption of solid particles to interfaces was first discovered by Ramsden. He stabilised air bubbles and oil droplets in water using solid particles²⁵ and four years after him, Pickering found that hydrophilic particles prefer to form water continuous emulsions.²⁶ The next section provides a deeper understanding of the role of solid particles as emulsion and foam stabilisers.

1.3.2 Solid particles at fluid-fluid interfaces

Solid particles with colloidal dimensions can adsorb at a liquid-liquid or liquid-vapour interface. Unlike surfactant molecules, solid particles with homogeneous properties over the surface of the particle do not have distinct hydrophilic and hydrophobic sections and hence are not amphiphilic. The three-phase contact angle, θ , that particles make with an oil-water interface measured through the more polar phase is thought to be the determining factor in curving the interface towards oil or water, in an emulsion.²⁷ Figure 1.3 shows adsorption of a spherical solid particle at an oil-water interface. It is shown for hydrophilic particles (left) that curving of the interface occurs in a way to surround the oil phase and produce oil-in-water emulsions or in other words it is concaved with respect to the water phase. For hydrophobic particles (right) the interface is convex with respect to water phase and produces water-in-oil emulsions.²⁸

Figure 1.3. Schematic diagram of a spherical solid particle at a planar (top) and curved (bottom) oil-water interface showing the interfacial energies and the three-phase contact angle measured through water. For $\theta < 90^\circ$, oil-in-water emulsions are more likely to form and for $\theta > 90^\circ$, water-in-oil emulsions are more common.



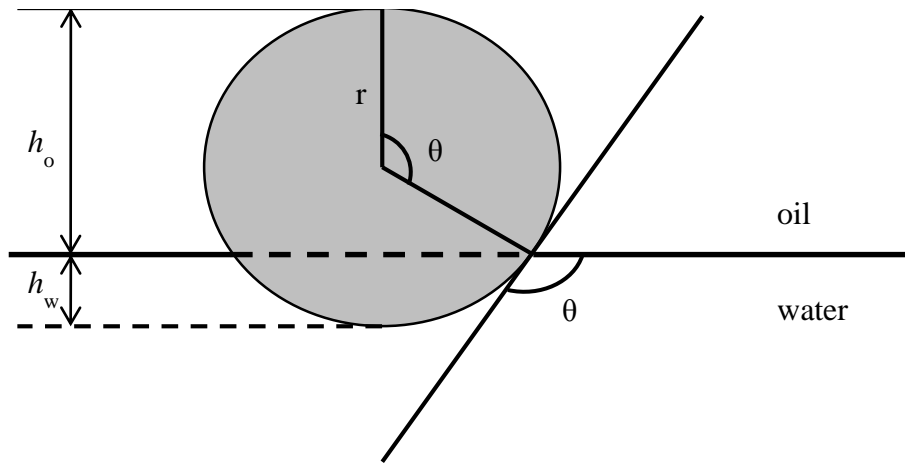
The wettability of a particle is also affected by other factors such as particle shape and surface roughness.²⁹ As shown above, a hydrophilic particle has a contact angle less than 90° (measured through water) and as a result a bigger fraction of the particle's surface remains in water. The monolayer of the particles at the interface curves in a manner that a larger area of the particle remains in contact with water. Hydrophobic particles have contact angle values bigger than 90° and hence the particle remains more in oil than in water. The former situation ($\theta < 90^\circ$) gives rise to oil-in-water emulsions and the latter condition ($\theta > 90^\circ$) prefers to form a water-in-oil emulsion.²⁷ When the particle is adsorbed at the oil-water interface, three interfaces namely solid-water (sw), solid-oil (so) and oil-water (ow) are produced with a surface tension γ associated with each. The Young equation, shown below, relates the three interfacial tensions to the three-phase contact angle for a solid particle at an oil-water interface.²⁹

$$\gamma_{so} - \gamma_{sw} = \gamma_{ow} \cos \theta \quad (1.1)$$

Colloidal solid particles with intermediate hydrophobicity are capable of strongly adsorbing to an oil-water or air-water interface. The removal of an area from the interface

between the two fluids, with high interfacial tension, is believed to be the driving force for this phenomena. The strength of the adsorption of a solid particle at an oil/air-water interface is therefore influenced by the value of the interfacial tension associated with the interface, γ_{ow} , as well as the positioning of the solid particle at the oil-water interface, characterised by the three phase contact angle θ .³⁰ Figure 1.4 schematically represents a spherical hydrophobic solid particle at equilibrium with an oil-water interface.

Figure 1.4. Representation of a spherical solid particle at equilibrium with an oil-water interface. The effect of gravity is assumed to be negligible for small particles ($< 5 \mu\text{m}$) so that the oil-water interface remains planar up until the contact line with the particle.



For such a single spherical particle with radius r , adsorbed at an oil-water interface forming a contact angle θ measured through the water phase the depth of immersion into the water phase, h_w , is equal to $r(1 + \cos \theta)$. The surface area of the particle in contact with water, A_{sw} , is given by $2\pi r h_w = 2\pi r^2(1 + \cos \theta)$. The planar area of oil-water interface removed by the adsorption of the particle is therefore:

$$A_{ow} = \pi r^2 \sin^2 \theta = \pi r^2 (1 - \cos^2 \theta) \quad (1.2)$$

The energy, E_{des} , required for desorption of the particle from the interface into the oil phase is given by:

$$E_{des} = 2\pi r^2 (1 + \cos \theta) (\gamma_{so} - \gamma_{sw}) + \pi r^2 (1 - \cos^2 \theta) \gamma_{ow} \quad (1.3)$$

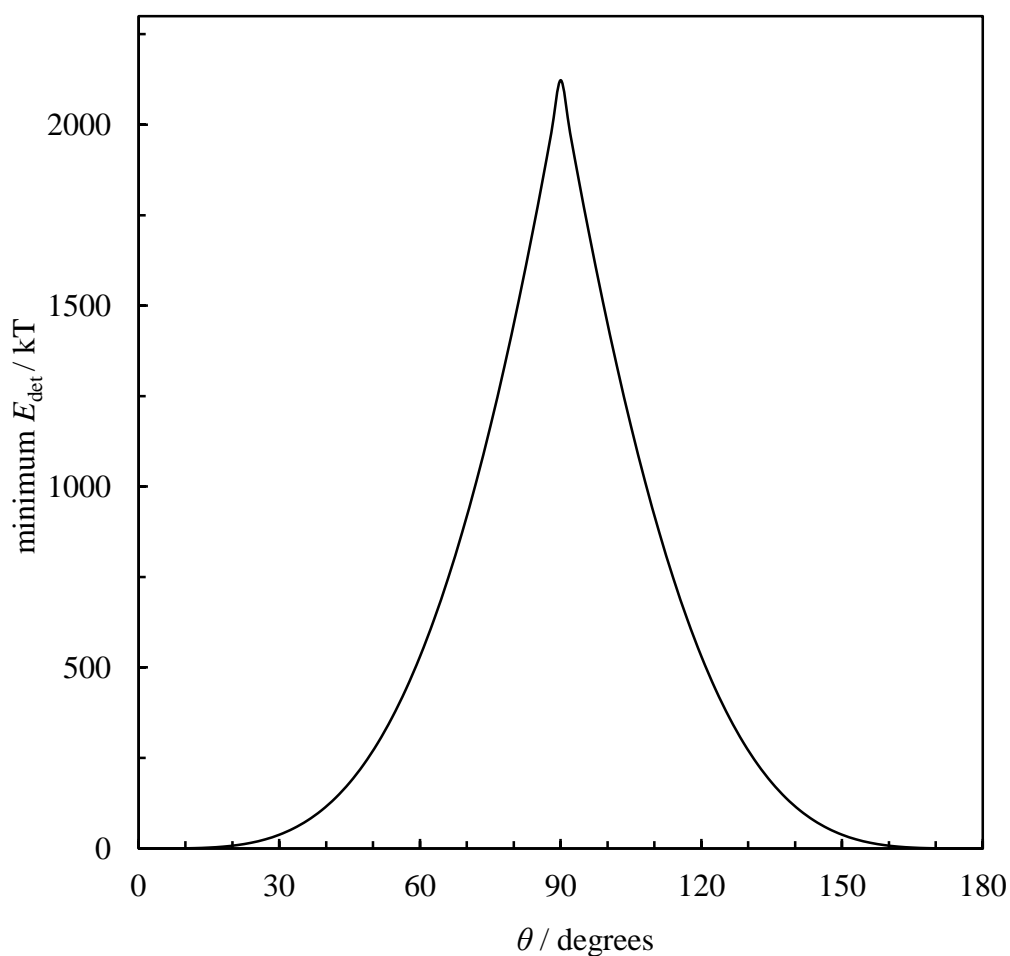
where γ represents the appropriate interfacial tension and the subscripts o, w and s refer to oil, water and solid phases, respectively.

Combining equation (1.3) with the Young equation results in the equation below:²⁹

$$E = \pi r^2 \gamma_{ow} (1 + \cos \theta)^2 \quad (1.4)$$

The sign inside the bracket is negative for detachment towards the water phase. From equation 1.4, it can be concluded that for particles with $\theta > 90^\circ$, removal of the particle into the oil phase is easier but for hydrophilic particles ($\theta < 90^\circ$), removal into the water phase is easier. The change in the minimum energy of detachment of a solid particle with the contact angle θ at constant γ_{ow} and particle radius is shown in Figure 1.5.

Figure 1.5. Variation in calculated minimum energy of detachment of a spherical particle of radius $r = 10$ nm with contact angle θ , at the planar isopropyl myristate-water interface of interfacial tension $\gamma_{ow} = 27.32$ mN m⁻¹ at 298 K.



It can be seen from the graph that solid particles are most strongly adsorbed at an oil-water interface with a contact angle of 90° . The energy of detachment of such

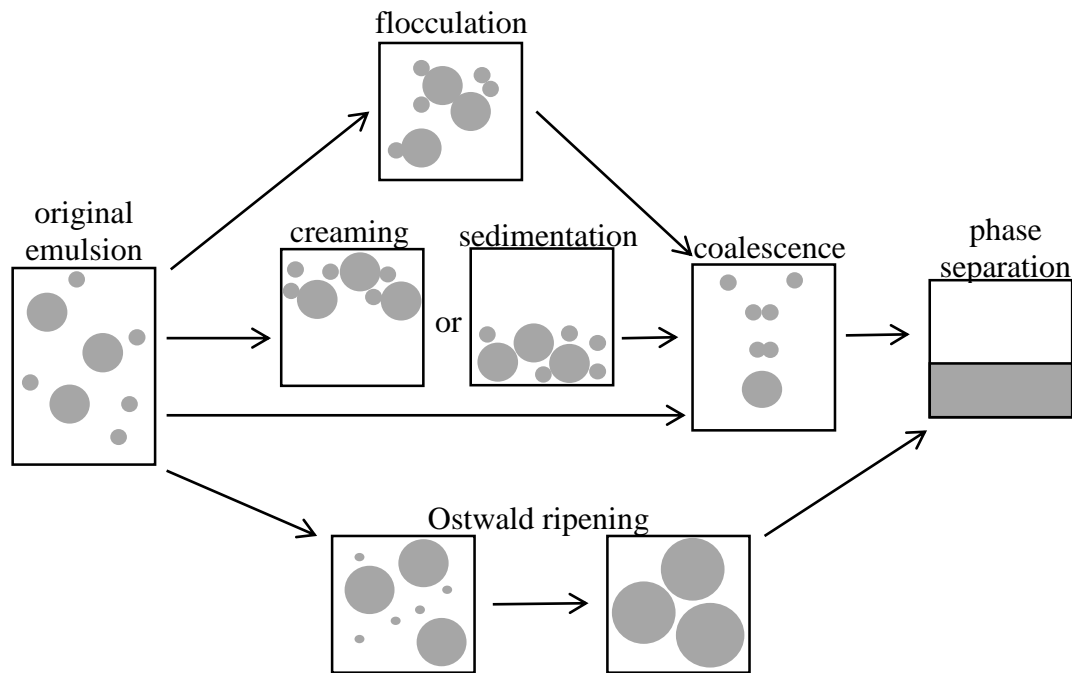
particles from interfaces is typically orders of magnitude higher than the thermal energy of the particle, as presented in Figure 1.5. Therefore attachment of particles to the interface can be considered as an irreversible process. The minimum detachment energy falls sharply on either side of 90° such that for particles with a contact angle between 0 and 20° or between 160 and 180° , the energy is only around 10 kT or even less. This is in contrast with surfactant molecules, which adsorb and desorb relatively fast.²⁷ The irreversible adsorption of solid particles to oil-water interfaces significantly improves the stability of emulsions towards coalescence and Ostwald ripening.³¹

A wide variety of particle types has been used as emulsion stabilisers to date. Some examples include silica, latexes, metal oxides and sulphates, clays, carbon, waxes and microgel particles.^{27, 32-38} Their effectiveness as emulsion stabiliser depends on their shape and size, their wettability and inter-particle interactions, as well as the properties of the two phases (dispersed and continuous) in the emulsions.²⁹ Some particles such as microgels are able to invert the type of emulsions (from oil-in-water to water-in-oil) they stabilise upon varying the pH or temperature of the emulsion.^{39, 40} A class of paramagnetic particles is capable of preventing or inducing the destabilisation of an emulsion upon applying an external magnetic field.⁴¹

1.3.3 *Emulsion stability*

Producing stable food emulsions is very important in the food industry. There are different chemical and physical processes during which an emulsion becomes unstable. Oxidation and hydrolysis are examples of chemical instability processes, which result in alteration in the chemical structure and properties of the molecules. In physical instability processes, the structural organisation or spatial distribution of the molecules changes. Creaming, sedimentation, coalescence, flocculation, Ostwald ripening and phase inversion are physical instability processes of emulsions.⁵ These processes are shown schematically in Figure 1.6.

Figure 1.6. Schematic representation of the different processes involved in the physical instability of an emulsion.



Creaming or sedimentation in emulsions is the movement of droplets, and they can either form a concentrated layer by moving to the top of the sample or settle to the bottom by gravity or centrifugal forces. The term creaming comes from the familiar separation of cream from raw milk. The density difference between the dispersed and continuous phases causes a vertical concentration gradient in the system. In creaming and sedimentation processes the size distribution of the droplets does not change and the process is reversible by simple agitation of the vessel.^{13, 42} The creaming speed v_s of an isolated, spherical drop of radius r moving through a fluid medium of density ρ_0 and shear viscosity η_0 is given by equation below based on Stokes' Law:⁴³

$$v_s = -\frac{2gr^2(\rho_0 - \rho)}{9\eta_0} \quad (1.5)$$

where g is the acceleration and ρ is the density of the dispersed phase. In dilute emulsions, this equation indicates that creaming or sedimentation can be retarded by reducing the size of the emulsion droplets, increasing the viscosity of the continuous phase or by decreasing the density difference between the two phases.

Coalescence occurs when two or more emulsion droplets join together to form a single one with a higher volume but lower interfacial area which is energetically favourable. The speed of thinning of the film between the droplets and the stability of the film against rupture are important factors determining the stability of the emulsion towards coalescence.^{7, 44} In emulsions stabilised with solid particles, droplets usually coalesce until the interfaces are sufficiently covered with particles to be stable; this phenomenon is called limited coalescence.^{45, 46}

In flocculation the emulsion droplets come into close proximity with each other without rupture of the stabilising interfacial film. The affinity of droplets to flocculate depends mainly on the balance of attractive and repulsive forces between them. The droplets will tend to aggregate if attractive forces dominate (van der Waals, depletion and hydrophobic forces), whereas they will be stable towards aggregation if the repulsive forces dominate (electrostatic and steric forces).⁴³ The interaction between them here can either be strong and irreversible or weak and reversible, depending on the forces acting between them. In polydispersed emulsions (where the size of the droplets are not the same), the chance of flocculation occurring is higher than in monodispersed emulsions. The difference in creaming speed for small and large droplets causes them to collide more often compared to monodispersed systems.⁷

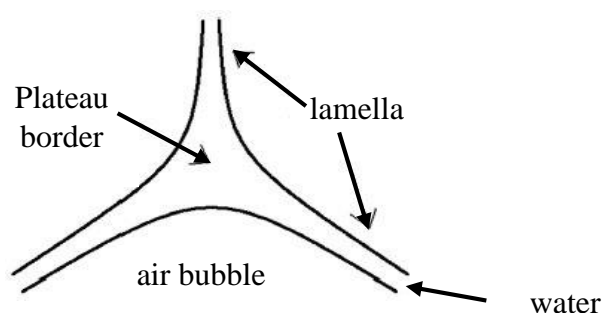
Ostwald ripening is a result of differences in solubility between droplets with different sizes. In polydispersed emulsions the solubility of the dispersed phase in continuous phase depends on the size of droplets. The difference in the solubility of smaller droplets to the solubility of bigger droplets is due to the curvature effect. The smaller droplets start to disappear and the molecules of them diffuse through the continuous phase and finally deposit on the bigger droplets. This results in shifting the droplet size distribution to bigger droplet sizes.⁷ Ostwald ripening is of less importance in food emulsions because of the limited solubility between the aqueous and oil phases.¹¹

1.4 Foams and aerated emulsions

Foam is a colloidal dispersion of gas bubbles in a liquid (usually water) or solid phase. Air is the most common gas used to make bubbles in food systems and unique properties of carbon dioxide such as being non-toxic, natural and its preservative action makes it the second candidate to be used in food foams.¹² Similar to emulsions, foams are commonly found in consumer and industrial products such as foods, pharmaceutical

and personal care products, cleaning detergents and fire-fighting applications.⁴⁷⁻⁵¹ Aeration and structural properties of foams are greatly influenced by the stabiliser used as they can reduce the interfacial tension and increase the viscosity of the liquids. For example, proteins stabilise air bubbles in foams by forming a rigid film of adsorbed protein molecules around air bubbles, whereas in surfactant-stabilised foams, the reduction in the interfacial tension of the air-water interface is the main mechanism for foam stability.⁵²⁻⁵⁵ The thin walls of bubbles comprising a foam are called lamellae and the point where film lamella join together in between air bubbles are known as Plateau borders.⁵⁶ These are shown schematically in Figure 1.7.

Figure 1.7. Schematic representation of three adjacent air bubbles. The Plateau border and lamella are highlighted.



1.4.1 Foam formation and stability

Pure liquids do not foam due to the high energy associated with liquid-gas interfaces, and they require adsorption of a foam stabiliser in order to stabilise gas bubbles. Surfactant and protein molecules have been extensively studied as foam stabilisers in the food industry. However, there are some examples of foams stabilised by fat droplets (whipped cream) and ice crystals (ice-cream).⁵⁷⁻⁵⁹ There are two main structural situations existing for foams. Wet foams consist of spherical smaller bubbles separated by thick foam lamella, while dry foams possess large polyhedral gas bubbles separated by thinner foam lamella. The gas bubble geometry depends on the gas volume fraction (ϕ_{gas}) within the system. In wet foams, ϕ_{gas} can have a value of up to 0.74, which represents the maximum volume fraction possible for an internal phase made up of incompressible spheres. In dry foams, with $\phi_{\text{gas}} > 0.74$, the foam bubbles start to distort taking on a variety of polyhedral shapes and the lamella between air bubbles become

thinner than wet foams, which enhances the chance of film rupture and foam breakdown.⁶⁰

Similar to emulsions, foams are also thermodynamically unstable. The high free energy of the air-water interface is the main reason for foam instability. There are three main physical processes to reduce the overall system free energy leading to foam destabilisation. The instability processes include disproportionation, drainage (creaming) and coalescence. The driving force for disproportionation is the difference in Laplace pressure between bubbles of different size. The Laplace pressure inside a gas bubble arises from the curvature of the air-water interface.^{12, 29} For spherical bubbles of radius R with a gas-liquid interfacial tension of γ , the Laplace pressure is given by:⁶¹

$$\Delta p = \frac{2\gamma}{R} \quad (1.6)$$

This results in the smaller bubbles having higher pressure than the larger ones. According to Henry's law the solubility of a gas increases with pressure; therefore more gas dissolves in water near the small bubbles than near the larger ones. As a result of this, larger bubbles grow at the expense of the smaller bubbles. Drainage (creaming) is another instability process, which is a result of gravity and leads to separation between the gas and liquid phases. During drainage lighter gas bubbles move upward forming a dense foam layer on the top, while the heavier liquid concentrates at the bottom. Coalescence (film rupture) occurs when the thin film between adjacent gas bubbles is not stable enough and results in joining the gas bubbles together forming a single larger bubble.¹²

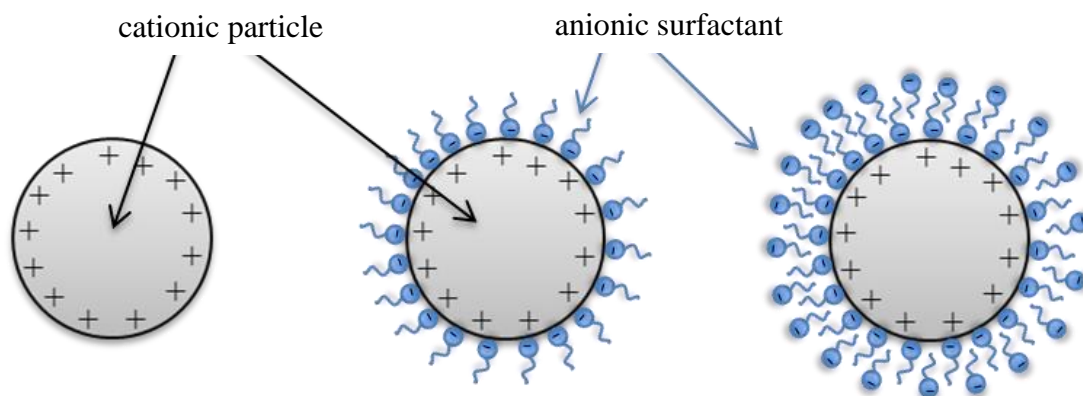
1.4.2 Particle-stabilised foams

Stabilisation of food foams by solid nanoparticles has received great attention recently as foams with better textural properties and longer shelf-life can be produced. Binks and Horozov demonstrated that stable aqueous foams can be formed using partially hydrophobic silica nanoparticles in the absence of any added surfactant.⁶² Results from a study carried out by Ip *et al.* on foams showed that addition of silica particles with the correct wettability stabilises the air bubbles. They concluded that the stability of foams enhances by increasing the concentration of the particles and decreasing the particle size.⁶³ All these results and many from other scientists^{21, 64, 65} show the interest of researchers in stabilising foams by solid particles.

As with Pickering emulsions, in particle-stabilised foams the effectiveness of particle binding to the interface is controlled by the particle wettability characterised by the contact angle (measured through water).^{66, 67} Particles exhibiting a contact angle slightly below or beyond 90° are highly surface-active because of the higher adsorption free energy of the particles compared with the thermal energy.^{27, 29} The commercially available raw nanoparticles such as silica and calcium carbonate are not surface-active due to their extreme hydrophilicity. As a result of this there is an interest in modifying the surface properties of such solid particles in order to control their behaviour at interfaces. One way of doing this is *via* a homogeneous surface coating. Using this *ex situ* method, hydrophilic silica particles can be modified to have variable wettability by surface silylation.²⁷ The most common method to modify the surface properties of the particles is *via in situ* surface activation using amphiphilic molecules. It has been found that using this protocol, ultra-stable emulsions and foams can be produced.^{34, 68-70} Another less common approach is the preparation of “Janus” particles, which introduces asymmetry properties over the surface of the particle and renders them amphiphilic and suitable for adsorption at interfaces.⁷¹⁻⁷⁴

Gonzenbach *et al.*⁷⁵ reported the formation of ultra-stable particle-stabilised foams that were entirely stable towards coalescence and disproportionation. They hydrophobised alumina particles with short chain amphiphiles to stabilise aqueous foams. Cui *et al.*⁷⁶ prepared stable aqueous foams by *in situ* surface activation of Precipitated Calcium Carbonate (PCC) nanoparticles with negatively charged Sodium Dodecyl Sulphate (SDS) molecules. Non-modified PCC nanoparticles are positively charged at their natural pH and negatively charged SDS molecules adsorb on the particles with a head-on configuration. This results in neutralising the positive charge and renders the particles more hydrophobic by leaving their tail group towards the aqueous phase. In their results the synergistic effect on foamability and foam stability was observed for a certain range of surfactant concentration, above that the synergistic effect decreased. This could be a result of particles becoming hydrophilic again with the formation of a double surfactant layer (bilayer) or hemi-micelles⁷⁷ on their surfaces due to chain-chain interactions. The formation of a bilayer on a positively charged particle upon adsorption of negatively charged surfactant molecules is shown schematically in Figure 1.8.

Figure 1.8. Anionic surfactant monomers can adsorb on positively charged particles *via* electrostatic interactions. They initially form a monolayer and may then form a bilayer on the surface of the particles upon further adsorption of surfactant.



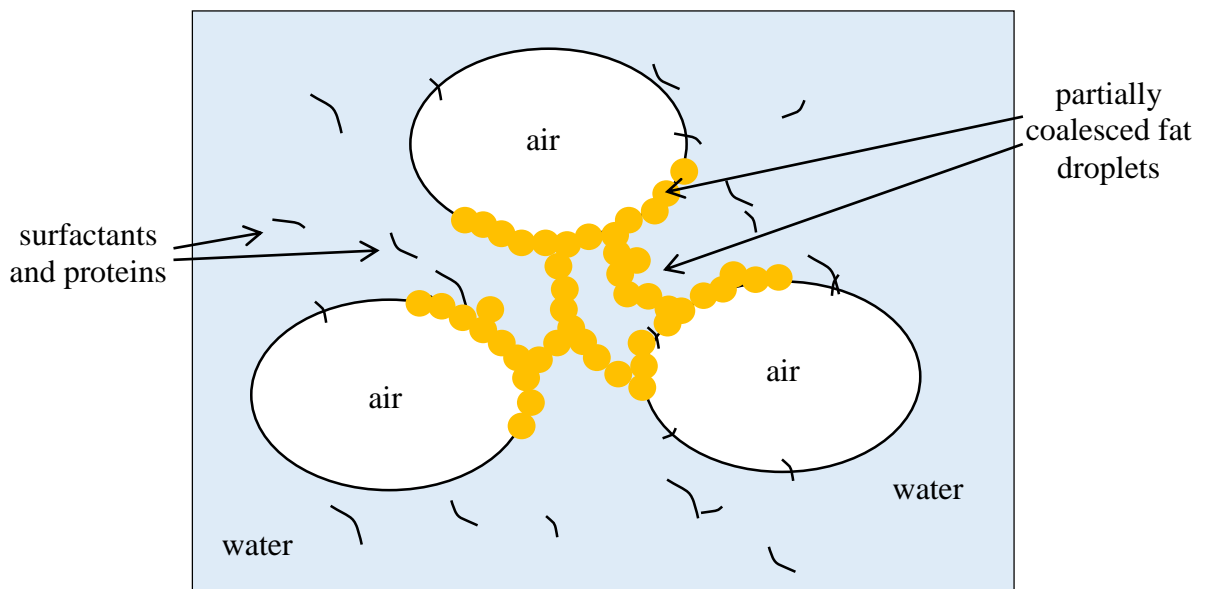
1.4.3 Whipped cream

Whipped cream is an aerated oil-in-water emulsion in which air bubbles in water are covered to varying degrees with fat droplets. The fat droplets in such a system only partially coalesce since they contain both crystallised and liquid portions. The rigid structure of the final whipped cream is supported by the formation of a three-dimensional network of partially coalesced fat droplets and a high viscous serum phase. Other factors controlling the structural properties of the whipped cream are the Solid Fat Content (SFC) of the oil, processing conditions, stabilisers and emulsifiers. Surfactants and proteins are known to improve the stability of whipped cream by increasing the viscosity of the continuous phase and retarding the thinning of the liquid films between adjacent air bubbles as well as their role as a surface-active ingredient at the air-water interface. A cream, an oil-in-water emulsion, with fat content of 30-40% is typically known as whipping cream, which can also be used un-whipped.^{78, 79} Whipped cream is a complex system containing various components such as an aqueous solution of sugars, proteins and surfactants, fat droplets, polymers and air cells. It is required to be stable before whipping, as an emulsion, and be partially unstable during whipping since fat droplet coalescence is an essential factor of foam formation.²²

The most common way of introducing air bubbles into whipping cream is by using an electric or manual mixer equipped with a ball shape whisk. During the whipping

process fat droplets adhere to air-water interfaces and form a protective layer around air bubbles.⁸⁰ Whipping of a cream using a whisk can be explained in a three step process.⁸¹ The first stage of whipping involves the incorporation of the air into the cream as large bubbles. Initially formed large bubbles are stabilised by quickly adsorbed proteins and surfactants. Bubble formation takes place immediately behind the moving wires of the whisk. The second stage involves a dynamic process of bubble break-up and oil droplet coalescence. The air bubbles break to smaller ones and fat globules from the aqueous phase adsorb to newly formed interfaces. After bubble break-up, fat globules are pressed together at the bubble surface and form aggregates at the surface of the bubbles. In the final stage of whipping fat aggregates grow at the bubble surface and form clumps of partially coalesced fat droplets in the continuous phase, which results in the formation of a rigid whipped cream. Figure 1.9 is a schematic representation of the air bubbles stabilised with partially coalesced fat droplets in whipped cream.

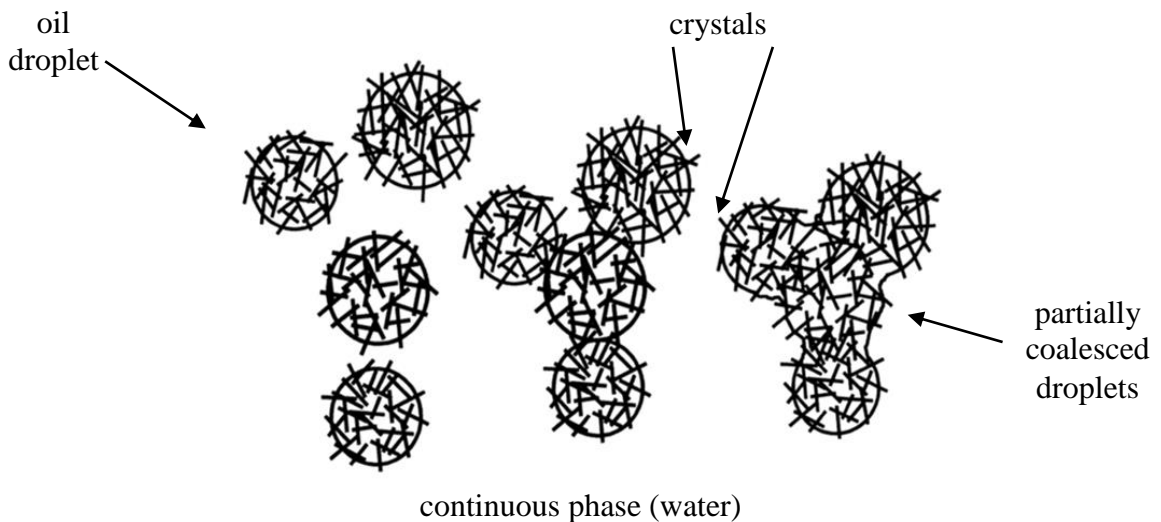
Figure 1.9. Partial coalescence of fat droplets forms a protective layer around air bubbles and stabilises them. Partially crystallised fat globules further grow and make a 3D network in the continuous phase and give stiffness to foam structure.



The role of fat globules in stabilizing air bubbles and giving stiffness to the whipped product can be explained due to their surface activity and adsorption to bubble interfaces and also to the formation of the partially coalesced fat droplet network in the continuous phase. In order for partial coalescence to occur during aeration, oil droplets

in the initial oil-in-water emulsions need to contain some degree of crystallinity. Crystals inside the oil droplets form a network and this solid network can extend out to the continuous phase. Upon collision with other droplets during whipping, the crystals rupture the stabilising film of the other droplet and make oil-oil contact as shown in Figure 1.10.⁸²⁻⁸⁴ Liquid oil droplets cannot form aggregates by clumping,⁵⁸ therefore to produce a stable rigid foam at least 40% of the fat is required to be crystalline to promote partial coalescence of oil droplets.⁸⁵

Figure 1.10. Partial coalescence occurs between partially crystallised oil droplets. A crystal from one droplet penetrates into the liquid part of another oil droplet.



Attaching of a fat droplet at an air-water interface during whipping can be thermodynamically described by the entering coefficient, E , defined as:

$$E = \gamma_{aw} + \gamma_{ow} - \gamma_{oa} \quad (1.7)$$

where γ_{aw} , γ_{ow} and γ_{oa} are the interfacial tensions of air-water, oil-water and oil-air respectively. When $E > 0$ adsorption of fat globules at the air-water interface is thermodynamically favourable.²⁹

As explained earlier the fat type and degree of crystallisation of fat in whipping cream significantly affect the whipping process, stability and properties of the whipped cream. As a result using a fat with desirable whipping properties has been of interest to food scientists. Whipping cream produced from whole milk is called dairy cream. Whole

milk contains about 4% of fat which is present as small droplets. In modern practice, whole milk can be taken to the stage of single cream (18% fat) or double cream (about 42% fat) using a centrifuge.⁸⁶ Whipping this cream produces a dairy whipped cream. On the other hand, there are many vegetable oils such as coconut, Palm Oil (PO) and Palm Kernel Oil (PKO) that are also used to produce whipping cream. The cream made from these oils is called non-dairy whipping cream. Non-dairy whipped toppings are more functional than dairy whipping cream because manufacturers can choose to use a more desirable fat characterized by a specific SFC profile with matching emulsifier systems. In addition, a high abundance of non-dairy fats in nature makes them good components for food and other consumer products. The stability of dairy whipped cream has been compared with PKO-based whipped cream in different studies and it was found that the latter is more stable than the former.^{87, 88}

1.5 Presentation of thesis

The general aim of this thesis was to investigate the incorporation of solid particles into food formulations as emulsion and foam stabilisers. It was investigated whether solid particles with the correct surface properties could fulfil all or part of the role played by fat droplets in stabilising air bubbles in whipped cream. PCC particles were used in this project and their behaviour at air-water and oil-water interfaces are studied systematically in separate chapters. In Chapter 3, oil-free aqueous foams, stabilised by surfactant alone and subsequently surfactant-particle mixtures, are investigated in terms of their foam formation and foam stability. The influence of key parameters such as surfactant concentration, particle concentration and particle wettability is studied in detail. In Chapter 4, model non-dairy whipping cream emulsions and aerated emulsions containing Palm Kernel Oil (PKO) as the oil phases are studied. The effect of particle concentration, oil volume fraction and whipping duration on the structural properties of the model foams are studied in depth. Various properties of such foams were compared with a commercial whipped cream manufactured by the sponsor of the project. The effect of temperature on the aeration and structural properties of the commercial whipping cream is also investigated. Surfactant-stabilised emulsions are compared with particle-stabilised emulsions in terms of their stability towards partial coalescence in Chapter 5. It is shown that for oil-in-water emulsions containing crystallisable oil, the type of stabiliser plays a crucial role in the stability of the

emulsions. In Chapter 6, several properties of surfactant-stabilised oil-in-water emulsions containing non-crystallisable oil are presented followed by their aeration properties. It is shown that the size of oil droplets influences the stability of the foams generated from the aeration of oil-in-water emulsions. Finally, a summary of conclusions, suggestions and future work is described at the end of this thesis.

1.6 References

1. <http://www.richs.com/about/>, Accessed 19.05.2014.
2. *Foundations of colloid science*, ed. R.J. Hunter, 2nd edn., Oxford University Press, New York, 2001.
3. *Colloidal Dispersions: Suspensions, Emulsions, and Foams*, I.D. Morrison and S. Ross, Wiley-Interscience, New York, 2002.
4. *Emulsions, Foams, and Suspensions: Fundamentals and Applications*, L.L. Schramm, Wiley, Weinheim, 2006.
5. *Food Emulsions: Principles, Practice and Techniques*, D.J. McClements, CRC Press, Boca Raton, 1999.
6. N. Garti, *Colloids Surf. A*, **123-124**, 233 (1997).
7. *Modern Aspects of Emulsion Science*, ed. B.P. Binks, The Royal Society of Chemistry, Cambridge, 1998.
8. T.S. Dunstan, P.D.I. Fletcher and S. Mashinchi, *Langmuir*, **28**, 339 (2011).
9. P.J. Wilde, *Curr. Opin. Colloid Interface Sci.*, **5**, 176 (2000).
10. T. Awad and K. Sato, *Colloids Surf. B*, **25**, 45 (2002).
11. D. Rousseau, *Food Res. Int.*, **33**, 3 (2000).
12. *An Introduction to Food Colloids*, E. Dickinson, Oxford University Press, Oxford, 1992.
13. *Emulsion Science and Technology: A General Introduction*, ed. T.F. Tadros, Wiley-VCH Weinheim, 2009.
14. E. Dickinson, *Food Hydrocoll.*, **17**, 25 (2003).
15. M.A. Bos and T. van Vliet, *Adv. Colloid Interface Sci.*, **91**, 437 (2001).
16. E. Ruckenstein, *Langmuir*, **12**, 6351 (1996).
17. B.P. Binks, *Langmuir*, **9**, 25 (1993).
18. W.C. Griffin, *J. Soc. Cosmet. Chem.*, **1**, 311 (1949).
19. R.C. Pasquali, M.P. Taurozzi and C. Bregni, *Int. J. Pharm.*, **356**, 44 (2008).
20. *Functionality of Proteins in Food*, J.F. Zayas, Springer Berlin 1997.
21. B.S. Murray and R. Ettelaie, *Curr. Opin. Colloid Interface Sci.*, **9**, 314 (2004).
22. Q. Zhao, M. Zhao, J. Wang, C. Wang and B.A.O. Yang, *J. Food Process Eng.*, **31**, 671 (2008).
23. B.P. Binks and S.O. Lumsdon, *Phys. Chem. Chem. Phys.*, **2**, 2959 (2000).
24. B.P. Binks and J.A. Rodrigues, *Langmuir*, **19**, 4905 (2003).

25. W. Ramsden, *Proc. Roy. Soc.*, **72**, 156 (1903).
26. S.U. Pickering, *J. Chem. Soc.*, **91**, 2001 (1907).
27. B.P. Binks, *Curr. Opin. Colloid Interface Sci.*, **7**, 21 (2002).
28. R. Aveyard, B.P. Binks and J.H. Clint, *Adv. Colloid Interface Sci.*, **100**, 503 (2003).
29. *Colloidal Particles at Liquid Interfaces*, ed. B.P. Binks and T.S. Horozov, Cambridge University Press, Cambridge, 2006.
30. S. Levine, B.D. Bowen and S.J. Partridge, *Colloids Surf.*, **38**, 325 (1989).
31. B.S. Murray, K. Durga, A. Yusoff and S.D. Stoyanov, *Food Hydrocoll.*, **25**, 627 (2011).
32. B.P. Binks and S.O. Lumsdon, *Phys. Chem. Chem. Phys.*, **1**, 3007 (1999).
33. S. Abend, N. Bonnke, U. Gutschner and G. Lagaly, *Colloid Polym. Sci.*, **276**, 730 (1998).
34. B.R. Midmore, *Colloids Surf. A*, **132**, 257 (1998).
35. N.P. Ashby and B.P. Binks, *Phys. Chem. Chem. Phys.*, **2**, 5640 (2000).
36. B.P. Binks and S.O. Lumsdon, *Langmuir*, **17**, 4540 (2001).
37. N. Yan, M.R. Gray and J.H. Masliyah, *Colloids Surf. A*, **193**, 97 (2001).
38. S. Fujii, E.S. Read, B.P. Binks and S.P. Armes, *Adv. Mater.*, **17**, 1014 (2005).
39. B.P. Binks, R. Murakami, S.P. Armes and S. Fujii, *Angew. Chem. Int. Ed.*, **44**, 4795 (2005).
40. B.P. Binks, R. Murakami, S.P. Armes and S. Fujii, *Langmuir*, **22**, 2050 (2006).
41. S. Melle, M. Lask and G.G. Fuller, *Langmuir*, **21**, 2185 (2005).
42. *Emulsions and Emulsion Stability*, J. Sjöblom, 2nd edn., CRC Press, Boca Raton, 2006.
43. D.J. McClements, *Crit. Rev. Food. Sci. Nutr.*, **47**, 611 (2007).
44. S. Simovic and C.A. Prestidge, *Langmuir*, **20**, 8357 (2004).
45. S. Arditty, C.P. Whitby, B.P. Binks, V. Schmitt and F. Leal-Calderon, *Eur. Phys. J. E.*, **11**, 273 (2003).
46. B.P. Binks and C.P. Whitby, *Langmuir*, **20**, 1130 (2004).
47. P.C. Vandevivere, R. Bianchi and W. Verstraete, *J. Chem. Technol. Biotech.*, **72**, 289 (1998).
48. C.A. Moody and J.A. Field, *Environ. Sci. Technol.*, **34**, 3864 (2000).
49. Y. Zhao, S.A. Jones and M.B. Brown, *J. Pharm. Pharmacol.*, **62**, 678 (2010).
50. A. Arzhavitina and H. Steckel, *Int. J. Pharm.*, **394**, 1 (2010).

51. H.D. Goff, *J. Dairy Sci.*, **80**, 2620 (1997).
52. D. Varade, D. Carriere, L.R. Arriaga, A.L. Fameau, E. Rio, D. Langevin and W. Drenckhan, *Soft Matter*, **7**, 6557 (2011).
53. S. Samanta and P. Ghosh, *Chem. Eng. Res. Des.*, **89**, 2344 (2011).
54. L.A. Pughaloni, E. Dickinson, R. Ettelaie, A.R. Mackie and P.J. Wilde, *Adv. Colloid Interface Sci.*, **107**, 27 (2004).
55. M.D. Eisner, S.A.K. Jeelani, L. Bernhard and E.J. Windhab, *Chem. Eng. Sci.*, **62**, 1974 (2007).
56. *The Physics of Foams*, D. Weaire and S. Hutzler, Clarendon Press, Oxford, 2001.
57. Y. Chang and R.W. Hartel, *J. Food Eng.*, **55**, 59 (2002).
58. K.E. Allen, E. Dickinson and B. Murray, *LWT - Food Sci. Technol.*, **39**, 225 (2006).
59. K.E. Allen, B.S. Murray and E. Dickinson, *Food Hydrocoll.*, **22**, 690 (2008).
60. *Colloid and Interface Science*, P. Ghosh, Prentice-Hall of India Pvt. Ltd., New Delhi, 2009.
61. *Capillarity and Wetting Phenomena: Drops, Bubbles, Pearls, Waves*, P.G. de Gennes, F. Brochard Wyart and D. Quéré, Springer, New York, 2004.
62. B.P. Binks and T.S. Horozov, *Angew. Chem. Int. Ed.*, **44**, 3722 (2005).
63. S.W. Ip, Y. Wang and J.M. Toguri, *Can. Metall. Q.*, **38**, 81 (1999).
64. B.S. Murray, *Curr. Opin. Colloid Interface Sci.*, **12**, 232 (2007).
65. T.N. Hunter, R.J. Pugh, G.V. Franks and G.J. Jameson, *Adv. Colloid Interface Sci.*, **137**, 57 (2008).
66. Z.P. Du, M.P. Bilbao-Montoya, B.P. Binks, E. Dickinson, R. Ettelaie and B.S. Murray, *Langmuir*, **19**, 3106 (2003).
67. E. Dickinson, R. Ettelaie, T. Kostakis and B.S. Murray, *Langmuir*, **20**, 8517 (2004).
68. B.P. Binks, A. Desforges and D.G. Duff, *Langmuir*, **23**, 1098 (2007).
69. B.R. Midmore, *Colloids Surf. A*, **145**, 133 (1998).
70. B.P. Binks, M. Kirkland and J.A. Rodrigues, *Soft Matter*, **4**, 2373 (2008).
71. B.P. Binks and P.D.I. Fletcher, *Langmuir*, **17**, 4708 (2001).
72. A. Perro, S. Reculosa, S. Ravaine, E.B. Bourgeat-Lami and E. Duguet, *J. Mater. Chem.*, **15**, 3745 (2005).
73. O. Cayre, V.N. Paunov and O.D. Velev, *J. Mater. Chem.*, **13**, 2445 (2003).
74. V.N. Paunov and O.J. Cayre, *Adv. Mater.*, **16**, 788 (2004).

75. U.T. Gonzenbach, A.R. Studart, E. Tervoort and L.J. Gauckler, *Angew. Chem. Int. Ed.*, **45**, 3526 (2006).
76. Z.G. Cui, Y.Z. Cui, C.F. Cui, Z. Chen and B.P. Binks, *Langmuir*, **26**, 12567 (2010).
77. R. Atkin, V.S.J. Craig, E.J. Wanless and S. Biggs, *Adv. Colloid Interface Sci.*, **103**, 219 (2003).
78. R. Kováčová, J. Stetina and L. Curda, *J. Food Eng.*, **99**, 471 (2010).
79. K.E. Allen, B.S. Murray and E. Dickinson, *Int. Dairy J.*, **18**, 1011 (2008).
80. *Advances in Food Emulsions and Foams*, ed. E. Dickinson and G. Stainsby, Elsevier Applied Science, London, 1988.
81. G.A. van Aken, *Colloids Surf. A*, **190**, 333 (2001).
82. K. Boode and P. Walstra, *Colloids Surf. A*, **81**, 121 (1993).
83. E. Fredrick, P. Walstra and K. Dewettinck, *Adv. Colloid Interface Sci.*, **153**, 30 (2010).
84. K. Boode, P. Walstra and A.E.A. de Groot-Mostert, *Colloids Surf. A*, **81**, 139 (1993).
85. A.K. Smith, H.D. Goff and Y. Kakuda, *Int. Dairy J.*, **10**, 295 (2000).
86. *Advanced Dairy Chemistry*, P.F. Fox and P.L.H. McSweeney, 3rd edn., Springer, New York, 2003.
87. K. Shamsi, Y. Che Man, M. Yusoff and S. Jinap, *J. Am. Oil Chem. Soc.*, **79**, 583 (2002).
88. K. Nesaretnam, N. Robertson, Y. Basiron and C.S. Macphie, *J. Sci. Food Agric.*, **61**, 401 (1993).

CHAPTER 2 EXPERIMENTAL

2.1 Materials

2.1.1 Water

Water was purified by passing through an Elgastat Prima Reverse Osmosis Unit and then a Millipore Milli-Q reagent water system. Measurements of the surface tension of the resulting Milli-Q water determined *via* the du Noüy ring method were typically around 71.8 mN m⁻¹ at 25 °C. This is in good agreement with the accepted literature value¹ for ultrapure water. The water had an average electrical resistivity value of 18 MΩ cm, in good agreement with specifications of ultrapure water.²

2.1.2 Oils

2.1.2.1 Palm kernel oil

Samples of Palm Kernel Oil (PKO) Encore 100 were kindly provided by the sponsor, purchased from Cargill Food Ingredients (North America). No further purification was necessary and it was used as received. PKO is a commercial oil and because it consists of a mixture of Triacylglycerides (TAGs), it melts and crystallises over a range of temperatures. In its liquid form, it is clear and pale yellow in appearance. Its fatty acid composition consists mainly of lauric acid (C12:0, about 50%), myristic acid (C14:0, about 16%) and palmitic acid (C16:0, about 8%), with other fatty acids raising the total percentage of saturates to about 82%.³ One of the main applications of PKO Encore 100, which contains citric acid added as a preservative, is in confectionary coatings as well as in whipped cream.⁴ Prior to its use, PKO was melted to 80 °C using a Grant Optima Digital Immersion Thermostat (GD120) connected to a R1-5L stainless steel refrigeration unit.

2.1.2.2 High oleic sunflower oil

High Oleic Sunflower Oil (HOSO), purchased from EULIP S.p.A Italy, was purified prior to use by column chromatography through activated basic aluminium oxide (99 %, Acros Organics). This was repeated twice in order to remove the more polar surface active impurities. HOSO is a vegetable fat that is manufactured from sunflower oil and has various applications in the food industry. HOSO has a pale yellow colour at

room temperature (23 °C) and is liquid down to 0 °C. It is more stable towards oxidation and it comprises of a mixture of TAGs. As its name implies it is rich in oleic (C18:1; monounsaturated) acid with a minimum amount of 81.3 %, ⁵ with some other varieties containing 83.5 % oleic acid. ⁶

2.1.2.3 Dodecane

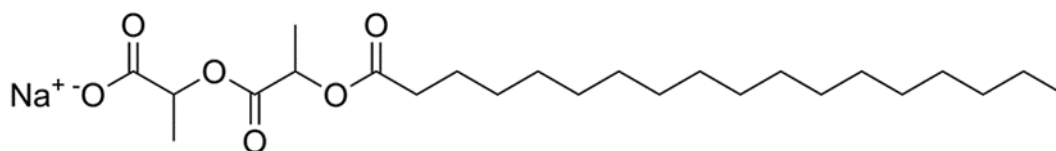
Dodecane is a liquid alkane hydrocarbon with the chemical formula of C₁₂H₂₆. It is a non-food grade oil and was used for comparison purposes. A sample of dodecane was purchased from Acros Organics (99% purity) and was further purified prior to use by column chromatography through activated basic aluminium oxide (99 %, Acros Organics). This was repeated twice in order to remove the more polar surface active impurities.

2.1.3 Surfactants

2.1.3.1 Sodium stearoyl lactylate

Samples of Sodium Stearoyl Lactylate (SSL, Emplex® 268) were kindly provided by the sponsor, purchased from Caravan Food Ingredients. SSL is a pale yellow powder at room temperature and it was used as received. SSL is produced by esterification of stearic acid with lactic acid in the presence of sodium hydroxide, which gives a mixture of stearyl lactylate (sodium salts), fatty acid salts and free fatty acids. The main component of stearyl lactylate is shown in Figure 2.1 and is sodium stearyl lactylate with a molecular weight of 450 g/mol.

Figure 2.1. Chemical structure of SSL molecule. It consists of a large head group and a C₁₈ hydrocarbon tail group.



2.1.3.2 Sodium dodecylsulphate

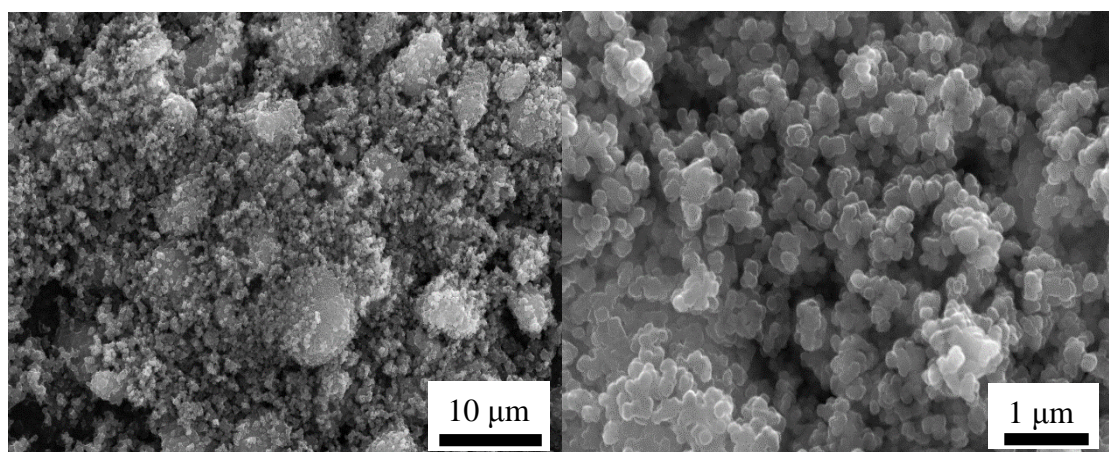
Sodium DodecylSulphate (SDS) is an anionic, non-food grade surfactant and was used for comparison purposes. A sample of SDS, Sigma Ultra, > 99% GC was purchased from Sigma-Aldrich.

2.1.4 Particles

2.1.4.1 Precipitated calcium carbonate

Precipitated Calcium Carbonate (PCC) is made by the hydration of calcium oxide to calcium hydroxide, followed by direct carbonation. It is of greater purity compared to naturally-available calcium carbonate as impurities are removed during the production process.⁷ PCC used in this study is a white microcrystalline powder characterised by a large surface area, controlled particle shape and high degrees of whiteness. Calofort U PCC was received from Specialty Minerals Inc. (SMI). This specific type of PCC is uncoated and its hydrophilic nature makes it a suitable ingredient in water-based systems.⁸ Figure 2.2 shows SEM images of dry Calofort U PCC particles. The images show that particles have a primary particle diameter of approximately 150 nm and are partially fused together and form aggregates of several μm .

Figure 2.2. SEM images of dry Calofort U PCC particles.



2.1.5 *Vanilla Bettercreme[®] commercial whipping cream*

Vanilla Bettercreme[®] (VBC) produced and kindly provided by the sponsor of the project is an oil-in-water non-dairy ready-to- whip cream. VBC contains water, oil, high fructose corn syrup and less than 2 % of the following: sodium caseinate, soy protein concentrate, carbohydrate gum, polysorbate 60, salt, artificial flavour, soy lecithin, polyglycerol esters of fatty acids, potassium sorbate and xanthan gum. The oil phase in VBC is a mixture of partially hydrogenated PKO and partially hydrogenated soybean oil.⁹ VBC as an oil-in-water emulsion containing all the main ingredients of a whipping cream was used as a reference in the experiments and the results from its characterisation was of importance for comparison purposes.

2.1.6 *Xanthan gum*

Xanthan gum was manufactured by FMC BioPolymers and was kindly provided by the sponsor of the project. It was used as received. It is produced from the fermentation of glucose in the presence of the bacterium *Xanthomonas campestris*¹⁰ and is one of the most common hydrocolloids used as thickening agents in various food formulations. Xanthan gum is a heteropolysaccharide with a primary structure consisting of repeated pentasaccharide units formed by two glucose units, two mannose units, and one glucuronic acid unit.¹¹

2.1.7 *Other chemicals*

Within the specific sections of this work, materials other than those already detailed have been used. These materials along with their supplier and purity are listed in Table 2.1. All these chemicals were used as received.

Table 2.1. Source and purity of other chemicals used within this study.

Chemical	Source	Purity / %
Sodium hydroxide	VWR International	> 99
Aqueous hydrochloric acid	Fluka	37 wt., analytical grade
Chloroform	Fisher	Analytical grade
Ethanol	Fisher	Analytical grade

2.2 Methods

2.2.1 *Characterisation of sodium stearyl lactylate powder*

2.2.1.1 Differential scanning calorimetry

Differential Scanning Calorimetry (DSC) measurements enable precise determination of the temperature range at which a material melts, as well as the amount of energy associated with the melting transition. A Perkin-Elmer DSC-7 was used for SSL thermal analyses. Nitrogen was used as the purge gas and the instrument was calibrated with indium (melting point 156.8 °C, $\Delta H_f = 28.87$ J/g). Approximately 5 mg of SSL powder was weighed using a Mettler Toledo XS105 Analytical Balance into 20 μ L aluminium pans and the covers were sealed using a crimper. An empty, sealed aluminium pan was used for reference and the base line was obtained prior to the analysis of samples using the empty reference pan. One temperature program was used to obtain the thermogram of the SSL sample. The sample was held isothermally at -10 °C for 2 minutes, heated to 80 °C at 10 °C/min, held at 80 °C for 2 minutes, cooled to -10 °C at 10 °C/min and re-heated to 80 °C at 10 °C/min. The plotted results (heat flow as a function of temperature) were used to obtain the onset, major peak and end of the melting/solidification transitions, while the software determined the associated heats by standard methods.

2.2.2 *Preparation of sodium stearyl lactylate aqueous dispersions*

2.2.2.1 Heat treated and non-heat treated

A concentrated aqueous stock solution of SSL was prepared in a volumetric glass vessel for each experiment. For heat treated solutions, the stock solution was kept at 60 °C using a Grant Optima Digital Immersion Thermostat (GD120) for 30 minutes while stirring with a magnetic bar on a Heidolph MR 3001 magnetic hot plate. For non-heat treated samples, the stock solution was stirred for 30 minutes with a magnetic bar whilst being kept at 25 °C. Later, selected surfactant solutions were prepared by dilution from the stock solution. The solutions were magnetically stirred at all temperatures in sealed vessels. The level of stirring was adjusted to prevent foaming but rapid enough to enable the equilibrium dispersion/dissolution of SSL in the water phase. Unless stated otherwise, the pH of the samples was not modified.

2.2.3 Characterisation of sodium stearyl lactylate aqueous dispersions

2.2.3.1 Optical microscopy

Aqueous dispersions and foams were observed using an Olympus BX51 optical microscope at 23 ± 1 °C. A normal glass microscope slide was used. Digital micrographs of the dispersions were taken using a 12-bit Olympus DP70 camera and the images were edited using Microsoft PowerPoint and scale bars were added to them. Crossed-polarised light was used by applying the reflected light analyser (U-AN, Olympus) and the U-POT polariser when needed.

2.2.3.2 Cryo-scanning electron microscopy

For Cryo-Scanning Electron Microscopy (Cryo-SEM) analysis, dispersions and foams were placed in double aluminium rivets (1 mm bore) and submerged in a liquid nitrogen slush (-210 °C). Frozen samples were then transferred under vacuum into the Cryo preparation chamber where the top rivet was fractured off. The dispersion was then sublimated for 1 hour at -90 °C. Samples were gold coated and transferred under vacuum onto the cold stage (-150 °C) of the SEM, Hitachi S-570 (10 kV). Digital images were captured using Quartz PCI Version 7, Quartz Imaging Corp.

2.2.3.3 Surface tension

The air-water surface tension of the solutions was measured with a Krüss K10 digital tensiometer. The measurements were performed by the static maximum pull method using the du Noüy ring method. For each solution, at least three measurements were recorded and the reproducibility was within ± 0.5 mN m⁻¹. To retain a stable temperature of 25 °C a Grant Optima Digital Immersion Thermostat (GD120) was used. Before each use the balance was checked and the surface tension of dodecane measured. The measured surface tension values were corrected as explained by Bayramli *et al.*¹² The cleaning procedure consisted of rinsing the glass vessel in ethanol followed by washing with Milli-Q water. The ring was heated to glowing in a blue Bunsen flame.

2.2.4 Characterisation of particles

2.2.4.1 Scanning electron microscopy

PCC particles were studied using SEM in order to gain information regarding their shape, size and aggregation state. A carbon-impregnated sticky disk was applied to the surface of a standard 12 mm diameter aluminium SEM mount. The prepared mount was then brought into contact with a small quantity of the particle sample that adhered to the sticky surface. The mounted sample was coated with a thin film of carbon by thermal evaporation using an Edwards High Vacuum E12E Vacuum Coating Machine. Finally, the samples were examined and a representative area was imaged at various magnifications using a Zeiss EVO 60 SEM instrument.

2.2.4.2 Surface area

The surface area of PCC particles was determined *via* gas adsorption using a Micromeritics TriStar 3000 instrument. The Brunauer, Emmet and Teller (BET) theory is the most popular model used to determine the surface area. When analysing samples on this instrument, the samples are first out-gassed using vacuum. Clean solid surfaces adsorb surrounding gas molecules and the BET theory provides a mathematical model for the process of gas adsorption. Measuring the surface area involved chilling the surface of the pre-weighed powder using nitrogen leading to surface adsorption; then taking the chilling away, leading to desorption. The specific surface area of a powder is estimated from the amount of nitrogen adsorbed in relation to its pressure at the boiling temperature of liquid nitrogen under normal atmospheric pressure. A weight of approximately 0.03 g of calcium carbonate was used for the analysis and the sample's temperature was kept at -195 °C using a liquid nitrogen bath during adsorption. The effect of sonication on breaking any particle clumps and consequently on the surface area of particles was checked. The samples were placed in a sonicator bath for 10 minutes prior to analysis. Sonication was found to have no effect on the surface area of the particles.

2.2.4.3 Contact angle

The contact angle through water of sessile drops of SSL solution on Calofort U disks under air was measured using a Krüss DSA 10 MK2 Drop Shape Analyser at $23 \pm$

1 °C. The instrument consisted of a camera and a closed chamber. The chamber was connected to the thermostated water bath to control the temperature. A drop of water or SSL solution (20 µL) was placed on the disk using a micro-syringe in the measuring chamber and sealed to saturate the vapour space with water. Advancing (20 µL, formed by expanding) and receding (10 µL, formed by contracting) contact angles of the liquid on the disks were then obtained. They were determined directly from the images by drawing a tangent between the liquid drop and the solid surface using the drop shape analyser software. The calculation was done on both sides of the drop and the average was calculated.

Compact disks of Calofort U were prepared at the School of Food Science and Nutrition at Leeds University. For preparing them a Clarke Strong Arm High Pressure Press with a highly polished stainless steel punch and a die of 1 cm diameter was used. Approximately 0.08 g of dry powder of particles were compressed into a circular disk of 1 mm thickness by applying a mass of 7 tonnes for 10 seconds. Each contact angle value was averaged for at least three drops. New drops were formed at different locations on the surface. The reproducibility of contact angles was generally $\pm 3^\circ$.

2.2.5 Preparation of particle dispersions in water and in surfactant aqueous dispersions

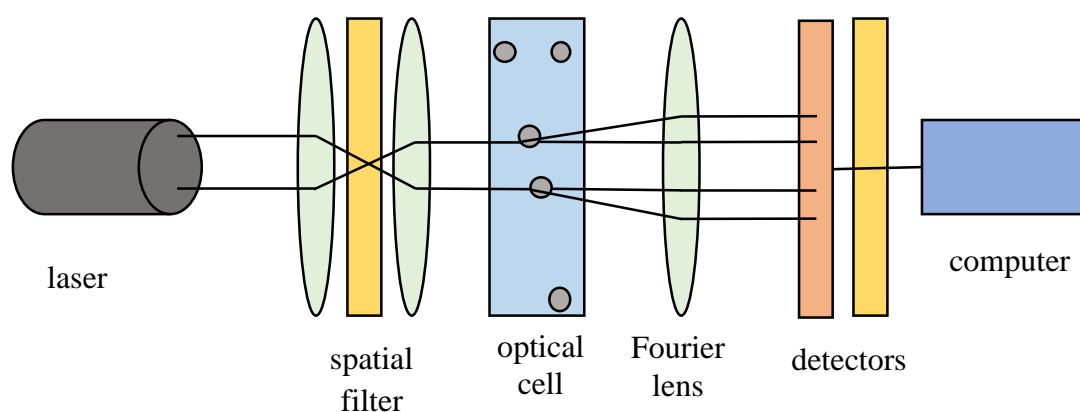
Dispersions of Calofort U PCC particles were prepared in Milli-Q water and in SSL aqueous solutions using a High Intensity Ultrasonic Processor, Vibra-cell VC100 with a 20 kV CV18 ultrasonic probe of 2.30 mm diameter (Sonic & Materials). A selected mass of particles was weighed into a glass sample tube of dimensions 7.5 cm (*h*) by 2.5 cm (*d*) and this was followed by adding pure water or SSL solution. The particles were then dispersed by operating the apparatus at 5 W for 2 minutes. The dispersion was processed at 23 ± 1 °C. The pH of the dispersion was adjusted using HCl or NaOH and was measured using a Fisherbrand, Hydrus400 digital pH meter. The appearance of the dispersions was photographed at various times after their preparation to check their stability to sedimentation. Since water was used to prepare the dispersions in the presence of air, no attempt was made to keep air out of the glass bottles.

2.2.6 Characterisation of particle dispersions in water and in surfactant aqueous dispersions

2.2.6.1 Particle size distribution

The size distribution of particles in dispersions was determined *via* a light diffraction method using a Malvern MasterSizer 2000 Droplet Size Analyser at 23 ± 1 °C. Figure 2.3 shows a representation of the components of the instrument. A Helium-Neon laser beam of 633 nm wavelength is spatially filtered and collimated to produce a clean parallel beam of light. This beam is then focused using a Fourier lens to a photosensitive detector. The laser beam then passes through a pinhole at the centre of the detector and falls on a second detector known as the obscuration detector. If no particles are present in the sample port all light from the laser beam hit the obscuration detector. However, if particles are added they scatter light at an angle inversely proportional to their size.¹³ Scattering of the laser beam generates a scattering pattern of the particle distribution which is subsequently analysed by the software using Mie light scattering theory. Mie theory correlates the light energy distribution with the particle size distribution.¹⁴ The refractive indexes of both continuous phase and dispersed phase were required by the instrument software.

Figure 2.3. Schematic representation of Malvern MasterSizer 2000 particle size analyser. Sample is introduced between the spatial filter and the Fourier lens.



A few droplets of the dispersion (approximately 0.1 mL) were added to the sample dispersion unit (model Hydro 2000SM) filled with the continuous phase of the dispersion (approximately 125 mL). This caused the particles to become dispersed in

larger volumes of continuous phase. The mixture was stirred in the dispersion unit at 350 rpm in order to minimise the interactions between particles. Values presented here are the average of four measurements. The particle size distribution was characterized by the median diameter ($d(0.5)$), which is the size at which 50% of the particles are smaller and 50% are larger. The accuracy of the measurements was assessed using latex particles of known average diameter of 4 μm .

2.2.6.2 Conductivity

The conductivity of the dispersions was measured immediately after preparation using a Jenway 4510 Digital Conductivity Meter with Pt/Pt black electrodes. The conductivity value of Milli-Q water, κ water = 1.20 $\mu\text{S cm}^{-1}$ (23 °C). The instrument was calibrated using a standard solution of 0.01 M KCl as recommended by the manufacturer.¹⁵

2.2.6.3 Zeta potential

The zeta potential of Calofort U particles in pure water and in SSL aqueous solutions was determined using a Malvern Instrument Nano zs Zetasizer at 23 ± 1 °C. 1 wt. % Calofort U particles, with respect to total dispersion volume, were dispersed in pure water or in SSL solution. The pH was adjusted when necessary by adding small volumes of HCl (1M) or NaOH (1M) to the dispersion just after preparation. The dispersions were then left on the bench for 30 minutes prior to measurements. Each zeta potential reading was averaged from at least three measurements.

2.2.6.4 Adsorption isotherm

The method employed to determine the adsorption of SSL surfactant onto Calofort U PCC particles at natural pH of the dispersions was *via* depletion from solution. After preparation, the dispersions were thermostated at 25 °C for 24 hours. After removing the suspended particles by centrifuging at 2000 rpm for 10 minutes in a Thermo Scientific Sorvall Biofuge Primo Bench Top Centrifuge, the equilibrium concentration of free SSL in the supernatant liquid was determined using the two phase Epton titration.¹⁶

Hyamine 1622 was used as the cationic titrant. It was purchased from Fluka as 98 % pure and was used as received. The two dyes were both purchased from Sigma and

used as received. Dimidium bromide was ~ 95 % pure and disulfine blue had a 50 % dye content. The amount of surfactant adsorbed was then calculated from the difference between the initial concentration and that measured in the solution after equilibration with particles. The adsorbed amount of surfactant on the particles, Γ / mmol g⁻¹, was then calculated by equation 2.1:

$$\Gamma = \frac{V(C_0 - C)}{W} \quad (2.1)$$

where V is the volume of the solution (mL), C₀ and C are the initial and equilibrium concentrations (M) of SSL respectively and w is the weight (g) of Calofort U particles.

2.2.7 Preparation of aqueous foams from particles alone, surfactant alone and surfactant-particle mixture dispersions

2.2.7.1 Hand shaking

20 mL of particles alone, surfactant alone or surfactant-particle mixture dispersion was added into a 120 mL Jaytec glass measuring cylinder. The vessels were sealed and vigorously hand shaken for 30 seconds to produce the foam. It was checked that this procedure gave foams with properties that were reproducible within the estimated uncertainties. This was done using repeated experiments performed by two different researchers.

2.2.7.2 Hand mixer

For the dispersions to be aerated using the hand mixer, Calofort U particles were dispersed in 200 mL SSL aqueous solutions using a IKA Werke EURO-ST D S2 mixer equipped with a 3 blade propeller blade of 5 cm diameter. A known mass of Calofort U particles was weighed into a 960 mL glass vessel followed by adding the SSL solution. The particles were then dispersed by operating the apparatus at 200 rpm for 5 minutes.

The Cuisinart Hand mixer CSB800U (shown in Figure 2.4) was used to aerate the dispersions. It consists of a whisk (cylindrical cage, radius r = 2.5 cm, length 11 cm) composed of 6 stainless steel wires with diameter = 1 mm. 200 mL of dispersion was added to a 960 mL glass vessel (diameter = 10 cm) and the whisk was submerged into the liquid before operating the instrument. The whisk made a planetary movement that

effectively covered the whole volume of the vessel. The mixer was operated at 1100 rpm for 30 s.

Figure 2.4. Appearance of the Cuisinart CSB800U hand mixer. Scale bar is 5 cm.



As different volumes were used for hand shaking and the Cuisinart hand mixer, the Foamability Parameter (F) is defined to compare the foaming efficiency of the two methods:

$$F = \frac{f_0}{l_0} \quad (2.2)$$

where f_0 is the initial foam volume (mL) and l_0 is the solution volume (mL) prior to foaming.

2.2.8 Characterisation of aqueous foams from particles alone, surfactant alone and surfactant-particle mixtures

2.2.8.1 Particle association with foam

In order to correlate the foam stability to the adsorption of particles at the air-water interface for SSL-PCC foams, the loss of particles from the dispersion to the foam was determined. For SSL-PCC foams, the drained dispersion at the bottom of the foaming vessel was transferred into a glass beaker. The dispersion was then dried in an oven at 85 °C. The percentage by weight (x) of Calofort U particles adsorbed at the air-water interface was calculated using:

$$x = \frac{w_0 - w}{w_0} \times 100 \quad (2.3)$$

where w_0 is the mass of Calofort U particles initially dispersed in SSL solutions and w is the mass of Calofort U particles drained in the beaker. At some high SSL concentrations (>10 mM) the mass of SSL present in the drained solution was high

enough to effect w . As a result, a correction was applied to w by determining the approximate mass of SSL adsorbed on the particles and subtracting it from w .

2.2.9 *Characterisation of bulk palm kernel oil*

2.2.9.1 Solid fat content determination *via* Differential Scanning Calorimetry

The same instrumentation and method, as detailed in section 2.2.1.1, was used to determine the crystallinity of PKO at different temperatures. Approximately 5 mg of bulk PKO was sampled and a temperature program with a tempering step was applied as follows: 80 °C isotherm for 5 minutes, cooled at -10 °C/minute to -30 °C, isotherm for 5 minutes, heated from -30 °C to 30 °C at 10 °C/minute, isotherm for 5 minutes, cooled from 30 °C to -30 °C at -10 °C/minutes, isotherm for 5 minutes and finally heated to 80 °C at the same rate.

Values of the Solid Fat Content (SFC) can be calculated by determining the area under the melting curve at a particular temperature. The Perkin Elmer software provides this measurement and the SFC was deduced as a function of temperature from the integration of the second melting curve.

2.2.10 *Preparation of model whipping cream emulsions*

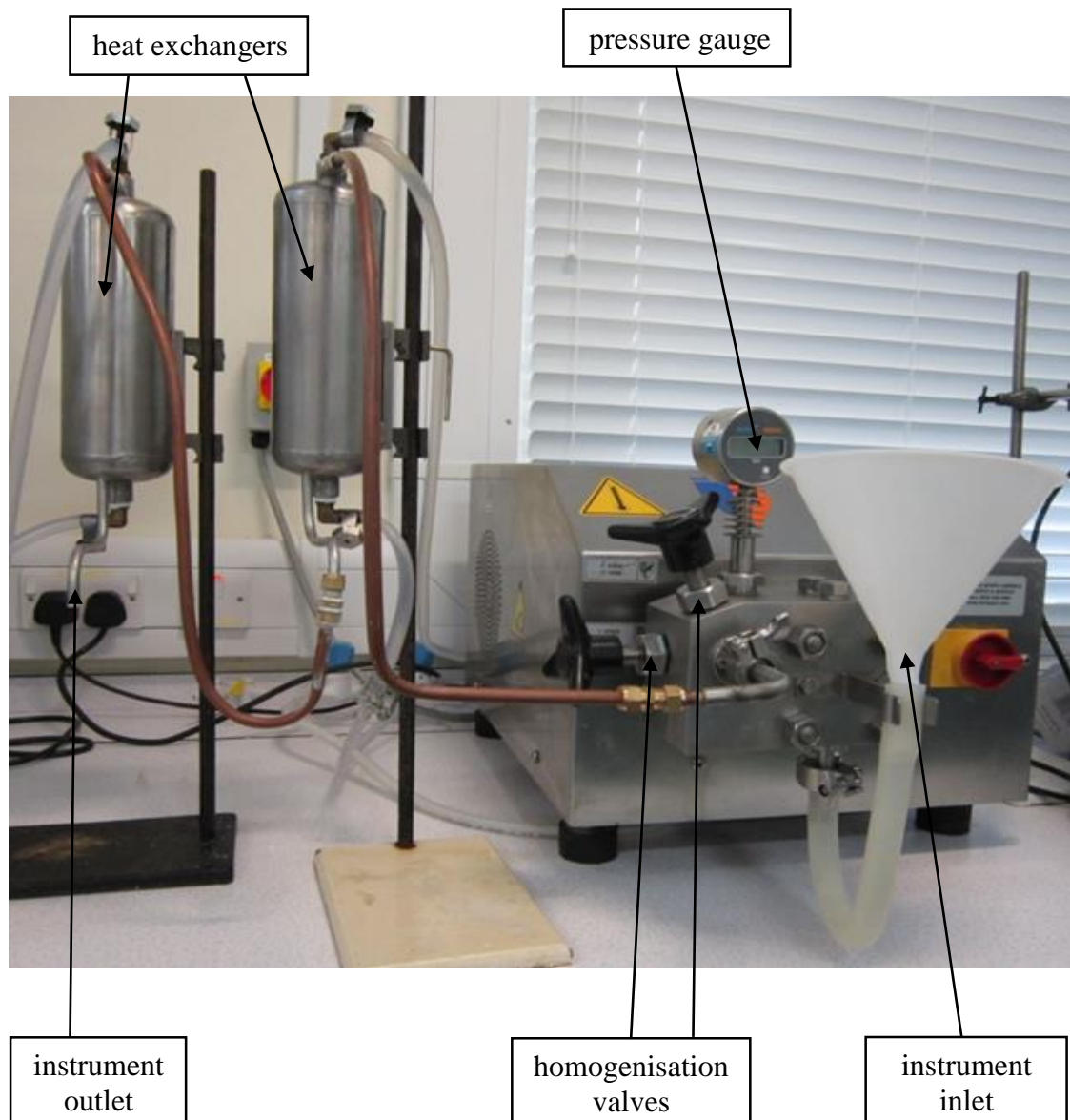
2.2.10.1 High pressure homogeniser

2.2.10.1.1 *Laboratory table top homogeniser*

A two-stage NS 1001L Panda - High Pressure Homogeniser (HPH), manufactured by GEA Niro Soavi S.P.A. Italy, was used to prepare model whipping cream emulsions. PKO was melted at 80 °C prior to emulsification. In a separate double boiler, mixtures of water, xanthan gum and SSL were heated up to 80 °C whilst stirring with an IKA Werke EURO-ST D S2 mixer (equipped with a 3 blade propeller blade of 5 cm diameter) at 300 rpm for 30 minutes to fully melt the SSL and xanthan gum. This was followed by adding hot PKO to the dispersion and emulsifying using a Bosch hand blender (model CNHR9EV) for 10 minutes and a stable pre-emulsion was formed. The homogeniser apparatus was heated by running hot water (80 °C) through the system to avoid crystallisation of PKO. The hot pre-emulsion was then transferred into the inlet of the homogeniser and was emulsified in two stages of 180 and 30 bar respectively. In this

two-stage emulsification, most of the emulsification occurs in the first stage. In the second stage, any droplet aggregates formed after the first stage are broken up. The hot emulsion was then passed through two heat exchangers to achieve the optimum foamability properties. The two heat exchange tanks were adjusted to cool the temperature of the emulsion to 35 °C and 4 °C respectively (as advised by the sponsor) before its release from the outlet. The emulsion was then kept in a fridge at 6 °C for 24 hours prior to whipping. The Panda laboratory homogeniser equipped with two heat exchangers is shown in Figure 2.5.

Figure 2.5. Panda NS 1001L two-stage laboratory high pressure homogeniser equipped with two heat exchangers.



2.2.10.1.2 Pilot laboratory homogeniser

The pilot scale homogenisation line consisted of large mixing tanks equipped with propeller mixers to prepare a stable pre-emulsion. The pre-emulsion was then pumped into the HPH (APV Gaulin G 5.5 10B), where the emulsion was further homogenised in two stages of 180 and 30 bar respectively. The hot emulsion was then passed through heat exchangers and collected in plastic buckets from the outlet. The temperatures of the heat exchangers were the same as those for the table top homogenisation (section 2.2.10.1.1). The emulsions prepared in the pilot laboratory, similar to those made with table top HPH, were stored in the fridge at 8 °C for 24 hours prior to their aeration.

2.2.11 Characterisation of model whipping cream emulsions

2.2.11.1 Droplet size distribution

The size of oil droplets after homogenisation was determined using the instrumentation detailed in section 2.2.6.1. A Grant Optima Digital Immersion Thermostat (GD120) water bath was connected to the sample dispersion unit of the instrument to perform size determination at 80 °C (emulsion temperature before it passed through the heat exchangers). For whipped emulsions, due to partial coalescence of the initial PKO droplets and formation of larger and fragile clusters, a different procedure was followed as explained by Gravier *et al.*¹⁷ One gram of foam was diluted in 10 mL water and heated at 60 °C for 30 min., at this temperature, PKO is fully melted and the aggregates comprising partially coalesced droplets undergo shape relaxation (under the effect of surface tension) that generates spherical droplets. The dilution was made under extremely low agitation conditions in order to avoid flow-induced fragmentation of the aggregates. After dilution, a small volume of the sample was identically added into the inlet of the sample dispersing unit. In aerated emulsions, partial coalescence was revealed by the occurrence of one or several modes at larger PKO size distributions that were not present in the primary emulsion.

2.2.11.2 Stability

The stability of model whipping cream emulsions to creaming and coalescence was determined by observing the change of the water-emulsion boundary and oil-

emulsion interfaces. The appearance of the emulsions was photographed at various times after preparation.

2.2.12 Aeration of model whipping cream emulsions and Vanilla Bettercreme®

A Hobart bench top mixer was used to aerate model whipping cream emulsions and the VBC. The Hobart mixer N50 (Hobart Corporation) consisted of a stainless steel beaker (diameter = 20 cm) and a whisk rotating at a controlled speed. The whisk consisted of a wire cage (cylindrical cage, radius $r = 6.5$ cm, length 17 cm) composed of 11 stainless steel wires with diameter = 2 mm. The whisk made a planetary movement that effectively covered the whole volume of the beaker. The emulsions were kept in the fridge at 6 °C for 24 hours prior to whipping and was whipped at 10 °C as advised by the sponsor. The emulsion was stirred well before whipping and 650 g of it was added to the whipping bowl. Whipping was carried out at 130 rpm. The whipping time was determined by immersing the whisk into the whipped product and observing the pyramid formed at the bottom of the whisk for a period of 30 seconds. When the pyramid of cream present at the top of the inverted whisk was stiff and remained standing over the 30 second period, this meant that the cream was ideally whipped. Figure 2.6 shows the appearance of the Hobart bench top mixer.

Figure 2.6. Appearance of the Hobart N50 bench top mixer used for aeration of model whipped cream emulsions and the VBC.



2.2.13 Characterisation of model whipped emulsions and whipped Vanilla Bettercreme[®]

2.2.13.1 Overrun

There are different approaches to calculating the amount of air introduced into a liquid. One common approach is to measure the foam overrun. Overrun is the relative increase in the volume of the emulsion by the inclusion of gas. In this research, the overrun values were calculated as follows. A 150 ml plastic vessel was filled with the un-whipped emulsion and all the air bubbles were removed from the surface of the emulsion using a spatula. The weight of the liquid product was recorded. The same vessel was then filled with the same volume of the whipped sample of the emulsion and its weight recorded in order to calculate the overrun using equation 2.4:

$$\text{Overrun \%} = \frac{\text{weight of unwhipped emulsion}}{\text{weight of whipped emulsion}} \times 100 \quad (2.4)$$

2.2.13.2 Cryo-scanning electron microscopy

Cryo-SEM characterisation was carried out for model whipping cream emulsions, foams and VBC foam. Samples were prepared by mounting a small volume of the emulsion or foam onto a copper holder. The holder was submerged in liquid nitrogen (-210 °C) where the sample was frozen by complete submersion. Frozen samples were transferred under vacuum into the Quorum Technologies PP3010T Cryogenic sample preparation chamber where a thin layer of it was fractured off to reveal a fresh surface of the sample. The sample was then sublimated for 1 hour at -90 °C. The fresh surface was coated with a thin (<10 nm) layer of platinum. Finally, the samples were examined with an accelerator voltage of 15 kV and a representative area was imaged at various magnifications using a Zeiss EVO 60 SEM instrument.

2.2.13.3 Quiescent foam stability

Model whipped cream foams and aerated VBC samples were transferred into a 250 mL glass beaker straight after aeration and this was left on the bench at room temperature of 23 ± 1 °C. The appearance of the foam was photographed at various times after aeration to record the foam volume loss. The beakers were covered with a plastic lid to prevent water evaporation.

The stability of the model whipped cream foams and aerated VBC towards drainage was investigated by recording the amount of liquid drained under gravity from 20 g of the foam. Samples were carefully removed from the whipping bowl and transferred to a nylon sieve (pore size 5 mm) supported by a glass funnel. Drained liquid from the foam was collected in a measuring cylinder. Sieves containing the foams were covered with a plastic lid to prevent contact with the air and evaporation.

2.2.13.4 Rheology

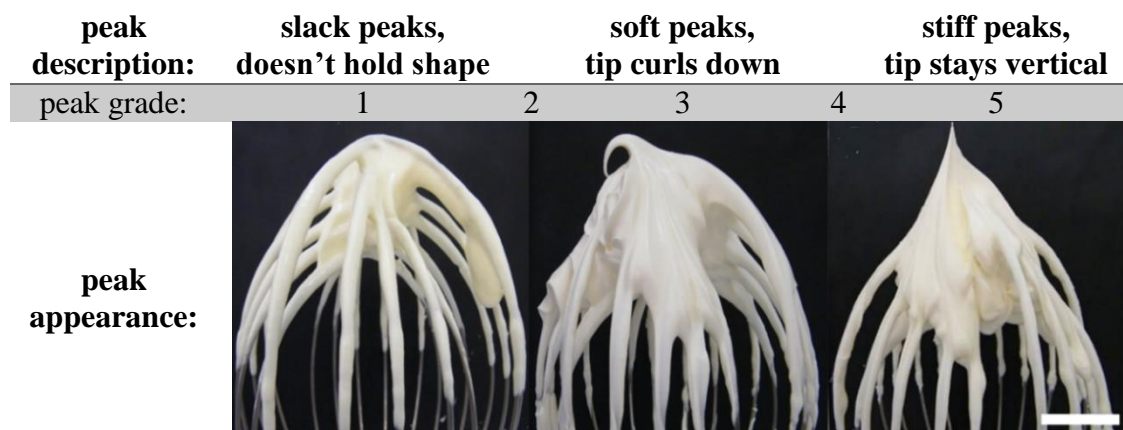
The rheology of model whipping cream emulsions, model whipped cream foams and aerated VBC samples was studied by oscillatory rheometry using a Bohlin CVO 120 High-Resolution rheometer. Experiments were performed using parallel-plate (40 mm diameter) geometry with a gap of 500 μm and rough surfaces in order to avoid wall slipping. Other values of gap size (250 μm and 1 mm) were examined and yielded the same results. For analysis of non-aerated emulsions, they were gently stirred to mix the

creamed oil droplets back into the released water prior to sampling. For examination of foams, freshly aerated samples (age < 10 minutes after aeration) were carefully transferred from the whipping bowl to the lower plate of the rheometer. The upper parallel plate was slowly lowered onto the sample until the gap size was reached and any excess foam gently removed. An amplitude sweep test at a fixed frequency (1 Hz) over 30 minutes was applied to determine the viscoelastic properties of the emulsions and foams. For non-aerated samples the analysis was performed at the sample temperature before aeration (10 °C) and for foam samples the measurements were performed at the sample temperature after aeration (13 °C). The geometries were cleaned by sonicating in ethanol for about 10 minutes in a Decon FS300b Ultrasonic Bath.

2.2.13.5 Peaking assessment

The texture of the model whipped emulsions and VBC was evaluated immediately after their aeration. For peaking evaluation, a peak was formed on top of the whipping whisk as explained in Section 2.2.12. The peaking of the foam was then graded according to its sharpness and stiffness based on the scale in **Figure 2.7** (advised by the sponsor of the project). The approximate appearance for grades 1, 3 and 5 is also shown in the figure.

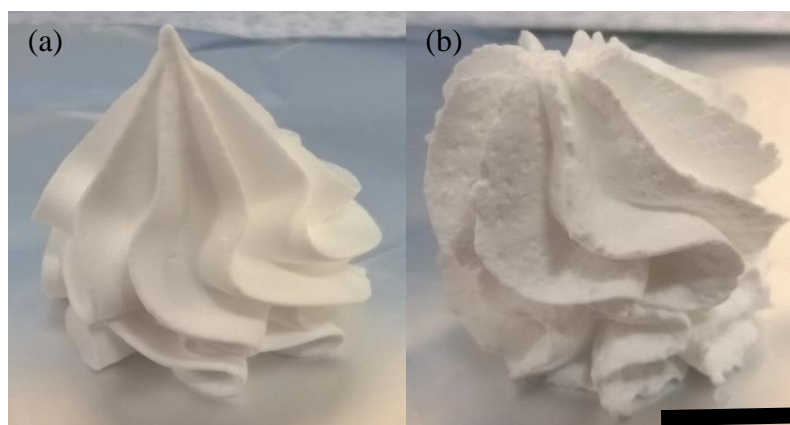
Figure 2.7. Grading scale based on peak appearance with the approximate appearance of grades 1, 3 and 5. Scale bar represents 3 cm.



2.2.13.6 Pastry bag evaluation

Textural properties of the model whipped emulsions were further investigated by determining their pastry bag time. A pastry bag, fitted with a standard star tip was approximately half-filled (500 mL) with the aerated emulsion straight after aeration. A rosette (star) was then made by dispensing the foam out of the pastry bag onto baking paper at 5 minute intervals. The pastry bag time of the foam was then recorded as the maximum amount of time for which the appearance of the rosette was acceptable. The rosette was considered to have a poor appearance when its edges were rough and/or the rosette lost shape and/or air cell coalescence made the rosette look poor. The approximate appearances of a good rosette and a poor rosette are shown in Figure 2.8.

Figure 2.8. Approximate appearance of a good rosette (a) and a poor rosette (b) made from model whipped emulsions. Scale bar represents 2 cm.



2.2.14 Preparation of palm kernel oil-in-water emulsions

PKO-in-water emulsions were prepared and stabilised by either particles or surfactants in Chapter 5. The emulsions prepared by this protocol were different from batches of model whipping cream emulsions (also PKO-in-water emulsions) prepared by HPH in Chapter 4. The powdered particle method was used to prepare PKO-in-water emulsions stabilised by PCC particles. In this method, particles were added as a powder on top of the water phase followed by the addition of the oil phase. A 10 ml mixture of water, PKO and known mass of particles were emulsified using an IKA Ultra-Turrax T25 homogeniser. For the emulsions stabilised by surfactants, a 10 ml mixture of surfactant (stock solution), water and oil was emulsified using the same homogeniser.

The rotor-stator mixing head with an 8.2 mm internal diameter was immersed in the mixture before homogenisation. Homogenisation was carried out at 11000 rpm for 2 minutes at 80 °C in a thermostated water bath. Homogenisation was carried out at this temperature in order to ensure that the PKO is fully melted. Emulsions were prepared and stored in foil lined screw-capped glass sample tubes of 18 mm inner diameter and 70 mm height.

2.2.15 Preparation of oil-in-water emulsions containing non-crystallisable oils

Oil-in-water emulsions containing non-crystallisable oils (HOSO and dodecane) were prepared to study their stability and also their aeration properties. For the stability study, a 10 ml mixture of SSL (stock solution), water and oil was emulsified with an IKA Ultra-Turrax T25 homogeniser. Homogenisation was carried out at 11000 rpm for 2 minutes at room temperature (23 ± 1 °C). The rotor-stator mixing head with an internal diameter of 8.2 mm was immersed in the mixture before starting the homogeniser. This produced intense shear, which resulted in the breakdown of oil or water into emulsion droplets. Emulsions with a volume of 200 mL were prepared to investigate the aeration properties of the emulsions. Homogenisation was performed using the same apparatus as for smaller volume emulsions, however it was equipped with a large dispersing head (12 mm inner diameter).

2.2.16 Aeration of oil-in-water emulsions containing non-crystallisable oils

For the aeration of oil-in-water emulsions containing non-crystallisable oils (HOSO and dodecane), the Cuisinart Hand mixer CSB800U as detailed in section 2.2.7.2 was used to aerate 200 mL of emulsion. The emulsions were aerated immediately after their emulsification in 1 L glass jars at room temperature of 23 ± 1 °C for 2 minutes at 1100 rpm.

2.2.17 Characterisation of oil-in-water emulsions and aerated emulsions

2.2.17.1 Optical microscopy

Emulsions and aerated emulsions were observed using the optical microscope detailed in section 2.2.3.1. Emulsions were observed without dilution on a dimple cell microscope slide, covered with a cover slip. Samples of aerated emulsions were taken

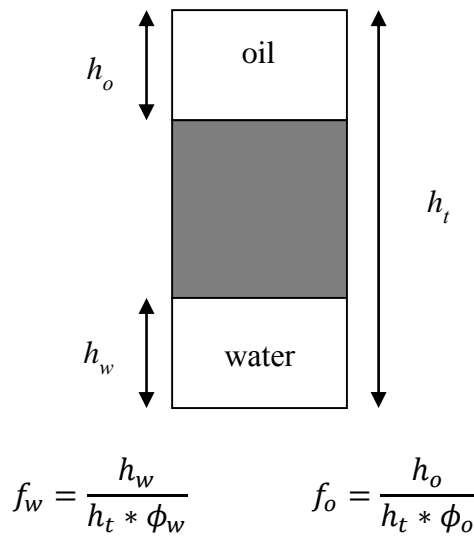
carefully to prevent foam breakdown and were observed on a dimple cell microscope slide without a cover slip.

2.2.17.2 Stability

Emulsions were stored in the vessels used in the homogenisation process, these being screw-capped glass sample tubes of internal diameter 18 mm and height 70 mm, at room temperature of 23 ± 1 °C. The stability of oil-in-water emulsions to creaming and coalescence was determined by observing the change of the water-emulsion boundary and oil-emulsion interfaces. For water-in-oil emulsions, the change of the oil-emulsion boundary and the water-emulsion interface was monitored in order to determine the stability of the emulsion to sedimentation and coalescence respectively. Figure 2.9 depicts how the fraction of water (f_w) and oil (f_o) resolved from an emulsion are determined from the height of water resolved (h_w), height of oil resolved (h_o), initial volume fraction of water (ϕ_w) and oil (ϕ_o) and the total height of emulsion plus water and oil resolved (h_w).

For oil-in-water emulsions, f_o indicates the stability of the emulsion to coalescence and f_w indicates its stability to creaming. For water-in-oil emulsions, f_w refers to the stability of the emulsion to coalescence and f_o indicates its stability to sedimentation. According to this explanation, f_o and f_w will both have values of 0 for stable emulsions whereas the values of f_o and f_w will be equal to 1 for totally unstable emulsions (total phase separation).

Figure 2.9. Representation of the determination of water and oil fraction resolved in an emulsion. The shaded area shows the volume of the sample occupied by the emulsion.



2.2.17.3 Droplet size distribution

The size of oil droplets in the emulsions was determined using light diffraction method as detailed in section 2.2.6.1 at various times after emulsification to check their stability towards coalescence and Ostwald ripening.

2.2.17.4 Surface and interfacial tension

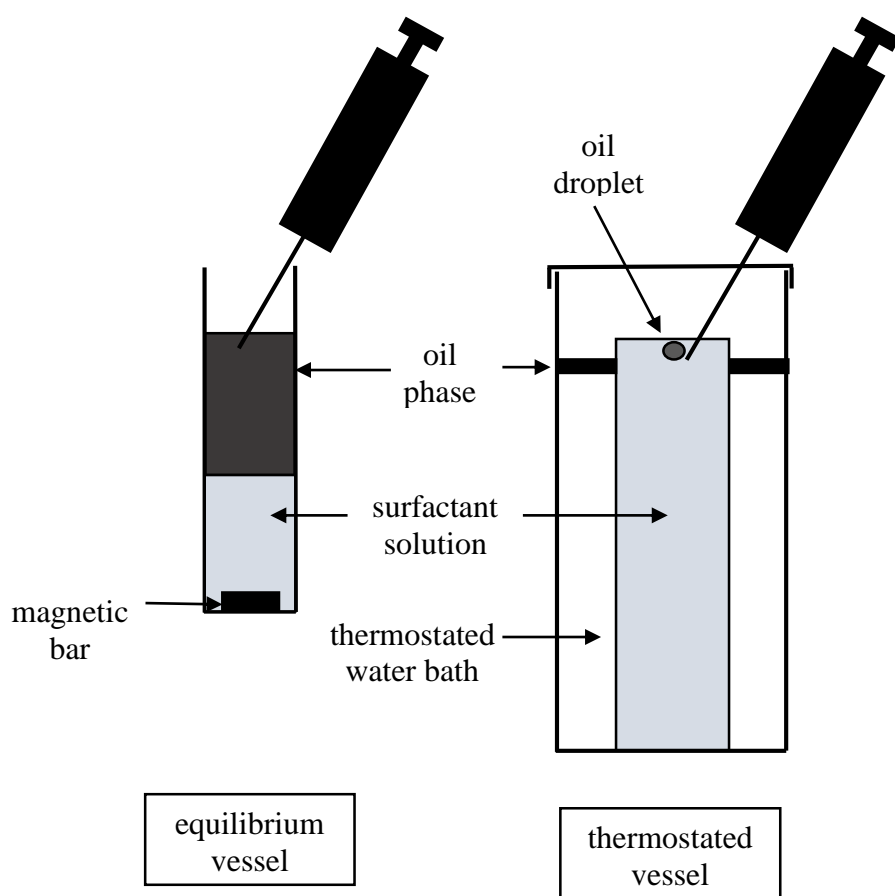
The air-water, air-oil and oil-water tensions were measured with a Krüss K10 digital tensiometer as detailed in section 2.2.3.3. For oil-water interfacial tension measurements, the measuring system was adjusted to zero in the oil phase initially. This is done to compensate the buoyancy and the surface tension which acts on the shafts.

2.2.17.5 Life-time of single oil droplets at the air-surfactant solution interface

The life-time of a single oil droplet beneath the air-SSL solution interface was measured by the method explained by Aveyard *et al.*¹⁸ The apparatus is shown in Figure 2.10 and consisted of a cylinder which contained the surfactant solution placed in a sealed water bath chamber. A collar was designed around the top of the cylinder containing the oil under study to saturate the vapour above the surfactant solution. Equal volumes of surfactant solution and oil were first pre-equilibrated at 25 °C for 1 hour in

a separate vessel while stirring gently with a small magnetic bar. Then without unsealing the water bath chamber a drop of known volume (usually 5 μl) of the equilibrated oil was carefully placed *ca.* 1 cm below the surfactant solution-air interface in the thermostated vessel. The time taken for the drop to enter the interface, as observed visually, was recorded.

Figure 2.10. Apparatus for determination of single droplet life-time at the air-surfactant solution interface.



2.3 References

1. *CRC Handbook of Chemistry and Physics*, D.R. Lide, 89th edn., CRC Press, Boca Raton, 2008.
2. Milli-Q Product Information, Millipore Corporation, September 2002.
3. W.L. Siew, *Eur. J. Lipid Sci. Technol.*, **103**, 729 (2001).
4. Palm Kernel Oil Encore 100 Product Information, Cargill, 2010.
5. *Fats and oils formulating and processing for applications*, R.D. O'Brien, 3rd edn., CRC Press, Boca Raton, 2009.
6. V. Dossat, D. Combes and A. Marty, *Enzyme Microb. Tech.*, **30**, 90 (2002).
7. S. Teir, S. Eloneva and R. Zevenhoven, *Energy Convers. Manage.*, **46**, 2954 (2005).
8. Calofort U Precipitated Calcium Carbonate Product Information, Specialty Minerals Inc., UK, 2004.
9. <http://www.richs.com/about/>, Accessed 19.7.2012.
10. S. Rosalam and R. England, *Enzyme Microb. Tech.*, **39**, 197 (2006).
11. F. García-Ochoa, V.E. Santos, J.A. Casas and E. Gómez, *Biotechnol. Adv.*, **18**, (2000).
12. E. Bayramli, C. Huh and S.G. Mason, *Can. J. Chem.*, **56**, 818 (1978).
13. Basic Principles of Particle Size Analysis -Technical paper MRK034, Malvern Instruments Limited, UK.
14. Z. Stojanović, S. Marković and D. Uskoković, *Technics – New Mat.*, **67**, 11 (2012).
15. Jenway Model 4510 Conductivity Meter Manual Rev. A/03-03, Bibby Scientific Limited, England, 2003.
16. V.W. Reid, G.F. Longman and E. Heinerth, *Tenside*, **4**, 292 (1967).
17. E. Gravier, N. Drelon, L. Boisserie, A. Omari and F. Leal-Calderon, *Colloids Surf. A*, **282-283**, (2006).
18. R. Aveyard, B.P. Binks, P.D.I. Fletcher, T.-G. Peck and P.R. Garrett, *J. Chem. Soc. Farad. T.*, **89**, 4313 (1993).

CHAPTER 3 AQUEOUS DISPERSIONS AND FOAMS OF PRECIPITATED CALCIUM CARBONATE, SODIUM STEAROYL LACTYLATE AND THEIR MIXTURES

3.1 Introduction

Aqueous foams are thermodynamically unstable and destabilisation happens through a combination of drainage, coalescence and disproportionation to reduce the total free energy of the system.¹ Generally, foams stabilised by surfactants and proteins are inherently unstable and collapse within a day or so. Stabilisation of foams by solid particles has received great attention recently as foams with better stability can be produced.²⁻⁶ Solid particles with colloidal dimensions can adsorb at a gas-liquid interface and reduce the high interfacial energy of the interface. Adsorption of the appropriate particles at a gas-liquid interface is known to be irreversible due to the high energy of attachment of these particles compared to their thermal energy.⁷ The irreversible adsorption of such particles at the interface enhances the stability of foams towards coalescence and disproportionation compared to foams stabilised by surfactant or protein molecules.^{7,8}

As with Pickering emulsions, in particle-stabilised foams the effectiveness of particle binding at the interface is controlled by the particle wettability, characterised by contact angle (measured through water).^{3,4} Commercially available raw solid particles such as silica and calcium carbonate are not surface active due to their high hydrophilicity. As a result of this there is an interest in modifying the surface properties of such particles in order to promote their adsorption at interfaces. For stabilisation of aqueous foams, an appropriate degree of hydrophobic particle character can be achieved in different ways. One way to achieve the hydrophobicity is *via* a homogeneous surface coating. Using this *ex situ* method, hydrophilic silica particles can be modified to have variable wettability by surface silylation.⁷ Binks and Horozov⁶ used fumed silica particles coated with dichlorodimethylsilane groups to varying degrees to prepare aqueous foams. They found that foams of high stability can be prepared with particles of intermediate hydrophobicity.

Another common approach used to hydrophobise particles is by binding amphiphilic molecules to the surface of hydrophilic particles, which eventually renders

them hydrophobic.⁹⁻¹³ Using this *in situ* method, very stable foams can be produced.^{14, 15} Some examples of this approach to hydrophobise particles include silica particles with cationic surfactants (alkylamine and alkyltrimethylammonium bromides),^{9, 12} laponite clay with cationic surfactants (alkylammonium bromides),¹³ laponite with nonionic surfactants (C₁₂E₄, tetraethylene glycolmonododecylether),¹⁶ calcium carbonate with anionic surfactants (sodium dodecylsulphate, SDS, and sodium-2-ethylhexylsulphosuccinate, AOT)¹⁵ and alumina with short chain carboxylic acids.¹⁴ Cui *et al.*¹⁵ reported that stable aqueous foams can be produced by *in situ* surface activation of Precipitated Calcium Carbonate (PCC) nanoparticles with anionic SDS molecules. They also showed that there is no synergistic effect on foam stability for PCC nanoparticles with a cationic (Cetyltrimethylammonium bromide) or with a non-ionic (octylphenylpolyoxyethylene (10) ether) surfactant.

PCC particles were selected as foam stabilisers to be studied in this project since they are easily accessible, cheap and edible.¹³ In addition, their synergistic effect on the stabilisation of aqueous foams has already been studied in non-edible systems.¹⁵ The aim here is to modify the wettability of the hydrophilic PCC nanoparticles using an anionic food-grade surfactant, Sodium Stearoyl Lactylate (SSL). SSL, a key ingredient of the Vanilla Bettercreme[®] emulsion produced by the sponsor of the project, acts as an emulsion stabiliser, whipping agent and conditioning ingredient in a wide variety of food products.¹⁷⁻²¹ SSL is prepared by esterification of stearic acid with lactic acid in the presence of sodium hydroxide. Unlike many other surfactants like SDS, SSL molecules when dispersed in water do not aggregate into micelles but instead form bilayer structures in the form of vesicles or lamellar liquid crystals.

There are limited studies on the foaming properties of SSL in the literature despite its extensive application in food manufacture. However there are some papers which report it as an active component at air-water interfaces.^{22, 23} Bezelgues *et al.*²² compared the foamability (volume of foam formed initially) and foam stability (volume of foam with respect to time) of SSL (lamellar phase forming) and Polysorbate 80 a non-ionic surfactant (micelle forming) surfactants. They found that SSL produces foams of higher stability than Tween 80, which is believed to be due to the 'compact, tight and ordered surface layers around bubbles'. Neat SSL is normally composed of α crystals (hexagonal sub-cell) which melts at around 45 °C.²⁴ A schematic phase diagram of this surfactant in mixtures with water shows that up to around 45 °C, hydrated crystals are

formed.²⁴ Upon heating above this temperature and up to 40 wt. % surfactant, the crystals melt and a dispersion of lamellar structures (including vesicles) is formed, known as the L_{α} phase in which water penetrates between opposing layers of head groups and a transition from a solid state to a liquid state takes place in the hydrocarbon chain layer. Upon cooling below the chain melting temperature, a gel may form known as the L_{β} phase whose structure is similar to that of the L_{α} phase but in which the hydrocarbon chains are solid again and orientated parallel to each other. Similar phase behaviour has been reported in detail recently for a polyglycerol fatty acid ($C_{16/18}$) ester surfactant in water.²⁵

Foaming properties of SSL alone and in mixtures with PCC are studied in detail in this chapter. In addition, the characteristics of SDS aqueous foams are also presented for comparison with properties of foams made with SSL alone. It is shown how initially hydrophilic PCC particles are rendered hydrophobic *via* SSL adsorption and how this in turn changes the preference for the attachment of the particles at the air-water interface. We also attempt to make the link between the surface properties of the coated PCC particles and the stability of foams produced from PCC-SSL mixtures using a variety of experiments including determination of the extent of adsorption of SSL on PCC particles, Zeta potentials of particle dispersions and appropriate contact angle measurements.

3.2 Characterisation of precipitated calcium carbonate particles

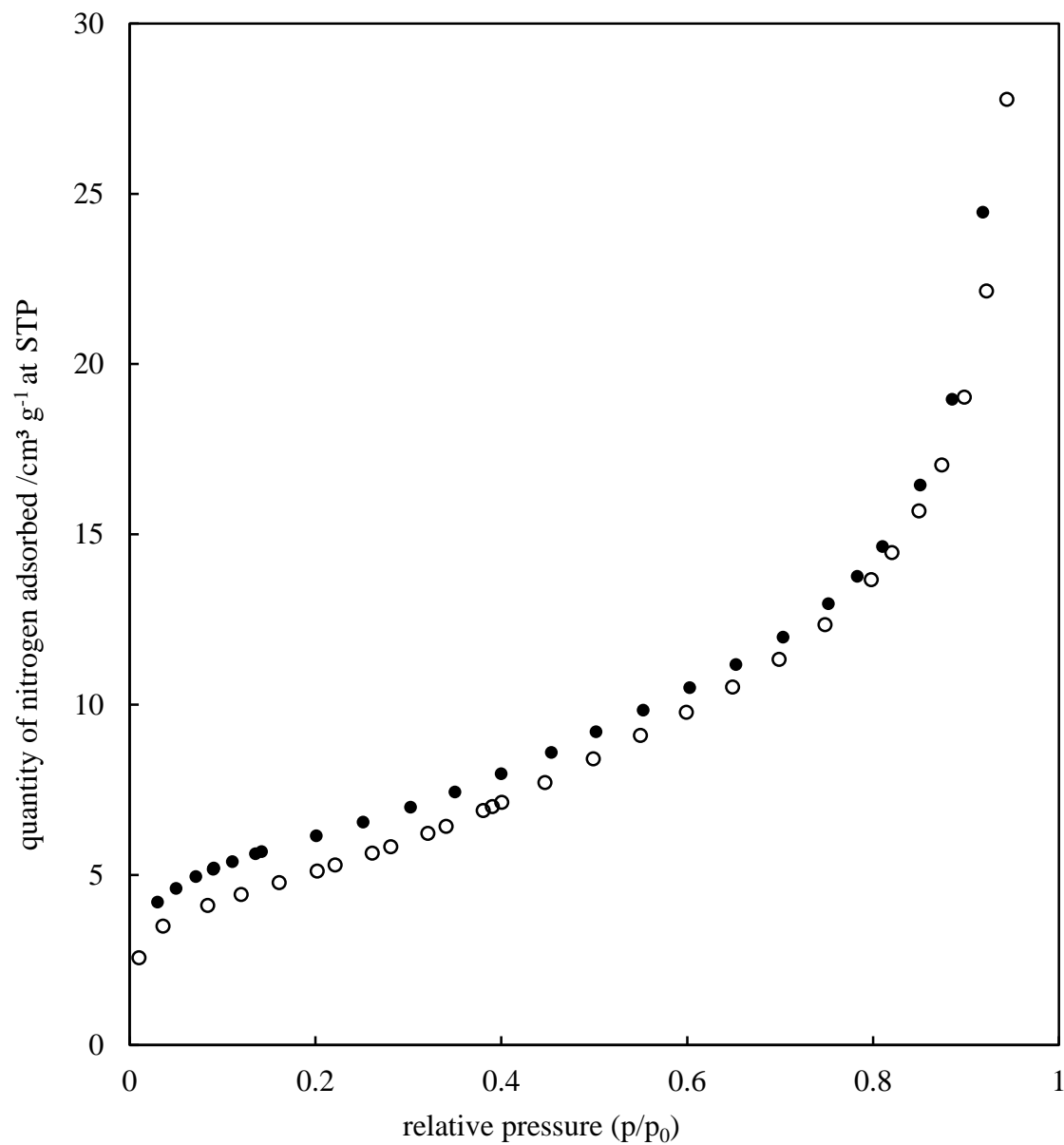
3.2.1 Scanning Electron Microscopy

Calofort U PCC particles were examined with Scanning Electron Microscopy (SEM) in order to determine their size, shape and the aggregation state within a dry powder. The micrographs were shown in the previous chapter (Figure 2.2). The images showed that the primary particles are quasi-spherical with diameters no more than 150 nm. It was also observed that some of the particles were partially fused and form aggregates of several μm .

3.2.2 Surface area

The specific surface area (SSA) and porosity of Calofort U particles were determined *via* nitrogen adsorption. An accurate measurement for the amount of SSL adsorbed on Calofort U particles is *via* adsorption isotherm determination and this will be discussed in Section 3.7.3.1. Exact measurements of the adsorption isotherm requires the SSA of Calofort U particles to be known. Figure 3.1 shows the adsorption and desorption isotherms of nitrogen on Calofort U particles. The points on the isotherm corresponding to monolayer adsorption (unfilled points) and desorption (filled points) were analysed using the BET method.²⁶ The particles were found to have an SSA of $18.7 \pm 0.5 \text{ m}^2 \text{ g}^{-1}$ and a porosity of $0.093 \pm 0.01 \text{ cm}^3 \text{ g}^{-1}$. The SSA measured is within the range of that specified in the manufacturer's technical data sheet of the particles²⁷ ($17\text{-}29 \text{ m}^2 \text{ g}^{-1}$), that differs from $26 \text{ m}^2 \text{ g}^{-1}$ reported by Renaudin *et al.*²⁸ This could be due to the difference in the aggregation state of the particles at the time of measurement. The analysis also reveals that the particles are slightly porous.

Figure 3.1. Isotherms showing nitrogen adsorption (unfilled points) and desorption (filled points) from the BET analysis of Calofort U particles. The samples were cooled to $-195\text{ }^{\circ}\text{C}$ using liquid nitrogen in order to induce adsorption.



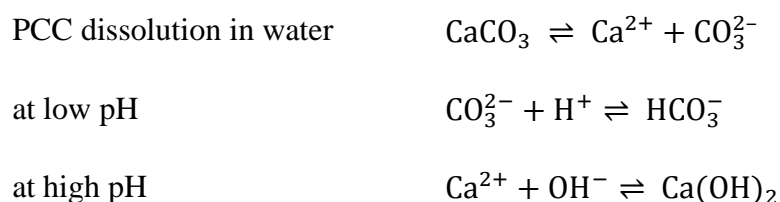
3.3 Aqueous dispersions of precipitated calcium carbonate particles

Calofort U PCC particles are naturally hydrophilic and disperse in water. Ultrasound was used to disperse the particles in water and once they were dispersed, these dispersions were found to be unstable and particles sediment at the bottom of the vessel as a white layer at concentrations ≤ 1 wt. %. This is due to the formation of large aggregates and also due to the density difference with water. The density of PCC particles is 2.7 g cm^{-3} .²⁹ Figure 3.2 shows the appearance of the dispersions at varying particle concentrations immediately and one day after preparation. Clearly the dispersions are not stable and the height of the sediment layer increases upon increasing the particle concentration.

Figure 3.2. Appearance of Calofort U PCC aqueous dispersions, at their natural pH (depending on particle concentration), immediately (upper image) and one day (lower image) after preparation. Particles sediment due to formation of large particle aggregates. Numbers below the samples represent the concentration of particles (wt. % with respect to total mass of dispersion).



Figure 3.3 shows the particle size distribution of a 1 wt. % Calofort U dispersion in pure water obtained from laser diffraction. It shows a median diameter of roughly 10 μm , indicating the formation of aggregates from primary particles. The solubility of precipitated CaCO_3 particles in water is around 0.014 g dm^{-3} (at normal atmospheric CO_2 partial pressures and $25 \text{ }^\circ\text{C}$) such that Ca^{2+} and CO_3^{2-} ions become dissolved in water.¹⁵ At low pH, carbonate ions attach a proton to form HCO_3^- ions, which repeat this process forming H_2CO_3 in solution. This causes the Ca^{2+} ions to be in excess and act as charge-determining ions. At high pH, the high concentrations of OH^- ions bind to the Ca^{2+} ions, forming $\text{Ca}(\text{OH})_2$. This causes an excess of CO_3^{2-} ions, which act as the charge-determining ions. These reactions are shown below.



The natural pH of a 1 wt. % PCC dispersion in pure water was found to be 9.3, in agreement with a pH of 9.05 reported by Cui *et al.* for a different source of hydrophilic CaCO_3 particles.¹⁵ The zeta potential of the Calofort U particles in pure water as a function of pH is shown in Figure 3.4. As shown in the figure, particles are cationic at pH values between 8 and 11 with an isoelectric point around $\text{pH} = 12$.

Figure 3.3. Particle size distribution of a 1 wt. % Calofort U PCC particles ultrasonically dispersed in pure water at pH=9.3 determined by light scattering at 23 ± 1 °C. PCC particles aggregate when dispersed in water and show a mono-modal peak at around 10 μm .

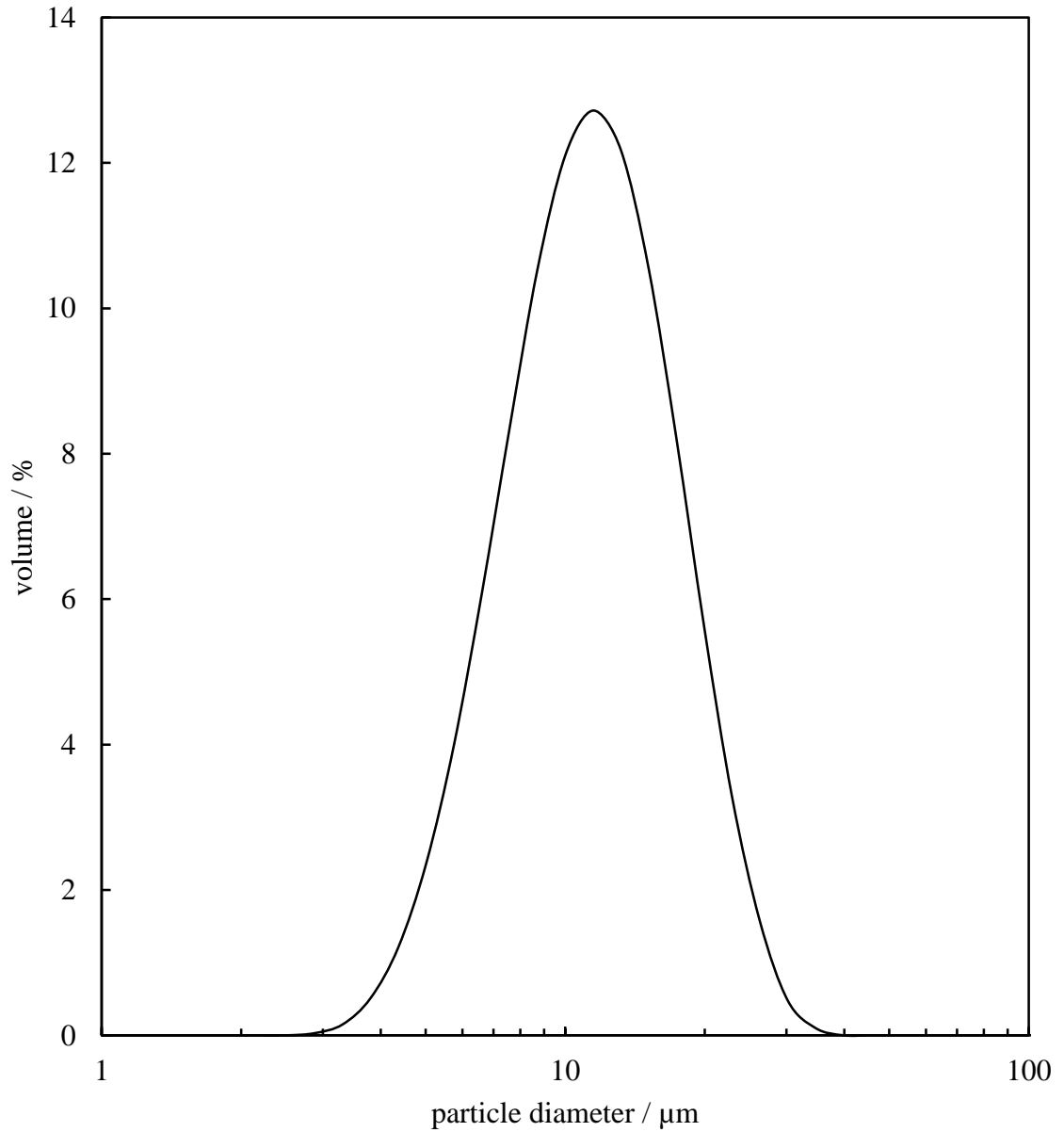
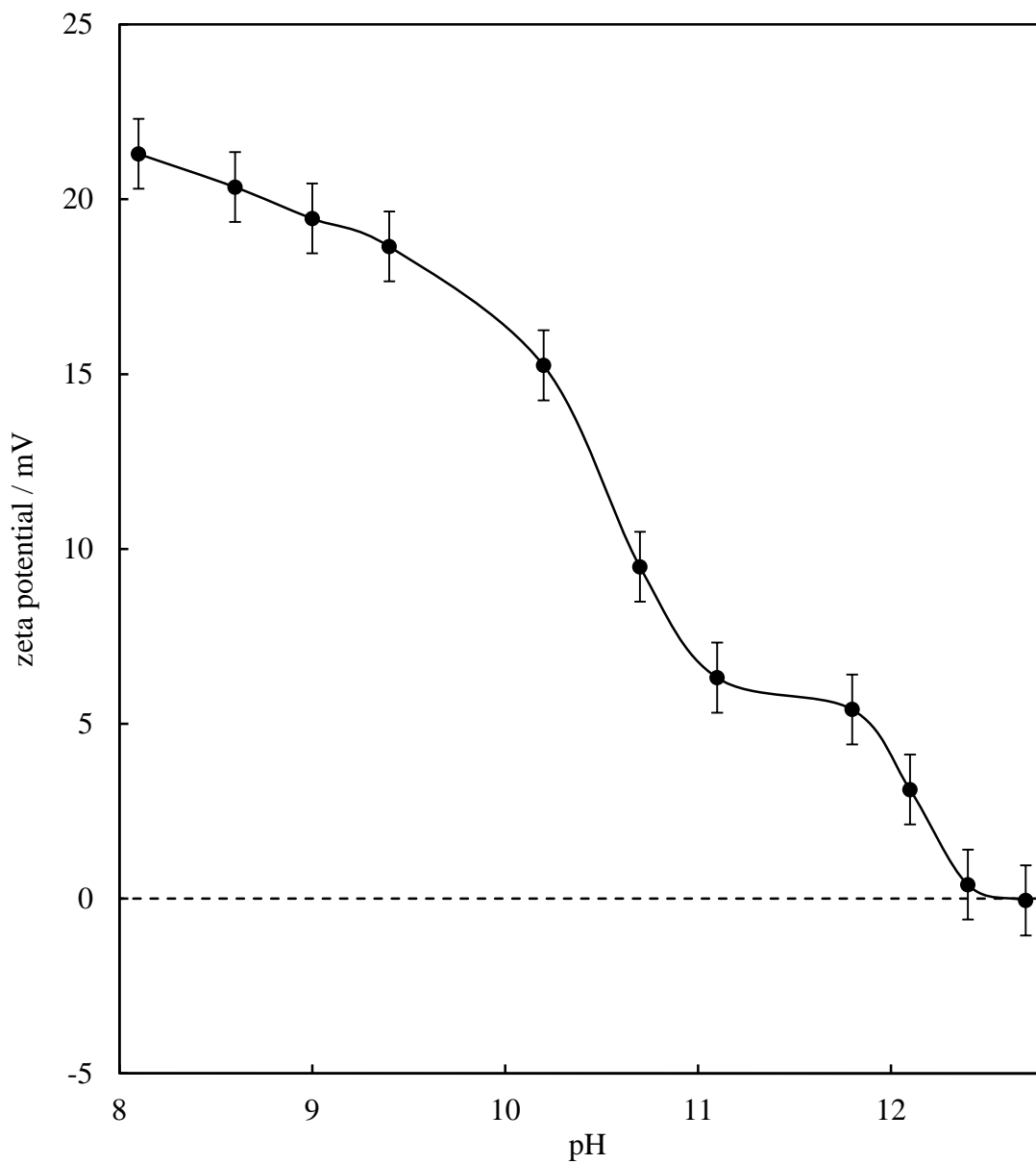


Figure 3.4. Zeta potential of 1 wt. % Calofort U PCC particles dispersed in pure water as a function of pH. The natural pH of the dispersion is 9.3.



3.4 Foaming properties of aqueous dispersions of particles

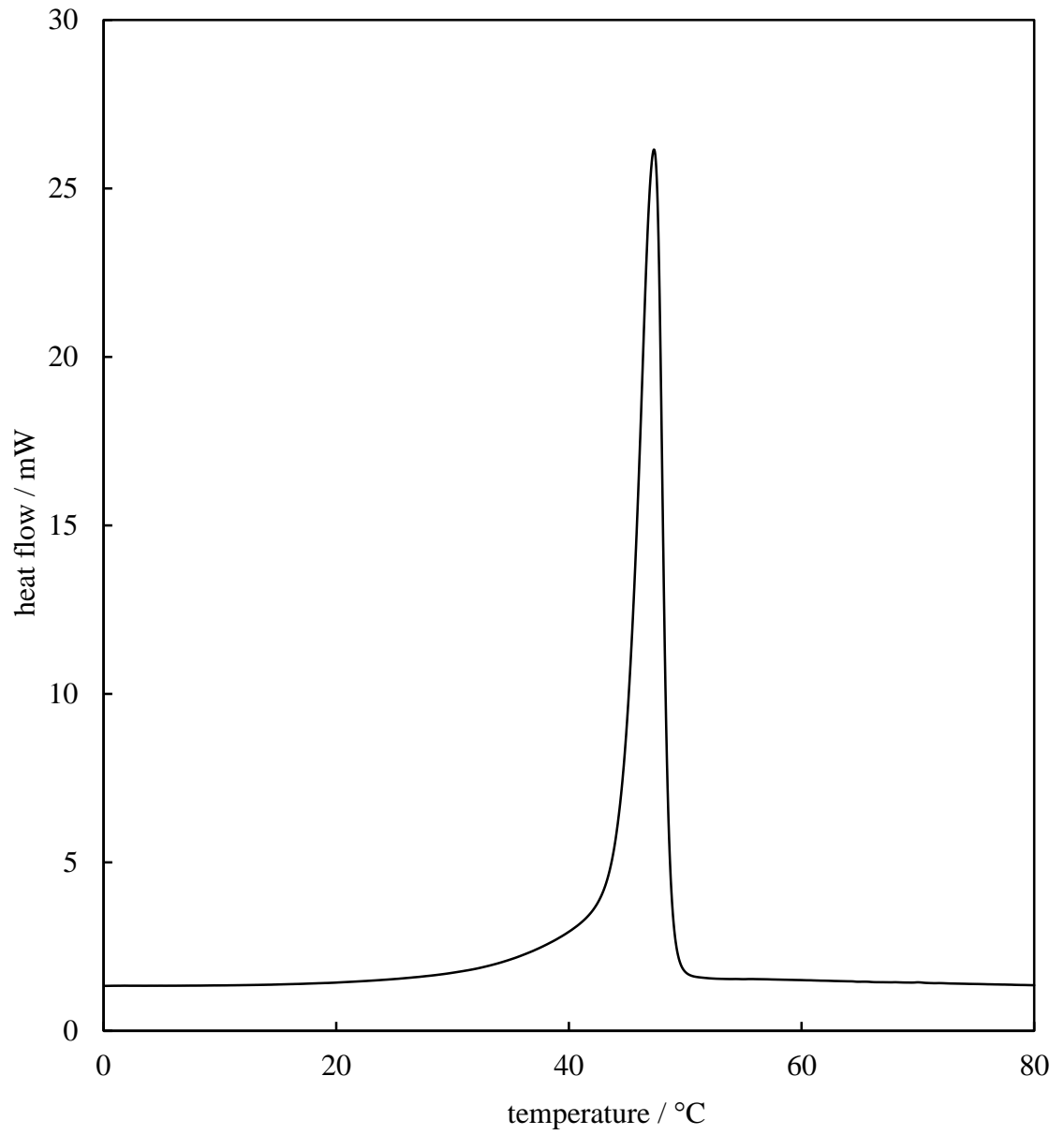
Aqueous dispersions of Calofort U PCC particles were aerated by hand shaking at pH values from 8 to 12 in order to assess their surface activity at air-water interfaces. Aeration of Calofort U aqueous dispersions at concentrations between 0.1 and 1 wt. % did not produce any stable foam and the few bubbles produced were very unstable and disappeared after five seconds. This confirms that Calofort U PCC particles are not surface active at the air-water interface and that they require surface modification to promote adsorption. They prefer to stay in the water phase as they are very hydrophilic and charged; those that adsorb quickly desorb due to the low energy of attachment to the air-water interface.

3.5 Characterisation of sodium stearyl lactylate

3.5.1 Melting point determination by thermal analysis

A neat SSL powder sample was analysed with DSC to determine the melting point and the DSC thermogram is shown in Figure 3.5. Upon heating at 10 °C min⁻¹, a transition was observed at around 47 °C with onset of 44 °C and an enthalpy change of 84 J g⁻¹. This melting point is close to that of 46 °C reported by Kokelaar *et al.*³⁰ for a sample of SSL from a different source and is believed to be due to the melting of α crystals.

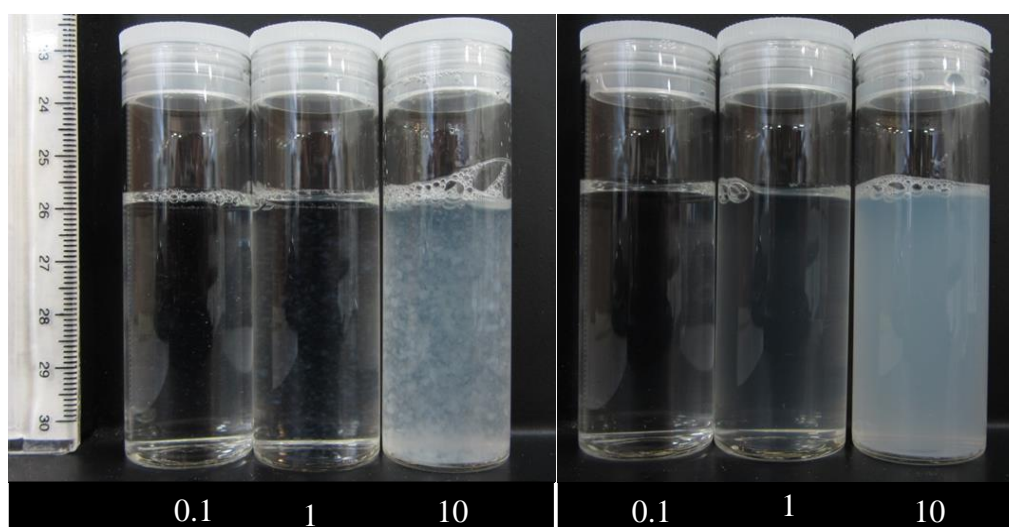
Figure 3.5. DSC thermogram of dry SSL powder (5.38 mg). The sample was held at $-10\text{ }^{\circ}\text{C}$ for 5 minutes and heated to $80\text{ }^{\circ}\text{C}$ at $10\text{ }^{\circ}\text{C min}^{-1}$ (endo is up).



3.5.2 Bilayer and multilayer vesicle formation in water

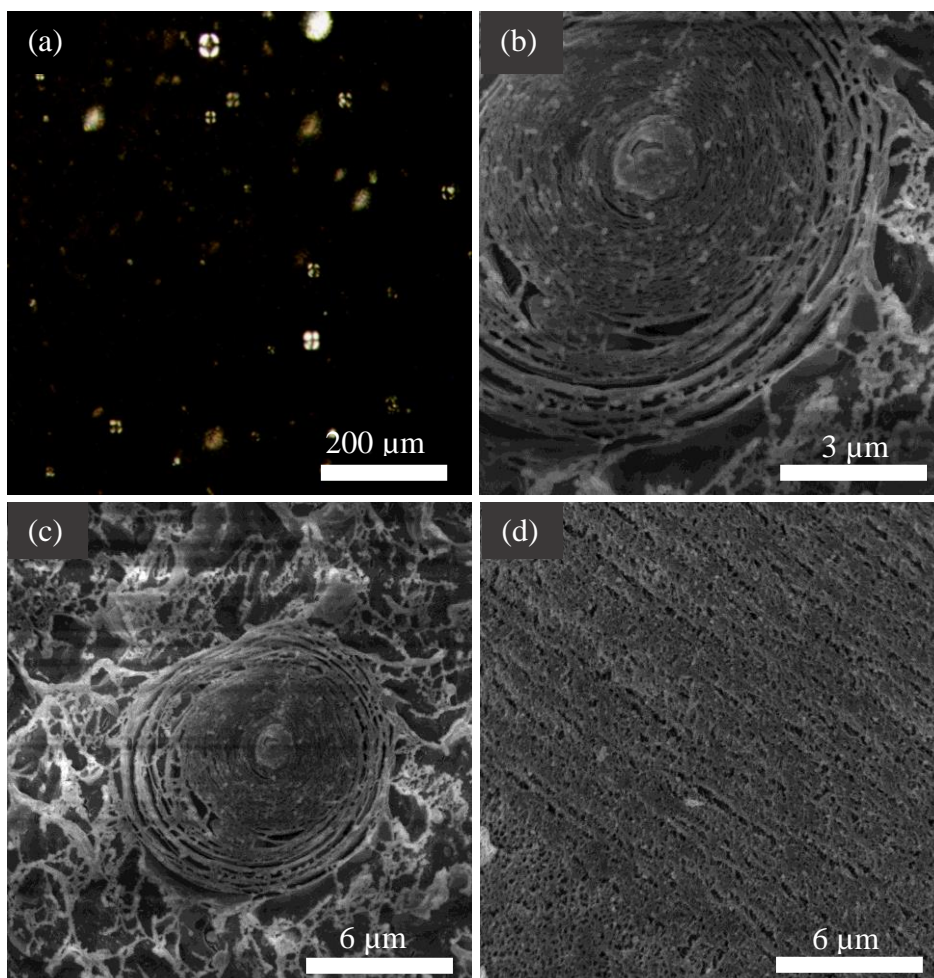
When dry SSL was added to water at room temperature, followed by stirring, the surfactant powder hydrated and two separate phases could be distinguished visually in the vessel. The appearance of the SSL aqueous dispersions one hour after mixing is shown in Figure 3.6 (left). Over time, the volume occupied by the surfactant phase increased; however after a week of preparation the solution with 10 mM SSL remained inhomogeneous. If however these dispersions were heated to 60 °C sufficient to melt the crystals, those at higher concentrations become homogeneously cloudy and remained this way upon cooling naturally to room temperature. A similar observation was reported by Kokelaar *et al.*³⁰, where they also showed that the crystalline structure of the SSL powder disappears after heating an SSL aqueous solution and that it does not reform to any great extent upon cooling. The appearance of the heat-treated solutions after cooling naturally to room temperature (23 ± 1 °C) is shown in Figure 3.6 (right). As shown in the figure the turbidity of the solutions was increased with increasing SSL concentration.

Figure 3.6. Photograph of vessels containing SSL surfactant in water at various concentrations (in mM) one hour after preparation for samples prepared at room temperature (left) and samples heated to 60 °C and then cooled to room temperature (right).



The morphology of the surfactant aggregates causing the turbidity in the heat-treated solutions was explored using cryo-SEM and optical microscopic techniques. Figure 3.7 contains some of the images from a heat-treated 30 mM SSL aqueous dispersion after it was cooled to room temperature. In (a) optical microscopy with crossed polarisers show birefringent spherulites with an approximate diameter of 10 μm that display an interference design of two crossing black lines forming a Maltese cross. The appearance of maltese crosses represent multi-lamellar vesicles in surfactant solutions.²⁵ Cryo-SEM images after water sublimation given in (b) and (c) further confirm the presence of closed spherical shapes representing multilamellar vesicles with diameters of approximately 10 μm . In these images, the grey areas represent surfactant layers and darker areas voids where water was present. Streaky planar lamellar structures in the same dispersions as seen in (d) were also observed previously by Heertje *et al.*³¹ for a monoglyceride surfactant with a chain length of C16/18 in water.

Figure 3.7. Microscopy images of 30 mM SSL dispersions in water after heat treatment using (a) optical microscopy and (b) - (d) cryo-SEM.



3.5.3 Surface activity of the surfactant at air-water surface

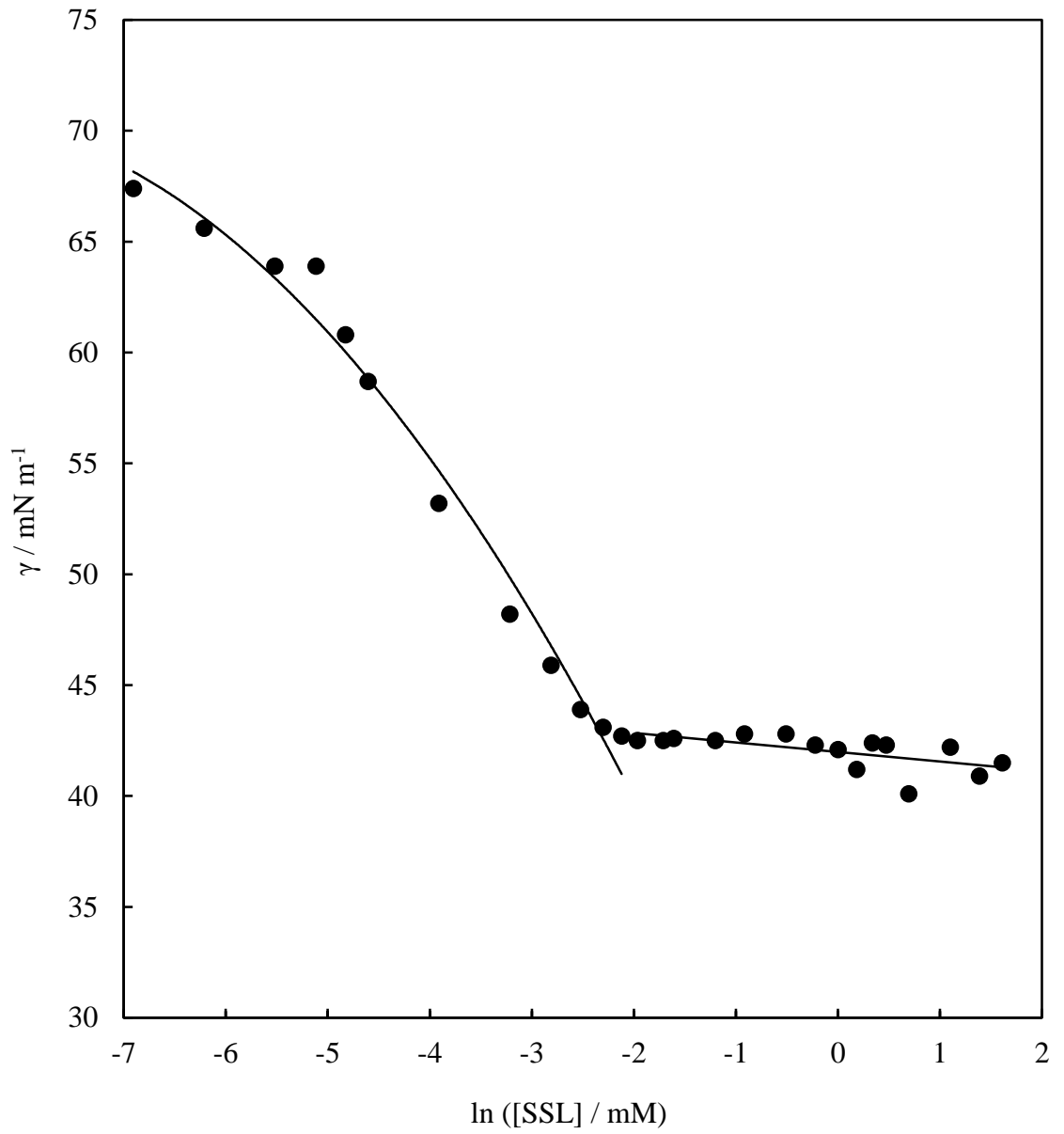
The critical aggregation concentration, c_{ac} , of SSL was determined by carrying out equilibrium surface tension measurements for a series of solutions of different surfactant concentrations at 25 °C by means of the du Noüy ring method. For this, a stock solution of 30 mM SSL prepared and heated to 60 °C was allowed to cool naturally to room temperature and diluted appropriately with water. Figure 3.8 shows the variation of the surface tension with SSL concentration, from which a c_{ac} value of 0.1 mM is derived from the breakpoint in the curve. Surface tension values decrease with SSL concentration up to around the c_{ac} and then level off.

The area per SSL molecule at the air-water interface was calculated from the slope of the surface tension curve just before the c_{ac} using the Gibbs adsorption equation for an ionic surfactant in the absence of electrolyte. The equation is shown below,³²

$$\Gamma = -\left(\frac{1}{2RT} \times \frac{d\gamma}{d\ln a}\right) \quad (3.1)$$

where γ is the surface tension, Γ is the surface excess concentration, T is the absolute temperature, R is the gas constant and a is the activity of the surfactant. Using this method, the area per molecule of SSL was found to be $1.1 \pm 0.1 \text{ nm}^2 \text{ molecule}^{-1}$, a value typical for single chain surfactants with a relatively large head group.³³

Figure 3.8. Variation of the air-water surface tension as a function of SSL concentration in water at 25 °C for samples prepared by heating to 60 °C and cooling naturally to room temperature, 23 ± 1 °C.



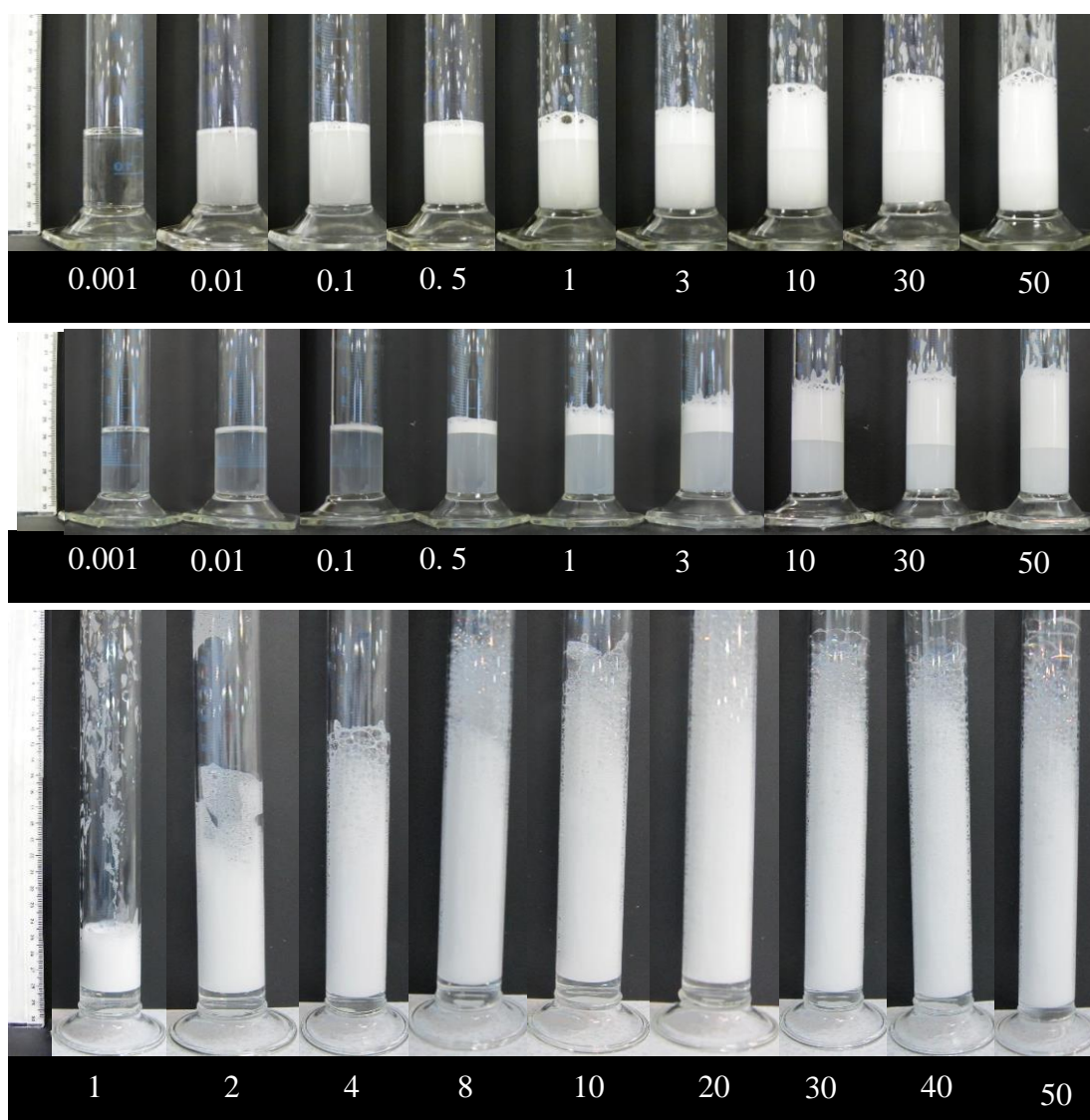
3.6 Aqueous foams of sodium stearyl lactylate

3.6.1 Foamability

Foaming properties of SSL dispersions were characterised with regards to their foamability and foam stability for both heat-treated and non heat-treated SSL aqueous dispersions. Two different foaming methods, hand shaking and use of a hand mixer, were examined and the effect of surfactant concentration on the foaming properties of the dispersions were studied. In addition, the foaming characteristics of SSL are compared with those of a micelle forming surfactant SDS, with a critical micelle concentration, cmc, of 8 mM. SDS aqueous solutions were prepared at room temperature by dispersing SDS powder in pure water followed by stirring and clear solutions were formed. Figure 3.9 shows the appearance of the foams for the three systems foamed by hand-shaking immediately after their preparation. This is followed by the foamability values of the dispersions plotted as a function of surfactant concentration in Figure 3.10. As shown in both figures, the foamability increases progressively with concentration in the case of SDS up to and slightly beyond the cmc, after which it reaches a plateau value. The foamability profile of SDS is in close agreement with that reported by Binks *et al.*³⁴ By contrast, although the volume of foam formed with SSL also increases with concentration, much lower foam volumes appear (30 vs. 250 mL at high concentration) for both heat-treated and non heat-treated SSL dispersions. It was also observed that non heat-treated SSL dispersions produce slightly more foam than heat-treated ones in general. The decrease in foam volume above 30 mM SSL for heat-treated samples is due to the dramatic increase in the dispersion viscosity hindering air incorporation. This was not the case for non heat-treated SSL samples, where the viscosity of the solutions did not increase with surfactant concentration and the foamability continued to increase with concentration.

It is worth noting also that no foam is formed at SSL concentrations below the cac, *i.e.* foaming only occurs once the surfactant aggregates. Below the aggregation concentrations, the reduced foaming of SSL compared with SDS is due to the reduced monomer concentration, by up to a factor of 80, at the cac/cmc. Above the cmc/cac, diffusion and breakdown of either micelles or dispersed lamellar phases (vesicles) is potentially an important aspect in the transport of the surfactant to the air-water (bubble) surface.

Figure 3.9. Appearance of heat-treated SSL aqueous foams (upper), non heat-treated SSL aqueous foams (middle) and SDS aqueous foams (lower) immediately after preparation. The samples were left on the bench at room temperature following their preparation. Numbers below each sample correspond to the concentration of the surfactant in mM.



Garrett and Gratton³⁵ studied the foaming properties of a homologous series of nonionic surfactants, n-dodecyl polyethylene glycol mono ethers; $C_{12}E_n$. The aqueous solutions prepared from the surfactants were clear, isotropic and micellar when $n \geq 5$ and were turbid, containing lamellar phases when $n < 5$. Their foamability results (by cylinder shaking) showed that lower foam volumes were produced for the lamellar phase-forming surfactants compared to micellar solutions. Garrett and Gratton correlated the low foamability of lamellar phase-forming surfactants to the slow transport of surfactant monomers to the air-water interface. Slow transport means low dynamic adsorption levels which in turn leads to an enhanced probability of foam film rupture and thereby diminished foamability. It is likely that similar arguments apply here in the case of SSL. They concluded that the transport of surfactant from the aggregated lamellar phase to the surface does not occur *via* breakdown to monomers unlike the case for micelles, but may occur by a combination of direct emergence of aggregates into the air-water surface followed by spreading.

The effect of foaming method on the foamability of heat-treated SSL aqueous dispersions was also studied. It was found that the foamability of SSL dispersions is dependent on the foaming method as shown in Figure 3.11. It is clear from the graph that foaming is more efficient (parameter F is higher) in hand-shaken foams at all SSL concentrations. As different solution volumes were used for hand shaking and Cuisinart hand mixer methods, the foamability parameter F is used as defined in section 2.2.11.

Figure 3.10. Initial foam volume *versus* surfactant concentration in water for SSL (heat-treated: triangles and non heat-treated: circles) and SDS (squares) foams from 20 mL of each dispersion formed *via* hand shaking for 30 seconds at room temperature. SDS (a micelle forming surfactant) produces higher foam volumes compared to SSL (a lamellar phase forming surfactant).

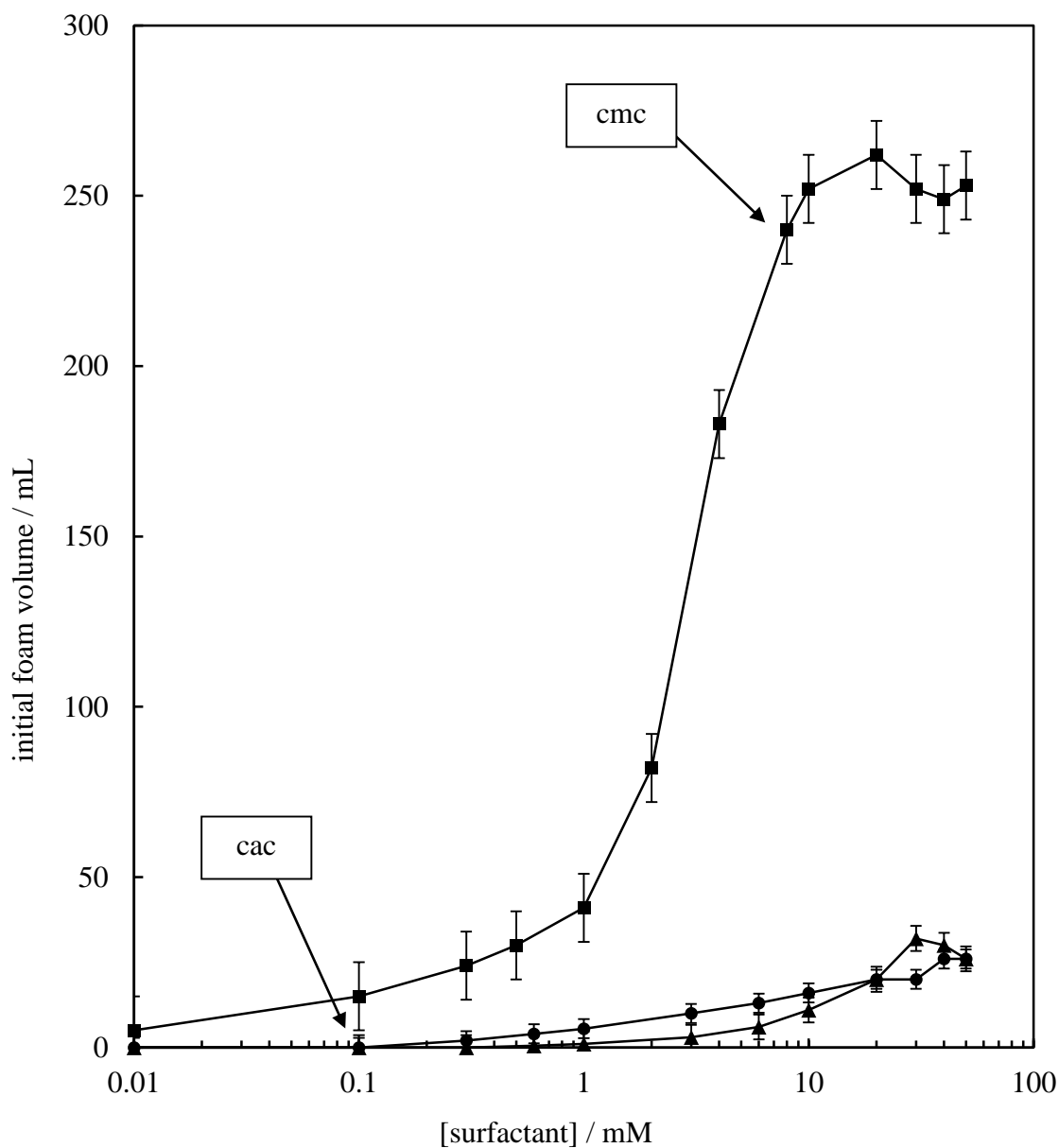
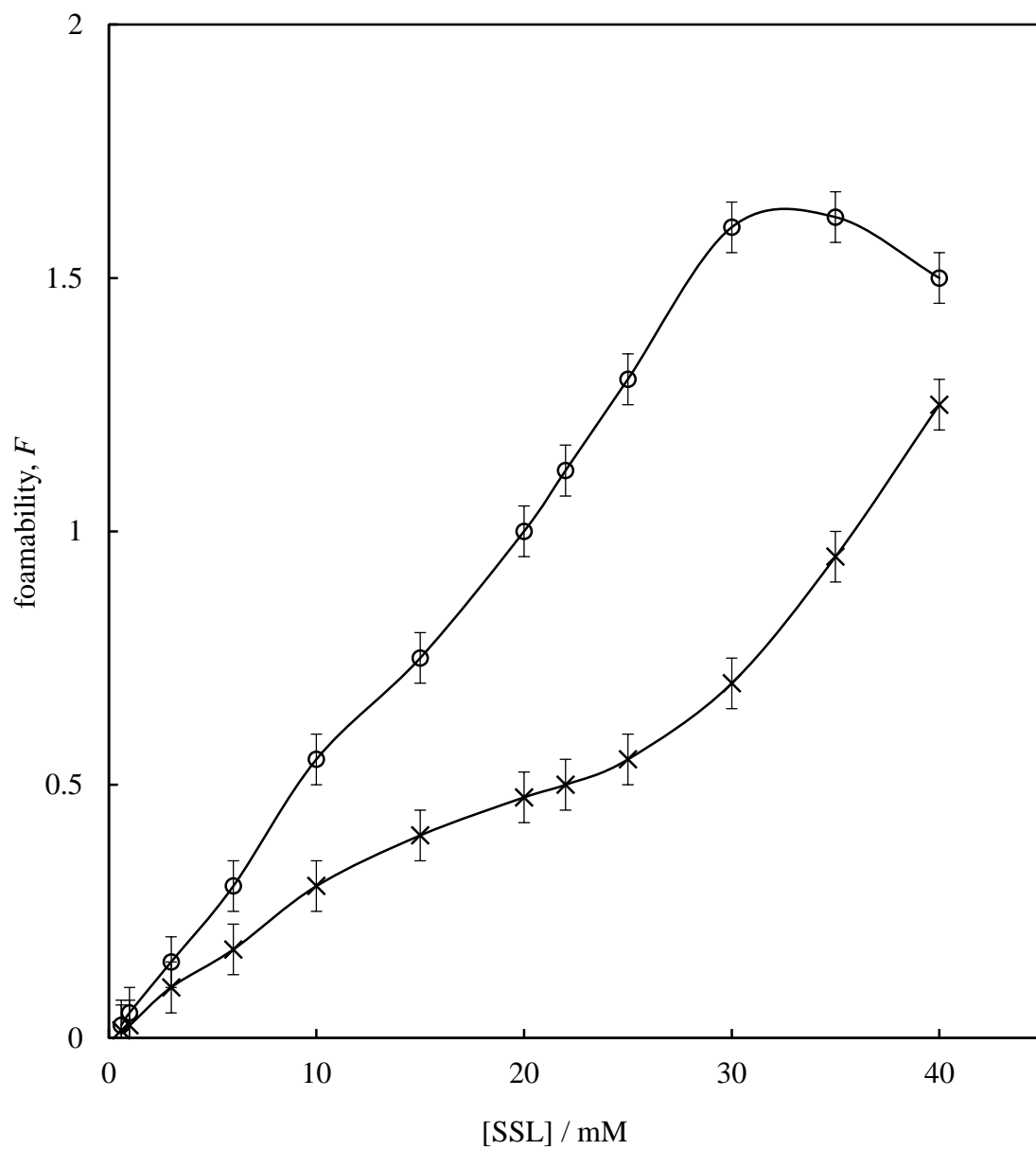


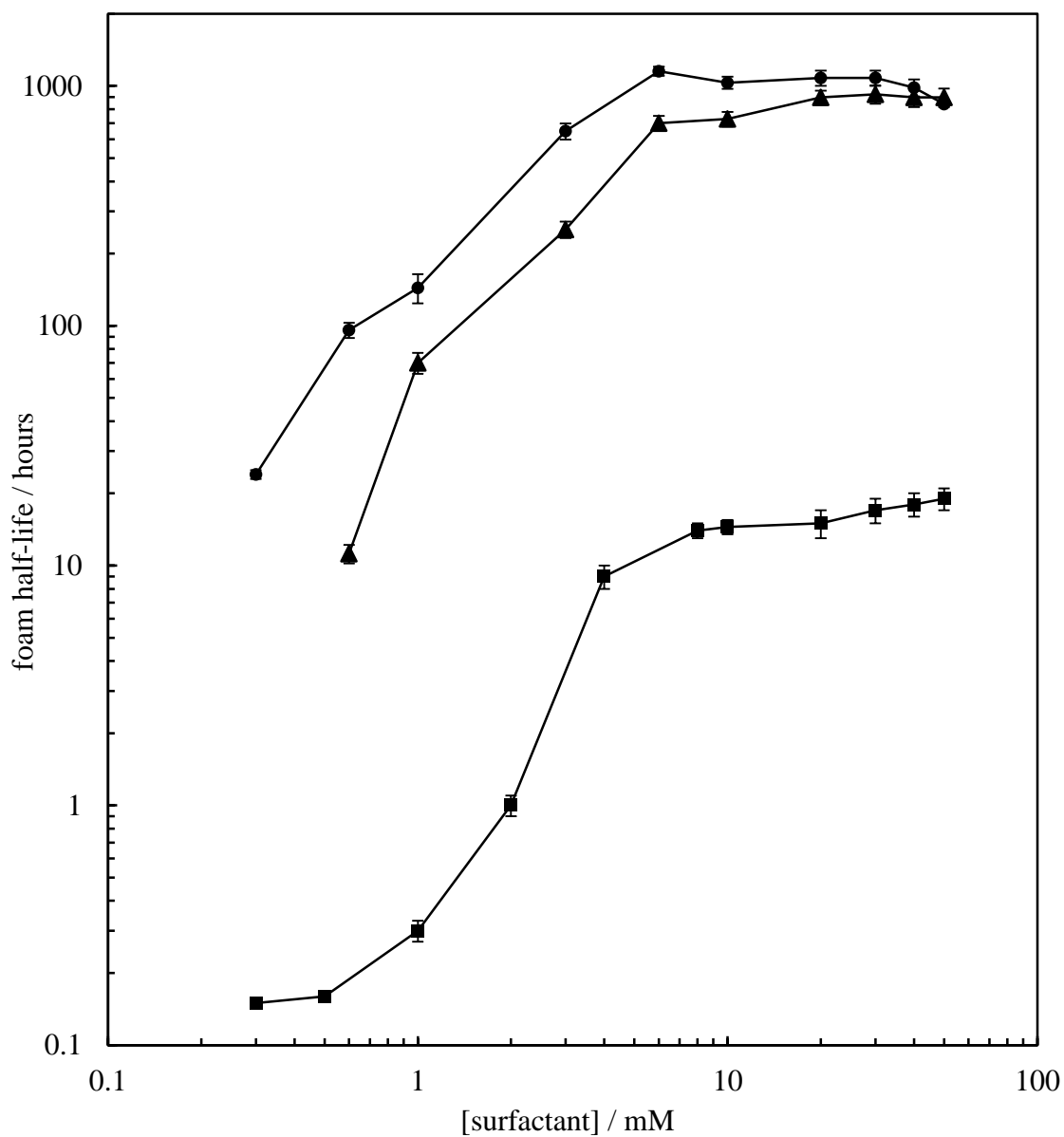
Figure 3.11. Foamability, F , of SSL dispersions by hand-shaking (20 mL, circles) and Cuisinart hand mixer (200 mL, crosses) as a function of SSL concentration.



3.6.2 *Foam stability*

In terms of the stability of the foams, SSL foams were far more stable than those of SDS. The half-lives (time taken for the initial foam volume to fall by 50%) are plotted against surfactant concentration for all SSL (heat-treated and non heat-treated) and SDS foams in Figure 3.12. It can be clearly seen that half-lives are nearly two orders of magnitude higher for SSL compared to SDS at all concentrations. The life-time (time taken for complete foam collapse) of SDS-stabilised foams was within 48 hours, whereas SSL-stabilised foams can remain stable for up to 80 days. In both systems, complete foam collapse occurred *via* initial drainage of the aqueous phase followed by coalescence and disproportionation. The initial bubble diameters for SDS foams were several millimetres with very thin films in between the bubbles and these foams appeared dry. On the other hand, bubbles were much smaller ($< 50 \mu\text{m}$) for SSL and the foams had a creamy, fluid-like appearance and maintained a significant amount of liquid in comparison to SDS-stabilised foams.

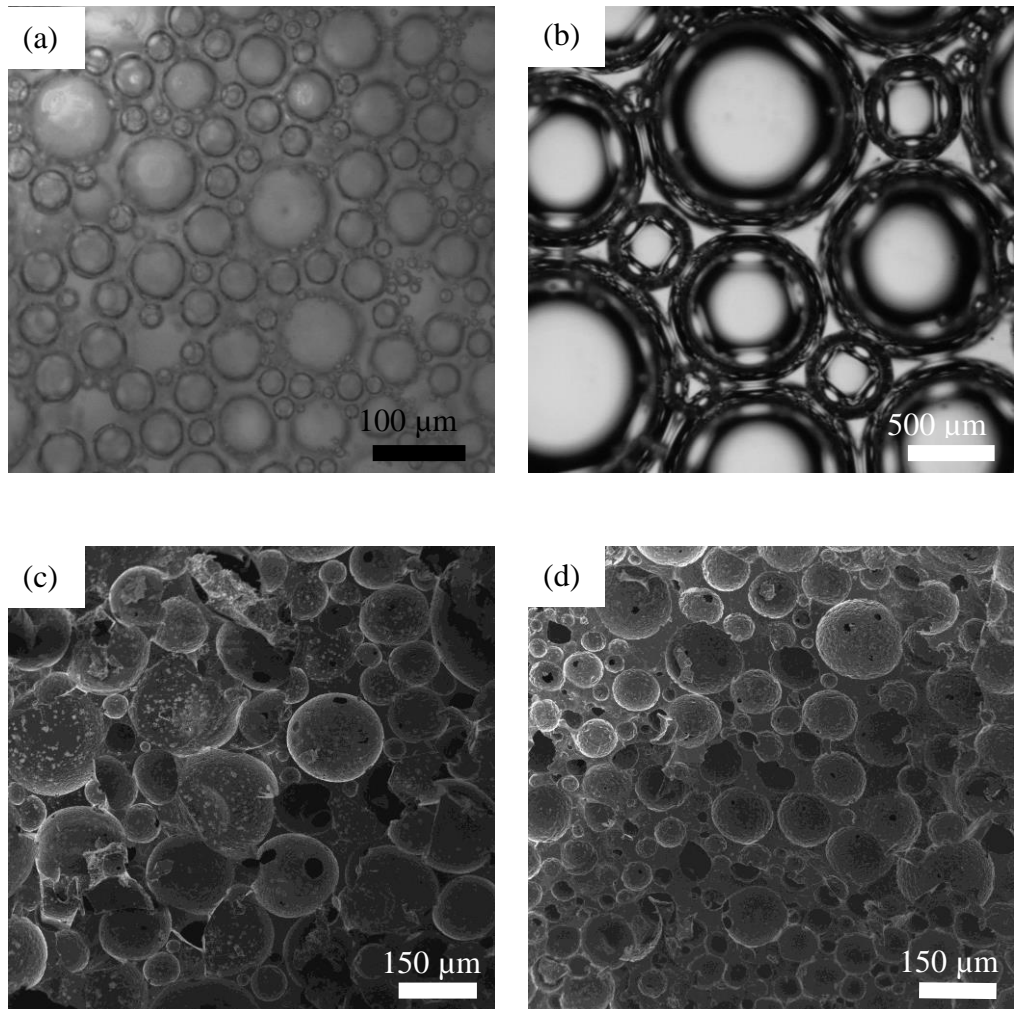
Figure 3.12. Half-life of aqueous foams *versus* surfactant concentration for SSL (heat-treated: triangles and non heat-treated: circles) and SDS (squares) foams from 20 mL dispersion/solution. Foams were prepared by handshaking for 30 seconds and were left at 23 ± 1 °C. To determine the half-lives, the volume of the foam and subnatant solution were recorded at various times after foaming.



Foaming properties of vesicle forming surfactants have been compared with those of micelle forming surfactants by Novales *et al.*³⁶ They studied the foaming properties of fatty acid-lysine (1:1) salts with different alkyl chain lengths. The dodecyl analogue formed micelles in water and yielded foams with large bubbles of low stability (complete foam collapse after 15 minutes). The longer chain length (tetradecyl and hexadecyl) analogues however assembled into vesicles when in water and produced foams, which were stable for at least several hours with small bubbles. In another study, Varade *et al.*³⁷ investigated the foaming properties of a mixture of anionic (myristic acid) and cationic (cetyltrimethylammonium chloride) surfactants. They prepared aqueous foams *via* hand shaking and explained the extreme stability of the foams by a synergy effect between two fundamentally different mechanisms. Firstly, such mixtures form highly close-packed monolayers of surfactant mixtures at the air-water surface with high interfacial viscoelasticities. This eventually confers a high disjoining pressure (enhancing stability) between two approaching surfaces. Secondly, micron-sized vesicles reside in the thin aqueous films between bubbles and block the Plateau borders slowing down drainage and reducing bubble coalescence and inter-bubble gas transfer. It is believed that the same mechanisms are involved in stabilising SSL aqueous foams. SSL foams are stabilised by the open ended planar lamellar aggregates that cover the air cells as well as the micron-sized vesicles blocking the thin films and Plateau borders hence increasing the stability of the foams towards coalescence, disproportionation and drainage.

Figure 3.13 shows optical microscopy and cryo-SEM images of bubbles in SSL foams. Comparing the optical microscopy image of a 30 mM SSL aqueous foam initially (a) and one week after preparation (b) clearly shows the increase in size of the air bubbles due to disproportionation and coalescence. Cryo-SEM images of the same foams with and without heat treatment of the aqueous dispersion show no significant change in the shape and size of the air cells due to heat treatment and all the bubbles are spherical in both cases.

Figure 3.13. Optical microscopy image of 30 mM SSL (heat-treated) aqueous foam (a) initially and (b) one week after preparation. Cryo-SEM images of the same foams initially (c) with and (d) without heat treatment of the aqueous dispersion.



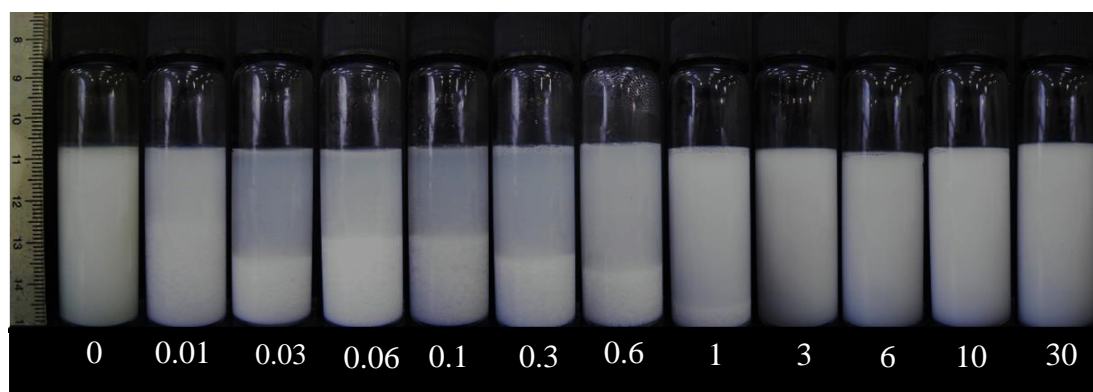
3.7 Aqueous dispersions of precipitated calcium carbonate and sodium stearyl lactylate mixtures

3.7.1 Dispersion stability

The adsorption behaviour of negatively charged SSL on positively charged PCC particles was studied in detail. Aqueous dispersions of 1 wt. % Calofort U particles on adding increasing concentrations of SSL were prepared without modifying the pH. In fact the pH decreases from 9.3 (natural pH of 1 wt. % PCC dispersion) without surfactant to 7.5 with 30 mM SSL. Figure 3.14 shows the appearance of SSL-PCC mixtures immediately after preparation. It is clear from the image that addition of SSL affects the stability of the dispersions significantly. Addition of surfactant at low concentrations (0.03 mM) induces particles sedimentation, which increases in extent initially and then decreases with increasing surfactant concentration (up to 1 mM). Dispersions remain stable with surfactant concentration above 1 mM and those above 10 mM remain stable to sedimentation indefinitely. This pattern of behaviour (stable-unstable-stable) is reported by Binks *et al.*⁹ for mixtures of anionic silica particles and cationic surfactant in terms of surfactant adsorption on particle surfaces and the resultant changes in the stability of dispersions. This pattern could be explained in terms of the colloidal structural forces.³⁸ In the presence of PCC particles and low concentration of non-adsorbed SSL vesicles the potential can develop an attractive well because of the depletion effect. Upon approaching PCC particles, the SSL vesicles are expelled from the area between particles when their surface separation becomes smaller than the size of the SSL vesicles. This creates an unbalanced osmotic pressure difference pushing the particles together, which results in an effective attraction between PCC particles and eventually their sedimentation. At higher SSL concentration (e.g. 30 mM) the behaviour is different and the particles were stable towards sedimentation. It is known that in aqueous dispersions of surfactant-particle mixture, the presence of high concentration of non-adsorbed surfactant vesicles and molecules causes an effective repulsion force between solid particles due to the colloidal structural forces. In these dispersions the distribution of surfactant vesicles between particles is oscillatory. The surfactant vesicles tend to order in layers as they come closer to the surface of the particles. The average surfactant vesicle concentration between the two particle surfaces oscillates with the separation as only separations close to a whole number of particle diameters (i.e. $D=2Rn$,

D = separation, R = vesicle diameter and $n = 1,2,3,\dots$) favour close packing of surfactant vesicle in layers. The stability of the particles to aggregation is then enhanced due to change of the osmotic pressure of the solvent when the particle concentration between the surfaces is changing oscillatory with the particle separation. This is known as volume exclusion effect.³⁸

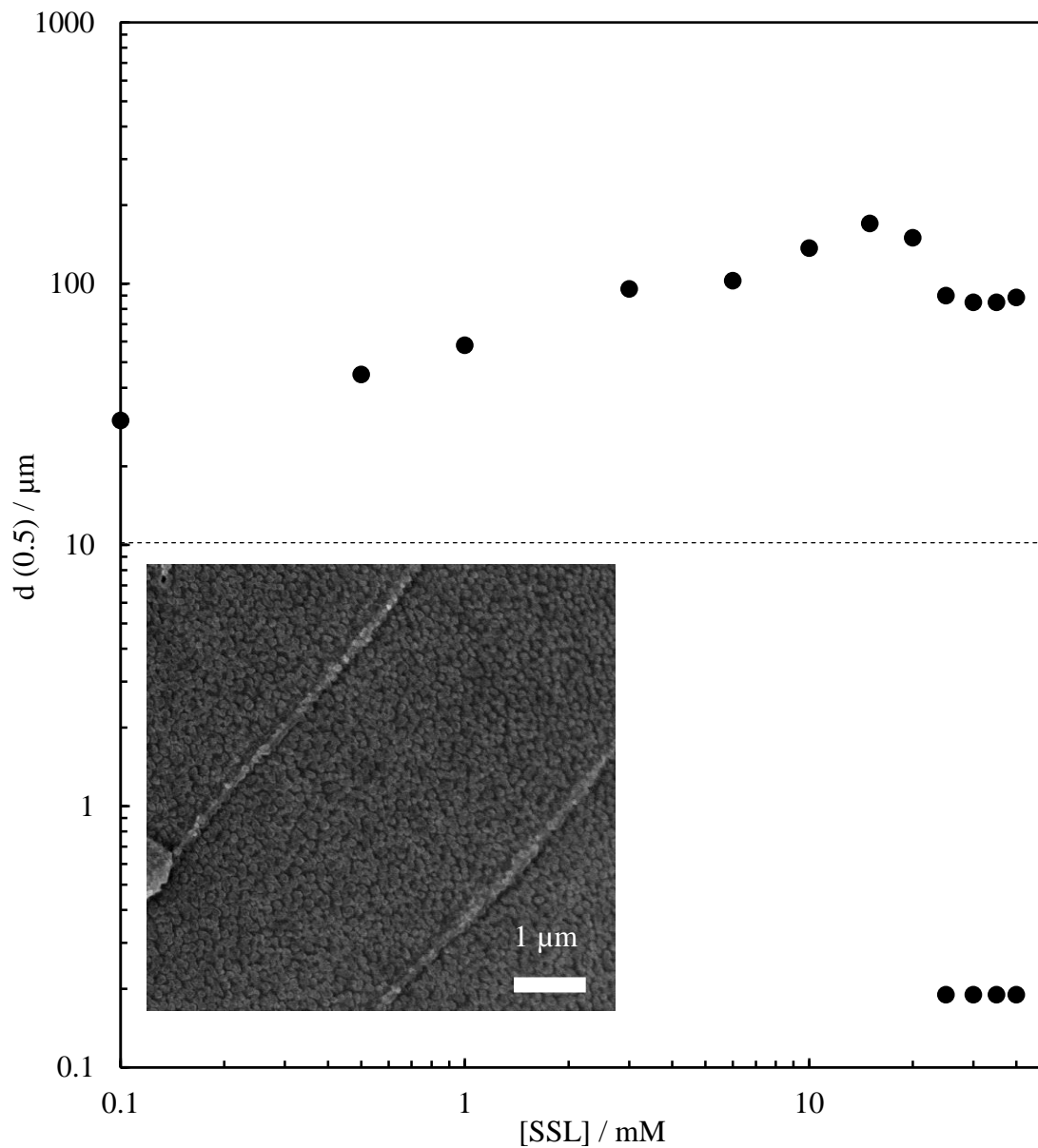
Figure 3.14. Appearance of SSL-PCC aqueous dispersions immediately after preparation. The concentration of particles is fixed at 1 wt. % and SSL concentration is varied (given in mM). All samples are at their natural pH. The sedimentation state of the particles depends on SSL concentration.



3.7.2 Particle size distribution evolution upon surfactant adsorption

The particle size distributions of PCC in SSL-PCC mixtures were measured by light scattering immediately after preparation and the data are shown in Figure 3.15. As shown in the figure the distributions are unimodal for dispersions with up to 20 mM SSL. The median diameter, $d(0.5)$, value rises from about 10 μm in pure water (shown previously in Figure 3.3) to around 100 μm for the dispersion with 20 mM surfactant. The results show that surfactant addition induces further particle aggregation. At SSL concentrations ≥ 25 mM however, size measurements reveal bimodal distributions with a population of discrete particles of median diameter around 180 nm (that of primary particles) separated entirely from the larger particle aggregates. The population of the smaller particles present increases relative to the aggregates with SSL concentration since surfactant adsorption aids particle dispersion. The inset in Figure 3.15 shows a cryo-SEM image of a dispersion containing 1 wt. % PCC particles in 30 mM surfactant solution where individual primary particles appear between surfactant layers within planar lamellar aggregates.

Figure 3.15. Median diameter of PCC particles in SSL-PCC aqueous dispersions as a function of SSL concentration. The concentration of particles was fixed at 1 wt. %. Note switch from monomodal distribution to bimodal. Inset is a cryo-SEM image of a dispersion at 30 mM SSL.

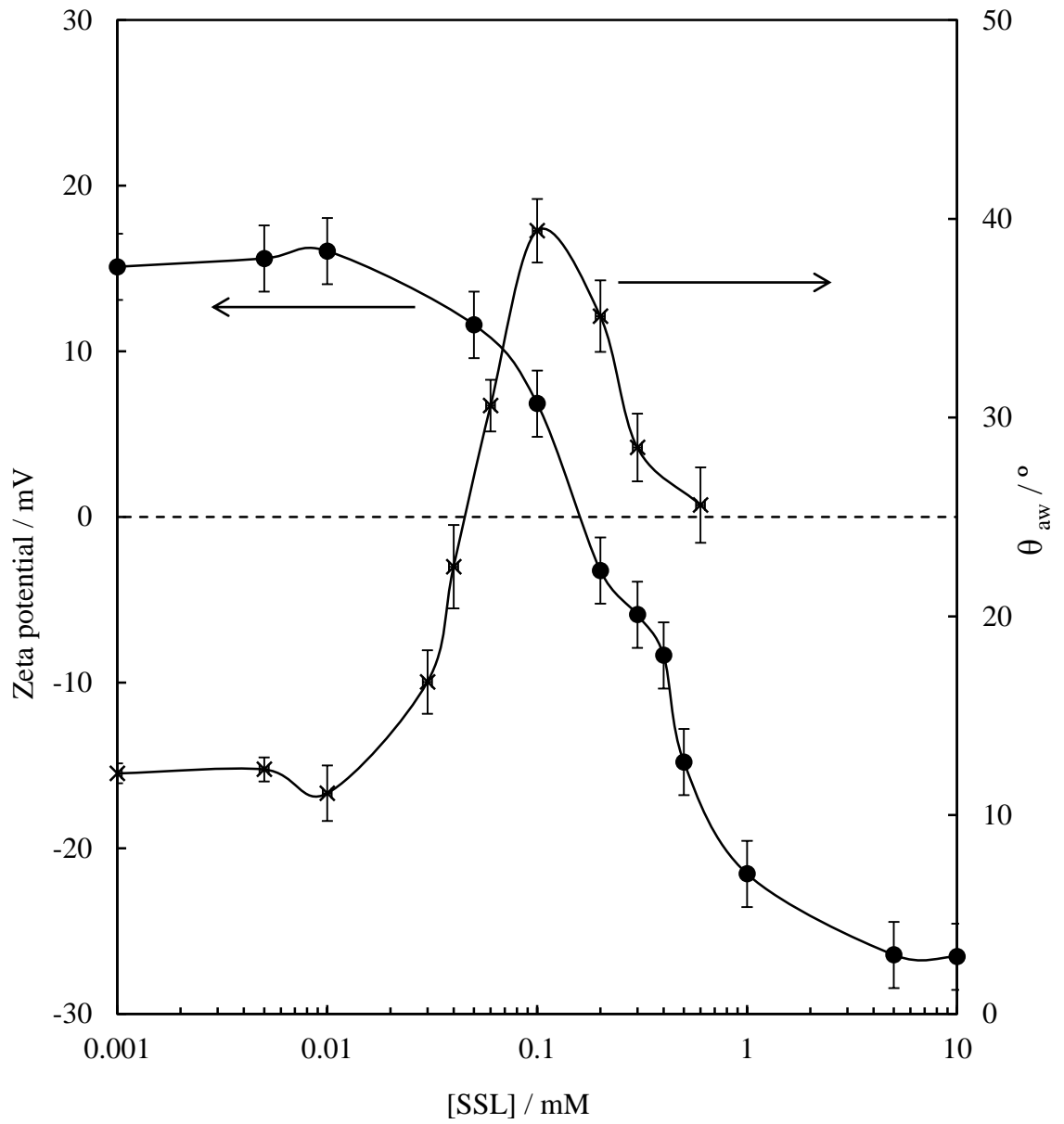


3.7.3 *Zeta potential of particles and contact angle of aqueous surfactant on particle disks*

The change in the zeta potential of PCC aqueous dispersions accompanying adsorption of surfactant monomers to particle surfaces is shown in Figure 3.16 (filled points). Cationic PCC particles in the absence of surfactant lose their charge approaching the cac of the surfactant and subsequently become negatively charged at higher concentrations. At low concentrations, surfactant molecules adsorb to particles *via* electrostatic interactions of their anionic headgroups with cationic sites on the surface. Charge neutralisation is thought to occur following completion of an adsorbed monolayer rendering particles more hydrophobic. Adsorption continues *via* chain-chain interactions as a surfactant bilayer develops and particles become anionic since surfactant headgroups are now exposed to water.

The *in situ* surface activation of PCC particles by adsorption of SSL monomers is backed up by determining the contact angle of aqueous SSL droplets in air on substrates composed of PCC particles. Since determination of the contact angle using nanoparticles themselves is not possible, circular disks (1 cm approx. diameter and 1 mm thickness) of the particles using a high pressure press were made for the purpose. It is worth mentioning that there are several reasons which make obtaining a valid, reproducible contact angle difficult such as contamination of the droplet, surface cleanliness, surface heterogeneity, surface roughness and environmental conditions, however extra care was taken to ensure all these factors were minimised for the measurements. The advancing contact angle values measured are given in Figure 3.16 (crosses) over a limited concentration range (up to 0.6 mM). The contact angle of pure water was 13°, indicative of a very hydrophilic surface. This is in close agreement with the contact angle measured by Cui *et al.* for a different source of PCC particles.¹⁵ It increases initially on adding surfactant as the surface becomes more hydrophobic and decreases above 0.1 mM (= cac) as surfaces become hydrophilic again. At SSL concentrations ≥ 1 mM, difficulties were encountered measuring the angles as aqueous drops became quite viscous. As shown in the figure the maximum advancing contact angle measured overlays with the zero point of charge of the particles. This is believed to be the point of the completion of an adsorbed monolayer of surfactant on the surface of the particles rendering them hydrophobic.

Figure 3.16. Zeta potential of 1 wt.% Calofort U aqueous dispersions (filled points, left hand ordinate) and advancing contact angle of aqueous droplets containing SSL in air on pressed discs of Calofort U particles (crosses, right hand ordinate) *versus* concentration of SSL.



3.7.3.1 Adsorption isotherm of surfactant on particles

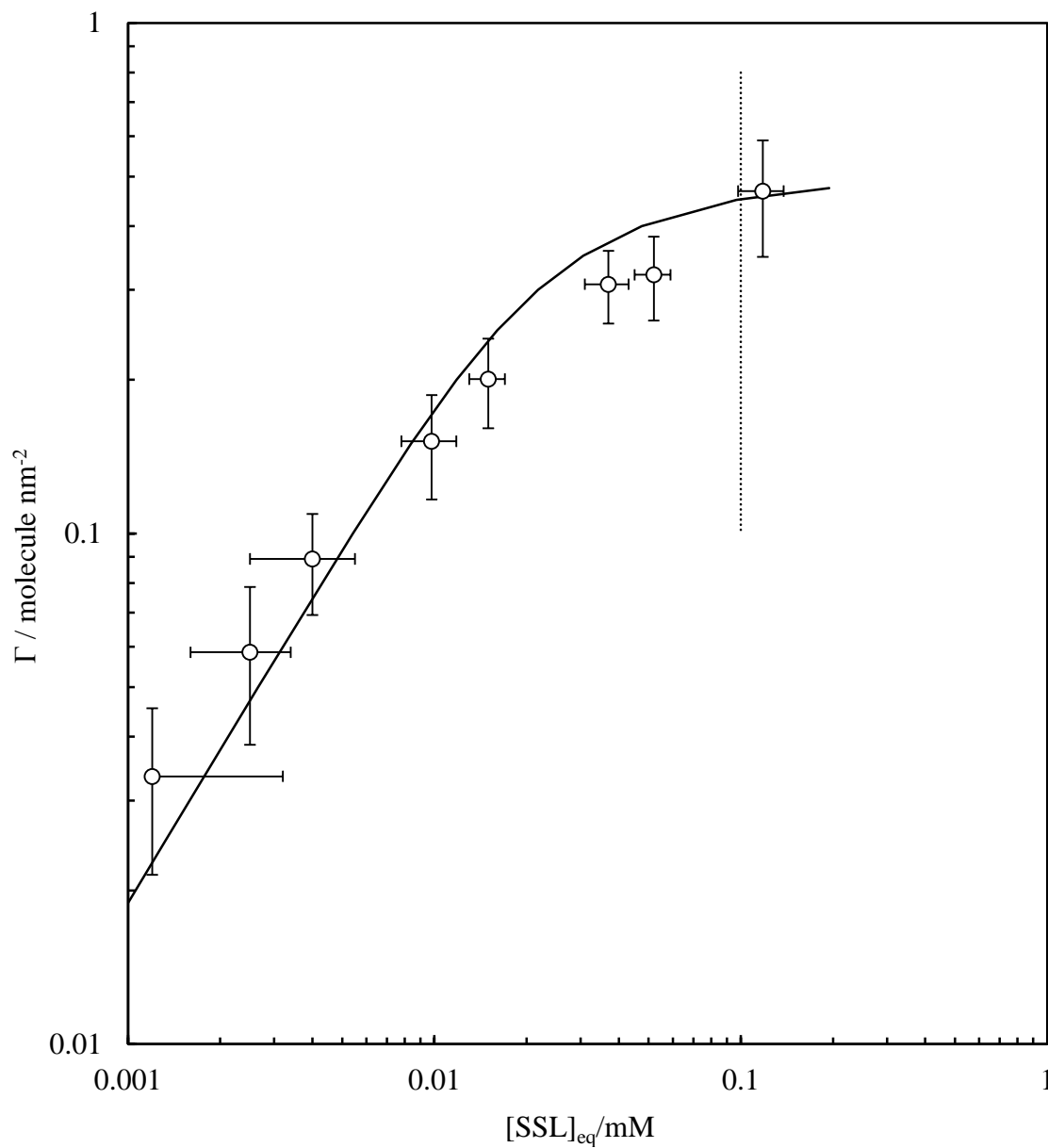
In order to quantify the extent of SSL adsorption on CaCO₃ particles in water, the adsorption isotherm using depletion from solution was determined and is given in Figure 3.17. A problem was encountered at higher surfactant concentrations (> 0.5 mM) as vesicles and aggregates of SSL were also sedimented with particles upon centrifugation, invalidating this method. Due to this only the values from the dispersions up to the cac were taken into account.

The isotherm profile was found not to be a Langmuirian type possibly due to the adsorption being highly cooperative in nature. Cooperative adsorption is presented when the energy of adsorption becomes more negative with increasing surface coverage or in other words adsorption of one surfactant can assist the others to adsorb on the surface.¹¹ In addition, the electrostatic adsorption of surfactant to the substrate may lower the activation energy of aggregate formation promoting the formation of vesicles, on the solid surface, below the solution cac similar to the findings of Subramanian and Ducker,³⁹ for the adsorption of hexadecyltrimethylammonium (CTA⁺) on hydrophilic silica surface. The adsorption isotherm of SSL on PCC particles may be explained in terms of cooperative adsorption laterally between adsorbed molecules. The concentration of non-adsorbed surfactant C_{eq} is given by:⁴⁰

$$C_{eq} = \frac{\theta}{(1 - \theta)e^{-E/RT} e^{-\beta\theta}} \quad (3.2)$$

where $\theta = \Gamma/\Gamma_{max}$, *i.e.* the ratio of the amount of surfactant adsorbed to the maximum amount adsorbed, E is the adsorption energy, R is the gas constant, T is temperature and β (degree of cooperativity) is a parameter linked to the strength of the attractive lateral interactions between adsorbed surfactant molecules. Values of E and β were floated simultaneously to obtain the best fit to the data and were found to be $E = -4.5 \text{ kJ mol}^{-1}$ and $\beta = -1$, comparable to those determined for long chain esters on steel.⁴⁰ A negative β value means the adsorption of SSL on PCC particles is cooperative (attractive). The value of Γ_{max} of $0.5 \text{ molecule/nm}^2$ corresponds to an area per SSL molecule adsorbed on the particles of 2 nm^2 , which is higher than that near the cac at the air-water surface from surface tension data.

Figure 3.17. Adsorption isotherm of SSL onto Calofort U particles in water. The fit is that to the cooperative model (eqn. 3.2). No measurements were taken at concentrations above 0.5 mM due to sedimentation of vesicles and aggregates of SSL with particles upon centrifugation. Dotted line = cac.



3.8 Aqueous foams of sodium stearyl lactylate – precipitated calcium carbonate mixtures

3.8.1 Foamability

Aqueous foams were prepared from mixtures of Calofort U PCC particles (1 wt. %) and increasing concentrations of SSL. The appearance of the foams prepared from 20 mL mixtures by hand-shaking three weeks after preparation is shown in Figure 3.18. All foams have a white appearance and the residual foam volume after three weeks increases with surfactant concentration. A white layer of sedimented PCC particles at the bottom of the vessel can be seen for the foam with 0.05 mM SSL. The foamability of the mixtures is compared to that of SSL alone in Figure 3.19. As is clear from the graph, there is no significant change in the initial foam volume between the two systems via hand-shaking. This is in contrast to the results of Cui *et al.*¹⁵, where they reported differences in the foamability of SDS alone and SDS-PCC mixture foams. Their results showed an increase in the foamability of the SDS aqueous solutions in the presence of 1 wt. % PCC particles, with a maximum foamability at concentrations between 1 and 2 mM SDS, after which foamability decreased. Similar to SSL systems alone, in SSL-PCC mixtures there is no foaming at concentrations below the cac (0.1 mM). Above the cac the initial foam volume increases gradually with surfactant concentration and then reaches a maximum for 30 mM SSL after which it decreases slightly. The highest foamability occurs at a concentration where there is a significant population of discrete particles following de-aggregation of particle aggregates as well as a high concentration of SSL aggregates (planar and lamellar structures). After this point there is a slight decrease in foamability, which is due to an increase in the viscosity of the solution, also observed for foams of SSL alone. A similar profile was obtained for foams prepared using the hand mixer, however this yielded slightly better foamability. This is shown in Figure 3.20 with the inset showing the appearance of a foam from an SSL (30 mM)-PCC (1 wt. %) mixture aerated using the hand mixer one day after preparation.

Figure 3.18. Appearance of SSL + Calofort U PCC (1 wt. %) aqueous foams three weeks after preparation. The foams were produced from 20 mL of mixture by hand-shaking at 23 ± 1 °C. Concentrations of SSL in mM are given.

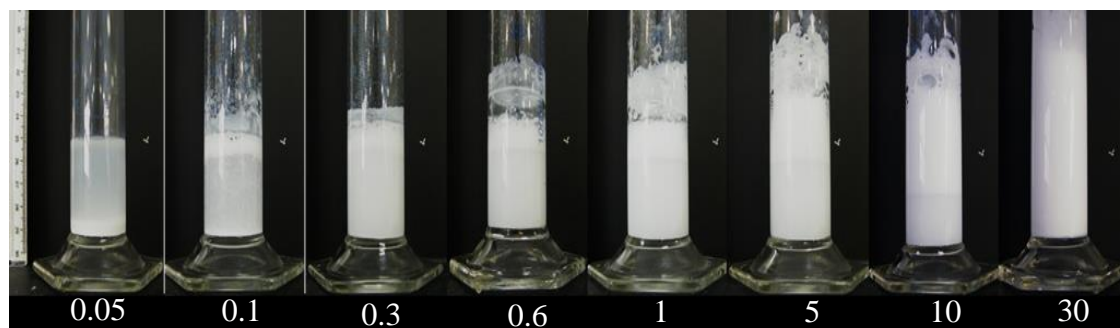


Figure 3.19. Initial foam volume vs. surfactant concentration foams of SSL alone (crosses) and SSL-Calofort U PCC (1 wt. %) mixtures (circles) produced from 20 mL initial dispersion at their natural pH by 30 seconds hand shaking.

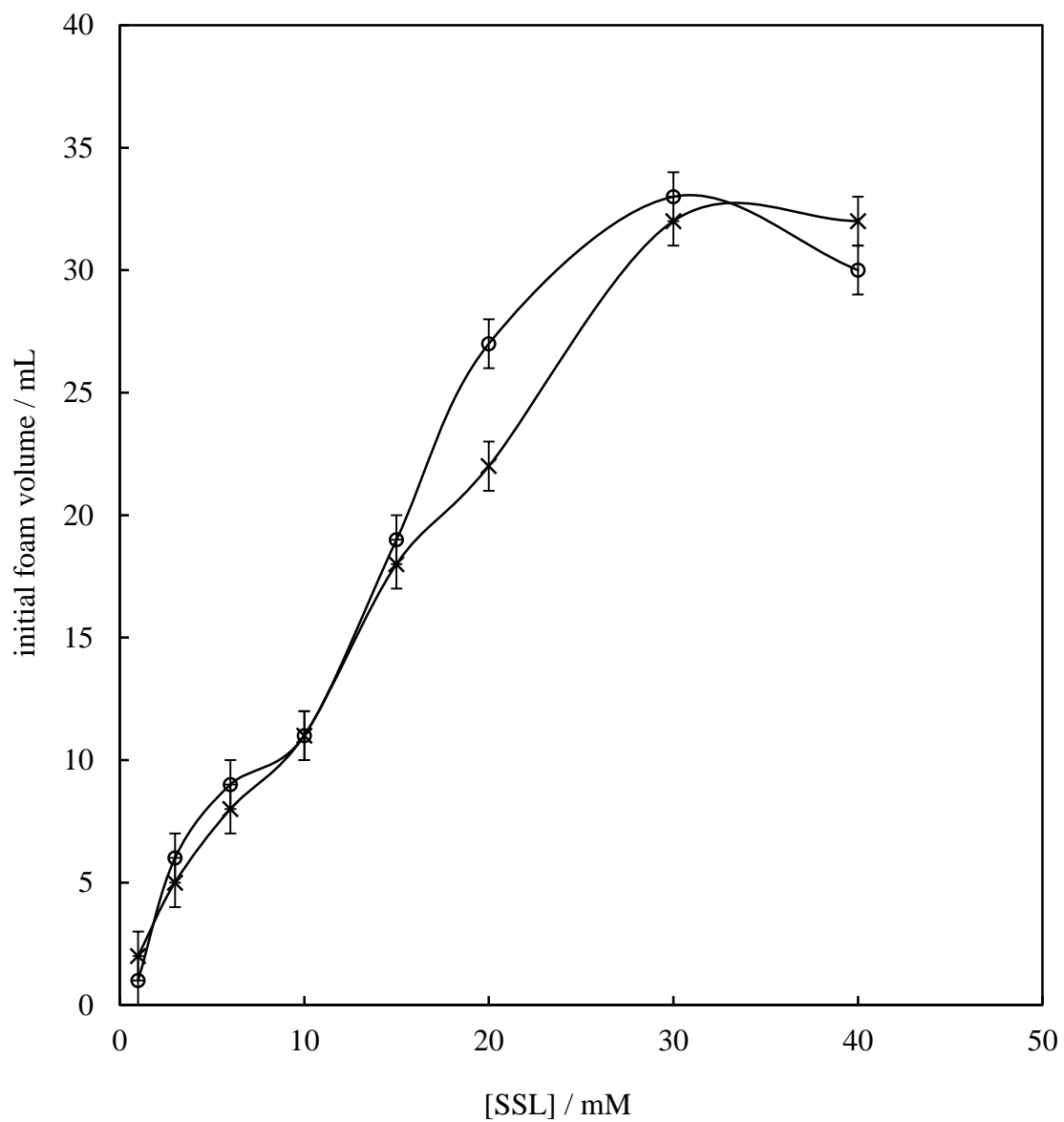
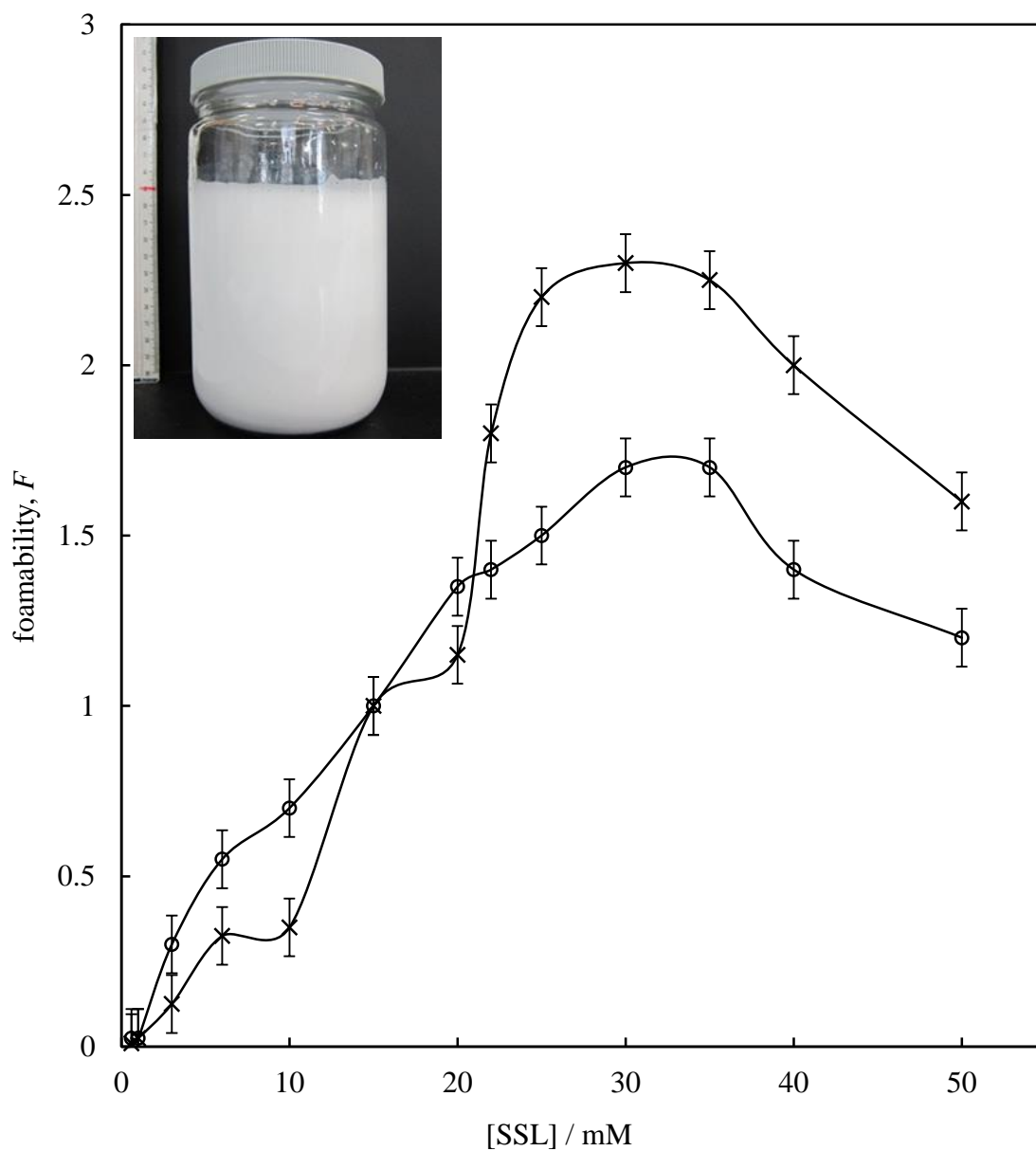


Figure 3.20. Foamability, F , of SSL + Calofort U PCC (1 wt. %) mixtures using hand-shaking (20 mL, circles) and Cuisinart hand mixer (200 mL, crosses) as a function of SSL concentration. The inset shows the appearance of a foam from an SSL (30 mM)-PCC (1 wt. %) mixture aerated using the hand mixer one day after preparation.



3.8.2 *Foam stability*

Unlike foams stabilised solely by SSL, the foams from SSL-PCC mixtures are very stable and retain their volume for much longer periods. The foam half-lives of both systems are plotted in Figure 3.21. The graph shows the significant improvement in stability for foams upon addition of 1 wt. % PCC particles at all SSL concentrations. The foams were monitored in sealed vessels for a year to determine the foam volume evolution with time. The half-lives of the foams from mixtures increased rapidly with concentration to over 280 days (not determined). This is to be compared with foams of SSL alone (filled points) possessing maximum half-lives of only 40 days. Above 30 mM surfactant concentration, foams are so stable that a half-life could not be determined.

The percentage of particles associated with the foams, x , was determined by analysing the supernatant aqueous phase following water drainage one day after preparation. The results are plotted versus surfactant concentration in Figure 3.22. At low SSL concentrations the measured loss of particles to foams is below 20% but increases dramatically to a maximum of 95% at 30 mM surfactant, followed by a sharp decrease above 30 mM. The similarity in both the shape and position of this variation with that of the foam stability data implies that particle presence within foams is advantageous to stability.

Figure 3.21. Aqueous foam half-life for SSL alone (filled points) and SSL + Calofort U PCC (1 wt. %) mixtures (empty points) as a function of SSL concentration. At and above 30 mM, no half-life arises (arrows).

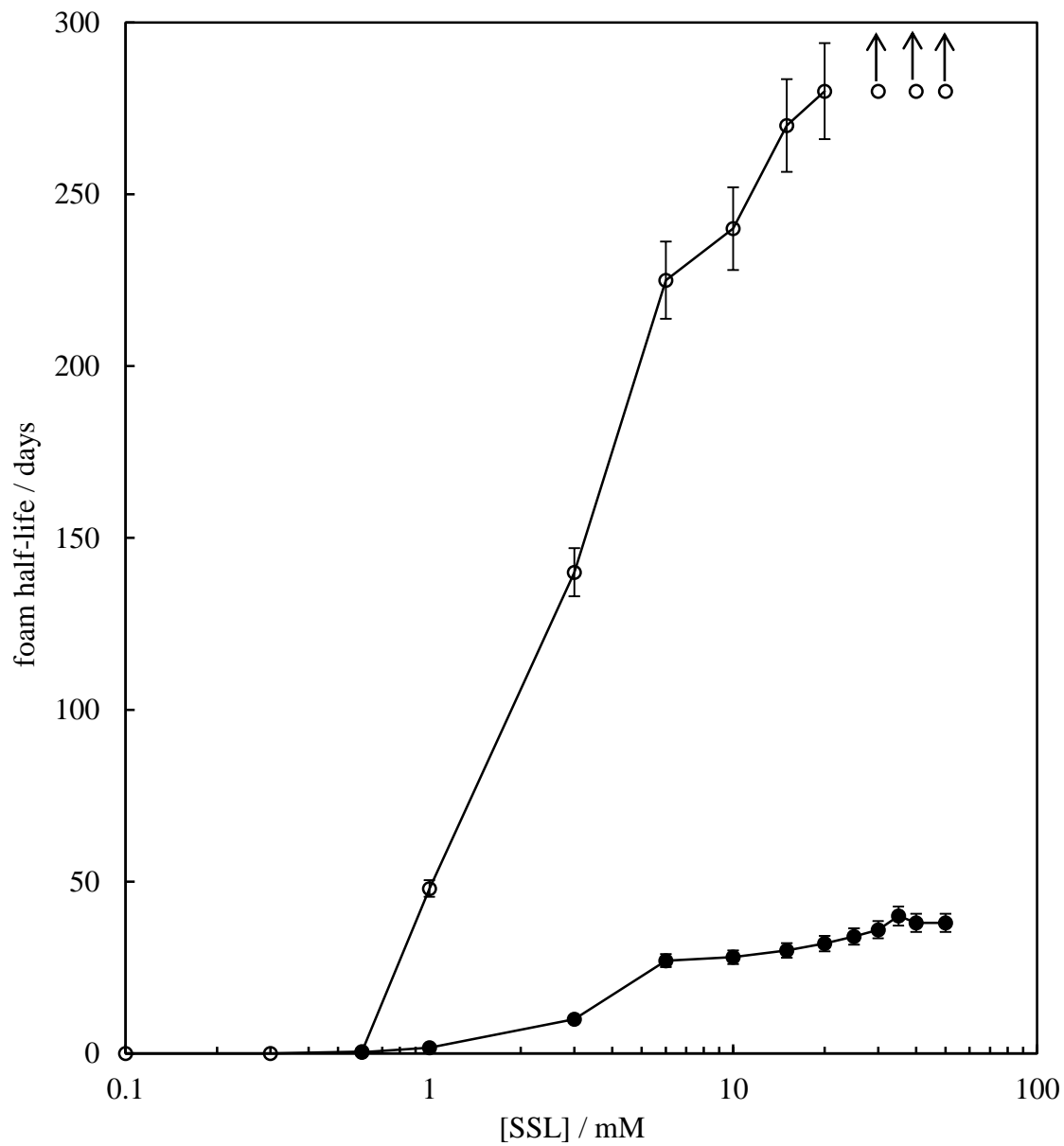


Figure 3.22. Percentage of particles associated with the foam *versus* surfactant concentration for foams from SSL + Calofort U PCC (1 wt. %) mixtures aerated by hand shaking for 30 seconds.

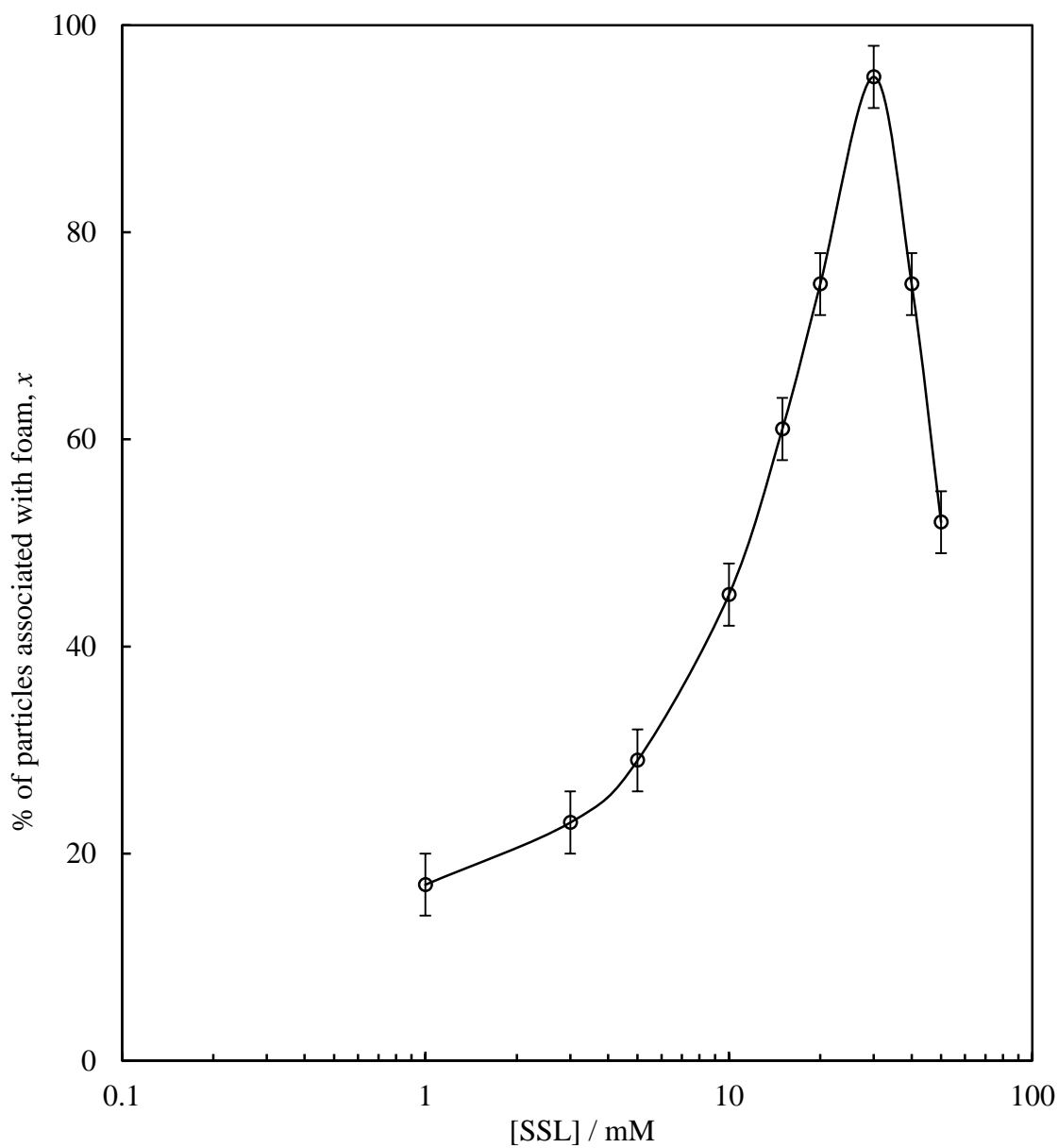
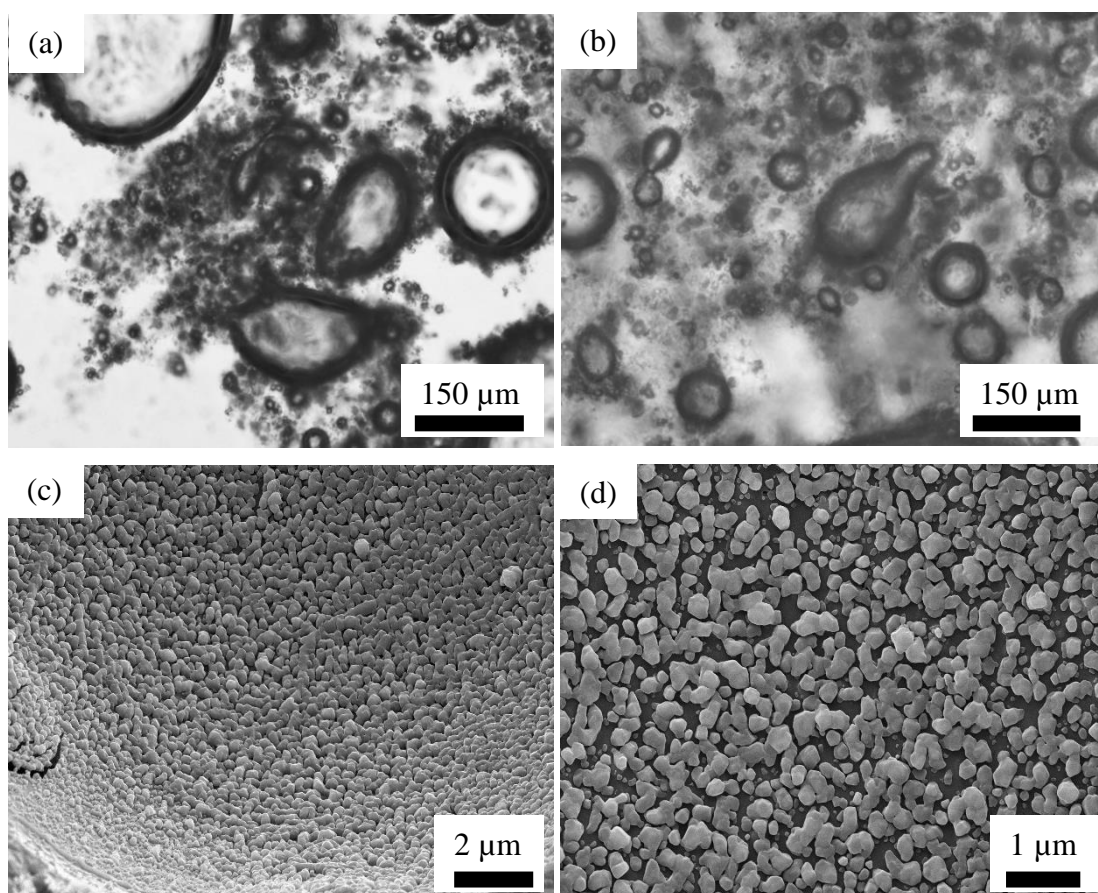


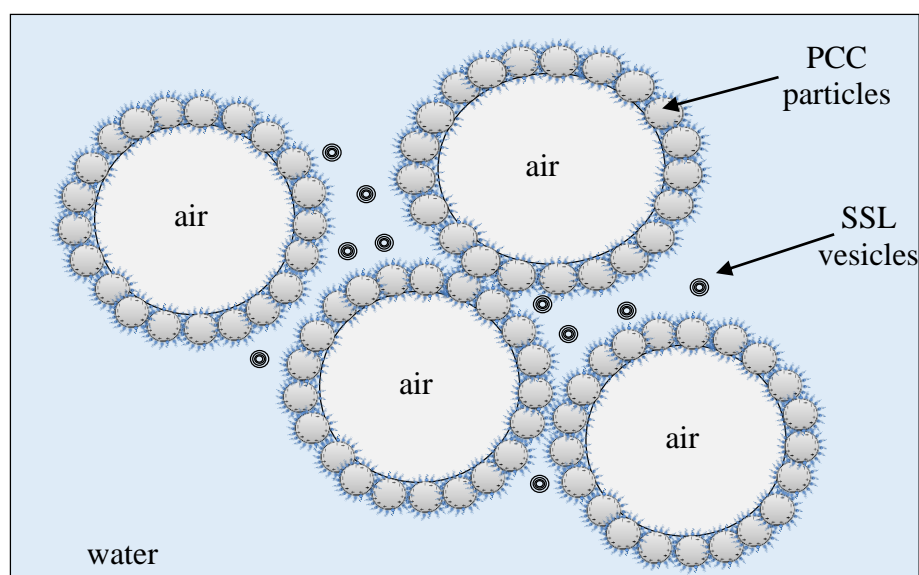
Figure 3.23 shows optical microscope and cryo-SEM images of SSL-PCC aqueous foams prepared by hand shaking for 30 seconds. In optical micrographs (a) and (b), non-spherical bubbles and the appearance of rough textured bubble surfaces are signatures of the presence of adsorbed particles. The adsorbed particles form a rigid layer around the air bubbles, which prevents shape relaxation to spheres during the aeration. From the cryo-SEM images (c) and (d) for 30 mM surfactant, a high coverage by particles of two adjacent bubble surfaces viewed from inside the bubbles can be seen clearly. At highest magnification (d), the discrete PCC particles of size around 200 nm are clearly evidenced on the surface of one of the bubbles.

Figure 3.23. Optical microscopy (a and b) and cryo-SEM (c and d) images of aqueous foams formed by hand shaking mixtures of 1 wt.% Calofort U particles and SSL at concentrations of (a) 1 mM and (b)-(d) 30 mM taken a few hours after formation. In (a) and (b) rough textured bubble surfaces and non-spherical shape are signatures of the presence of adsorbed particles. In (c) and (d) high coverage by particles of two adjacent bubble surfaces viewed from inside the bubbles are clearly visible.



It is believed that the high stability observed in foams from the mixtures compared to SSL alone foams arises from a combination of mechanisms. As explained in foams of SSL alone, SSL aggregates formed in the continuous phase enhance the stability of the aqueous film in between two adjacent air bubbles by reducing the rate of liquid drainage. In addition to that in SSL-PCC foams, discrete PCC particles adsorb around air cells as shown in the cryo-SEM images and create a rigid barrier around them, which eventually enhances the total stability of the system towards disproportionation and coalescence. This is shown schematically in Figure 3.24.

Figure 3.24. Schematic presentation of the behaviour of PCC particles and SSL aggregates within SSL-PCC aqueous foams.



The results from both foamability and foam stability can be compared with earlier ones in oppositely charged surfactant-particle systems for micelle-forming surfactants. For SDS-PCC mixtures, more foam is produced in mixtures at low surfactant concentration compared with surfactant alone whereas it is less at higher concentrations.¹⁵ In Aerosol OT (di-chain anionic)-PCC mixtures, the foamability is reduced at all surfactant concentrations,¹⁵ as it is in di-chain cationic-SiO₂ systems.⁹ It is thus clear that foam formation in the presence of particles is both system dependent and surfactant concentration dependent. In all cases however, the stability of foams is improved in the presence of particles and it passes through a maximum with respect to surfactant concentration.

Table 3.1 presents the stability data for aqueous foams of SDS, SSL and SSL-PCC solutions/dispersions aerated by hand shaking for 30 seconds at room temperature. Comparing SDS and SSL foams in terms of the time taken for complete foam collapse clearly shows the greater stability of SSL foams compared to SDS foams. SSL foams retain their volumes up to about 80 days for some concentrations, whereas SDS foams have a maximum life-time of around 2 days. Heat treatment was found to have no significant effect on the stability of SSL foams. Finally, aqueous foams of SSL-PCC mixtures showed exceptional stability with some at higher SSL concentrations losing only 30 % of their initial volume within a year.

Table 3.1. Stability of aqueous foams from 20 mL solutions/dispersions of SDS, SSL alone and SSL-PCC mixtures aerated by hand shaking for 30 seconds at room temperature (23 ± 1 °C). For non-heated samples surfactant powder was dispersed in water at room temperature. Heated samples were prepared by adding surfactant powder to water at room temperature and heated to 60 °C while stirring for 30 minutes. The samples then allowed to cool to room temperature naturally.

[surfactant] / mM	SDS	SSL		SSL + 1 wt. % Calofort U PCC
	time for complete foam collapse/hours	time for complete foam collapse/days		residual foam volume after 1 year as % of initial
	non-heated	non-heated	heat-treated	
0.1	4	1	no foam	0
0.3	16	3	no foam	0
0.6	18	9	1	0
1	18	14	4	17
3	28	30	21	33
6	52	69	60	38
10	51	77	62	33
20	53	81	80	37
30	50	80	78	76
40	51	76	72	73
50	48	75	76	60

3.9 Conclusions

A detailed study into the properties of aqueous foams stabilised by SSL alone and foams stabilised by mixtures of Calofort U PCC particles and SSL at their natural pH has been carried out.

Aqueous dispersions of Calofort U PCC particles were shown to be unstable towards sedimentation. Calofort U particles aggregate strongly and form structures with approximate diameter of 10 μm when they disperse in water. The particles were found to be positively charged at their natural pH and had an isoelectric point of $\text{pH} = 12$. Particles alone are shown to be ineffective foamers due to their extreme hydrophilicity, aggregation state and charge.

A detailed microscopic study of SSL aqueous dispersions revealed the formation of ordered lamellar phases and multi-layer vesicles. Aqueous foams produced from SSL alone were compared with those produced by the micelle-forming surfactant, SDS. The results confirmed that SSL foams are much more stable to coalescence with half-lives of up to forty days although SDS foams had better foamability. In SSL foams, the bubbles are stabilised by the open-ended planar lamellar aggregates that cover the air cells as well as micron-sized vesicles that block the thin films and Plateau borders hence increasing the stability of the foams towards coalescence, disproportionation and drainage.

Adsorption of anionic SSL monomers onto the surface of positively charged Calofort U PCC particles was confirmed by zeta potential measurements and the results were confirmed with contact angle measurements of SSL aqueous droplets on pressed disks of PCC particles. The adsorption isotherm of SSL monomers on Calofort U particles was also determined, showing a cooperative adsorption up to 0.1 mM SSL. In addition, the *in situ* surface activation of particles was shown to prevent the strong aggregation between particles and particle size distribution results confirmed the presence of primary particles. This also increased the hydrophobicity of PCC particles promoting their adsorption to the surface of the bubbles in the foam prepared from the SSL-PCC mixture. The foamability of the mixtures was similar to that of foams of SSL alone but the foams from mixtures showed very high stability with half-lives around an order of magnitude higher at low concentrations and foams which only lose around 30% of their volume within a year at high concentrations. A high surface density of discrete

surfactant-coated particles at foam bubble surfaces was observed using cryo-SEM, which is believed to promote the stability of these foams to coalescence and disproportionation.

3.10 References

1. *The Physics of Foams*, D. Weaire and S. Hutzler, Clarendon Press, Oxford, 2001.
2. Y.Q. Sun and T. Gao, *Metall. Mater. Trans. A-Phys. Metall. Mater. Sci.*, **33**, 3285 (2002).
3. Z.P. Du, M.P. Bilbao-Montoya, B.P. Binks, E. Dickinson, R. Ettelaie and B.S. Murray, *Langmuir*, **19**, 3106 (2003).
4. E. Dickinson, R. Ettelaie, T. Kostakis and B.S. Murray, *Langmuir*, **20**, 8517 (2004).
5. R.G. Alargova, D.S. Warhadpande, V.N. Paunov and O.D. Velev, *Langmuir*, **20**, 10371 (2004).
6. B.P. Binks and T.S. Horozov, *Angew. Chem. Int. Ed.*, **44**, 3722 (2005).
7. B.P. Binks, *Curr. Opin. Colloid Interface Sci.*, **7**, 21 (2002).
8. B.S. Murray and R. Ettelaie, *Curr. Opin. Colloid Interface Sci.*, **9**, 314 (2004).
9. B.P. Binks, M. Kirkland and J.A. Rodrigues, *Soft Matter*, **4**, 2373 (2008).
10. I. Grosse and K. Estel, *Colloid Polym. Sci.*, **278**, 1000 (2000).
11. P. Somasundaran and L. Zhang, *J. Petrol. Sci. Eng.*, **52**, 198 (2006).
12. L.R. Arriaga, W. Drenckhan, A. Salonen, J.A. Rodrigues, R. Íñiguez-Palomares, E. Rio and D. Langevin, *Soft Matter*, **8**, 11085 (2012).
13. Q. Liu, S. Zhang, D. Sun and J. Xu, *Colloids Surf. A*, **355**, 151 (2010).
14. U.T. Gonzenbach, A.R. Studart, E. Tervoort and L.J. Gauckler, *Angew. Chem. Int. Ed.*, **45**, 3526 (2006).
15. Z.G. Cui, Y.Z. Cui, C.F. Cui, Z. Chen and B.P. Binks, *Langmuir*, **26**, 12567 (2010).
16. S. Zhang, D. Sun, X. Dong, C. Li and J. Xu, *Colloids Surf. A*, **324**, 1 (2008).
17. E. Armero and C. Collar, *J. Cereal Sci.*, **28**, 165 (1998).
18. M. Gómez, S. del Real, C.M. Rosell, F. Ronda, C.A. Blanco and P.A. Caballero, *Eur. Food Res. Technol.*, **219**, 145 (2004).
19. R.S. Manohar and P.H. Rao, *J. Sci. Food Agric.*, **79**, 1223 (1999).
20. R.B. Swanson, L.A. Garden and S.S. Parks, *J. Food Qual.*, **22**, 19 (1999).
21. P.M. Kelly, D.J. Oldfield and B.T. O'Kennedy, *Int. J. Dairy Technol.*, **52**, 107 (1999).
22. J.B. Bezelgues, S. Serieye, L. Crosset-Perrotin and M.E. Leser, *Colloids Surf. A*, **331**, 56 (2008).

23. E.N.C. Mills, P.J. Wilde, L.J. Salt and P. Skeggs, *Food Bioprod. Process.*, **81**, 189 (2003).
24. *Food Emulsions*, ed. K. Larsson, S.E. Friberg and J. Sjöblom, 4th edn., Marcel Dekker Inc., New York, 1997.
25. N. Duerr-Auster, J. Kohlbrecher, T. Zuercher, R. Gunde, P. Fischer and E. Windhab, *Langmuir*, **23**, 12827 (2007).
26. TriStar 3000 Operator's Manual V6.08, Micromeritics Instrument Corporation, United States, 2007.
27. Calofort U Precipitated Calcium Carbonate Product Information, Specialty Minerals Inc., UK, 2004.
28. G. Renaudin, A. Bertrand, M. Dubois, S. Gomes, P. Chevalier and A. Labrosse, *J. Phys. Chem. Solids*, **69**, 1603 (2008).
29. S. Teir, S. Eloneva and R. Zevenhoven, *Energy Convers. Manag.*, **46**, 2954 (2005).
30. J.J. Kokelaar, J.A. Garritsen and A. Prins, *Colloids Surf. A*, **95**, 69 (1995).
31. I. Heertje, E.C. Roijers and H.A.C.M. Hendrickx, *LWT - Food Sci. Technol.*, **31**, 387 (1998).
32. *Applied Surfactants: Principles and Applications*, T.F. Tadros, Wiley-VCH, Weinheim, 2005.
33. *Surfactants and Interfacial Phenomena*, M.J. Rosen, Wiley, New Jersey, 2004.
34. B.P. Binks, A.J. Johnson and J.A. Rodrigues, *Soft Matter*, **6**, 126 (2010).
35. P.R. Garrett and P.L. Gratton, *Colloids Surf. A*, **103**, 127 (1995).
36. B. Novales, A. Riaublanc, L. Navailles, B. Houinsou Houssou, C. Gaillard, F. Nallet and J.P. Douliez, *Langmuir*, **26**, 5329 (2010).
37. D. Varade, D. Carriere, L.R. Arriaga, A.L. Fameau, E. Rio, D. Langevin and W. Drenckhan, *Soft Matter*, **7**, 6557 (2011).
38. *Intermolecular and surface forces*, J. Israelachvili, 2nd Edition, Academic Press Ltd, London, 1992.
39. V. Subramanian and W.A. Ducker, *Langmuir*, **16**, 4447 (2000).
40. T. Kurth, G. Biresaw and A. Adhvaryu, *J. Am. Oil Chem. Soc.*, **82**, 293 (2005).

CHAPTER 4 MODEL WHIPPING CREAM EMULSIONS AND AERATED EMULSIONS

4.1 Introduction

Whipped cream is a classic food foam, an aerated oil-in-water emulsion, in which the air bubbles are surrounded to varying degrees by partially-coalesced fat droplets. The fat droplets in a whippable cream contain both crystallised and liquid portions. During aeration of such cream, the crystals of one droplet pierce the film of another, which eventually allows droplets to clump irreversibly together to form a network. The identity of the initial individual fat droplets in the clumps is still retained due to the Solid Fat Content (SFC) of the droplets.¹⁻⁴ The structural properties of a whipped cream sample is crucial for its applications such as cake toppings. The stiff structure of a whipped cream sample is known to be supported by the rigid three-dimensional network, formed from partial coalescence of the fat droplets during the aeration process and also high viscosity in the serum phase.⁵⁻⁸

Commercial whipped creams are complicated colloid systems and they contain multiple phases including; aqueous solutions of sugar, proteins, surfactants, fat droplets, polymers and air cells. Aeration of a whipping cream such as Vanilla Bettercreme® (VBC), a non-dairy ready-to- whip cream manufactured by the sponsor of the project, yields a foam in which not all the destabilisation processes are halted. From a thermodynamical point of view, these foams are by definition unstable systems and instability processes such as disproportionation, drainage and coalescence still occur to varying degrees after whipping. This is not desirable in their applications and there are several studies attempting to improve the overall stability of whipped cream using new stabilisers and techniques. Camacho *et al.*^{9, 10} studied the influence of locust bean gum and λ -carrageenan mixtures, as thickening agents, on the whipping properties and stability of dairy creams. They found that the stability of whipped dairy products increased upon addition of locust bean gum and λ -carrageenan mixtures due to an increase in the aqueous phase viscosity. Sajedi *et al.*¹¹ examined the addition of conformationally modified Whey Protein Concentrate (WPC), as stabilisers, on the stability of low fat model whipped cream samples. They found that addition of modified WPC to model whipped cream increased the viscosity (of the un-whipped cream), firmness and decreased the syneresis of the whipped cream, leading to a better stability

in the final products. In different studies, Zhao *et al.* studied the effects of hydroxypropyl methylcellulose,¹² sodium caseinate and whey proteins¹³ and xanthan gum¹⁴ on the structure and stability of whipped cream.

The role of fat droplets is known to be crucial for stabilising air cells as well as rheological and sensory properties of the final whipped cream product. Recent advances in stabilising aqueous foams using solid particles¹⁵⁻¹⁹ initiated the desire to investigate the effect of such particles on the aeration properties of whipping cream. As explained in detail in Chapter 3, PCC particles were selected to investigate whether they could fulfil all or part of the role played by fat droplets in stabilising air bubbles in whipped cream. In addition, this may enable a decrease in the fat content of such whipped cream products, desirable for certain consumers. Studies have been done recently on reducing the fat content of whipped cream. For instance, Padiernos *et al.*²⁰ investigated the effect of modified whey proteins using high hydrostatic pressure to improve the foaming properties of low-fat whipping cream. Starch particles and starch derivatives have also been of interest for scientists^{21, 22} as fat replacements in dairy emulsions and foams and their addition has shown to improve the viscosity and minimise the syneresis from dairy foams.

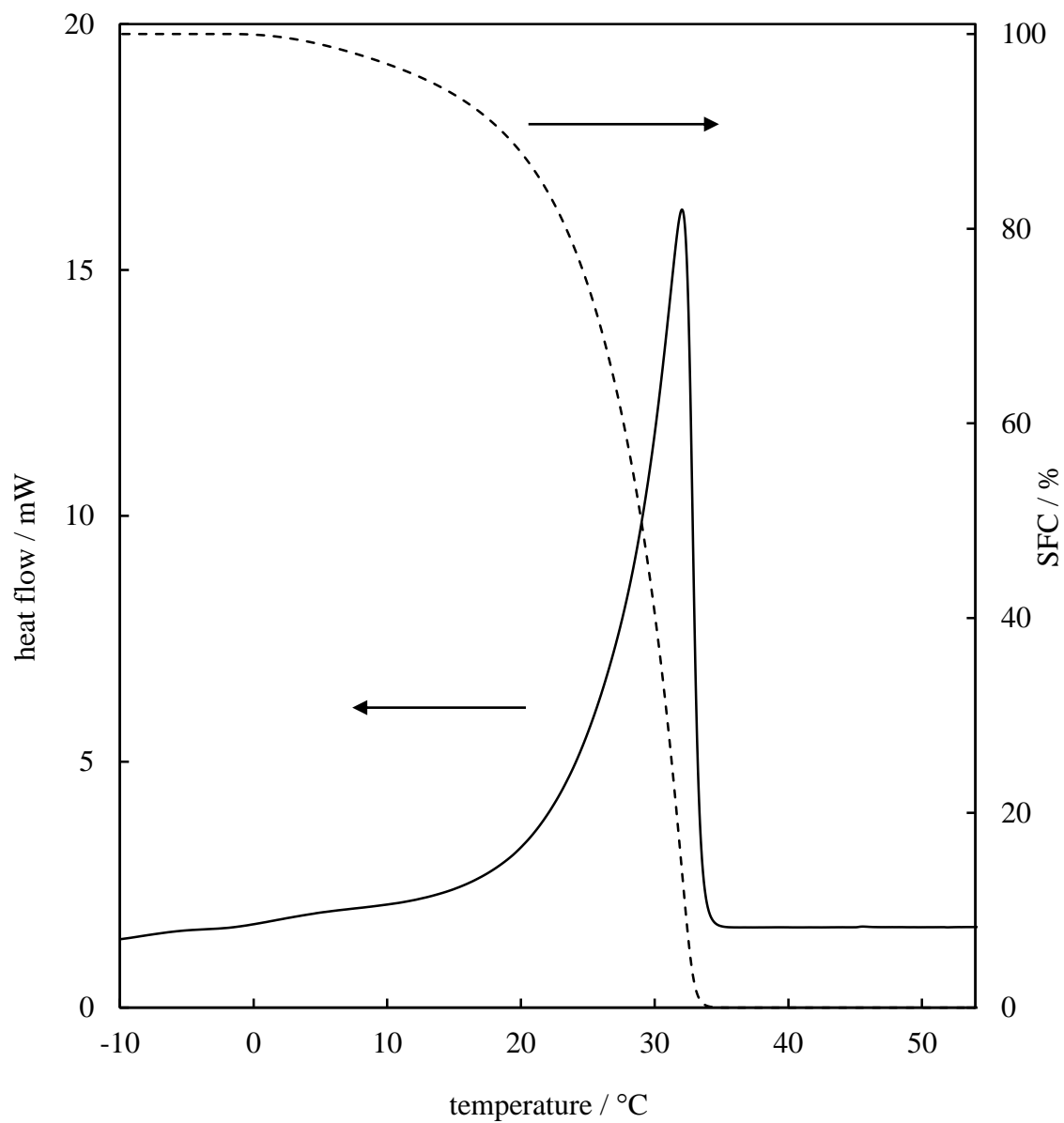
As detailed in Chapter 3, the initial step in this project was to study the foaming behaviour of one of the key ingredients of VBC, Sodium Stearoyl Lactylate (SSL). The interactions between SSL and PCC particles were studied in detail and the synergistic effect in stabilising aqueous foams using mixtures of SSL-PCC was shown. This chapter continues the progress in the preparation of model whipping cream samples by incorporating PKO as the oil phase in the dispersions. The melting behaviour of bulk PKO is studied using DSC to determine its SFC at different temperatures. The PKO droplet size distributions in model cream emulsions are compared with those in un-whipped VBC. The quality parameters of model whipped samples such as the increase in volume (overrun), stiffness and elasticity of the whipped cream, definition of the rosette made from whipped creams and their physical stability (*i.e.* the extent of drainage) are characterised and the results are compared to the properties of whipped VBC. The effect of particle concentration, PKO volume fraction and whipping duration on various properties of the foams are also investigated. It has also been attempted to make the link between the stability of the model whipped cream samples and the adsorption of SSL-coated PCC particles at the air-water interface using cryo-SEM.

4.2 Melting behaviour of bulk palm kernel oil *via* thermal analysis

Palm Kernel Oil (PKO) is used in a range of non-dairy food foams such as VBC, produced by the sponsor of the project. As mentioned earlier in Chapter 2, PKO is a commercial oil and because it consists of a mixture of different TAGs, it melts and crystallises over a range of temperatures rather than at a single point. This causes the PKO to have different SFC values at different temperatures. An understanding of the SFC of PKO is important for developing the structure, stability and rheology of whipped cream samples. DSC is the technique used to characterise bulk PKO regarding its melting behaviour and also to determine its SFC. The DSC trace for a 3.32 mg sample of PKO is given in Figure 4.1 in which heat flow and SFC curves are plotted versus temperature. It can be seen that upon heating, a single melting curve arises gradually from an onset temperature of 27.6 °C up to the melting peak at 32.6 °C. Jin *et al.*²³ characterised a sample of PKO from another source using DSC and they also found a single melting peak around the same temperature range. The enthalpy change associated with the melting peak was calculated to be 150.4 J g⁻¹. The melting temperature and enthalpy values are comparable with those reported by Siew²⁴ for a different source of PKO.

The variation of the SFC of PKO as a function of temperature is also shown in Figure 4.1. The SFC values were deduced as a function of temperature from the integration of the area below the melting curve using the Perkin Elmer software. As can be seen, the SFC decreases when the temperature is increased from -10 °C (when the oil is fully crystallised, 100% SFC) to 40 °C (when the oil is fully melted, 0% SFC). There is no change in SFC when there is no phase transition. The melting range below human body temperature results in a pleasant mouth feeling during consumption of the whipped creams produced using PKO as the oil phase.

Figure 4.1. DSC curve of the melting peak (solid line, left hand coordinate) and SFC (dashed line, right hand coordinate) of bulk PKO. (endo is up).



4.3 Model whipping cream emulsions

Having studied various properties of aqueous SSL-PCC mixtures dispersions and foams (Chapter 3) as well as the melting properties of bulk PKO, the next step towards the preparation of model whipping cream was to include PKO droplets in to the dispersions. From the previous chapter, it was found that aqueous dispersions with 30 mM SSL had high foamability and showed great foam stability in the presence of PCC particles. An SSL concentration of 1.35 wt % with respect to total emulsion volume (equivalent to 30 mM of SSL) was selected to apply in the formulation of the model cream emulsions. Xanthan gum was also added as a thickening agent in the model cream formulations as recommended by the sponsor of the project and is known to have no activity at an air-water interface. Variation of the xanthan gum concentration was found to have no effect on the overrun of the model whipped cream, similar to the finding of Zhao *et al.*¹⁴ Model whipping cream emulsions containing PKO (20 wt. %), SSL (1.35 wt. %), xanthan gum (0.1 wt. %) and water (78.55 wt. %) were prepared as detailed in Section 2.2.10.1.1. The concentrations of the ingredients are expressed with respect to the total emulsion volume. The homogenisation was carried out at 80 °C to ensure PKO was fully melted (0 % SFC).

Initially it was attempted to homogenise the PKO with the mixture of SSL-PCC at 80 °C in the HPH. However in this protocol there was no control on the adsorption of PCC particles around oil droplets. Using optical microscopy and light scattering techniques it was found that homogenisation of the emulsion in the presence of both PCC and PKO caused the formation of large clumps (> 500 µm) of PKO-PCC and accumulation of such clumps caused blockage in the homogenisation apparatus. Therefore, it was decided to stabilise PKO droplets in the model emulsions using SSL only and add PCC particles at a later stage. It was found that when the PCC particles were added as an aqueous dispersion to the prepared emulsion just before aeration, the whipped samples presented high overrun values and great stability. It is thought that PCC particles would interact with excess SSL within the emulsion and gain the hydrophobicity required for their adsorption around air bubbles during whipping.

All the processing, storage and whipping conditions of model whipping cream samples were advised by the sponsor of the project. These include the homogenisation temperature of 80 °C, homogenisation pressures of 180 and 30 bar at the first and second

stages of the HPH, cooling to 35 and 4 °C at the first and second heat exchangers, storage of the prepared emulsion in a fridge at 6 °C for 24 hours after emulsification (before aeration), a whipping temperature of 8 °C and an aeration speed of 130 rpm using the bench top Hobart mixer.

As detailed in Section 2.2.10.1.1. the model cream emulsion was passed through heat exchangers to induce crystallisation in PKO droplets and give optimum whipping characteristics to the model cream. The model cream was therefore at 4 °C when exiting the HPH. The model cream was confirmed to be an oil-in-water emulsion using the drop test immediately after preparation. Approximately 50 mL of the model cream was collected in a glass vessel and left in a fridge at 6 °C to assess its stability towards creaming and coalescence. Figure 4.2 shows the appearance of the model cream emulsion immediately and one day after preparation. The emulsion had a white appearance and no visual change was observed in its appearance after one day and the emulsion was found to be fully stable towards creaming.

Figure 4.2. Appearance of a model whipping cream emulsion containing 20 wt. % PKO, 1.35 wt. % SSL, 0.1 wt. % xanthan gum and 78.55 wt. % water taken immediately (left) and one day (right) after preparation. The emulsion was at 4 °C immediately after exiting the HPH (left) and was stored in a fridge at 6 °C overnight (right). The emulsion was found to be fully stable towards creaming one day after preparation.



The size distribution of PKO droplets within the model cream emulsions was determined immediately and one day after homogenisation to assess the stability of the droplets towards coalescence when stored at 6 °C overnight. In addition, a sample of the pre-emulsion before passing through the HPH was analysed to evaluate the effect of homogenisation on the size of PKO droplets. Figure 4.3 shows the size distribution data for the model cream emulsion before passing through the HPH (pre-emulsions), immediately after exiting the HPH and after one day storage at 6 °C. The size distribution of PKO droplets in un-whipped VBC, stored at 6 °C overnight, is also presented, which shows a similar distribution to the model cream after homogenisation. It is clear from the curves that HPH significantly decreases the size of PKO droplets; a median $d(0.5)$ of 10 μm in the pre-emulsion becomes around 150 nm in the final emulsion released from the HPH. The particle size distribution of the droplets measured one day after storage at 6 °C shows a major peak at around 150 nm and a small shoulder at around 600 nm. The major peak shows that the PKO droplets were stable towards coalescence, however the small peak reveals that PKO droplets aggregate to some extent during storage. Since it was aimed to produce model whipping cream emulsions with PKO droplets of the same size as those in the un-whipped VBC, pressures applied for homogenisation were not varied for any sample within this project. In a recent study, Kurukji *et al.*²⁵ prepared sunflower oil-in-water emulsions stabilised by SSL using a similar HPH pressure of 100 bar. The size distribution of oil droplets in their emulsions had a $d(3,2)$ of 2 μm and their experiments showed that SSL concentration had no effect on the droplet size at fixed homogenisation pressure.

Figure 4.3. Size distribution of PKO droplets in the model cream emulsion (20 wt. % PKO, 1.35 wt. % SSL, 0.1 wt. % xanthan gum and 78.55 wt. % water) measured before homogenisation in HPH as a pre-emulsion (blue), immediately after exiting the HPH (red) and one day after storage at 6 °C (black). The green curve shows the size distribution of PKO droplets in un-whipped VBC. The pre-emulsion was prepared by mixing the ingredients using a Bosch hand blender at 80 °C in a double boiler. As shown by the curves, homogenisation in the HPH breaks down the PKO droplets by a factor of 100. The size of PKO droplets in the model cream are similar to those in VBC.

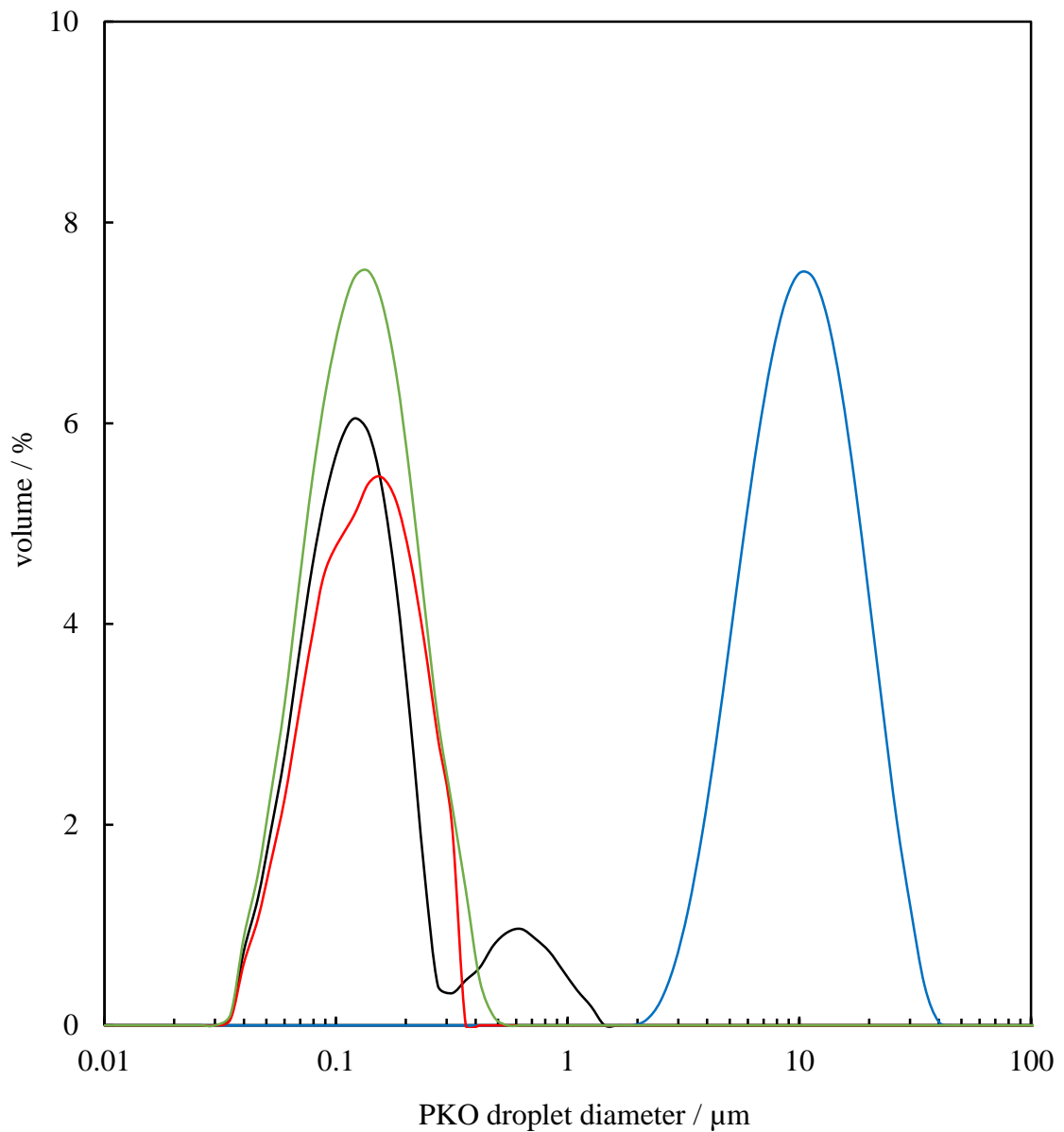
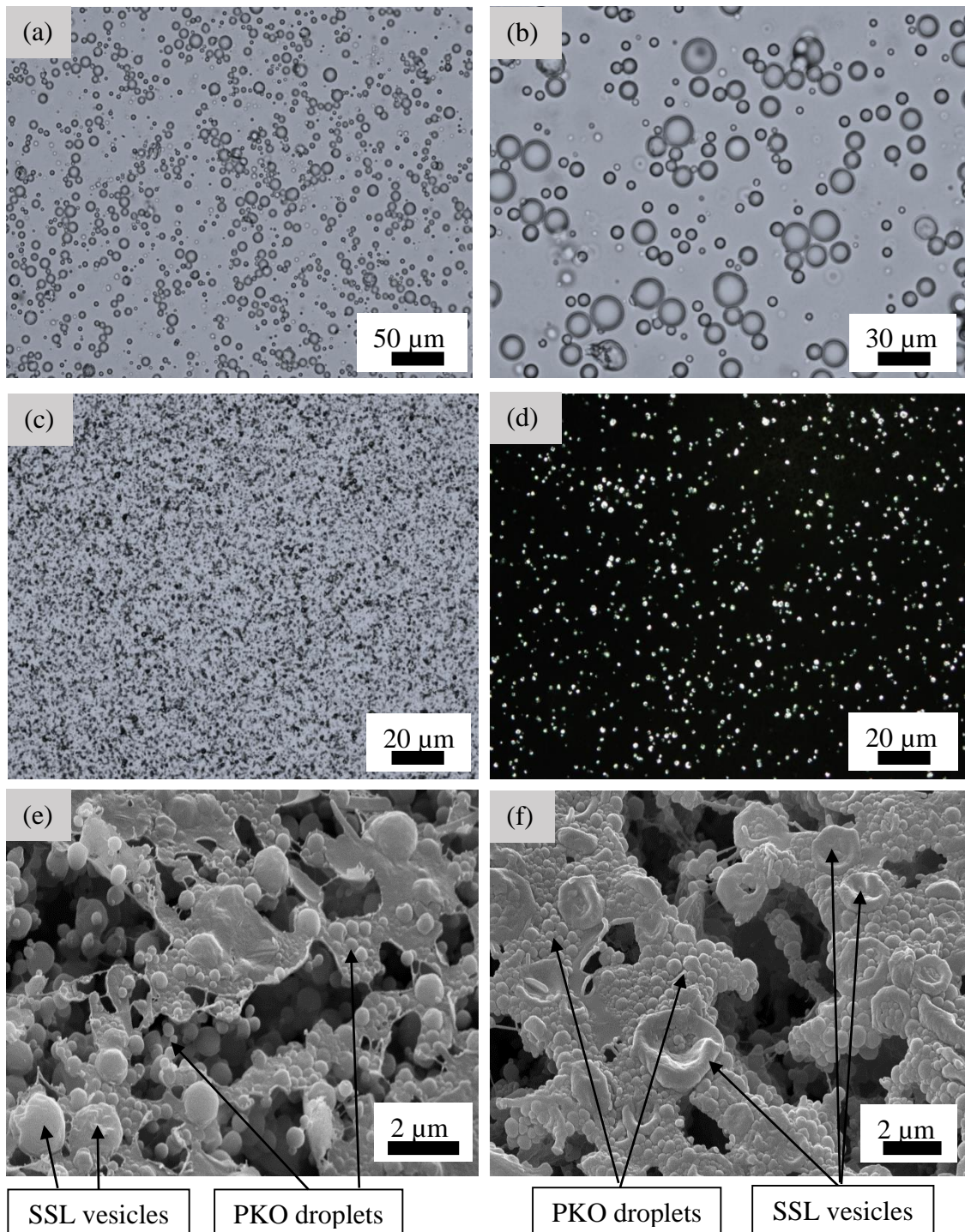


Figure 4.4 shows optical microscope and cryo-SEM images of the model cream as a pre-emulsion (a and b) and after homogenisation in the HPH (c-f). In (a) and (b) PKO droplets in the pre-emulsion are shown to be all spherical and polydisperse. The images show that the size of droplets are in agreement with a median diameter $d(0.5)$ of 10 μm obtained using light scattering. Image (c) shows the optical micrograph of the emulsion after homogenisation in the HPH in which individual PKO droplets are not recognisable being sub-micron. The same sample was observed using crossed-polarizers and crystallised PKO droplets and/or SSL vesicles are shown as bright spots in image (d). Cryo-SEM images of the model cream emulsion in (e) and (f) clearly show spherical PKO droplets together with SSL vesicles. The size of the droplets in the model cream emulsion shown in the images is in agreement with the median diameter $d(0.5)$ of 150 nm obtained using light scattering.

Figure 4.4. Optical microscope and cryo-SEM images of the model cream emulsion (20 wt. % PKO, 1.35 wt. % SSL, 0.1 wt. % xanthan gum and 78.55 wt. % water). Images (a) and (b) are optical micrographs of the pre-emulsion made using the hand mixer before homogenisation in the HPH. Images (c) and (d) show optical micrographs without and with crossed polarisers of the model cream emulsion after homogenisation in the HPH. Images (e) and (f) are cryo-SEM images of the model cream emulsion taken one day after homogenisation in which PKO droplets and SSL vesicles are highlighted.



4.4 Model whipped cream foams

4.4.1 Influence of particle concentration on whipping properties

4.4.1.1 Overrun

The effect of PCC particle addition on the aeration properties of the model cream emulsions was studied. As mentioned earlier, model cream emulsions were stored in a fridge at 6 °C for 24 hours, before their aeration. The temperature of the model cream emulsions was 8 °C in the whipping bowl. The PCC particles were added as an aqueous dispersion (10 mL, 8 °C) to the emulsion followed by aeration at room temperature. For this purpose PCC particles were ultrasonically dispersed in pure water, similar to those prepared in Chapter 3. The particles were therefore aggregated and had a $d(0.5)$ around 10 μm determined using light scattering.

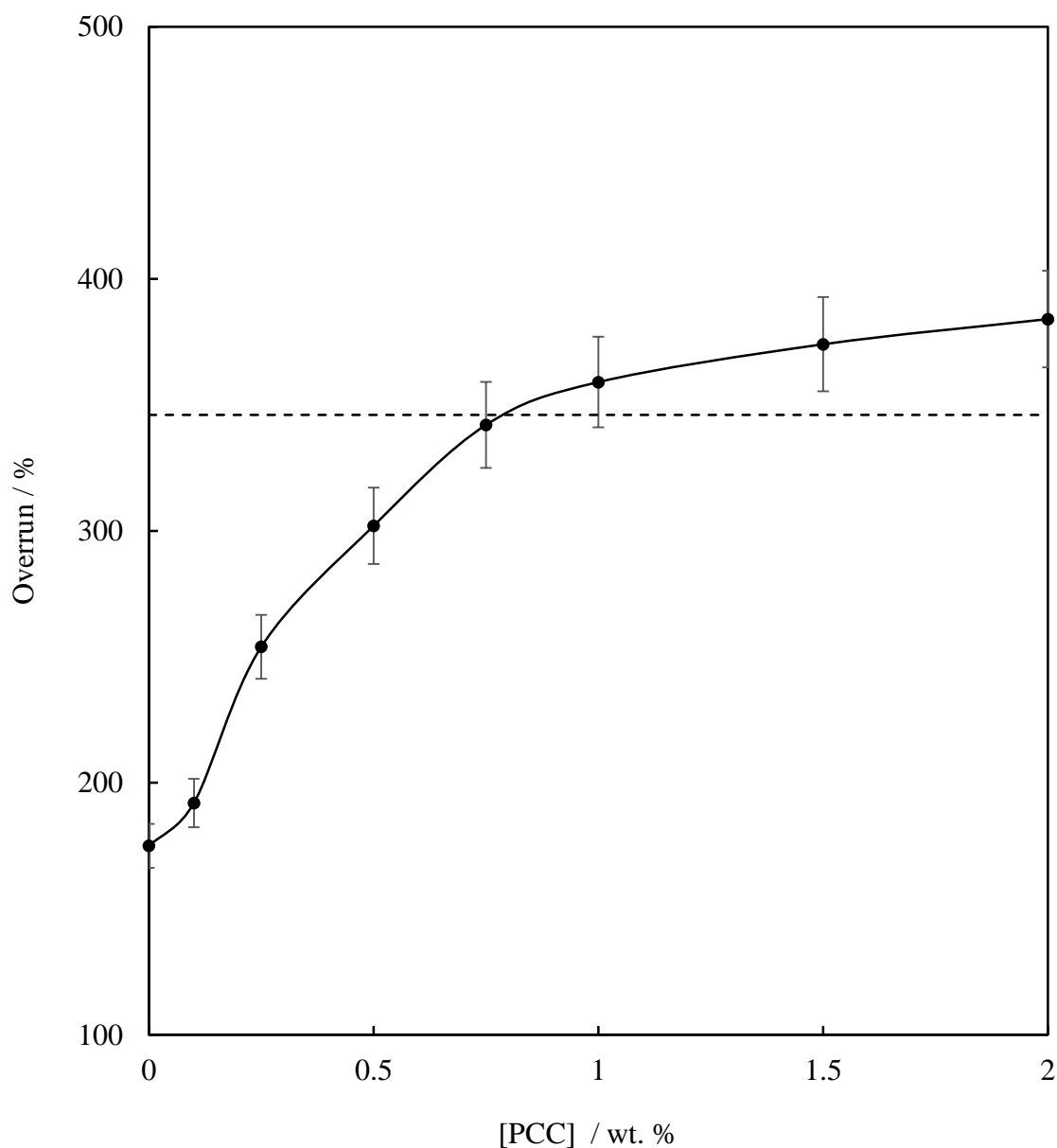
The method for calculating Overrun is given in equation 2.1 in Chapter 2 and the results are shown in Figure 4.5 with increasing PCC concentration. As shown in the figure, the sample without PCC particles had a very low overrun value. It was observed that after aeration such foam was watery and soft. As the concentration of PCC particles increased the overrun values were raised and reached 360 % at 1 wt. % PCC particles. This was higher than an overrun value of 346 % measured for whipped VBC (dashed line). The significant increase in the overrun values of the model foams, upon increasing PCC concentration, suggests that the PCC particles adsorb around air bubbles and eventually enhance the amount of air incorporated in the emulsions. The overrun value remained nearly constant above 1 wt. % particle concentration.

As mentioned earlier there are different ways to report the amount of air incorporated into an emulsion upon whipping. The method detailed in Chapter 2 was advised by the sponsor of the project, however the air volume fractions of the foams can also be calculated using the equation below for a clearer understanding of the amount of air in foams.

$$\phi_{air} = 1 - \frac{m_F}{V_F \rho} \quad (4.1)$$

where ρ is the density of emulsion, m_F is mass of foam (fixed volume) and V_F is volume of foam (fixed). For example, 346 % overrun represents $\phi_{air} = 0.73$ and 200% overrun is equivalent to $\phi_{air} = 0.52$.

Figure 4.5. Overrun values of model whipped cream foams upon increasing PCC particle concentration aerated for 12 minutes. 12 minutes was found to be the optimum aeration time for model cream samples, determined using peaking assessment (shown later). Dashed line shows the overrun of whipped VBC aerated for 6 minutes. The composition of the model cream was 20 wt. % PKO, 1.35 wt. % SSL, 0.1 wt. % xanthan gum and 78.55 wt. % water. The PCC concentration is with respect to the cream volume in the whipping bowl.



4.4.1.2 Structural properties and stability

Aerated model creams were analysed in terms of their stiffness and structural properties using peaking evaluation, rosette definition assessment and rheology measurements. Figure 4.6 shows the peaking evaluation of aerated model whipping creams with different PCC concentrations followed by the peaking evaluation grades presented in Table 4.1. Peaking evaluation was used to determine the optimum whipping duration and also the stiffness of whipped cream samples. In image (a) the peaking of the model whipped foam without PCC particles is shown, which does not hold its structure on the whisk and has no stiffness. The stiffness of the foams was improved with increasing PCC concentration and the model whipped cream with 1 wt. % PCC (e) shows similar peaking properties to whipped VBC shown in image (f). Whipped VBC has a pale yellow appearance due to the presence of other ingredients such as corn syrup, sodium caseinate and vanilla flavour, which are absent in the model foams.

Figure 4.7 shows the rosette structure of model whipped foams with different PCC concentrations formed immediately after whipping using a pastry bag equipped with a star shape nozzle. Similar to the observations from the peaking evaluation, definition of the rosette was improved with increasing PCC concentration and rosettes with sharp edges were formed for the sample with 1 wt. % PCC particles. The tailing of the top peaks and the surface roughness was also improved as the concentration of PCC increased. The model whipped cream sample with 1 wt. % PCC shows similar rosette properties to whipped VBC.

Figure 4.6. Peaking evaluation of the model whipped cream foams with 0, 0.1, 0.5, 0.75 and 1 wt. % PCC particles shown in images (a), (b), (c), (d) and (e) respectively. Image (f) shows whipped VBC on top of the inverted whisk taken immediately after aeration. Peaking test as explained in Chapter 2 was used to determine the optimum whipping time and to grade the stiffness of the whipped cream. It is clear that the stiffness increases with PCC concentration and the sample with 1 wt. % PCC produces similar results to the whipped VBC. The composition of the model cream (a-e) was 20 wt. % PKO, 1.35 wt. % SSL, 0.1 wt. % xanthan gum and 78.55 wt. % water. Scale bar represents 3 cm.

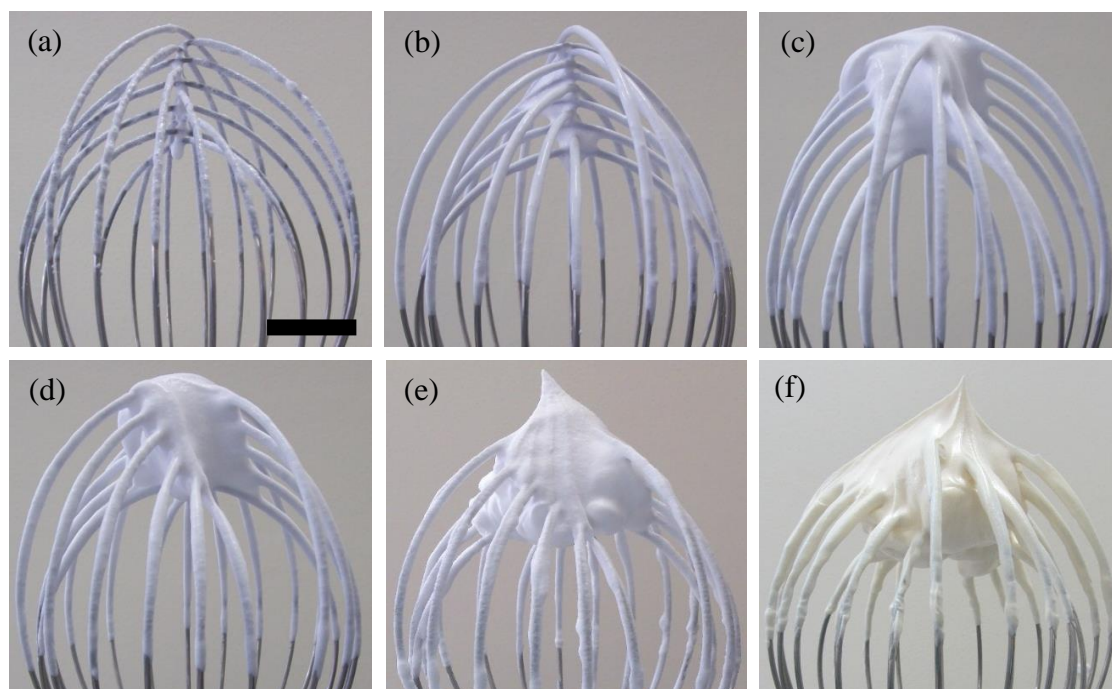
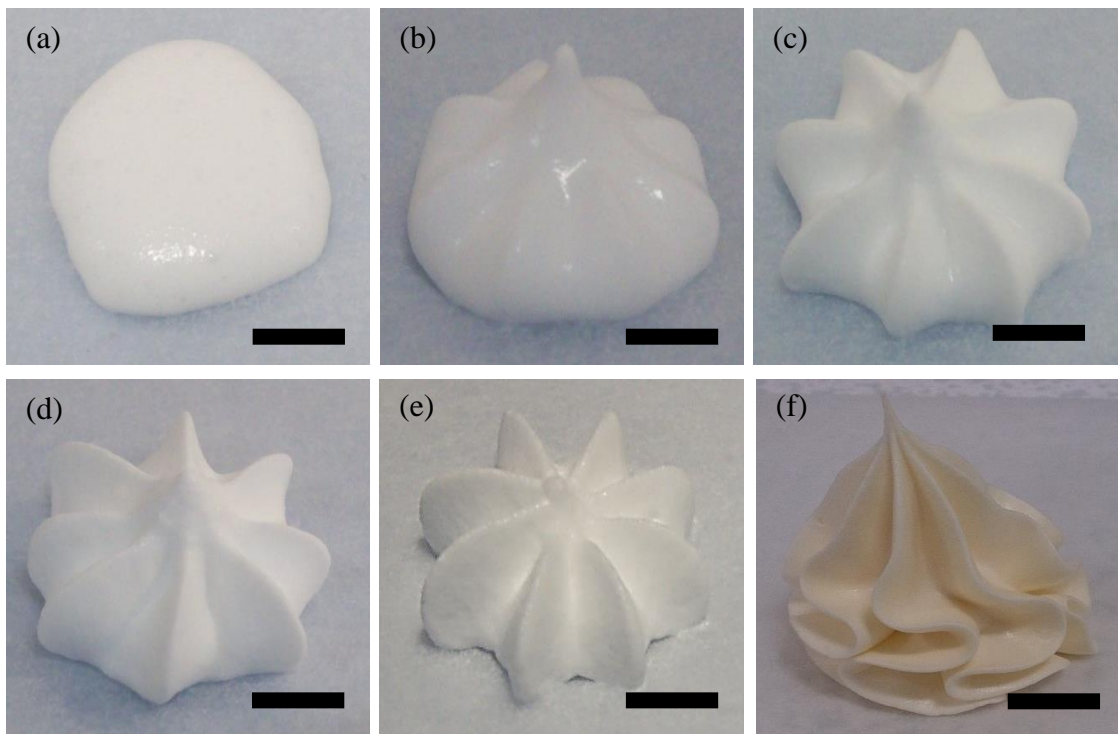


Table 4.1. Peaking evaluation grades for model whipped cream foams with different PCC concentrations based on the images in Figure 4.6. Last column shows the peaking grade of whipped VBC. The grading scale was explained in Chapter 2.

[PCC] / wt. %	0	0.1	0.5	0.75	1	VBC
Peaking grade	1	1	2	2	4	5

Figure 4.7. Rosette structure evaluation of the model whipped creams with 0, 0.1, 0.5, 0.75 and 1 wt. % PCC particles shown in images (a), (b), (c), (d) and (e) respectively. Image (f) shows a rosette of whipped VBC taken immediately after aeration. Rosette structure evaluation as explained in Chapter 2 was used to determine the life-time of the foam in a pastry bag and also to grade the definition of the rosette. It is clear that the definition of the rosette improves with PCC concentration and the sample with 1 wt. % PCC produces a similar rosette to the rosette from whipped VBC. The composition of the model cream (a-e) was 20 wt. % PKO, 1.35 wt. % SSL, 0.1 wt. % xanthan gum and 78.55 wt. % water. Scale bars represent 1 cm.



Aerated model cream foams were characterised using cryo-SEM to visually locate the position of PKO droplets and PCC particles in foam samples. Figure 4.8 and Figure 4.9 show the cryo-SEM images of model whipped cream samples without and with 1 wt. % PCC particles respectively. The foam without PCC particles, shown in Figure 4.8, was soft and brittle and this caused the formation of debris during sample preparation as shown in image (a). An average air bubble diameter of $610 \pm 30 \mu\text{m}$ was measured for this sample. Image (c) reveals the partially coalesced PKO droplets in the thin film between two air cells. The inner surface of an air cell is shown in image (d) in which closely packed and/or partially coalesced PKO droplets are visible. The adsorption of fat droplets to the surface of air cells in whipped cream has been shown previously.²⁶ Upon adding PCC particles to the model whipped samples, shown in Figure 4.9, the stiffness of the foam increases and the average bubble diameter decreased to $130 \pm 10 \mu\text{m}$ for the foam with 1 wt. % PCC particles. Unlike the sample without PCC particles, the whole volume of the emulsion was incorporated into the foam hence giving rise to thicker films between the bubbles. Inspecting the thin film in between two adjacent air bubbles reveals the three-dimensional network composed of fat droplets in a matrix of xanthan gum rods.^{27, 28} Close inspection of the inner surface of air bubbles shown in images (e) and (f) shows the presence of SSL vesicles together with PKO droplets and/or PCC particles. PCC particles were not distinguishable from PKO droplets in the Cryo-SEM images due to their similarity in size, the higher concentration of PKO droplets (20 wt. % PKO compared to 1 wt. % PCC) and also due to the Pt coating applied to the sample.

In contrast to the foams without PCC particles, it was observed that the inner surfaces of air bubbles were covered with SSL vesicles as can be seen in images (e) and (f). It is believed that SSL vesicles were driven to the air-water interface in the presence of PKO droplets and PCC particles or in other words SSL vesicles were pushed out of the water phase to the air-water interface upon formation of the three-dimensional network of partially coalesced PKO droplets. This further enhances the thickness and stability of the film around air bubbles, which eventually increases their stability.

Figure 4.8. Cryo-SEM images of the model whipped cream without PCC particles observed one day after whipping. The foam sample was stored at room temperature in a sealed vessel to avoid evaporation of water. The foam had a soft and brittle structure as shown in (a) by various debris formed during sample preparation for cryo-SEM analysis. In (b) a Plateau border in between three adjacent air cells is shown and image (c) shows the thin film in between two air cells. Image (d) shows the inner surface of an air cell clearly revealing the PKO droplets adsorbed around the air cell. The composition of the model cream was 20 wt. % PKO, 1.35 wt. % SSL, 0.1 wt. % xanthan gum and 78.55 wt. % water.

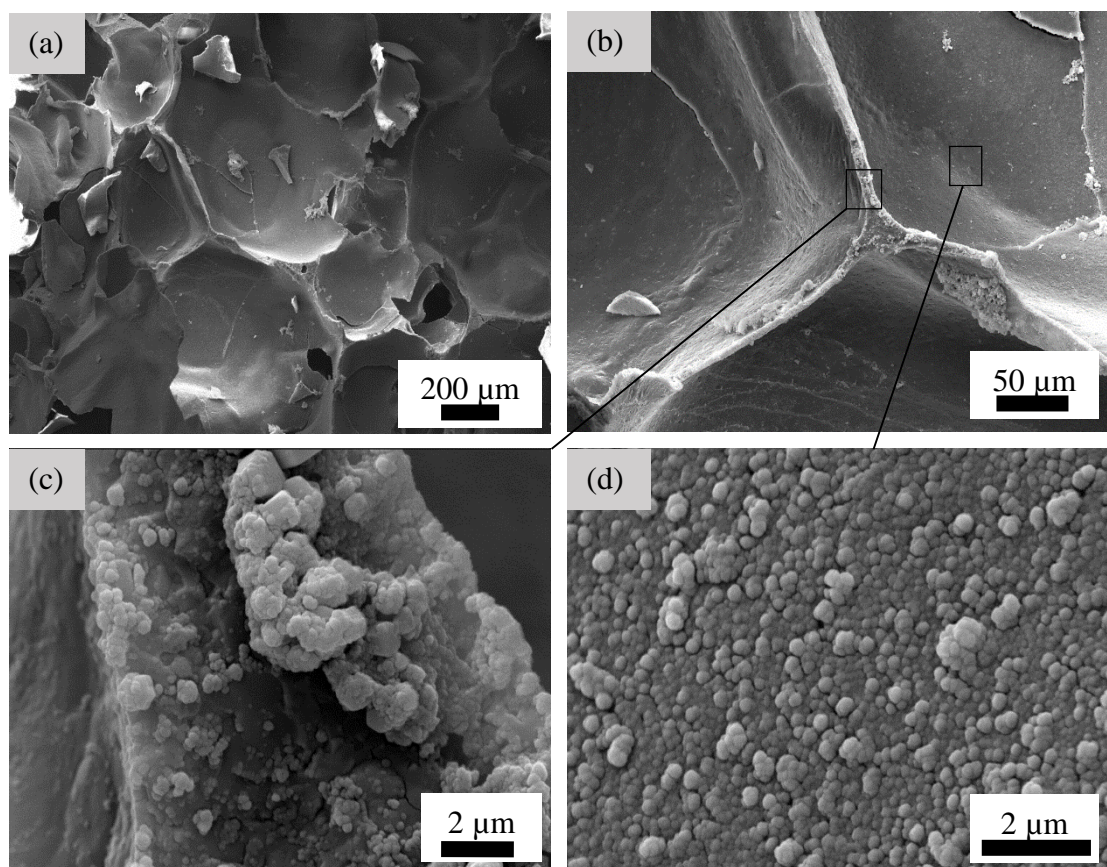
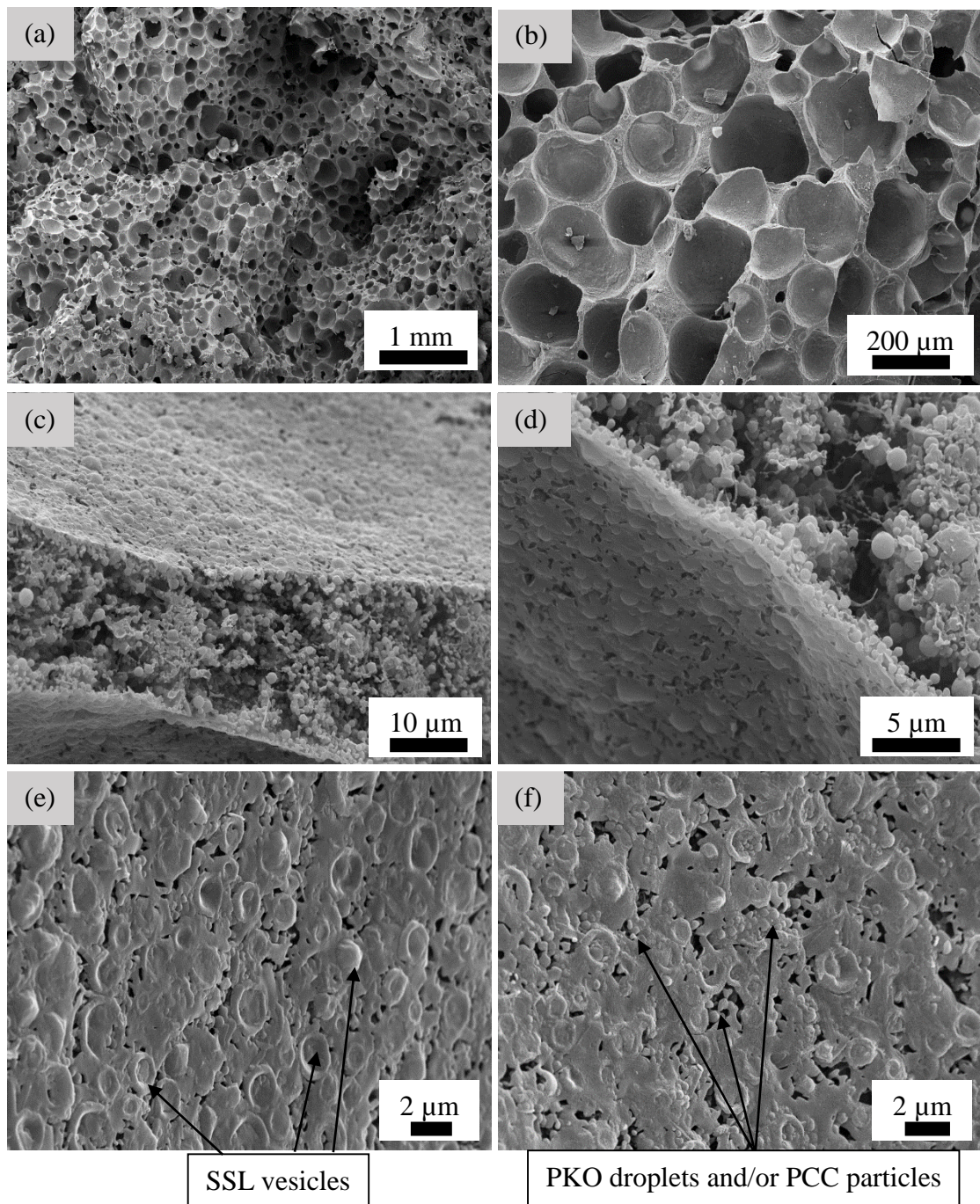


Figure 4.9. Cryo-SEM images of the model whipped cream with 1 wt. % PCC particles observed one day after whipping. The foam sample was stored at room temperature in a sealed vessel to avoid evaporation of water. As shown in (a) and (b) the foam had a high overrun with image (c) showing the thin film in between two air cells. Image (d) shows the edge and inner surface of an air cell clearly revealing the PKO droplets and micron sized SSL vesicles adsorbed around the air cell. Images (e) and (f) show the inner surface of an air cell in which SSL vesicles and PKO droplets and/or PCC particles are visible. The composition of the model cream was 20 wt. % PKO, 1.35 wt. % SSL, 0.1 wt. % xanthan gum and 78.55 wt. % water.



Whipped model cream samples without and with 1 wt. % PCC particles were further characterised using a Hitachi TM-1000 bench top SEM instrument. In this instrument the whipped samples could be observed without a Pt coating up to a certain magnification. A sticky disk was applied to the surface of a standard 12 mm diameter aluminium SEM mount. A small sample of the foam was carefully placed and adhered to the sticky surface of the disk. The aluminium mount was then fixed in the vacuum chamber of the microscope and the foams were observed at various magnifications. The aim was to check whether the sample without coating would reveal the position of PCC particles within the foam samples. Figure 4.10 shows the micrographs for samples without and with 1 wt. % PCC particles. The size and shape of the bubbles for both systems are comparable with those observed using cryo-SEM. The whipped sample with 1 wt. % PCC clearly shows some white fragments on the inner surfaces of air bubbles. Since no similar objects were found in the sample without PCC particles it is believed that the white fragments were PCC particles adsorbed around air bubbles. As can be seen in image (c) the fragments had different sizes, which shows that some PCC particles form aggregates with others existing as individual particles. This is in agreement with PCC particle size distribution data from SSL-PCC mixture aqueous dispersions presented in Chapter 3, where particles in both an aggregated state and a discrete state were evidenced. It is believed that SSL-coated PCC particles adsorb around air bubbles together with PKO droplets. The protective layer consisting of PKO droplets and PCC particles is believed to be the main stabilising factor for the model creams as will be discussed later. A schematic representation of what is believed to be happening in the model whipped creams is shown in Figure 4.11, where the PCC particles are shown to be adsorbed around air bubbles randomly in between PKO droplets.

Figure 4.10. SEM images of un-coated model whipped cream without PCC particles (upper) and with 1 wt. % PCC particles (lower) observed one day after whipping. The foam sample was stored at room temperature in a sealed vessel to avoid evaporation of water. Samples with 1 wt. % PCC clearly show white fragments, which are believed to be PCC particles. The composition of the model cream was 20 wt. % PKO, 1.35 wt. % SSL, 0.1 wt. % xanthan gum and 78.55 wt. % water.

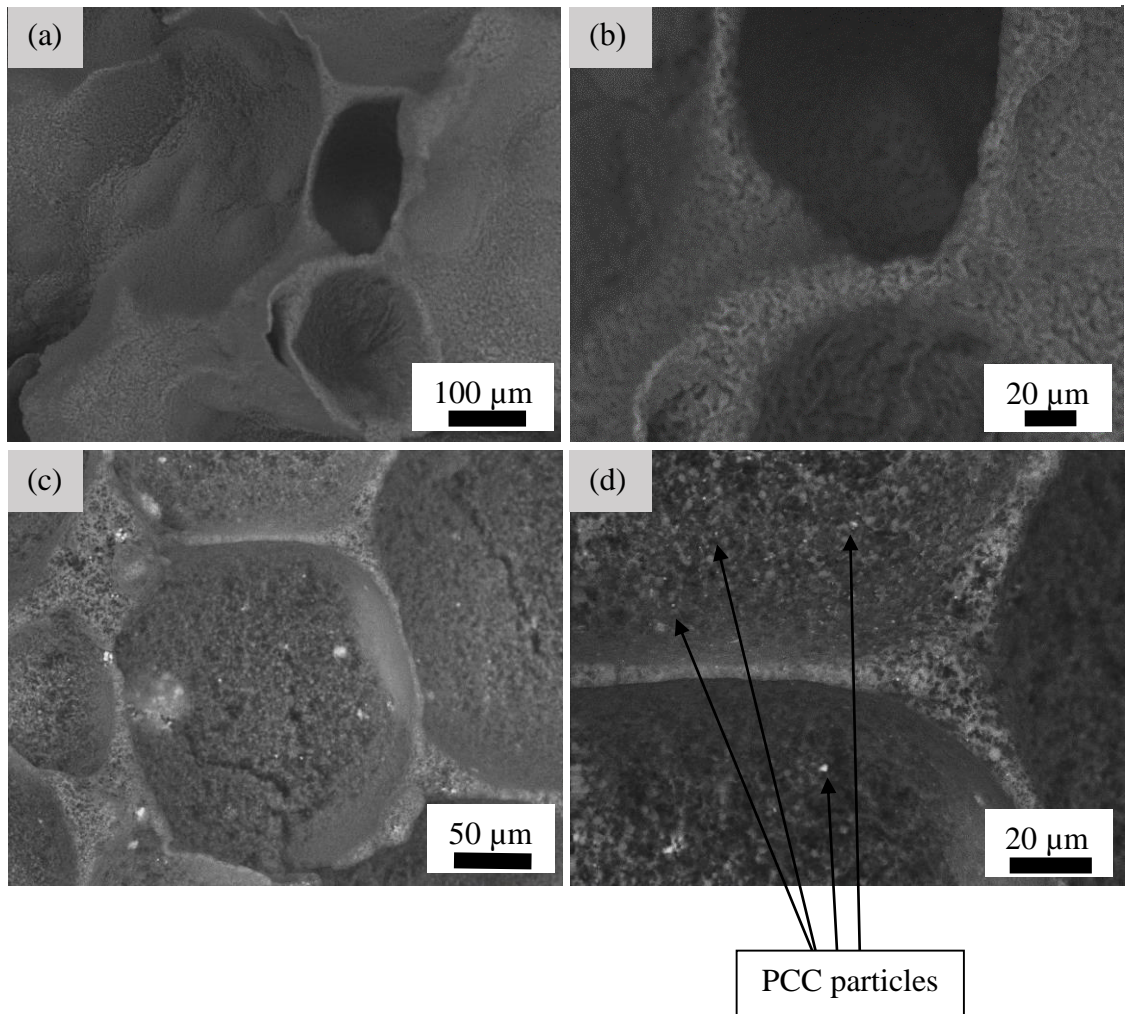
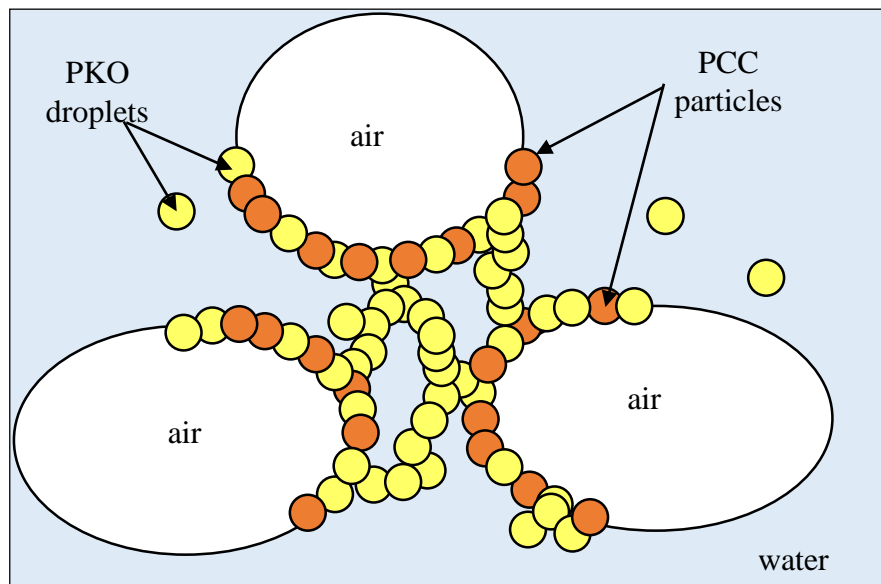
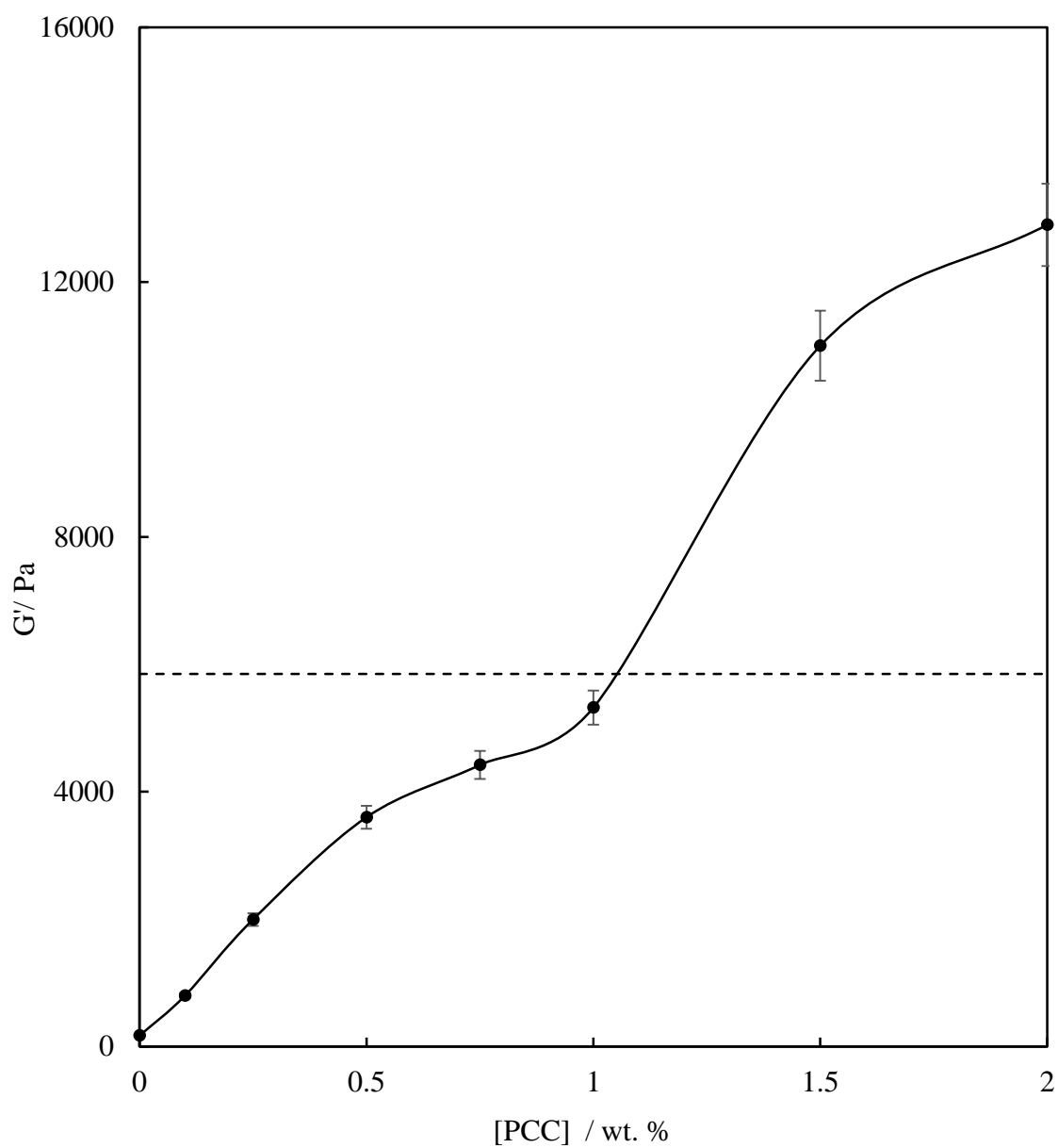


Figure 4.11. Schematic representation of the positioning of PKO droplets and PCC particles in a model whipped cream sample with 1 wt. % PCC particles. It is believed that PCC particles (orange) adsorb around air bubbles together with PKO droplets (yellow) and this improves both the foamability and foam stability of the model whipped cream samples. SSL vesicles and xanthan gum rods are not shown. Air bubbles have an average diameter of around 100 μm in model foams. The size of PKO droplets and PCC particles are increased in this illustration and they have approximate diameters of 140 nm and 150 nm respectively in model foams.



The structural properties of the model whipped cream samples were further studied using oscillation rheology. It is known that the stiffness of whipped cream is controlled by the extent of partial coalescence of fat droplets in the continuous phase. Figure 4.12 shows the variation of the elastic modulus (G') in the model whipped cream samples for different PCC particle concentration. Similar to the visual observation from peaking evaluation, incorporation of PCC particles increases the elastic modulus (G') of the whipped samples. One explanation is that the adsorption of PCC particles around air bubbles increases the stiffness of the protective film around air bubbles and creates a suitable base for the partial coalescence of PKO droplets further into the continuous phase, which did not occur in sample without PCC particles. The G' value of whipped VBC is also highlighted in the graph and shows a similar value to the model whipped cream with 1 wt. % PCC. Above 1 wt. % the G' value increases up to about 13000 Pa for the sample with 2 wt. % PCC particles. This value is much higher than that for whipped VBC and is not desirable in their application as a cake topping.

Figure 4.12. Variation of elastic modulus (G') in model whipped cream samples whipped for 12 minutes as a function of PCC particle concentration. The modulus was measured by oscillation mode at a frequency and stress of 1 Hz and 10 Pa, respectively. Dashed line shows the G' of whipped VBC. The composition of the model cream was 20 wt. % PKO, 1.35 wt. % SSL, 0.1 wt. % xanthan gum and 78.55 wt. % water.



4.4.1.3 Stability to liquid drainage

Model whipped cream samples were further characterised to assess their stability towards serum drainage. The data of serum drainage measurements for the model whipped cream samples with different PCC concentrations are shown in Table 4.2. As given in the table, the volume of liquid drained under gravity from 20 g of foam samples decreases with increasing PCC concentration. The improvement in drainage stability could be linked to the formation of a rigid three-dimensional network of partially coalesced PKO droplets due to the presence of PCC particles on the surface of air bubbles. The network is believed to be further supported by xanthan gum rods in the continuous phase. Xanthan gum rod-like chains entangle to form a complex network in the continuous phase as mentioned earlier.^{27,28} This is expected to further reduce the rate of drainage. The drainage occurs in model whipped creams with PCC concentration of ≤ 0.5 wt. %, while those above 0.5 wt. % PCC show no liquid drainage. The drainage stability of whipped VBC is also shown in the last row, where it shows 2 mL liquid drainage after 4 days despite possessing high viscosity and various other stabilising ingredients, which are absent in the model foams.

Table 4.2. Serum drainage volume from 20 g of model whipped cream samples for different PCC concentrations measured one and four days after whipping. The foam samples were stored at room temperature in sealed vessels to avoid evaporation of water. Adding PCC clearly improves the stability of model whipped creams towards drainage. Upon whipping of the sample without PCC particles not all the liquid was incorporated in to the foam and hence no data is shown for 0 wt. % PCC. The composition of the model cream was 20 wt. % PKO, 1.35 wt. % SSL, 0.1 wt. % xanthan gum and 78.55 wt. % water.

[PCC] / wt. %	Serum drainage day 1 / mL	Serum drainage day 4 / mL
0.1	8	9
0.25	4	6
0.5	1	2
0.75	0	0
1	0	0
1.5	0	0
2	0	0
VBC	1	2

4.4.2 *Effect of oil volume fraction*

4.4.2.1 Flow behaviour of emulsions before aeration

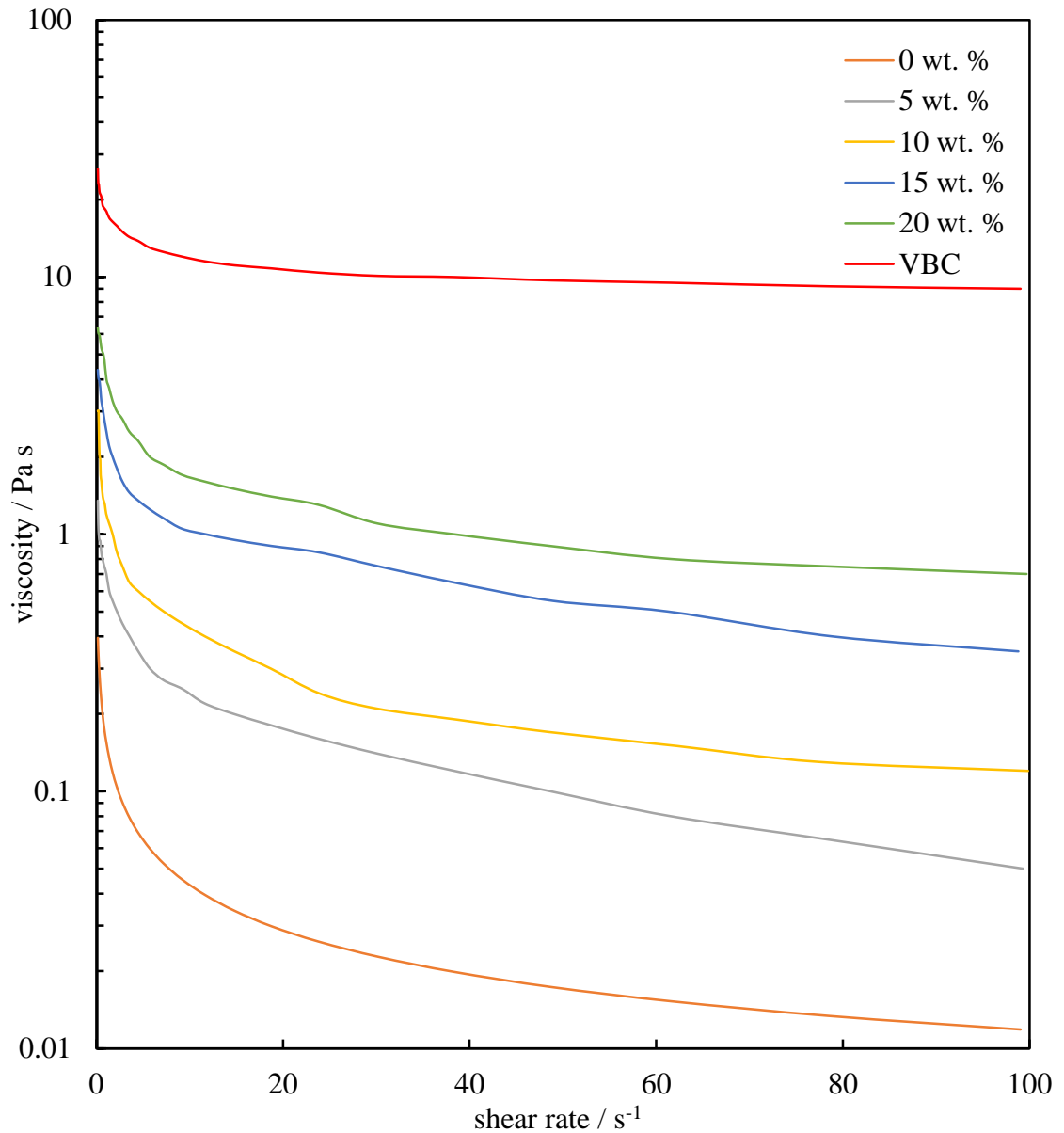
The effect of PCC particle addition on the aeration properties of model whipped cream samples was studied in the previous section. It was shown that upon increasing particle concentration the overrun values increased sharply and foams with better structural and stability properties were produced. Using SEM (both cryo and normal) micrographs the inner surfaces of air bubbles were shown and PCC particles were observed together with PKO droplets around the air bubbles. In order to evaluate the effect of PKO droplet concentration on the aeration properties of the model whipped creams, a series of model whipping cream emulsions were prepared with different PKO volume fractions. The PKO content was varied between 0 and 20 wt. %, with respect to the total emulsion volume. Since the pressure applied during homogenisation in the HPH was kept constant (180 and 30 bar at first and second homogenisation stages,

respectively) no change in the PKO droplet size was found and the droplet size distribution of emulsions, determined using light scattering, showed a mono-modal peak at around 150 nm for all model emulsions with PKO content between 5 and 20 wt. %.

Viscosity is an important property of food emulsions and foams. Viscosity of an emulsion is related to the strength of the interactions between dispersed phase droplets and also to the thickness of the continuous phase. The viscosity of the model cream samples prior to their aeration was measured using rotational rheology. Figure 4.13 shows the relationship between apparent viscosity and shear rate of the un-whipped model creams containing different contents of PKO measured at 10 °C. The viscosity of the un-whipped VBC is also shown for comparison. It can be seen that all of the model emulsions exhibited pseudo-plastic behaviour; *i.e.* the curves displayed shear-thinning behaviour. This is known to be due to weak associative interactions between the oil droplets.²⁹ Similar viscosity behaviour (shear-thinning) has been reported by Wang *et al.*³⁰ for PKO-in-water emulsions stabilised by sodium caseinate.

The viscosity of the model cream sample without PKO droplets (aqueous dispersion of SSL and xanthan gum) is shown by the orange curve and can be seen to have a very low apparent viscosity. Comparing the viscosities of the model cream emulsions, one can clearly see the increase in the viscosity with an increase in the PKO content. An increase in the viscosity of an emulsion upon increasing the volume fraction of the dispersed phase has been reported previously. Using rotational rheometry, Binks *et al.*³¹ showed that the viscosity of water-in-isopropyl myristate emulsions stabilised by clay particles increased when the water volume fraction increased from 0.1 to 0.5. It can also be seen in the figure that the viscosity of the model whipping cream emulsion with 20 wt. % PKO is significantly less than the viscosity of un-whipped VBC. The higher viscosity of the un-whipped VBC sample is due to the presence of various other stabilisers, sweeteners and thickening agents such as sodium caseinate and corn syrup.

Figure 4.13. Relationship between apparent viscosity and shear rate for un-whipped model creams containing different contents of PKO. The viscosities were measured by rotational rheology performing a shear rate scan at 10 °C. The model creams contained 1.35 wt. % SSL, 0.1 wt. % xanthan gum and water (calculated according to PKO wt. %). The PKO content in the emulsions is highlighted and is with respect to total emulsion volume. Red curve is the viscosity of the un-whipped VBC.

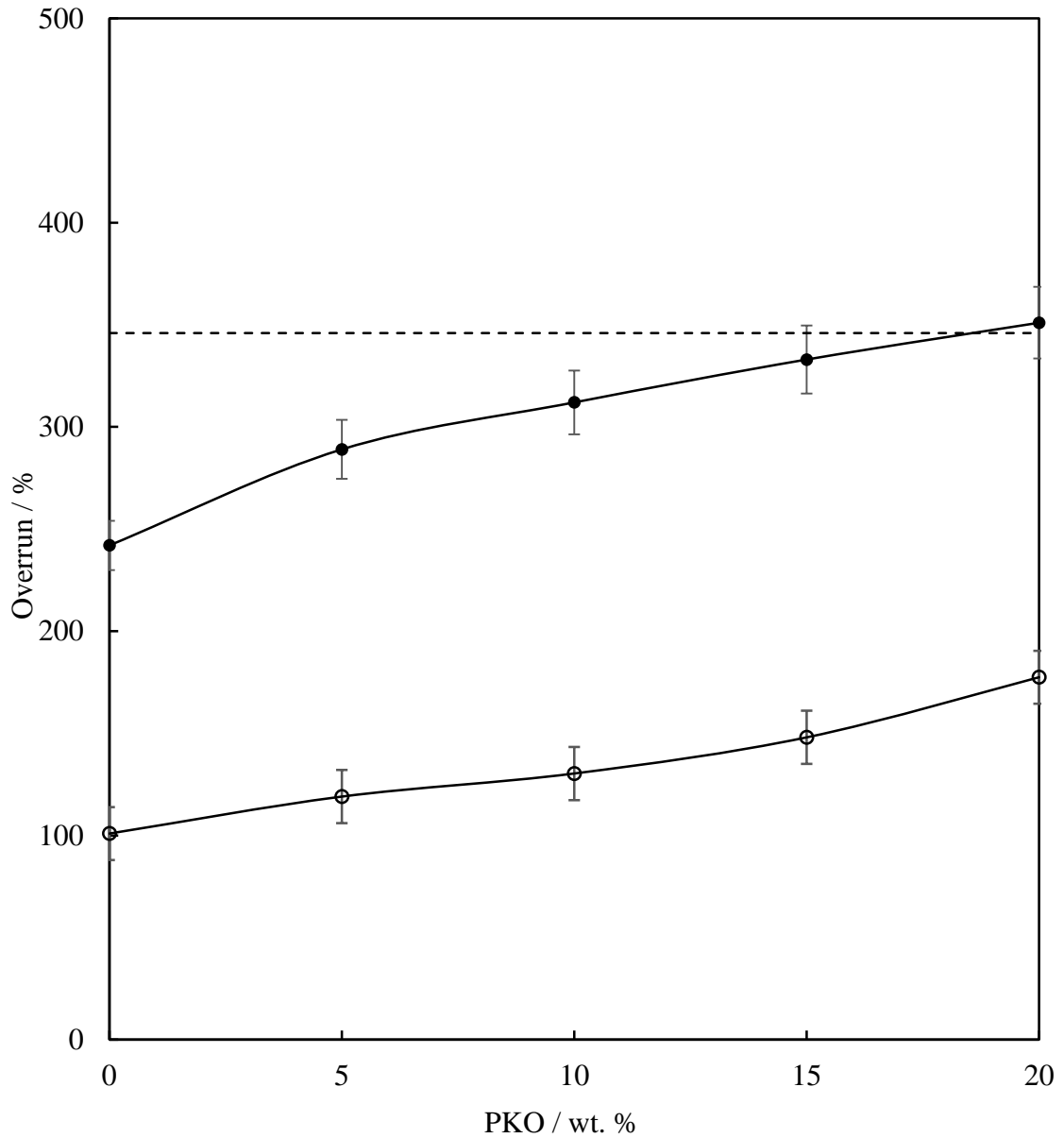


4.4.2.2 Overrun

The model whipping cream emulsions, with different PKO volume fractions, were characterised in terms of their foamability and foam stability in the presence and absence of PCC particles. The prepared emulsions were stored at 6 °C for 24 hours prior to their aeration. For samples containing PCC particles, 1 wt. % of particles with respect to the total emulsion volume, was added as an aqueous dispersion (10 mL at 10 °C) to the emulsion just before whipping. Figure 4.14 shows the overrun values of the model whipped creams in the presence and absence of PCC particles upon increasing PKO content. The overrun value of whipped VBC is also highlighted for comparison. As shown in the graph there is a significant difference in the overrun values of the samples with 1 wt. % PCC particles and those without PCC particles. Model samples with PCC particles showed higher overrun values as PCC particles adsorb around air bubbles during aeration and facilitate an increase in the amount of air incorporated into the emulsions.

A gentle increase in the overrun values was observed upon increasing the PKO content. The sample with 0 wt. % PKO showed an overrun value of 242 % ($\phi_{\text{air}} = 0.59$) and this increased to 346 % ($\phi_{\text{air}} = 0.73$) for the sample with 20 wt. % PKO. The slight effect of PKO volume fraction on overrun values means that increasing the concentration of PKO droplets does not influence the amount of air incorporated in the samples significantly. It is believed instead that this improves the structural properties and the stability of the prepared model whipped cream samples as shown later.

Figure 4.14. Overrun values of model whipped cream samples with 1 wt. % PCC particles (filled points) and without PCC particles (empty points) upon increasing PKO volume fraction. All samples were aerated for 12 minutes. Addition of PCC particles clearly enhances the incorporation of air into the foam for all PKO volume fractions. Dashed line shows the overrun of whipped VBC, aerated for 6 minutes. The model creams contained 1.35 wt. % SSL, 0.1 wt. % xanthan gum and water (calculated according to PKO wt. %).



4.4.2.3 Structural properties of foams

Structural properties and stiffness of the model whipped cream samples with varying PKO content were evaluated based on peaking appearance, rosette definition, cryo-SEM imaging and oscillation rheology. Figure 4.15 shows the appearance of the peaks made from the model whipped creams immediately after their aeration followed by the peaking evaluation grades presented in Table 4.3. As can be seen, the model foam without PKO droplets (aqueous dispersion of SSL-PCC-xanthan gum) had a watery and soft structure and no peak was formed. Since the formation of the three-dimensional network of partially coalesced PKO droplets is the main reason for the stiffness in whipped cream, such behaviour from the PKO-free foam was expectable. Both model whipped creams with 10 and 20 wt. % PKO showed high stiffness and the peak formed from them was found to be identical to the peak formed from whipped VBC shown in image (d). The peaking grading results presented in the table also confirms that the model cream foams with 10 and 20 wt. % PKO have similar peaking properties to the whipped VBC. Therefore can conclude that even at low PKO volume fractions (*i.e.* 10 wt. %) the model whipped cream had acceptable stiffness and peaking appearance.

Figure 4.15. Appearance of the peaks formed from model whipped creams with 0, 10 and 20 wt. % PKO shown in images (a), (b) and (c) respectively. Image (d) shows whipped VBC on top of the whisk taken immediately after aeration. Peaking test as explained in Chapter 2 was used to determine the optimum whipping time and to grade the stiffness of whipped cream. It is clear that the PKO-free foam, image (a), had a soft and watery structure and the samples with 10 and 20 wt. % PKO produces similar results to the whipped VBC. The composition of the model creams (a-c) was 1 wt. % PCC, 1.35 wt. % SSL, 0.1 wt. % xanthan gum and water (calculated according to PKO wt. %). The model cream foams and the VBC were aerated for 12 and 6 minutes respectively. Scale bar represents 3 cm.

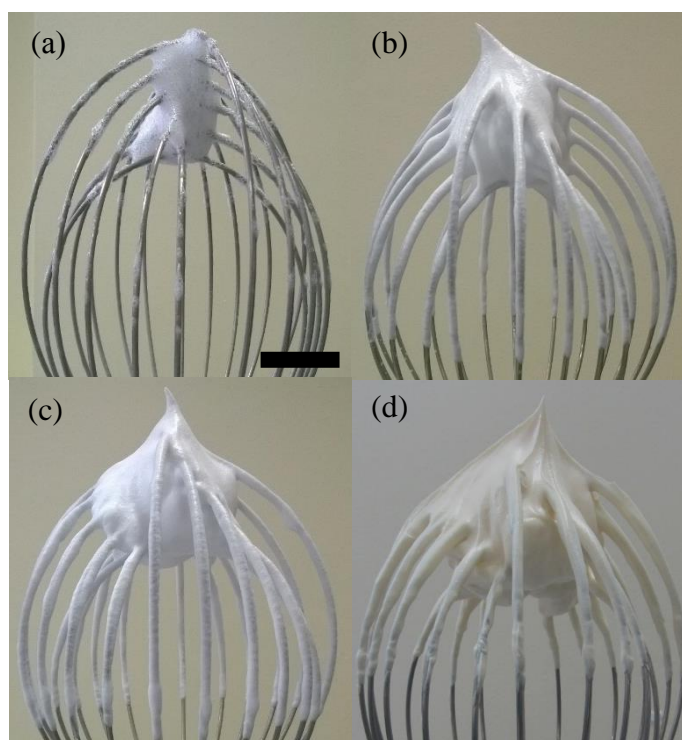
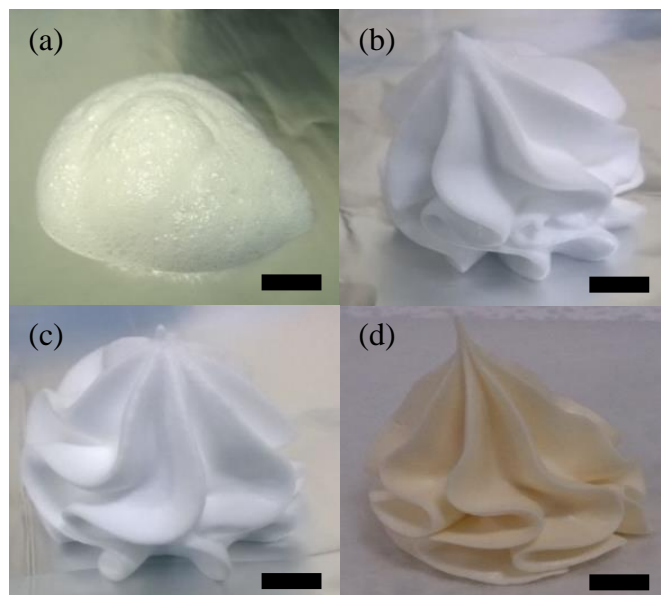


Table 4.3. Peaking evaluation grades for model whipped cream foams with different PKO content based on the images in Figure 4.15. Last column shows the peaking grade of whipped VBC. The grading scale was explained in Chapter 2.

PKO / wt. %	0	10	20	VBC
Peaking grade	1	4	4	5

The appearance of the rosettes made from the model whipped creams with varying PKO content are shown in Figure 4.16. In (a) it is seen that the rosette from the PKO-free foam had no structure and a poor appearance. The definition of the foams was significantly improved for the model cream samples with 10 and 20 wt. % PKO droplets as can be seen in images (b) and (c) due to the formation of the network of partially coalesced PKO droplets. The appearance and definition of the rosette from both of these samples are comparable to the rosette made from whipped VBC shown in image (d).

Figure 4.16. Appearance of the rosettes made from model cream foams with 0, 10 and 20 wt. % PKO shown in images (a), (b) and (c) respectively. Image (d) shows a rosette of whipped VBC. Rosette structure evaluation as explained in Chapter 2 was used to determine the life-time of foams in a pastry bag and also to grade the appearance of the rosette. It is clear that the definition of the rosette was significantly improved in samples with 10 and 20 wt. % PKO. The composition of the model creams (a-c) was 1 wt. % PCC, 1.35 wt. % SSL, 0.1 wt. % xanthan gum and water (calculated according to PKO wt. %). The model cream foams were aerated for 12 minutes and VBC for 6 minutes. Scale bar represents 1 cm.



Cryo-SEM imaging was used to observe the size of air bubbles and also to locate the position of the PCC particles and PKO droplets within the model whipped creams. Previously cryo-SEM images of the model whipped cream containing 20 wt. % PKO and 1 wt. % PCC were shown in Figure 4.9, where it was found that locating the PCC particles was challenging due to the similarity in the size of PCC particles and PKO droplets. However in Figure 4.10 SEM images of the same sample revealed white fragments of PCC particles adsorbed on the inner surfaces of air bubbles. In order to further investigate the role of PCC particles within the model cream foams, the fat-free model cream (0 wt. % PKO) with 1 wt. % PCC particles was analysed using cryo-SEM and the images are shown in Figure 4.17. The images show that the foam contained spherical bubbles with bubble diameter of no more than $75 \pm 10 \mu\text{m}$. Images (c-e) show the inner surfaces of different air bubbles in the sample at high magnification. The images clearly show that the inner surfaces of air bubbles are completely coated with PCC particles. Although it was not possible to show the similar proof for the samples containing both PCC particles and PKO droplets, it may be concluded that the same phenomenon is happening in those systems and PCC particles adsorb around air bubbles together with PKO droplets.

The foams with varying PKO content were characterised using oscillation rheology to assess their stiffness. The stiffness of the model whipped creams arises from the formation of a rigid film of PKO droplets and PCC particles around air bubbles as well as the three-dimensional network of partially coalesced PKO droplets in the continuous phase. The data are shown in Figure 4.18 for the samples without and with 1 wt. % PCC particles. The samples without PCC particles showed no significant development in elastic modulus upon increasing PKO volume fraction. This suggests that the adsorption of PCC particles around air bubbles is a requirement for the formation of the network of partially coalesced PKO droplets, which rises the stiffness and elastic modulus. The samples with 1 wt. % PCC particles showed different behaviour and the elastic modulus increased significantly upon increasing PKO droplet concentration as expected. The elastic modulus of the model foams containing 1 wt. % PCC particles increased gradually up to around the elastic modulus of whipped VBC at 20 wt. % PKO.

Figure 4.17. Cryo-SEM images of the fat-free model whipped cream (0 wt. % PKO) with 1 wt. % PCC particles observed one day after whipping. The foam sample was stored at room temperature in a sealed vessel to avoid evaporation of water. As shown in (a) and (b) the foam contained spherical bubbles with an average bubble size of $75 \pm 10 \mu\text{m}$. Images (c-e) show the inner surface of different air cells in which PCC particles are clearly visible. The composition of the model cream was 1wt. % PCC, 0 wt. % PKO, 1.35 wt. % SSL, 0.1 wt. % xanthan gum and 98.55 wt. % water. The sample was aerated for 12 minutes.

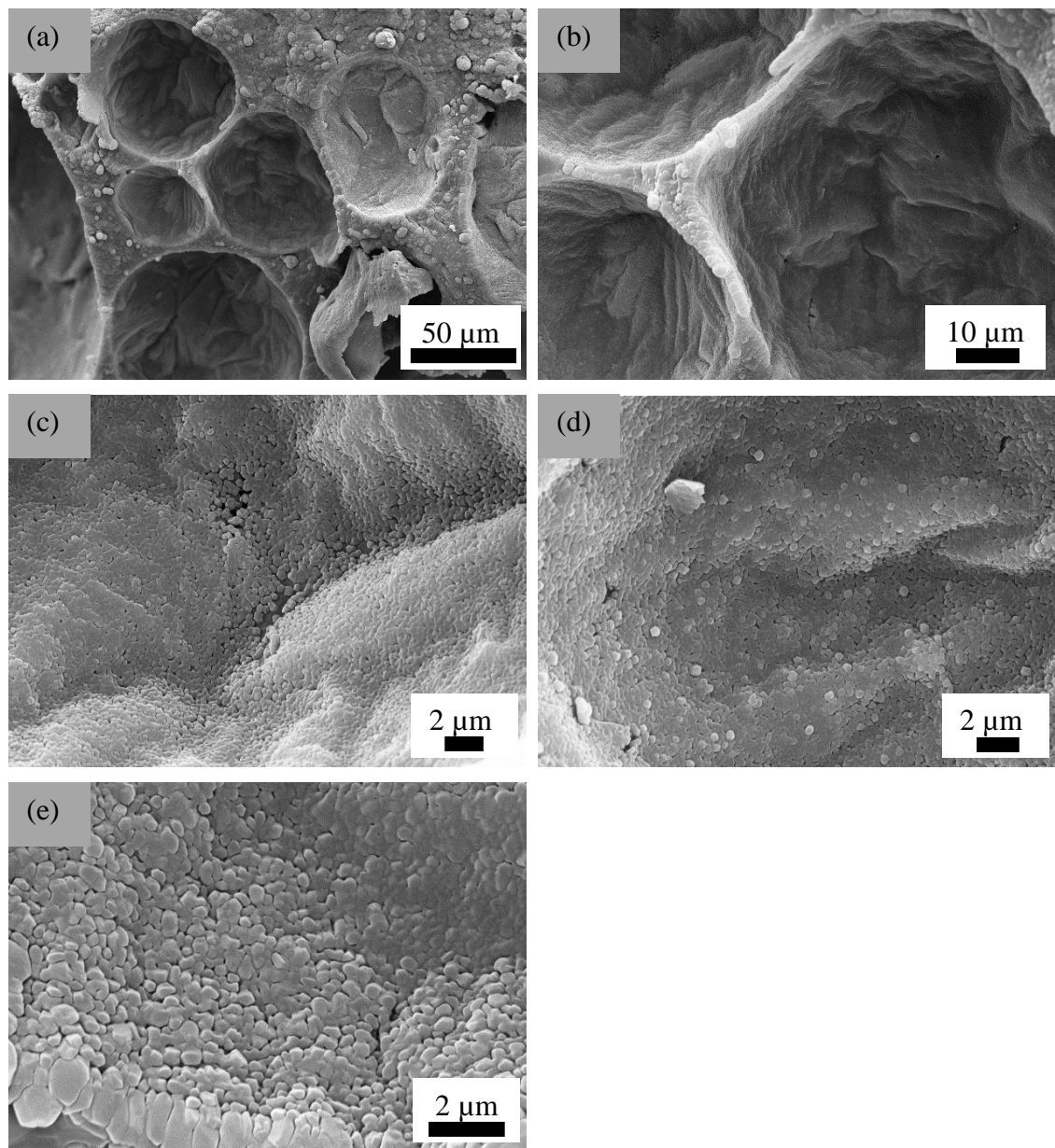
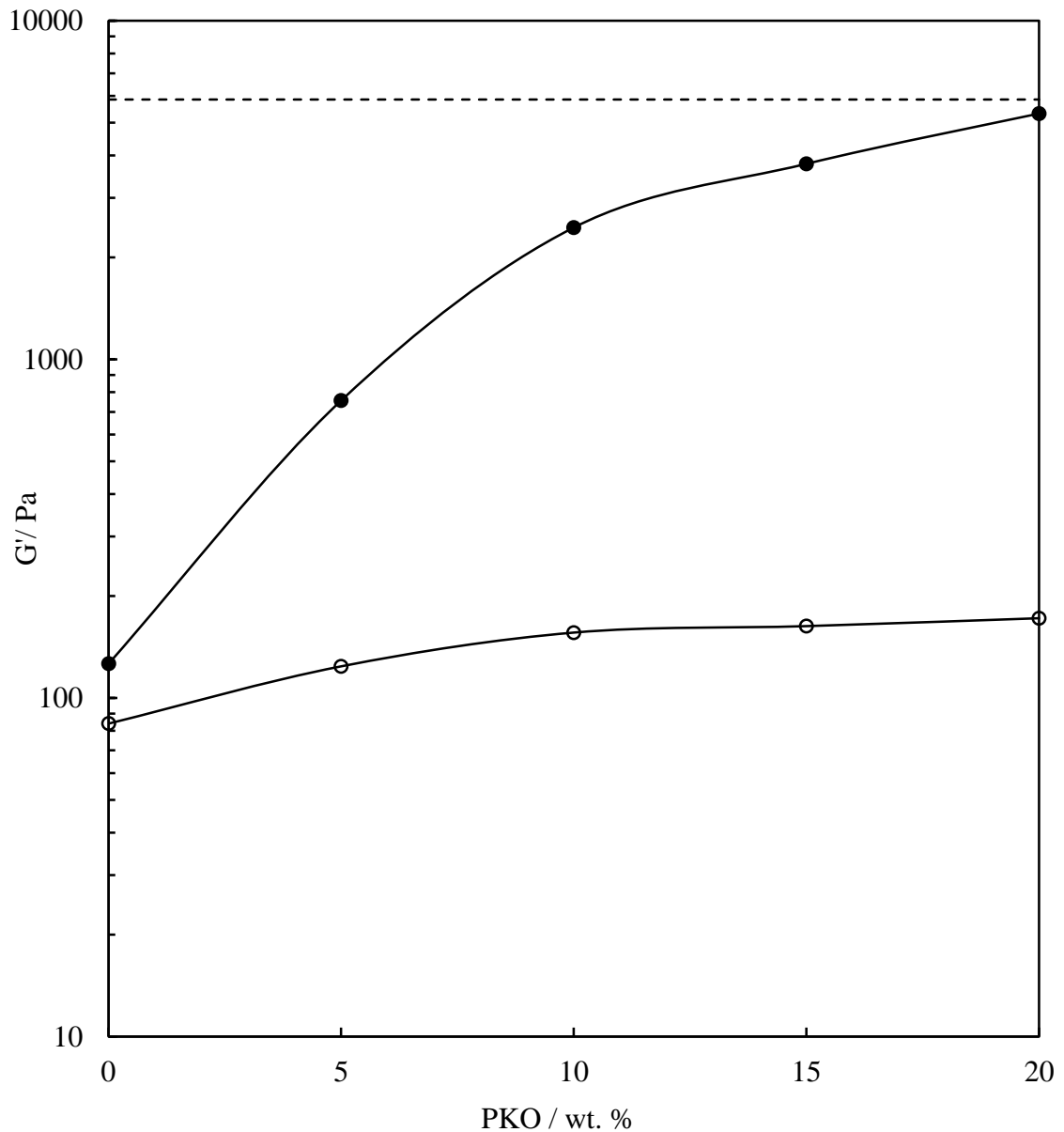


Figure 4.18. Variation of elastic modulus (G') of model whipped cream samples with 1 wt. % PCC particles (filled points) and without PCC particles (empty points) upon increasing PKO content. The modulus was measured by oscillation rheology at a temperature, frequency and stress of 10 °C, 1 Hz and 10 Pa, respectively. Dashed line shows the G' of whipped VBC. All samples were aerated for 12 minutes. Addition of PCC particles clearly enhances the stiffness of model whipped cream samples. The model creams contained 1.35 wt. % SSL, 0.1 wt. % xanthan gum and water (calculated according to PKO wt. %).



4.4.2.4 Stability of foam towards serum drainage

The model whipped creams with varying PKO content were characterised in terms of their stability towards liquid drainage. Table 4.4 shows the serum drainage from 20 g of foam samples without and with 1 wt. % PCC particles and varying PKO wt. %. The stability of the samples towards drainage was improved as the concentration of PKO droplets increased. This is believed to be due to an increase in extent of the network of partially coalesced PKO droplets, which reduces the extent and rate of liquid drainage. It was also noticed that the foams with 1 wt. % PCC particles showed greater stability to drainage compared to those without particles. The model whipped cream sample with 10 wt. % PKO was fully stable towards drainage and no liquid drainage was observed after 4 days, unlike the whipped VBC which had 2 mL serum drained after the same period of time.

Table 4.4. Serum drainage volume from 20 g of model whipped cream samples containing 1 wt. % PCC particles and varying PKO content. The data from the model whipped cream samples without PCC particles are also shown. The foam samples were stored at room temperature in a sealed vessel to avoid evaporation of water. Adding PCC clearly improves the stability of model whipped creams towards drainage. The composition of the model cream was 1.35 wt. % SSL, 0.1 wt. % xanthan gum and water (calculated according to PKO wt. %).

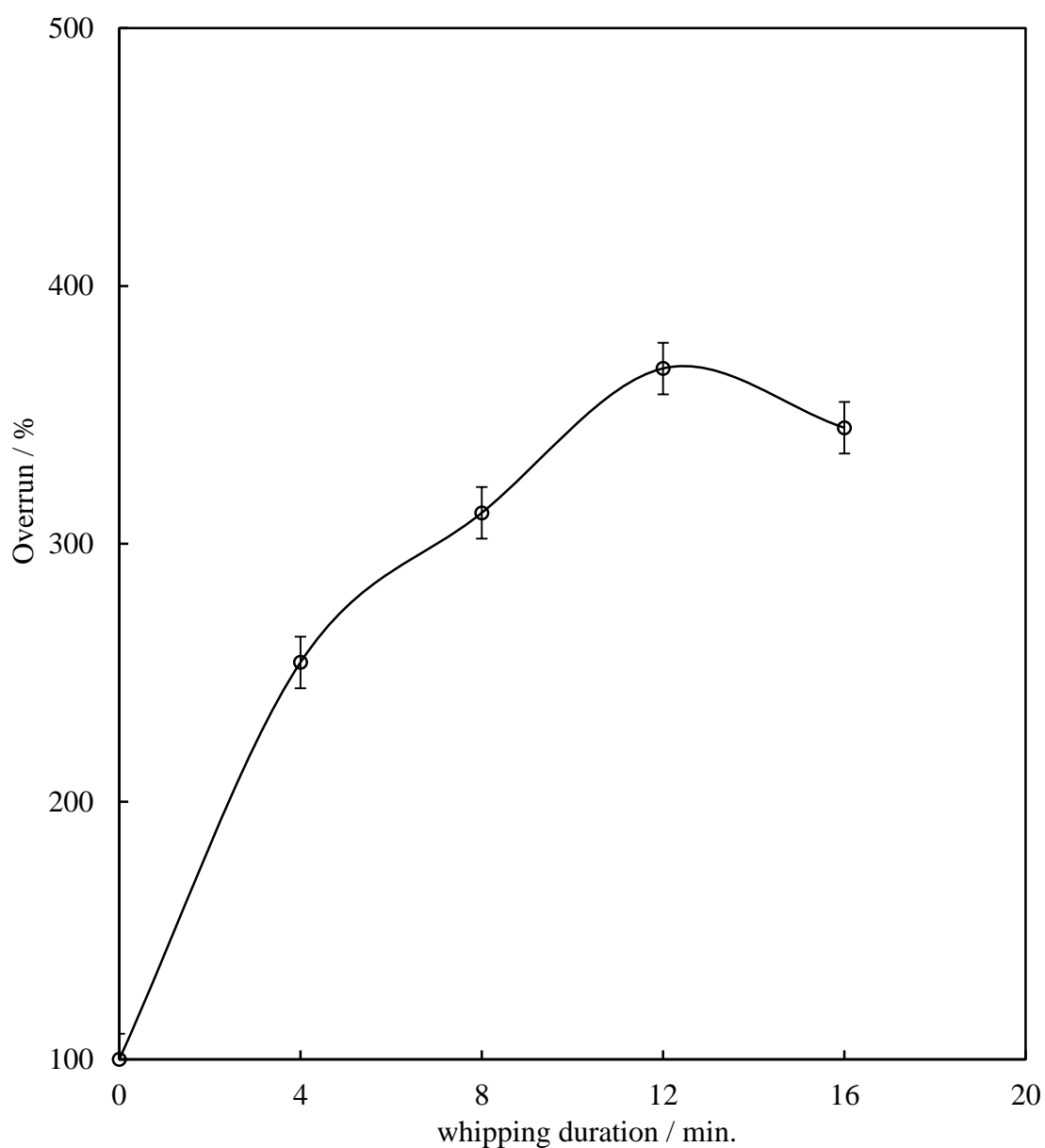
PKO / wt %	Serum drainage day 1 / mL		Serum drainage day 4 / mL	
	with 1 wt. % PCC	without PCC	with 1 wt. % PCC	without PCC
0	5	18	6	18
5	1	17	1	18
10	0	12	0	13
20	0	11	0	11
VBC	1	1	2	2

4.4.3 *Effect of whipping duration*

4.4.3.1 Overrun and bubble size evolution

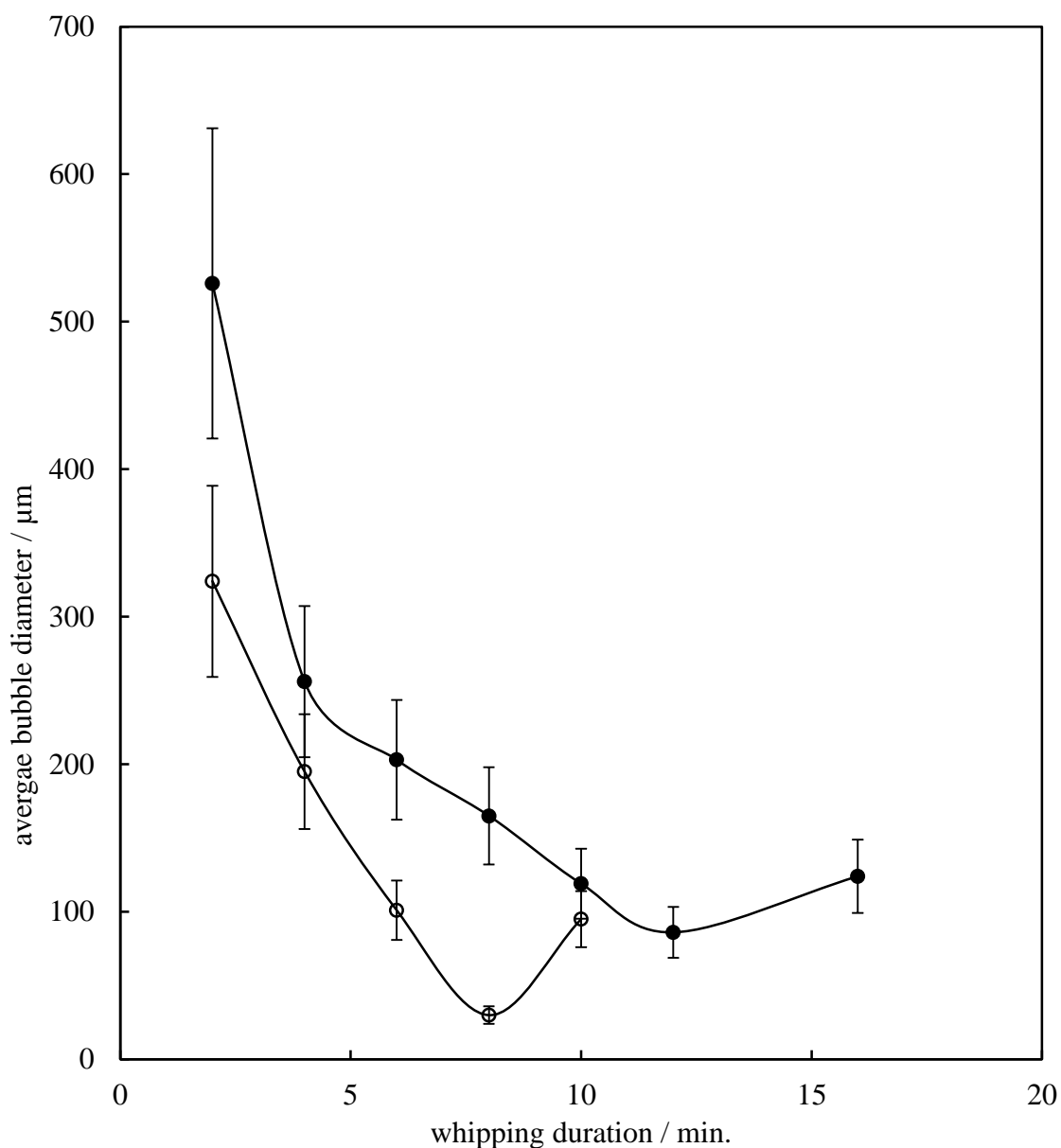
Whipping duration is known to have a large influence on air incorporation, stiffness and air bubble size distribution of the generated foams. Upon aeration of whipping cream, the overrun increases to a maximum and decreases thereafter as fat globules aggregate and the foam collapses. Figure 4.19 shows the overrun values determined from the aeration of the model whipped cream containing 20 wt. % PKO, 1.35 wt. % SSL, 0.1 wt. % xanthan gum and 78.55 wt. % water. 1 wt. % Calofort U PCC particles (with respect to the total volume of the cream in the whipping bowl, 650 g) was added as an aqueous dispersion on top of the cream in the whipping bowl just before aeration. Since whipping the sample without PCC particles did not produce much foam, those results are not included in the graph. As can be seen in the graph, the overrun increases sharply at the early stages of the aeration and reaches 254 % ($\phi_{\text{air}} = 0.61$) after 4 minutes. This is believed to be due to fast adsorption of SSL aggregates and PCC particles on the surface of air bubbles, at the initial stages of aeration. Further whipping the cream until 12 minutes resulted in the adsorption of PKO droplets around air bubbles, followed by their partial coalescence and increased the overrun to 368 % ($\phi_{\text{air}} = 0.73$). The optimum whipping time, determined using peaking evaluation, was found to be 12 minutes. Whipping the model cream further up to 16 minutes showed a decrease in the overrun. This is known to be due to the fact that the clumps of partially coalesced PKO droplets become very large that the lamellae stabilising the air cells are ruptured, air bubbles start to coalesce and the overrun decreases. This phenomenon, also known as over whipping, has been mentioned in several other studies on whipped cream.^{26, 32-34} The whipping times measured for the model creams here were found to be significantly longer than those reported for whipping of a natural dairy cream by van Aken⁷ and the whipping of VBC. This could be due to the absence of proteins in the model creams here, as they are known to adsorb around air bubbles at the initial stages of whipping and enhance the incorporation of air into the whipping cream.^{35, 36}

Figure 4.19. Effect of whipping duration on the overrun value of the model whipped creams. All samples stored at 6 °C for 24 hours before aeration. Calofort U PCC particles were added as an aqueous dispersion to top of the cream in the whipping bowl just before aeration. The composition of the model cream was 20 wt. % PKO, 1.35 wt. % SSL, 0.1 wt. % xanthan gum and 78.55 wt. % water. 1 wt. % PCC particle with respect to the volume of cream in the whipping bowl was added as an aqueous dispersion just before aeration.



Evolution in the average bubble size for model whipped cream samples and for whipped VBC as a function of whipping duration are shown in Figure 4.20. Generally, whipped VBC was shown to have smaller air bubbles compared to the model whipped cream. This could be due to the presence of various stabilisers in the VBC, such as sodium caseinate and methyl cellulose, which help reducing the air-water interfacial tension and creating smaller air bubbles. As aeration continues the bubble size distribution becomes more uniform and the average bubble size falls up to 12 minutes. Both data sets pass through a minimum, occurring at the optimum whipping time. Jakubczyk and Niranjana³⁷ also reported the formation of large air bubbles after whipping dairy cream samples for over 12 minutes. As mentioned previously, prolonged whipping of the model cream resulted in a loss of air bubbles due to air cell protective film rupture and hence the average bubble size increases after 16 minutes whipping.

Figure 4.20. Average bubble diameter evolution in model whipped cream (filled points) and whipped VBC (empty points) as a function of whipping duration. The size of air bubbles was determined using optical and cryo-SEM imaging and at least 100 bubbles were measured for each time. The composition of the model cream was 20 wt. % PKO, 1.35 wt. % SSL, 0.1 wt. % xanthan gum and 78.55 wt. % water. 1 wt. % PCC particle with respect to the volume of cream in the whipping bowl was added as an aqueous dispersion just before aeration.



4.4.3.2 Structural properties of foam

As performed for previous samples, structural properties and stiffness of the model whipped cream samples aerated for different durations were evaluated based on peaking appearance, cryo-SEM imaging and oscillation rheology. Figure 4.21 shows the appearance of the peaks formed from model whipped samples aerated for different durations followed by the peaking evaluation grades presented in Table 4.5. As can be seen the appearance of the peaks on top of the whisk taken at each stage showed the development of foam structure. The peaking appearance of the foams clearly improved by continuing the whipping up to 12 minutes. However the foam structure breaks upon continuing the aeration to 16 minutes and a fluffy texture was formed. Peaking evaluation data shown in the table clearly show that continuing the whipping up to 12 minutes improves the peak structure and then a poor peak forms when aerated up to 16 minutes.

Figure 4.21. Peaking evaluation of the model whipped creams aerated for 4, 8, 12 and 16 minutes shown in images (a), (b), (c) and (d) respectively. Peaking test as explained in Chapter 2 was used to determine the optimum whipping duration and to grade the stiffness of whipped cream. It is clear that whipping time significantly affects the peak formation on top of the whisk. The composition of the model cream was 20 wt. % PKO, 1.35 wt. % SSL, 0.1 wt. % xanthan gum and 78.55 wt. % water. 1 wt. % PCC particle with respect to the volume of cream in the whipping bowl was added as an aqueous dispersion just before aeration. Scale bar represents 3 cm.

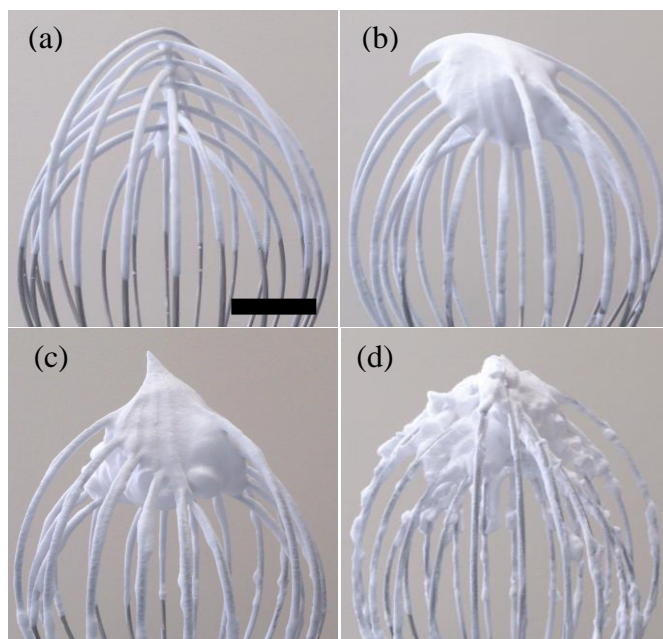


Table 4.5. Peaking evaluation grades for model whipped cream foams aerated for different durations based on the images in Figure 4.21. The grading scale was explained in Chapter 2.

Whipping duration / min.	4	8	12	16
Peaking grade	1	2	4	1

Cryo-SEM and optical micrographs of the model whipped cream aerated for 4, 8, 12 and 16 minutes are shown in Figure 4.22. Both cryo-SEM and optical micrographs show similar bubble sizes and are in agreement. Foams showed decrease in size of air bubbles and the films between air bubbles become thinner upon aeration until 12 minutes. It was also found that the size of air bubble becomes more uniform with increasing whipping time up to that point. Continuing the aeration for 16 minutes caused the formation of some large bubbles due to coalescence of smaller bubbles as can be seen in image (d). The same phenomena was reported by Jakubczyk and Niranjana³⁷ during the aeration of commercial dairy cream and is believed to be due to excessive extension of three-dimensional network of partially coalesced fat droplets, which breaks the film stabilising air bubbles.

Mechanical properties of the model whipped cream as a function of whipping duration was characterised by means of oscillation rheology. It is known that whipping changes the properties of cream by rendering it more viscoelastic than un-whipped cream. Figure 4.23 shows the variation of the elastic modulus (G') of model whipped cream samples and whipped VBC upon increasing whipping duration. In both series foams whipped for longer durations were found to have higher elastic modulus (G'), due to an increase in the extent of partial coalescence between PKO droplets and the formation of the rigid three-dimensional network in the continuous phase. Arboleya *et al.*³⁸ studied the rheological properties of aerated PKO-in-water emulsions stabilised by a mixture of methyl cellulose, sodium caseinate and Tween 60. They also showed that as aeration continues the bubble size decreases thus increasing the number contact points in the bubble network and hence increasing the overall elasticity of the foam.

Figure 4.22. Cryo-SEM (left) and optical microscopy (right) images of the model whipped cream aerated for 4, 8, 12 and 16 minutes shown in images (a), (b), (c) and (d) respectively. The images from both microscopy techniques shows similar bubble sizes. As shown the size of air bubbles decreases when the sample is aerated up to 12 minutes. Image (d) shows the sample aerated for 16 minutes at which some larger air bubbles started to form. The composition of the model cream was 20 wt. % PKO, 1.35 wt. % SSL, 0.1 wt. % xanthan gum and 78.55 wt. % water. 1 wt. % PCC particle with respect to the volume of cream in the whipping bowl was added as an aqueous dispersion just before aeration. Scale bars represent 500 μm .

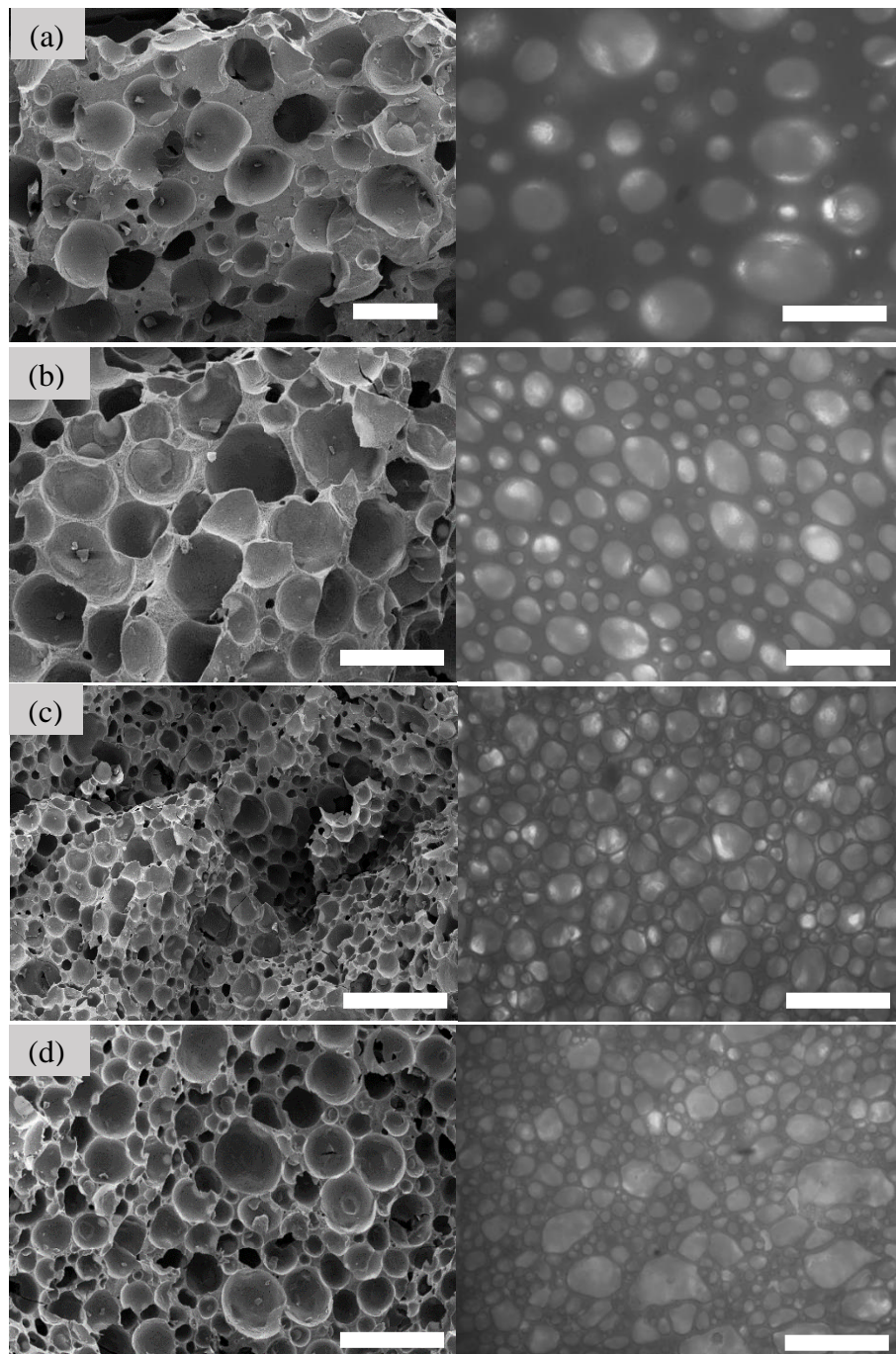
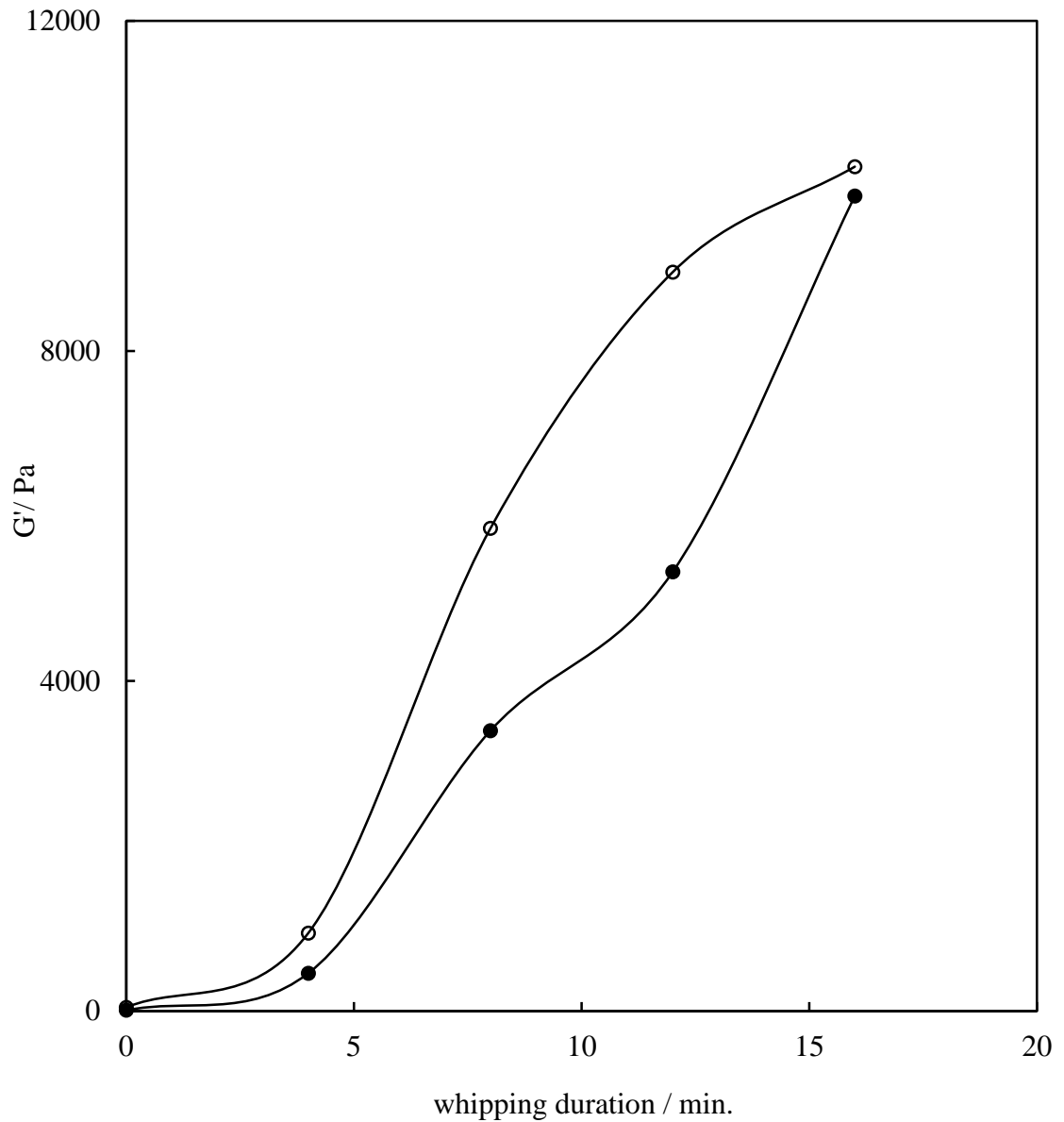


Figure 4.23. Variation of elastic modulus (G') of model whipped cream samples (filled points) and whipped VBC (empty points) upon increasing whipping duration. The modulus was measured by oscillation rheology at a temperature, frequency and stress of 10 °C, 1 Hz and 10 Pa, respectively. The composition of the model cream was 20 wt. % PKO, 1.35 wt. % SSL, 0.1 wt. % xanthan gum and 78.55 wt. % water. 1 wt. % PCC particle with respect to the volume of cream in the whipping bowl was added as an aqueous dispersion just before aeration.



4.4.3.3 Stability of foams towards serum drainage

The model whipped creams were characterised in terms of their stability towards liquid drainage at different stages of whipping. Table 4.6 shows the serum drainage data from 20 g of foam samples aerated for different durations. The stability of the samples towards drainage was improved as the whipping continued up to 16 minutes. Similar to the effect of PKO volume fraction, the improvement in serum drainage is due to the development of the partially coalesced network of fat droplets within the continuous phase, which reduces the extent and rate of liquid drainage by limiting the movement of the liquid. Model whipped cream with 1 wt % PCC particles showed no drainage after 4 days when aerated for 12 minutes, unlike the whipped VBC which showed 2 mL serum drainage after the same period of time.

Table 4.6. Serum drainage volume from 20 g of model whipped cream samples upon increasing whipping duration. The foam sample was stored at room temperature in a sealed vessel to avoid evaporation of water. The composition of the model cream was 20 wt. % PKO, 1.35 wt. % SSL, 0.1 wt. % xanthan gum and 78.55 wt. % water. 1 wt. % PCC particle with respect to the volume of cream in the whipping bowl was added as an aqueous dispersion just before aeration. Whipped VBC showed 1 and 2 mL drained serum after 1 and 4 days, respectively (data shown previously).

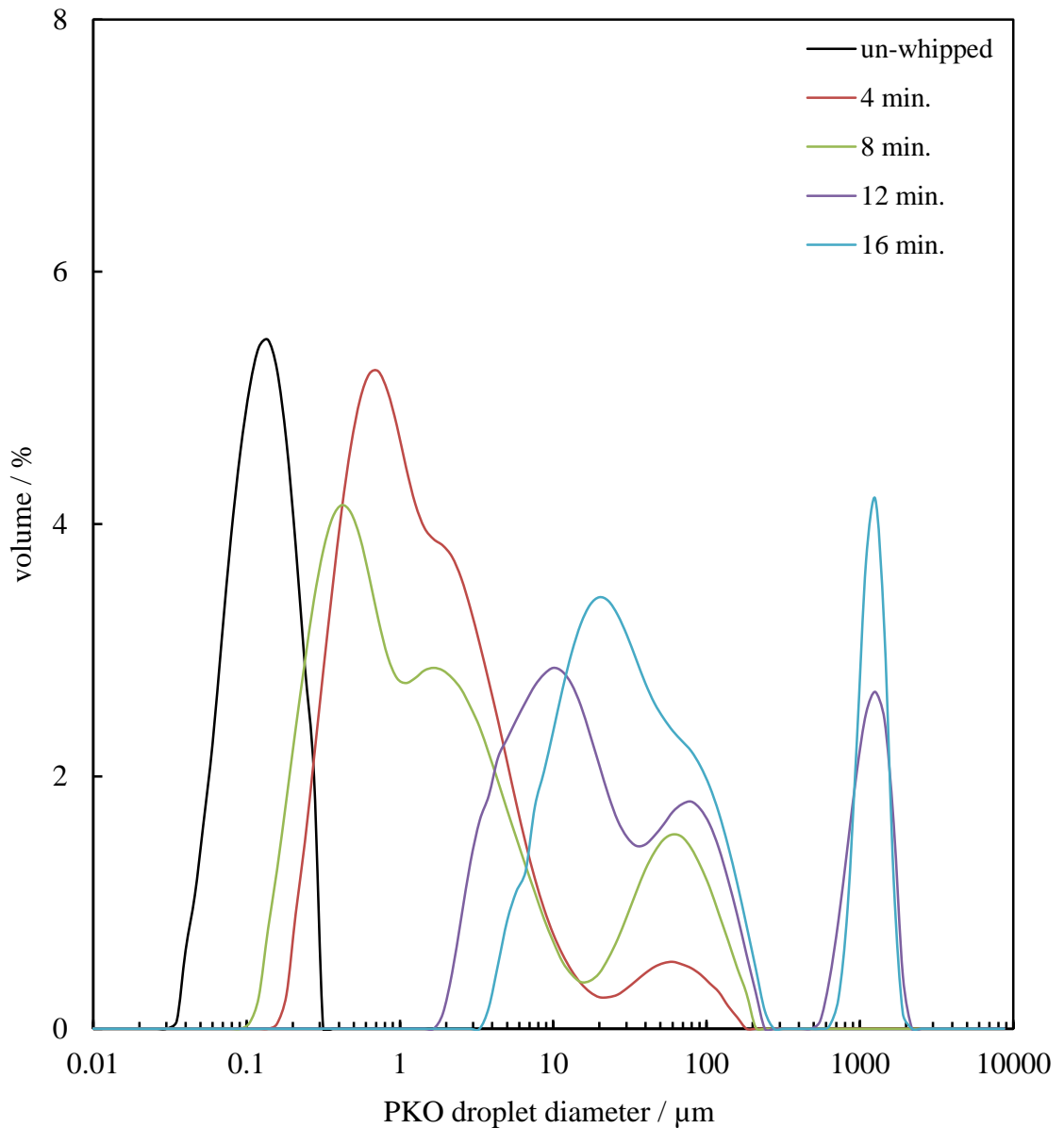
Whipping duration / minutes	Drained liquid after 1 day / mL	Drained liquid after 4 days / mL
4	4	6
8	0	1
12	0	0
16	0	0

4.4.3.4 PKO droplet size evolution upon whipping

PKO droplets coalesce with each other upon aeration and improve the viscoelastic properties of the foams. The size distributions of PKO droplets were measured in the model cream prior to whipping and at different stages of the whipping to assess the evolution of the droplet “connectivity” upon partial coalescence. Determining the size distribution of PKO droplets in the aerated emulsions requires a specific protocol due to partial coalescence of the initial PKO droplets, forming large and fragile clusters. If foam directly introduced in the apparatus, such clusters are easily broken by the agitation, and consequently, the droplet size distribution is not representative of the system. In addition, presence of air bubbles may give rise to peaks in the final distribution, which are not representation of PKO droplets. To overcome this difficulty as suggested by Gravier *et al.*³⁹ and explained in Section 2.2.11.1, one gram of foam was diluted in 10 mL water and heated at 60 °C for 30 minutes. At this temperature PKO is fully melted and the aggregates comprising partially coalesced droplets undergo shape relaxation (under the effect of surface tension) that generates spherical droplets. Using this method it was ensured that all the air bubbles were coalesced and collapsed during the heating stage and the peaks represented PKO droplets only. This was performed by observing the heated foam using optical microscopy to ensure no air bubbles were present.

Figure 4.24 shows the PKO droplet size distribution in model whipped cream, which varies due to partial coalescence at different stages of whipping. The size distribution of the model cream before whipping as shown previously in Figure 4.3 showed a single peak at around 140 nm, which is also included here. In whipped samples, partial coalescence was revealed by the occurrence of one or several peaks at larger PKO size distributions that were not present in the primary emulsion. As can be seen in the figure upon aeration the size distribution shifts to larger sizes. The size distributions of the samples whipped for 12 and 16 minutes show peaks at around 1 mm with the population of the droplets at those sizes increasing with whipping time. This evolution confirms that clusters of partially coalesced PKO drops are being connected during the whipping process and one of the causes of whipping is the increase of the connectivity between the PKO droplets due to partial coalescence.

Figure 4.24. Variation of PKO droplet size distribution in the model whipped cream due to partial coalescence during aeration. The duration of aeration for each curve is highlighted. The results clearly show the shift of the distribution towards larger PKO droplets as the whipping continues. The composition of the model cream was 20 wt. % PKO, 1.35 wt. % SSL, 0.1 wt. % xanthan gum and 78.55 wt. % water. 1 wt. % PCC particle with respect to the volume of cream in the whipping bowl was added as an aqueous dispersion just before aeration.



4.5 Homogenisation method

4.5.1 Pilot laboratory homogeniser

The model whipped cream samples were prepared in the pilot laboratory of the sponsor of the project in order to check the reproducibility of the data and for scale up the protocol. The apparatus used for homogenisation together with heat exchangers was detailed in Chapter 2. The homogenisation conditions in the pilot laboratory such as temperature and pressure applied were identical to the conditions applied using the table-top HPH, however the volume of the emulsions produced was 100 litres compared to 2 litres when the table-top HPH was used.

The size distributions of the model cream with the composition of 20 wt. % PKO, 1.35 wt. % SSL, 0.1 wt. % xanthan gum and 78.55 wt. % water, produced in the pilot laboratory was determined using light scattering prior to aeration. The results are shown in Figure 4.25 together with the data from the model cream produced using the table-top HPH. Both instruments produced emulsions with a monomodal size distribution of PKO droplets at 140 nm, which shows the emulsifying efficiency was independent of the homogeniser used and was mainly determined by the homogenisation conditions such as temperature and pressure.

The model whipped cream produced in the pilot laboratory was stored in a fridge at 6 °C for 24 hours before aeration, similar to previous samples. 1 wt. % PCC particles (with respect to the volume of emulsion in the whipping bowl) was added to the model cream as an aqueous dispersion and then aerated using the same Hobart mixer for 12 minutes. Aeration of the emulsions yielded overrun values of about 360 % for both instruments. The peaking appearance of the foams made in the pilot laboratory is shown together with the foam produced using the table-top HPH in Figure 4.26, where it can be seen both foams produced peaks of very similar stiffness and structure. Therefore one can conclude that the model whipped cream produced with three stabilising components (SSL, PCC particles and xanthan gum) are reproducible in the pilot laboratory and probably at larger scales.

Figure 4.25. Size distribution of PKO droplets in the model cream emulsion (20 wt. % PKO, 1.35 wt. % SSL, 0.1 wt. % xanthan gum and 78.55 wt. % water) measured after exiting the table-top HPH (solid line) or the pilot laboratory HPH (dashed line). As can be seen both HPH instruments yield similar PKO droplet size distribution.

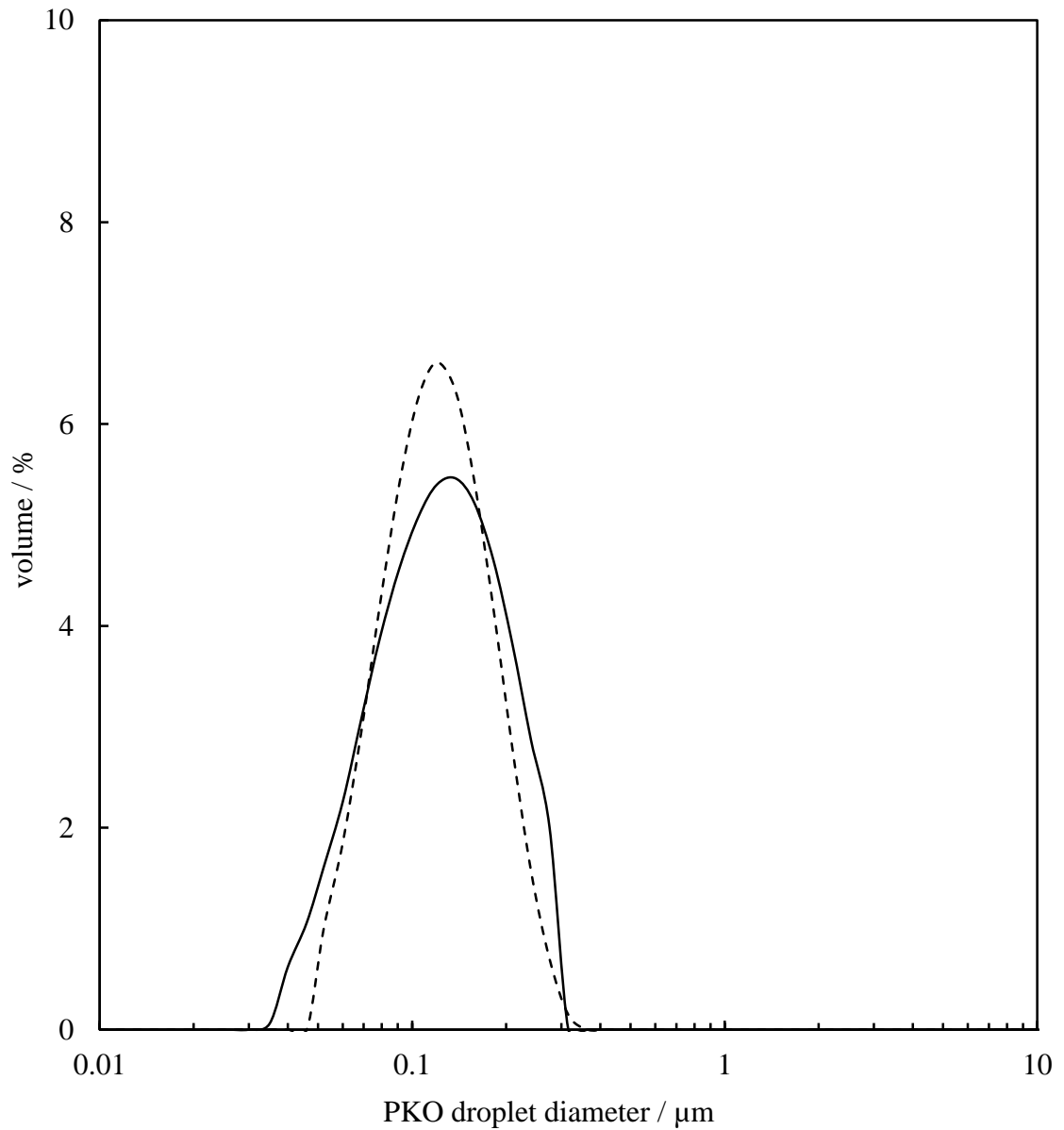


Figure 4.26. Appearance of a peak made from the model whipped cream homogenised using pilot laboratory HPH (left) and table-top HPH (right). Both model creams were aerated using the Hobart mixer for 12 minutes. The composition of both model creams included 1 wt. % PCC, 20 wt. % PKO, 1.35 wt. % SSL, 0.1 wt. % xanthan gum and 77.55 wt. % water.



4.6 Effect of temperature on whipping properties of VBC

In the final section of this chapter the data from the aeration of VBC at different temperatures together with cryo-SEM images of aerated VBC are presented. The aim was to further understand the relationship between the SFC of PKO droplets and the structural properties of whipped VBC. As mentioned earlier the three-dimensional network formed from the partial coalescence of the fat droplets is one of the main factors controlling the stability of the air bubbles and providing stiffness in whipped cream. The SFC of the PKO in fat droplets influences the extent of partial coalescence in the formed network and hence the structure of the whipped cream. VBC was whipped at different temperatures after being kept in a fridge at 6 °C for 24 hours. Whipping was carried out at temperatures of 5, 10, 20, 30, 40 and 50 °C. Different samples of VBC were stored in a thermostated water bath to reach the desired temperature and aeration was carried out for 6 minutes for all temperatures. Figure 4.27 shows the appearance of the whipped VBC on the whisk and also a section of the whipped VBC on a watch glass after whipping. As can be seen from the images, the stiffness of the whipped product decreases as the temperature VBC increases with the stiffest whipped cream produced at 5 and 10 °C. This is known to be as a result of the variation of the SFC of PKO with temperature.

Figure 4.28 shows the variation of the overrun with whipping temperature. It is clear that temperature has a large influence on the overrun values obtained from aeration of VBC. Aeration of the VBC at 50 °C did not incorporate much air into the emulsion with the overrun only being 130 % ($\phi_{\text{air}} = 0.24$). This is in agreement with the SFC of the PKO at 50 °C being 0 %, *i.e.* PKO is present in a liquid state and no partial coalescence occurs between PKO droplets. Whipping the emulsion at 10 °C was found to give the highest overrun value. This suggests that the crystals of PKO in fat globules provide maximum stability for air bubbles in whipped VBC at this temperature. This observation confirms that an aeration temperature of 8 °C for the model foams in this projects, suggested by the sponsor, was optimum for whipping of model creams also containing PKO as the oil phase.

Figure 4.27. Appearance of whipped VBC on the whisk (left images) and on a watch glass (right images) imaged immediately after whipping at different temperatures. Temperatures of the whipping and imaging were (a and b) 5 °C, (b and c) 10 °C, (e and f) 30 °C and (g and h) 50 °C. Scale bars represent 3 cm.

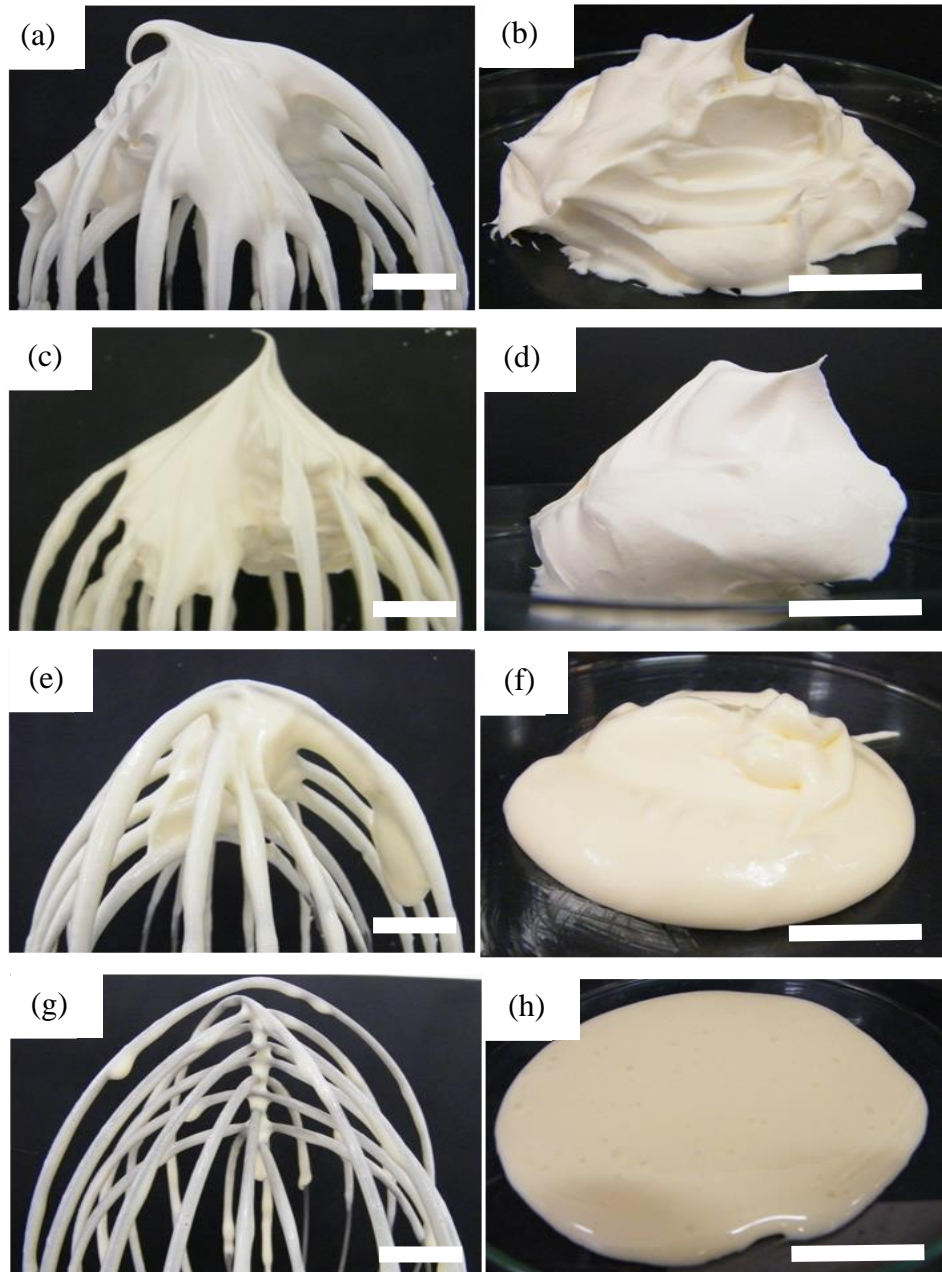
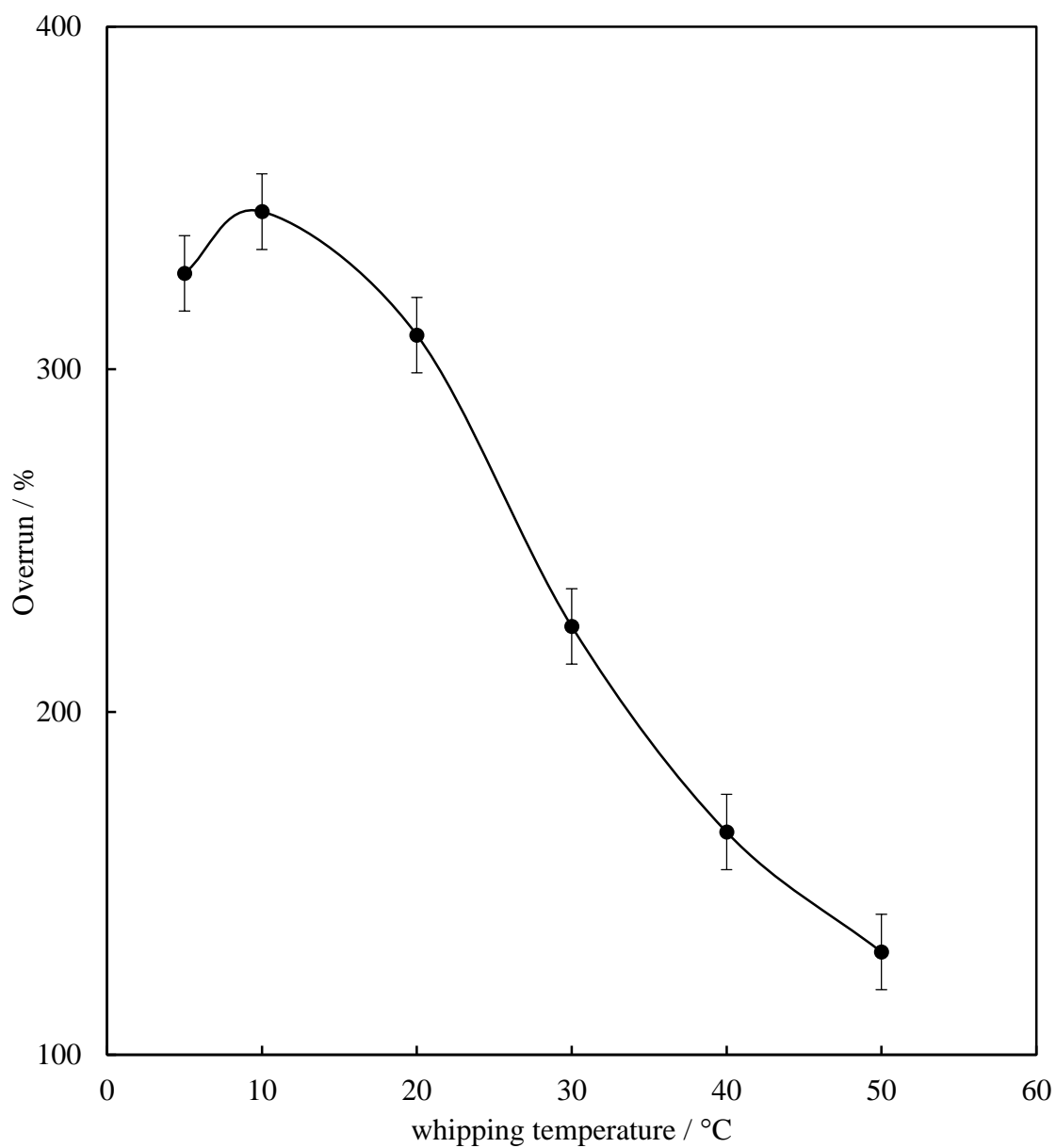
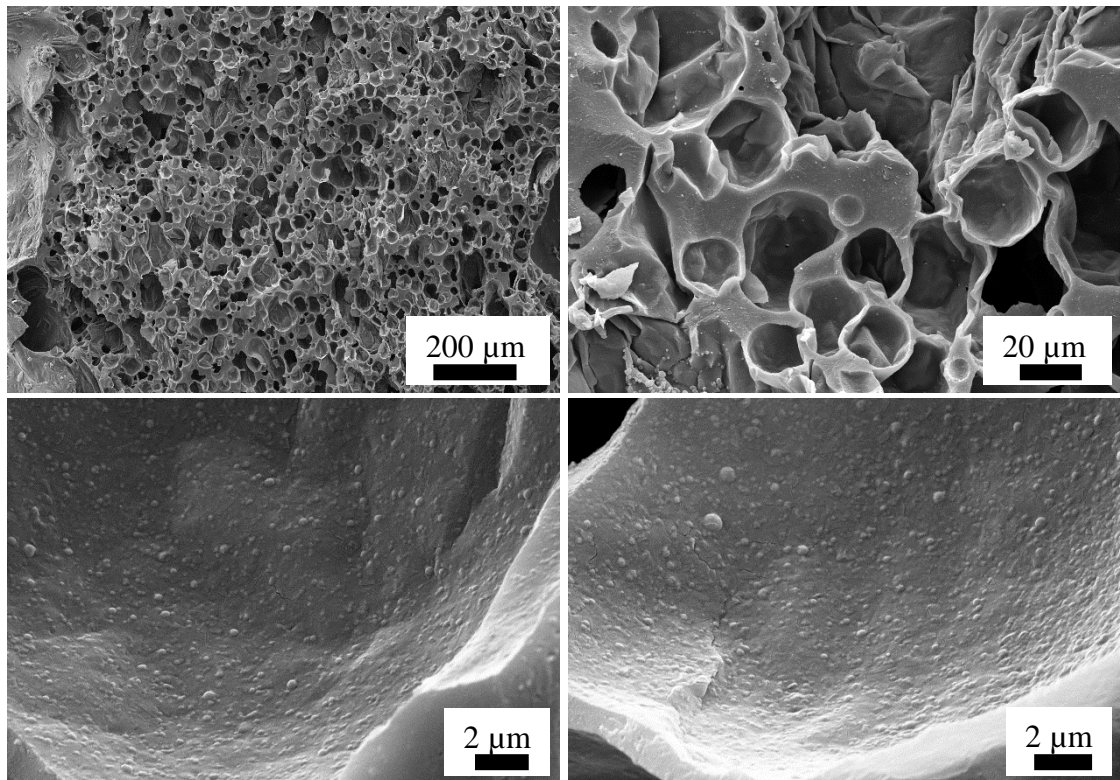


Figure 4.28. Variation of the overrun obtained from whipping VBC at different temperatures. Mass of VBC before aeration was 650 g for all temperatures.



The whipped VBC sample was further characterised using cryo-SEM imaging to visualise the positioning of PKO droplets around air bubbles. The images are shown in Figure 4.29. Comparing the size of air bubbles in whipped VBC, $30 \pm 3 \mu\text{m}$, with those of whipped model cream (containing 1 wt. % PCC particles), $90 \pm 10 \mu\text{m}$, reveals that whipped VBC contains smaller air bubbles. The smaller air bubbles in VBC as explained before is due to the presence of various stabilisers in the formulation, such as sodium caseinate and methyl cellulose, which help to reduce the air-water interfacial tension and create smaller air bubbles. The lower images in the figure show the inner surfaces of different air bubbles on which PKO droplets are visible.

Figure 4.29. Cryo-SEM images of whipped VBC immediately after aeration at 10°C for 6 minutes. PKO droplets on the inner surface of two air bubbles are visible in lower images.



4.7 Conclusions

Whipped cream is an aerated oil-in-water emulsion in which the air bubbles are surrounded to varying degrees by partially-coalesced fat droplets. The rigid network of partially coalesced fat droplets is known to be the major stabilising factor in whipped cream. PCC particles were applied in model whipping cream samples to investigate whether they can fulfil all or part of the role played by fat droplets in stabilising air bubbles in whipped cream. Model whipping cream samples were prepared and their aeration properties have been systematically studied.

The SFC of PKO, an important factor in partial coalescence of PKO droplets, was determined using DSC. As expected the SFC decreased when the temperature was increased between -10 °C (when the oil is fully crystallised, 100% SFC) and 40 °C (when the oil is fully melted, 0 % SFC).

PKO droplet size distributions of the model whipping cream before aeration were determined and were shown to be similar to the size distribution of PKO droplets in un-whipped VBC ($d(0.5) = 150$ nm). It was found that when the PCC particles were added as an aqueous dispersion to the prepared model whipping cream just before aeration, the cream yielded high overrun values and great stability. The effect of the addition of Calofort U PCC particles on the aeration properties of the model cream was explored and found to significantly improve the overrun, peaking, rosette definition and stability towards drainage. The influence of PKO volume fraction on the aeration properties of the model cream was also investigated. It was found that increasing PKO volume fraction increased the stiffness of the produced foams, however there was no significant effect on the overrun values. Using cryo-SEM analysis, various images of the whipped creams were taken and visually inspected to locate the position of PCC particles in the foams. It was found that when both PKO droplets and PCC particles were present in the model creams, SSL vesicles were driven to the air-water interface during aeration. It is believed that, SSL vesicles were pushed out of the water phase to the air-water interface upon formation of the three-dimensional network of partially coalesced fat droplets. Using cryo-SEM it was not possible to observe the Calofort U PCC particles at the surface of air bubbles in foams due to the Pt coating used and the similarity in the size of these particles with PKO droplets. However, SEM images without coating revealed white fragments of PCC particles on the surfaces of the air bubbles. In order to check the

adsorption behaviour of PCC particles at the air-water interface, a PKO-free model cream was prepared and analysed using cryo-SEM. The images showed that air bubbles were completely coated with PCC particles. Although it was not possible to show a similar trait for the samples containing both PCC particles and PKO droplets, can say that the same phenomenon occurs in these foams and PCC particles adsorb around air bubbles together with PKO droplets.

Aeration of VBC was carried out at different temperatures in order to understand the effect of the SFC on the overrun and stiffness of whipped VBC. It was shown that both overrun and stiffness depended strongly on the cream temperature and optimum whipping was obtained when the temperature was 10 °C. The PKO droplets contain 85 % SFC at that temperature.

Finally, it should be emphasised that the model cream samples studied here did not include many of the stabilisers normally present in VBC, such as sodium caseinate, soy protein concentrate, carbohydrate gum, polyglycerol esters of fatty acids, polysorbate 60 and soy lecithin. These creams however were shown to have similar overrun, elastic modulus and peaking properties compared to whipped VBC and they were shown to be fully stable towards serum drainage, unlike whipped VBC.

4.8 References

1. D. Rousseau, *Food Res. Int.*, **33**, 3 (2000).
2. K. Boode and P. Walstra, *Colloids Surf. A*, **81**, 121 (1993).
3. K. Boode, P. Walstra and A.E.A. de Groot-Mostert, *Colloids Surf. A*, **81**, 139 (1993).
4. H.D. Goff, *J. Dairy Sci.*, **80**, 2620 (1997).
5. *Advances in Food Emulsions and Foams*, ed. E. Dickinson and G. Stainsby, Elsevier Applied Science, London, 1988.
6. F. Leal-Calderon, *Oilseeds and fats, Crops and Lipids*, **19**, 111 (2012).
7. G.A. van Aken, *Colloids Surf. A*, **190**, 333 (2001).
8. *An Introduction to Food Colloids*, E. Dickinson, Oxford University Press, Oxford, 1992.
9. M.M. Camacho, N. Martínez-Navarrete and A. Chiralt, *Food Res. Int.*, **31**, 653 (1998).
10. M.M. Camacho, N. Martínez-Navarrete and A. Chiralt, *Int. Dairy J.*, **15**, 243 (2005).
11. M. Sajedi, A. Nasirpour, J. Keramat and S. Desobry, *Food Hydrocoll.*, **36**, 93 (2014).
12. Q. Zhao, M. Zhao, J. Li, B. Yang, G. Su, C. Cui and Y. Jiang, *Food Hydrocoll.*, **23**, 2168 (2009).
13. Q. Zhao, M. Zhao, J. Wang, C. Wang and B.A.O. Yang, *J. Food Process Eng.*, **31**, 671 (2008).
14. Q. Zhao, M. Zhao, B. Yang and C. Cui, *Food Chem.*, **116**, 624 (2009).
15. Q. Liu, S. Zhang, D. Sun and J. Xu, *Colloids Surf. A*, **355**, 151 (2010).
16. Z.P. Du, M.P. Bilbao-Montoya, B.P. Binks, E. Dickinson, R. Ettelaie and B.S. Murray, *Langmuir*, **19**, 3106 (2003).
17. E. Dickinson, R. Ettelaie, T. Kostakis and B.S. Murray, *Langmuir*, **20**, 8517 (2004).
18. R.G. Alargova, D.S. Warhadpande, V.N. Paunov and O.D. Velev, *Langmuir*, **20**, 10371 (2004).
19. B.P. Binks and T.S. Horozov, *Angew. Chem. Int. Ed.*, **44**, 3722 (2005).
20. C.A. Padiernos, S.Y. Lim, B.G. Swanson, C.F. Ross and S. Clark, *J. Dairy Sci.*, **92**, 3049 (2009).

21. Y. Ma, C. Cai, J. Wang and D.W. Sun, *J. Food Eng.*, **73**, 297 (2006).
22. E. Malinski, J.R. Daniel, X.X. Zhang and R.L. Whistler, *Cereal Chem.*, **80**, 1 (2003).
23. Q. Jin, T. Zhang, L. Shan, Y. Liu and X. Wang, *J. Am. Oil Chem. Soc.*, **85**, 23 (2008).
24. W.L. Siew, *Eur. J. Lipid Sci. Technol.*, **103**, 729 (2001).
25. D. Kurukji, R. Pichot, F. Spyropoulos and I.T. Norton, *J. Colloid Interface Sci.*, **409**, 88 (2013).
26. N.E. Hotrum, M.A. Cohen Stuart, T. Van Vliet, S.F. Avino and G.A. Van Aken, *Colloids Surf. A*, **260**, 71 (2005).
27. *Rheology of industrial polysaccharides: theory and applications*, R. Lapasin and S. Pricl, Blackie Academic & Professional, Gaithersburg, 1995.
28. *The Kitchen as Laboratory: Reflections on the Science of Food and Cooking*, C. Vega, J. Ubbink and E. van der Linden, Columbia University Press, Chichester, 2013.
29. M. Maskan and F. Göğüş, *J. Food Eng.*, **43**, 173 (2000).
30. C. Wang, X.W. He, Q. Huang, X. Fu and S. Liu, *J. Food Eng.*, **116**, 881 (2013).
31. B.P. Binks, J.H. Clint and C.P. Whitby, *Langmuir*, **21**, 5307 (2005).
32. K.E. Allen, E. Dickinson and B. Murray, *LWT - Food Sci. Technol.*, **39**, 225 (2006).
33. K. Ihara, C. Kajiya, Y. Shimada, Y. Asano and S. Kokubo, *Nippon Shokuhin Kagaku Kogaku Kaishi*, **52**, 553 (2005).
34. K. Ihara, K. Habara, Y. Ozaki, K. Nakamura, H. Ochi, H. Saito, H. Asaoka, M. Uozumi, N. Ichihashi and K. Iwatsuki, *J. Dairy Sci.*, **93**, 2887 (2010).
35. B.E. Brooker, M. Anderson and A.T. Andrews, *Food Microstruct.*, **5**, 277 (1986).
36. *Food emulsions and foams*, ed. E. Dickinson, Royal Society of Chemistry, London, 1987.
37. E. Jakubczyk and K. Niranjana, *J. Food Eng.*, **77**, 79 (2006).
38. J.C. Arboleya, M.J. Ridout and P.J. Wilde, *Food Hydrocoll.*, **23**, 1358 (2009).
39. E. Gravier, N. Drelon, L. Boisserie, A. Omari and F. Leal-Calderon, *Colloids Surf. A*, **282-283**, (2006).

CHAPTER 5 COMPARATIVE STUDY OF PALM KERNEL OIL- IN-WATER EMULSIONS STABILISED BY EITHER PARTICLES OR SURFACTANTS

5.1 Introduction

One of the main factors controlling the stability of oil droplets against coalescence in oil-in-water emulsions is the type of stabiliser. It has been shown in various studies that when solid particles are used as emulsion stabilisers, the emulsions show greater stability towards coalescence compared to those emulsions stabilised by surfactant molecules.¹

Another factor affecting the stability of oil-in-water emulsions is the oil type. Oil-in-water emulsions made of crystallisable oil have different properties to those containing only liquid droplets.² The general features of oil crystallisation in oil-in-water emulsions have been well studied in the literature.²⁻⁶ There are several factors that influence the rate and extent of crystallisation that takes place in the oil phase such as temperature, oil droplet size,⁷ nature of stabiliser,⁸ droplet-droplet interactions⁹ and cooling rate.¹⁰ Crystallisation in emulsion droplets is known to occur in two ways; homogeneous and heterogeneous. If the oil droplets have no impurities, then homogeneous crystallisation will occur. If impurities are present, the crystals will form in a heterogeneous manner. Crystallisation of the oil phase always starts with the formation of a nucleus, an ordered domain in the liquid; a process called nucleation. Nucleation may proceed *via* either a homogeneous or heterogeneous route depending on the size of the oil droplets, the abundance of impurities and the temperature.¹¹

The presence of fat crystals within the oil droplets has been shown to affect the stability of the emulsions and promote partial coalescence between crystallised oil droplets.^{4, 12} In partial coalescence, crystals at the surface of one droplet penetrate the surface of another droplet upon contact between them. The liquid oil in the second droplet then flows out and reinforces the contact point between the two droplets.^{2, 13}

Giermanska *et al.*¹⁴ studied the gelation of oil-in-water emulsions at quiescent conditions. They observed a significant change in the texture of the emulsions prepared and reported that the initially fluid emulsion turned into a strong gel that no longer flowed under its own weight. Their emulsions were made of hexadecane and paraffin

oils stabilised by polyoxyethylene (20) sorbitan monolaurate (Tween 20), a non-ionic surfactant. In another study Thivilliers *et al.*¹⁵ studied shear-induced gelation of oil-in-water emulsions containing natural anhydrous milk fat as the oil phase and stabilised by a mixture of sodium caseinate and Tween 20. Both studies proposed two mechanisms for the gelation, both induced by crystallisation of dispersed oil droplets. In one scenario, gelation in the emulsions is due to partial coalescence of oil droplets, which resulted in film rupture between the two droplets. In the other mechanism, gelation occurred without film rupture and was induced by surface roughness, which restricted droplets from internal dynamics, known as ‘jamming’. Both Giermanska *et al.*¹⁴ and Thivilliers *et al.*¹⁵ concluded that partial coalescence was more likely to occur if the oil droplets had a large average droplet size, and jamming was more likely to occur if the oil droplet size was small. They believed that jamming occurred with smaller droplets since the crystal growth was insufficient to cause film rupture, but was enough to cause surface roughness.¹⁵ Using temperature cycles, both Giermanska *et al.*¹⁴ and Thivilliers *et al.*¹⁵ also showed that if gelation of emulsions was due to jamming of the droplets, the emulsions did not phase separate upon re-heating. This was unlike gels formed *via* the partial coalescence mechanism.

In other studies, scientists have shown that the stability of an oil-in-water emulsion depends on the cooling rate of the emulsion after its preparation, which always occurs at a temperature above the melting point of the oil phase.^{10, 16} Tippetts and Martini studied the effects of different cooling rates on the stability of oil-in-water emulsions made of anhydrous milk fat and soybean oil, using whey protein as the emulsifier. They concluded that emulsions are more stable towards coalescence when a faster cooling rate is applied.¹⁰

To the best knowledge of the author, the work reported here shows that for the first time, oil-in-water emulsions containing crystallisable oil can be stabilised by solid particles. The properties of PKO-in-water emulsions stabilised by PCC particles and those stabilised by SSL are compared in this chapter. After preparation of the emulsions and upon cooling, PKO droplets crystallise and the initial fluid emulsions turn into hard gels with both stabilisers. The mechanism by which this occurred however was found to depend on the type of stabiliser used and this is explained later. The effects of stabiliser concentration on the stability of the emulsions and on the droplet size has also been studied. A further study was carried out on PKO-in-water emulsions stabilised by PCC

particles to analyse the effect of storage temperature on the stability and on the oil droplet size evolution.

5.2 Effect of stabiliser concentration

Equal volumes of melted PKO and water were homogenised with the two stabilisers to study the effect of stabiliser type on the stability of the emulsions. For particle-stabilised emulsions, the powdered particle method was used to add the PCC particles to make the emulsions.¹⁷ PKO was heated to 80 °C to ensure that the oil is fully melted and all nuclei are broken. The emulsification was carried out at 80 °C. Both sets of emulsions were left to cool naturally at an approximate rate of 1 °C min⁻¹ to room temperature (23 °C). For SSL-stabilised emulsions, melted PKO was emulsified at the same conditions detailed above with SSL aqueous dispersions. The hydrophilic nature of both stabilisers resulted in the production of water continuous emulsions in both cases. The results of the conductivity measurements also proved this and were the same for both stabilisers, with all emulsions having conductivities above the conductivity of pure PKO (0.65 µS cm⁻¹). This was further confirmed with drop test analysis, proving that emulsions produced were PKO-in-water.

Figure 5.1 shows the appearance of PKO-in-water emulsions stabilised by PCC particles and by SSL surfactant one day after their preparation. The samples without any stabiliser were immediately phase separated into bulk PKO and water phases after homogenisation. For the emulsions stabilised by SSL, the aqueous phase has an increasingly opaque and white appearance, resulting from the formation of liquid crystalline phases of non-adsorbed SSL in the water phase. This is unlike the emulsions prepared with PCC particles, which had clear water phases.

No coalescence was observed for any of the emulsions one hour after preparation. Previous studies have shown that the stability of emulsions increases with increasing stabiliser concentration.¹⁸⁻²⁰ Emulsions made from both stabilisers here similarly showed better stability towards creaming upon increasing the concentration of stabiliser. The effect was more noticeable in the case of emulsions stabilised by SSL. As mentioned earlier SSL molecules, form liquid crystalline structures, *i.e.* bi-layers and multi-layer vesicles, within the aqueous phase hence giving rise to the viscosity. According to Stokes law, the rate of creaming of a single oil droplet in an oil-in-water emulsion is proportional to the mass density difference between the oil and the water phase and the

square of the droplet diameter. It is also inversely proportional to the viscosity of the continuous phase, that is, the higher its viscosity, the lower the rate of creaming of the PKO droplets in these emulsions. In addition, decreasing the size of the PKO droplets with increasing stabiliser concentration also reduces the rate of creaming in these emulsions.

Figure 5.1. Appearance of PKO-in-water emulsions stabilised by PCC particles (upper image) and by SSL surfactant (lower image) one day after their preparation. The emulsions were prepared at 80 °C and were left to cool naturally at an approximate rate of 1 °C min⁻¹ to room temperature (23 °C). Numbers below each emulsion refer to the wt. % of stabiliser with respect to the total mass of PKO and water phases, $\phi_o = 0.5$.

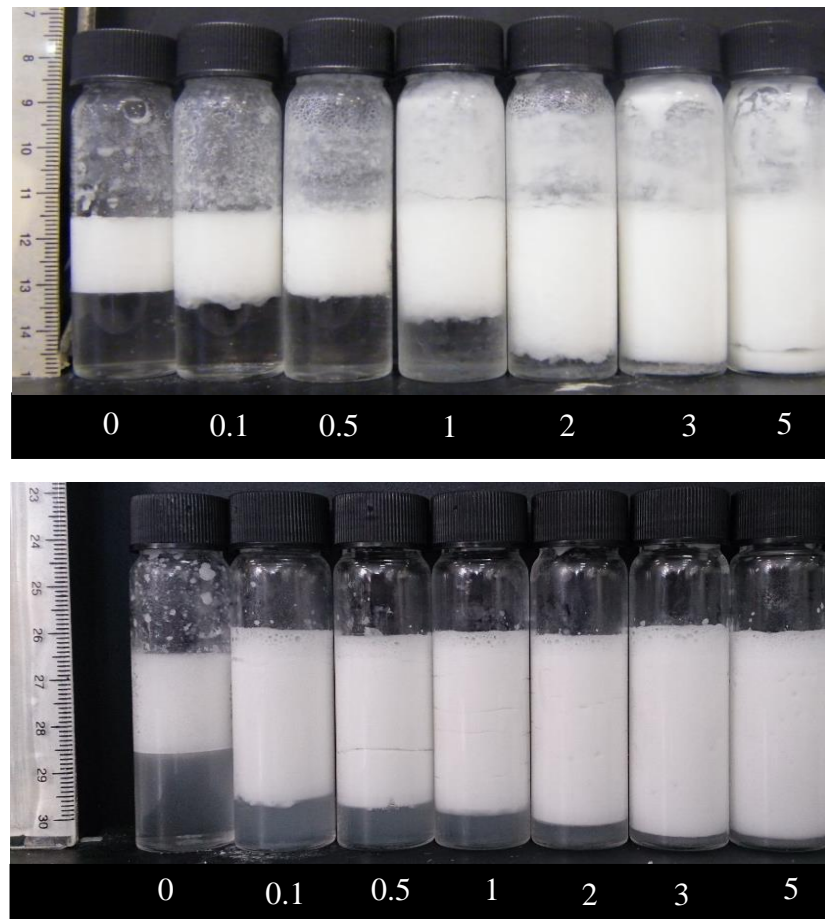


Figure 5.2 displays cryo-SEM images of a PKO-in-water emulsion stabilised by 1 wt. % Calofort U PCC particles and optical micrographs of a PKO-in-water emulsion stabilised by 1 wt. % SSL. The emulsions were observed one hour after preparation and were at room temperature (23 °C) at the time of sampling. For the emulsions stabilised by particles, cryo-SEM images clearly show that the surfaces of PKO droplets are coated

by PCC particles when viewed under high magnification. This is to be contrasted with the smooth surface of PKO droplets in the emulsion stabilised entirely by SSL, Figure 5.2 (b and d), which look featureless.

Another difference between the emulsions stabilised by PCC particles and those stabilised by SSL is the PKO droplet shape. As shown in Figure 5.2, all droplets in the emulsion stabilised by SSL are spherical whereas the emulsion stabilised with PCC particles reveals several non-spherical droplets. Formation of non-spherical particle-coated fluid dispersed phases has been reported previously.^{21, 22} This is believed to be due to jamming of particles at the interface preventing relaxation of the interface to a spherical geometry.

Reviewing Figure 5.2 in terms of the size of the droplets in the emulsions shows that PKO droplets stabilised by SSL were smaller than those stabilised by the same concentration of PCC particles. This was further confirmed by droplet size measurement data presented in Figure 5.3. The graph shows the influence of type and concentration of stabiliser on the average droplet diameter in PKO-in-water emulsions. The emulsion droplets prepared using the PCC particles are always larger than those stabilised by SSL. It is believed that since surfactant molecules are smaller than PCC particles, they adsorb to the PKO-water interface faster than PCC particles and hence give rise to smaller droplets. For both sets of data, the average size of PKO droplets decreases gradually with an increase in stabiliser concentration and then remains more or less constant above 3 wt. %.

The mechanisms by which surfactant molecules and solid particles stabilise the droplet are believed to be different. Surfactants decrease the interfacial tension between the two phases and facilitate droplet formation.²³ That is the higher the surfactant concentration, the easier oil droplets break into smaller ones, *i.e.* the smaller the emulsion droplets. This is unlike solid particles where they attach around the oil droplets and create rigid films that sterically stabilise the droplets.¹ That is the more particles there are available to adsorb around the oil droplets, the larger the area they can stabilise, *i.e.* the smaller the emulsion droplets.

Figure 5.2. The images on the left ((a), (c) and (e)) are cryo-SEM micrographs of a PKO-in-water emulsion stabilised by 1 wt. % Calofort U PCC particles. The images on the right ((b), (d) and (f)) are optical micrographs of a PKO-in-water emulsion stabilised by 1 wt. % SSL. Image (e) shows the surface of a PKO droplet covered with PCC particles. Image (f) shows crystallised PKO droplets stabilised by SSL observed using cross-polarised light revealing the presence of crystals inside droplets. The emulsions were observed one hour after preparation and were at room temperature (23 °C) at the time of sampling. $\phi_o = 0.5$.

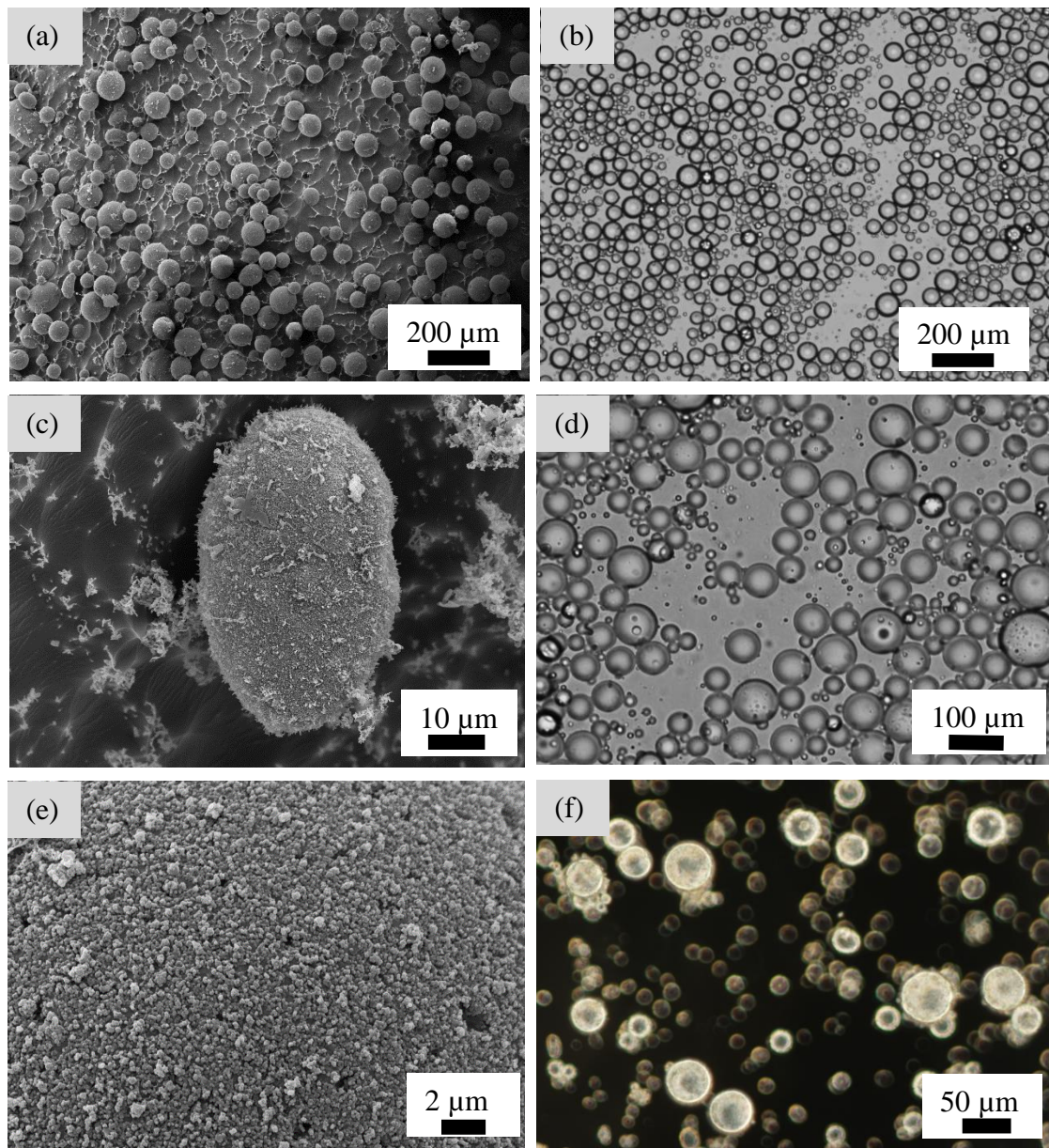
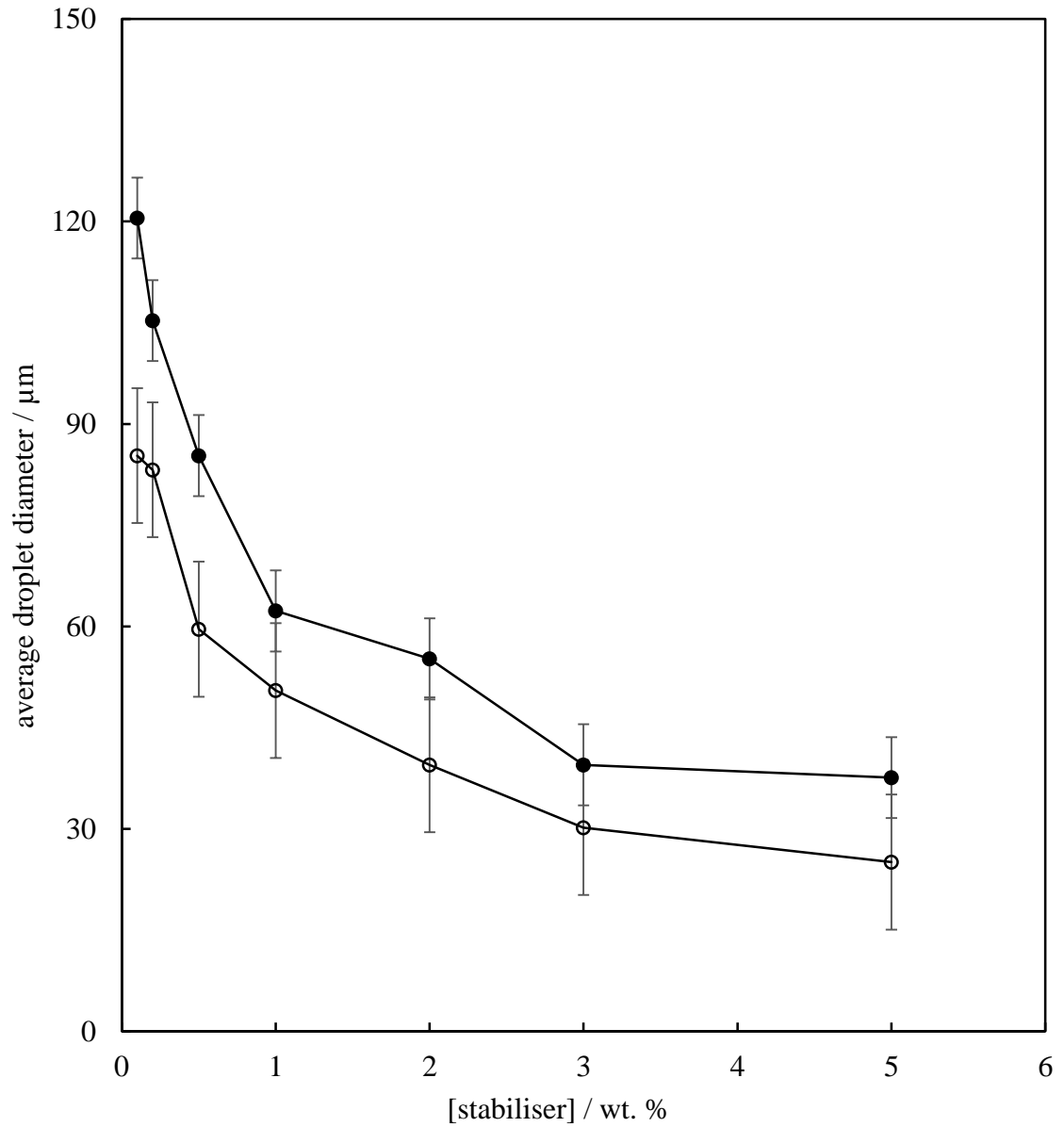


Figure 5.3. Average droplet diameter of PKO-in-water emulsions stabilised by Calofort U PCC particles (filled points) or SSL (empty points) as a function of stabiliser concentration. Droplet diameters were measured from optical microscopy images and the error bars show the standard deviation.



5.3 Gelling of emulsions

PKO-in-water emulsions were prepared at temperatures above the melting point of PKO to facilitate its breakdown into dispersed droplets. The emulsions were left to cool naturally at an approximate rate of $1\text{ }^{\circ}\text{C min}^{-1}$ to room temperature ($23\text{ }^{\circ}\text{C}$). It was observed that the initial fluid emulsions turned into hard gels one day after storage at room temperature ($23\text{ }^{\circ}\text{C}$). This was observed for emulsions stabilised by both PCC particles as well as those stabilised by SSL. Two distinct routes were detected for the gelation in the emulsions similar to the findings of Giermanska *et al.*¹⁴ and Thivilliers *et al.*¹⁵ According to their findings, the mechanism for gelation was dependent on the droplet size, *i.e.* partial coalescence was more likely to occur if the oil droplets had a large average drop size, while jamming was the more likely mechanism if the average droplet size was small. In contrast, the decisive factor in this research was found to be the nature of the stabiliser rather than the droplet size, as will be explained later. It was found that in emulsions stabilised by PCC particles (larger droplet size), gelation occurred *via* a jamming mechanism. In the case of SSL stabilised emulsions (smaller droplet sizes), gelation was found to occur by partial coalescence of the oil droplets.

The explanation proposed for these observations is that when PCC particles coat PKO droplets, they act as a mechanical barrier and stop the extension of crystals out through the droplet surface into the continuous phase. In the droplets stabilised by SSL however, upon cooling, the surface becomes rough and rippled as a result of the formation of irregularly shaped or irregularly oriented crystals, which can protrude into the continuous phase. It is well-known that when such crystals are present in the thin film separating two droplets, they may pierce the film and bridge the surfaces, causing the droplets to coalesce (partial coalescence).²⁴

The origin of the gelling process here was deduced from microscopic and macroscopic analysis of the emulsions. Figure 5.4 shows micrographs of the emulsions one day after their preparation. The initially spherical PKO droplets stabilised by SSL partially coalesced one day after emulsification. The PKO droplets in the emulsion stabilised by PCC particles however remained stable and no partial coalescence was observed.

To further clarify the difference in the mechanisms involved in the gelation of these emulsions, they were warmed to $80\text{ }^{\circ}\text{C}$ at an approximate rate of $1\text{ }^{\circ}\text{C min}^{-1}$. The

emulsions were simultaneously stirred using a magnetic stirrer bar (1 cm length at 100 rpm) to disperse the gelled phase back into the resolved water. Previous research³ has shown that partially coalesced droplets remain stable as long as there is a solid fat network to support their shape, but they fully coalesce when the solid fat network is melted upon heating. This causes the joined droplets to relax their shape under the effect of interfacial tension, which then leaves larger sized droplets than those measured initially. In some cases, warming may even result in complete phase separation.¹⁴

As shown in Figure 5.5, for the emulsions stabilised by PCC particles, warming and stirring did not result in the formation of larger droplets nor did it result in phase separation. The fluidity of the initial emulsions was recovered and droplet size measurement confirmed no change in the size of PKO droplets since their initial preparation. This again confirmed that the PKO droplets stabilised by PCC were not partially coalesced in the gelled emulsions but remained stable.

The results were different for the emulsions stabilised by SSL. After applying the warming and stirring step, the emulsions stabilised by 1 wt. % or lower SSL were completely phase separated into bulk PKO and water phases. It is thought that a high degree of coalescence led to this occurring. The emulsions with more than 1 wt. % SSL revealed centimetre-sized PKO droplets on top of the aqueous phase due to coalescence of PKO droplets during the warming process. These observations confirm that partial coalescence had occurred between PKO droplets in the gelled emulsions stabilised by SSL.

Figure 5.4. Optical micrographs of PKO-in-water emulsions stabilised by 1 wt. % PCC particles (upper images) and cryo-SEM images of PKO-in-water emulsions stabilised by 1 wt. % SSL (lower images) one day after preparation. The emulsions were prepared at 80 °C and were left to cool naturally at an approximate rate of 1 °C min⁻¹ to room temperature (23 °C). Crystallised PKO droplets stabilised by SSL can be seen to be partially coalesced whereas those stabilised by PCC particles are fully stable towards coalescence. $\phi_o = 0.5$.

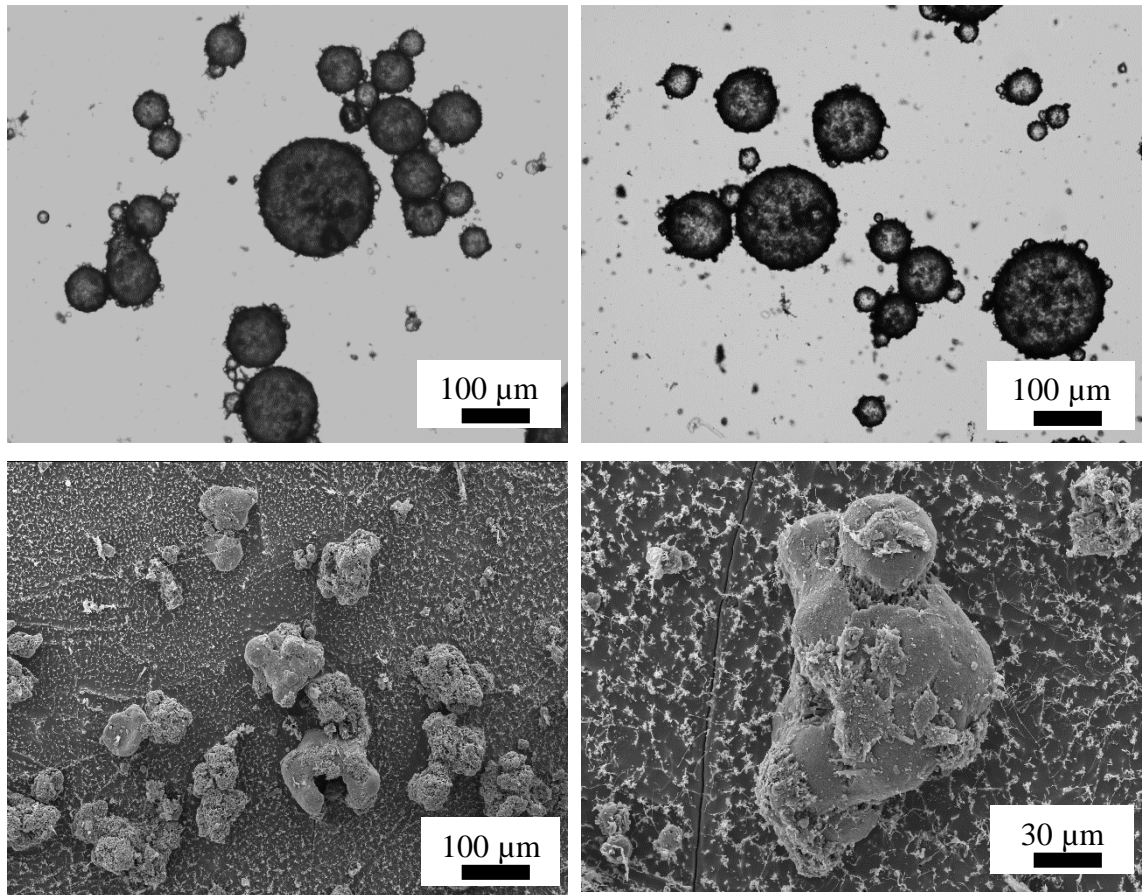
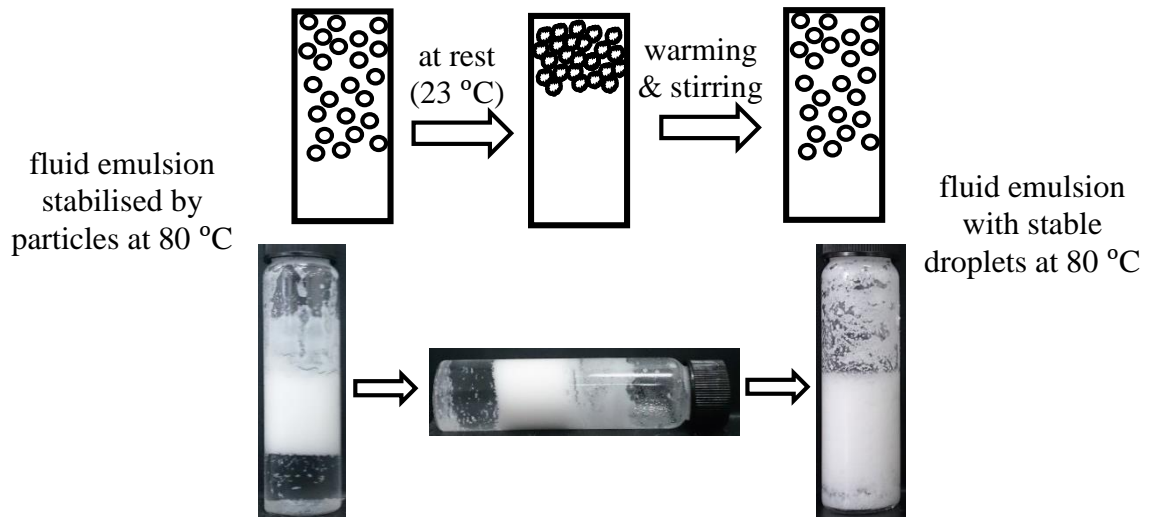
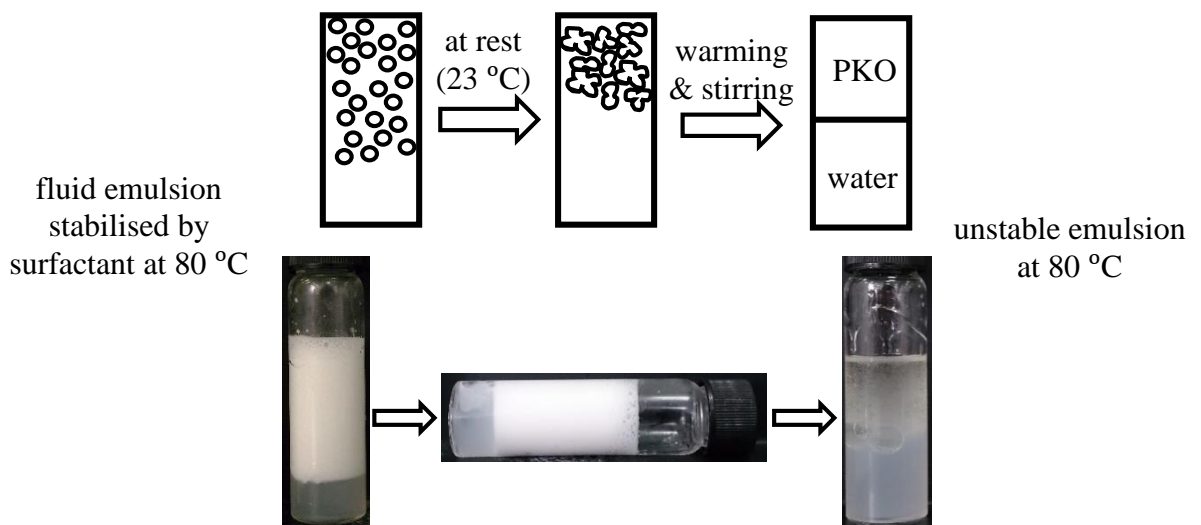


Figure 5.5. Schematic representations explaining the two different gelling mechanisms are shown together with actual images for the PKO-in-water emulsions stabilised by (a) particles and (b) by surfactant. The emulsions stabilised by PCC particles gel due to jamming after being stored at rest at room temperature. Since the gelation is due to jamming, the droplets retain their size and shape and become fluid after warming (above the melting point of PKO) and stirring. Emulsions stabilised by SSL gel due to partial coalescence of PKO droplets whilst stored at rest at room temperature. The droplets further coalesce upon warming and stirring, which eventually leads to phase separation. [stabiliser] = 1 wt. % and $\phi_o = 0.5$.

(a) Gelation due to jamming of PKO droplets in particle stabilised emulsions:



(b) Gelation due to partial coalescence of PKO droplets in surfactant stabilised emulsions:



5.4 Effect of oil volume fraction

The effect of oil volume fraction on the properties of PKO-in-water emulsions stabilised by both PCC particles and by SSL was also studied. All emulsions were prepared with a fixed stabiliser concentration of 1 wt. %. Figure 5.6 shows the appearance of the emulsions one day after their preparation. The type of emulsion prepared was checked using conductivity measurements and by the drop test method. The emulsions prepared were of the oil-in-water type for all volume fractions of oil (up to $\phi_o = 0.5$) regardless of whether the emulsions were stabilised by PCC particles or by SSL. No resolved PKO was observed on top of the emulsions one day after preparation.

Similar to the findings from the previous section, the emulsions prepared using SSL all gelled one day after storage at room temperature (23 °C). Therefore it can be concluded that even at low PKO volume fractions, these emulsions undergo partial coalescence. At low PKO volume fractions, the number of contacts between crystallised PKO droplets is less, however enough contact seems to occur for the crystals on the surface of the droplets to pierce the other droplet's surface and initiate partial coalescence, eventually leading to gelling.

Emulsions stabilised by PCC particles showed varying degrees of stability towards gelling depending on the volume fraction of PKO present. The emulsions with $\phi_o \leq 0.3$ remained fluid one day after preparation whereas those containing $\phi_o > 0.3$ gelled by the jamming mechanism described in section 5.3. It is believed that the lower the concentration of PKO droplets the lesser the chance of collisions between them hence they are more stable towards gelling. In addition, in the emulsions with $\phi_o \leq 0.3$ adsorption of PCC particles on the surface of PKO droplets decreases the density difference between PKO and the water phase, hence reducing the speed and extent of the vertical movements of PKO droplets within these emulsions. This caused the droplets to move slower within the aqueous phase hence reducing the contact between the droplets, reducing the chance of gelling occurring.

The emulsions at lower PKO volume fraction show PKO droplet sedimentation due to increase in the density of the droplets upon adsorption of PCC particles. The sedimentation degree was largest for $\phi_o = 0.05$, where all the heavily coated PKO droplets were sedimented. This is believed to be due to an increase in the density of the droplets upon adsorption of PCC particles ($\rho_{\text{CaCO}_3} = 2.7 \text{ g cm}^{-3}$)²⁵.

In Figure 5.6 (upper image) a sedimented layer can be seen in the emulsion at $\phi_o = 0.05$. Using optical microscopy, the layer was found to contain PKO droplets covered by a dense layer of PCC particles, with the excess PCC in the water phase. The images of this are shown in Figure 5.7. The sedimented layer could be re-dispersed into the emulsion by a gentle hand-shake whilst at room temperature (23 °C).

Figure 5.6. Appearance of PKO-in-water emulsions stabilised by 1 wt. % Calofort U PCC particles (upper image) and by 1 wt. % SSL surfactant (lower image) one day after their initial preparation. The emulsions were prepared at 80 °C and were left to cool naturally at an approximate rate of 1 °C min⁻¹ to room temperature (23 °C). Numbers below each emulsion refer to the volume fraction, ϕ_o , of PKO in the emulsion.

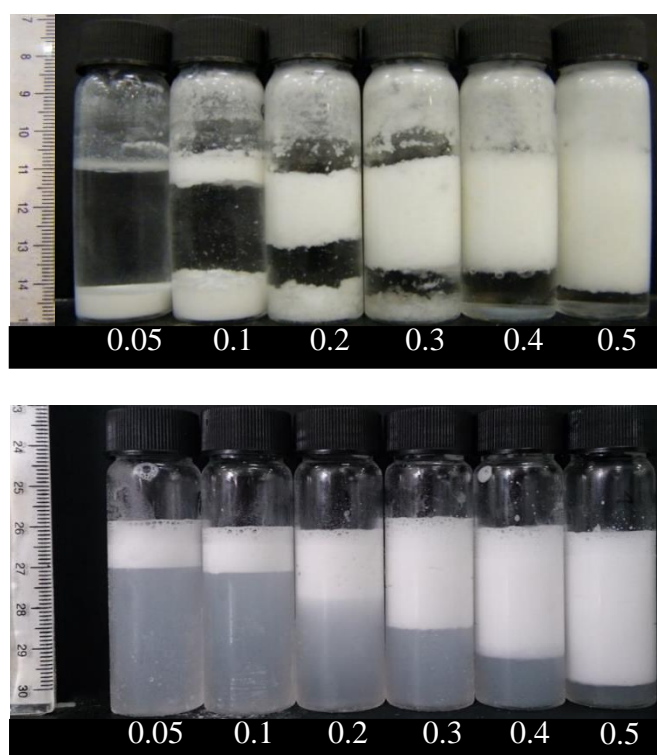
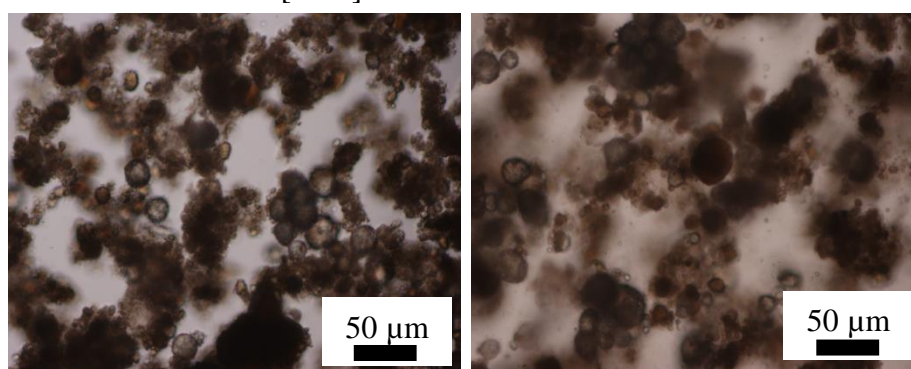


Figure 5.7. Optical micrographs of the sedimented layer in the particle-stabilised PKO-in-water emulsion at [PCC] = 0.05.



5.5 Conclusions

PKO-in-water emulsions can be stabilised by SSL, a food-grade surfactant and by PCC particles. The effects of the stabiliser nature and concentration on emulsions made from equal volumes of PKO and water have been systematically studied. As expected, the stability of emulsions towards creaming increased with increasing stabiliser concentration. The effect on the degree of creaming was more noticeable for the emulsions stabilised by SSL due to an increase in the viscosity of these emulsions. The increase in the viscosity was caused by an excess of SSL in the water phase. PKO-in-water emulsions with high stabiliser concentrations were also found to have smaller droplets.

Gelation of the PKO-in-water emulsions occurring one day after preparation was explored. It was shown that the mechanism by which gelation occurred was dependent on the nature of the stabiliser used. In the emulsions stabilised by PCC particles, gelation occurred via a jamming mechanism. In the case of SSL-stabilised emulsions, gelation was found to occur by partial coalescence of the oil droplets. It seems that when PCC particles coat PKO droplets, they act as a mechanical barrier and stop the extension of crystals out through the droplet surface into the continuous phase, which is the main cause of partial coalescence in crystallised droplets. The mechanism by which the emulsions gelled was further examined by applying a warming step. The emulsions containing PCC recovered their initial fluidity with no change in the PKO droplet size since their preparation. The emulsions stabilised by SSL however, were further destabilised as large droplets were formed. Even phase separation resulted at low SSL concentrations.

In addition, the effect of the PKO volume fraction on the stability of the emulsions towards gelling was studied. As expected, the emulsions prepared with SSL showed gelling one day after preparation. Therefore it can be concluded that even at low PKO volume fractions, emulsions stabilised by SSL undergo partial coalescence. Interestingly however, for emulsions stabilised by PCC particles, it was found that whether the emulsion turns into a gel or remains fluid depends on the oil volume fraction. The reduction in the speed of the vertical movement of the PCC-coated PKO droplets at certain PKO volume fractions and the limited contact between the droplets was thought to be the cause.

5.6 References

1. B.P. Binks, *Curr. Opin. Colloid Interface Sci.*, **7**, 21 (2002).
2. K. Sato, *Lipid / Fett*, **101**, 467 (1999).
3. S.A. Vanapalli and J.N. Coupland, *Food Hydrocoll.*, **15**, 507 (2001).
4. J.N. Coupland, *Curr. Opin. Colloid Interface Sci.*, **7**, 445 (2002).
5. T. Awad and K. Sato, *Colloids Surf. B*, **25**, 45 (2002).
6. K. Golemanov, S. Tcholakova, N.D. Denkov and T. Gurkov, *Langmuir*, **22**, 3560 (2006).
7. E. Dickinson, D.J. McClements and M.J.W. Povey, *J. Colloid Interface Sci.*, **142**, 103 (1991).
8. D.J. McClements, E. Dickinson, S.R. Dungan, J.E. Kinsella, J.G. Ma and M.J.W. Povey, *J. Colloid Interface Sci.*, **160**, 293 (1993).
9. S. Hindle, M.J.W. Povey and K. Smith, *J. Colloid Interface Sci.*, **232**, 370 (2000).
10. M. Tippetts and S. Martini, *Food Res. Int.*, **42**, 847 (2009).
11. S.D. Campbell, H.D. Goff and D. Rousseau, *Food Res. Int.*, **35**, 935 (2002).
12. D. Rousseau, *Food Res. Int.*, **33**, 3 (2000).
13. K. Boode and P. Walstra, *Colloids Surf. A*, **81**, 121 (1993).
14. J. Giermanska, F. Thivilliers, R. Backov, V. Schmitt, N. Drelon and F. Leal-Calderon, *Langmuir*, **23**, 4792 (2007).
15. F. Thivilliers, E. Laurichesse, H. Saadaoui, F. Leal-Calderon and V. Schmitt, *Langmuir*, **24**, 13364 (2008).
16. C. Lopez, A. Riaublanc, P. Lesieur, C. Bourgaux, G. Keller and M. Ollivon, *J. Am. Oil Chem. Soc.*, **78**, 1233 (2001).
17. B.P. Binks, P.D.I. Fletcher, B.L. Holt, P. Beaussoubre and K. Wong, *Phys. Chem. Chem. Phys.*, **12**, 11954 (2010).
18. *Colloidal Particles at Liquid Interfaces*, ed. B.P. Binks and T.S. Horozov, Cambridge University Press, Cambridge, 2006.
19. B.P. Binks and A. Rocher, *J. Colloid Interface Sci.*, **335**, 94 (2009).
20. D.E. Tambe and M.M. Sharma, *J. Colloid Interface Sci.*, **157**, 244 (1993).
21. B.P. Binks, A.J. Johnson and J.A. Rodrigues, *Soft Matter*, **6**, 126 (2010).
22. A.B. Subramaniam, M. Abkarian, L. Mahadevan and H.A. Stone, *Nature*, **438**, 930 (2005).

23. R. Aveyard, B.P. Binks and J.H. Clint, *Adv. Colloid Interface Sci.*, **100**, 503 (2003).
24. K. Boode, P. Walstra and A.E.A. de Groot-Mostert, *Colloids Surf. A*, **81**, 139 (1993).
25. S. Teir, S. Eloneva and R. Zevenhoven, *Energy Convers. Manag.*, **46**, 2954 (2005).

CHAPTER 6 OIL-IN-WATER EMULSIONS AND AERATED EMULSIONS CONTAINING NON-CRYSTALLISABLE OIL

6.1 Introduction

Oil-in-water emulsions and aqueous foams are dispersions of oil and air respectively in water, both of which are insoluble in water. They are thermodynamically unstable systems due to the unfavourable contact between the dispersed phase and the continuous phase.^{1, 2} The vast applications of aqueous foams and emulsions in our everyday lives has caused wide research activities to be carried out to inspect the routes to improve their stability and functionality. Aqueous foams containing emulsified oil droplets also have a wide variety of applications in food products,³ enhanced oil recovery⁴ and pharmaceutical products. Emulsified oil droplets can have different effects on air bubbles, however the effect of the oil droplets on the stability of air bubbles is of primary interest.⁵ A good example of stabilisation of air bubbles by oil droplets is in whipped cream. In whipped cream, air bubbles are surrounded to varying degrees by partially-coalesced oil droplets. The oil droplets in whipped cream contain both crystallised and liquid fat portions and during whipping, the crystals of one droplet pierce the film of another, which eventually allows droplets to clump irreversibly together to form a network. The identity of the individual fat droplets in the clumps is still retained due to the Solid Fat Content (SFC) of the droplets.⁶⁻¹⁰ So far, the focus on the study of incorporating air bubbles into oil-in-water emulsions has been on the systems containing partially/fully crystallised oil droplets.^{3, 11-15} Shamsi *et al.*¹¹ compared whipping properties of dairy whipping cream and palm oil-based whipping cream. They concluded that the oil type can influence the stability of the whipped emulsions. Hotrum *et al.*¹² studied whipping properties of artificial creams composed of a mixture of sunflower oil and palm fat stabilised by sodium caseinate or a mixture of sodium caseinate and low molecular weight surfactants (Tween 20 and Span 80). Their results show that the optimum whipping time depended on the fraction of bubble surface area at which fat droplet spreading was possible (depended on stabiliser concentration).

There are fewer studies present studying simpler systems and aerated emulsions containing fluid oil droplets. Koczo *et al.*¹⁶ studied the stability of aqueous foam films in the presence of octane, decane, dodecane and benzene oil droplets. They showed that oil droplets could accumulate within the Plateau borders of the foams and reduce

drainage rate, hence increasing the stability of the films. In another study by Salonen *et al.*¹⁷, aeration properties of dodecane-in-water and rapeseed oil-in-water emulsions stabilised by Sodium Dodecyl Sulphate (SDS) were studied. They concluded that more stable foams could be produced upon increasing the oil volume fraction due to an increase in bulk viscoelasticity and the formation of thicker layers of oil droplets around air bubbles. Allen *et al.*¹⁸ compared the aeration properties of acidified casein-stabilised emulsions containing groundnut oil droplets to the whipping of dairy creams. They produced stable foams of high overrun by aerating the sodium caseinate-stabilised emulsions and found that air bubbles were stabilised by aggregation (gelation) of the protein-coat surrounding the oil droplets.

There are several other studies where fluid oil droplets have been introduced onto pre-made foams¹⁹⁻²¹ and the interactions between the oil droplets and air bubbles have been investigated, however the main focus of these has been on the antifoaming effect of oil droplets.

Whether an oil droplet can enter the air-water interface and its behaviour after entry can be assessed from the interfacial tensions between the three phases (air, water and oil) involved. Entry and spreading coefficients, E and S respectively, are used to predict the behaviour of oil droplets at an air-water interface. Robinson and Woods²² defined the entering coefficient E as below:

$$E = \gamma_{aw} + \gamma_{wo} - \gamma_{oa} \quad (6.1)$$

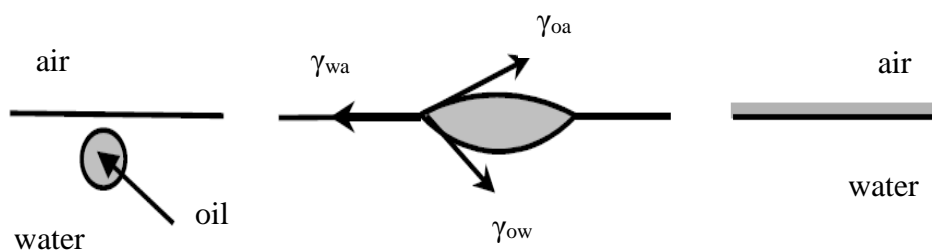
where γ_{aw} and γ_{oa} are the surface tensions of the aqueous phase and the oil phase respectively, and γ_{wo} is the interfacial tension at the water-oil interface. Thermodynamically, a positive value of E means the oil droplet enters the air-water interface. However there are several examples in which this is not applicable and the oil droplets do not enter at the air-water interface although possessing a positive E coefficient. Surfactants and proteins can adsorb at an air-water and oil-water interfaces providing mechanical stability to the interface, thus inhibiting droplet entering.^{23, 24}

When an oil droplet entered an air-water interface, it may either form a lens or spread out to form a film at the interface. The tendency of an oil droplet to spread at the air-water interface can be assessed by the spreading coefficient S , defined by Harkins and Feldman²⁵ as below:

$$S = \gamma_{aw} - \gamma_{wo} - \gamma_{oa} \quad (6.2)$$

When S is positive the oil droplet spreads at the interface. Therefore three conformations can be predicted based on the balance of interfacial tensions as illustrated schematically in Figure 6.1.

Figure 6.1. Schematic representation of the three possible conformations for an oil droplet at an air-water interface: (left) not entered, (middle) entered and formed a lens and (right) entered and spread.



The formation of a lens, after entry of an oil droplet an air-water interface, in foams may cause bridging of aqueous films. Such bridging is known to cause a capillary pressure in the foam film near the droplet leading to enhanced drainage rate and foam collapse eventually.²⁶

The present chapter considers the use of fluid oils in preparing aerated oil-in-water emulsions in order to understand the interactions of fluid oil droplets with the air-water interface. Two different types of oils were used, namely High Oleic Sunflower Oil (HOSO) and dodecane. Initially, various properties of oil-in-water emulsions are presented, which is followed by their aeration study. The emulsions and aerated emulsions were stabilised by Sodium Stearoyl Lactylate (SSL). SSL is a key component of the Vanilla Bettercreme[®] (VBC) produced by the sponsor of the project and is known to be an active component at oil-water and air-water interfaces.²⁷⁻²⁹ Foaming properties of SSL were reported in detail in Chapter 3. Effects of SSL concentration and the oil volume fraction on both emulsions and aerated emulsions are studied in this chapter. Emulsions and aerated emulsions were also monitored to determine their stability over time and were characterised by optical microscopy to determine oil droplet size and the position of oil droplets within the foams. Finally, the life-time of a single oil droplet at the air-water interface was determined and the results were attempted to link with the stability of aerated oil-in-water emulsions.

6.2 Oil-in-water emulsions

6.2.1 Surfactant concentration scan at fixed oil volume fraction

The effect of surfactant concentration on the preferred emulsion type and the stability of the prepared emulsions was investigated. For this purpose a fixed oil volume fraction of 0.2 was used with varying SSL concentrations. All the emulsification process was carried out at room temperature (23 ± 1 °C). Figure 6.2 shows the appearance of dodecane-water emulsions and Figure 6.3 shows the appearance of HOSO-water emulsions immediately and one week after emulsification. A high Hydrophilic Lipophilic Balance (HLB) number of 21^{30, 31}, makes SSL a suitable surfactant for water continuous emulsions. Using the drop test method, the emulsions were found to be oil-in-water for both oils used and at all SSL concentrations. Conductivity data of the prepared emulsions also agreed with this as they all had relatively large values of conductivity. As can be seen in both figures, production of foam during homogenisation of the emulsions was unavoidable and this increased with increasing SSL concentration. However it was attempted to minimise foaming during homogenisation. The turbidity of the resolved water in both series increases with SSL concentration and is known to be due to the formation of SSL bilayers and vesicles in bulk (see Chapter 3). In Figure 6.3 the decrease in volume seen for the emulsion with 0.01 mM SSL after one week was simply due to sampling for analysis.

The stability of both series of emulsions to creaming and coalescence was critically dependent on surfactant concentration. Homogenisation of a neat HOSO-water mixture (0 mM SSL) was found to form an unstable oil-in-water emulsion which completely phase separated after 1 day. However for dodecane-water without SSL no emulsion was formed upon homogenisation. This suggests that traces of impurities (e.g. free fatty acids) are present in HOSO, which are responsible for temporary stability of the emulsion in the case of HOSO.

The stability data of the emulsions against creaming and coalescence were recorded up to one week after emulsification and are presented in Figures 6.4 and 6.5 for dodecane-in-water and HOSO-in-water emulsions, respectively. As can be seen the emulsions become more stable against both creaming and coalescence as the concentration of SSL increases. Shortly after emulsification, both set of emulsions with SSL concentration of < 10 mM were found to be unstable against creaming (more

concentrated emulsion layer at the top surface and the resolved water phase at the bottom). The emulsions with SSL concentration of > 10 mM were stable towards creaming due to increase in the viscosity of the continuous phase and also due to a decrease in the size of the oil droplets (presented later). After one week the emulsions showed high degrees of creaming, even those at high SSL concentrations (> 10 mM) and approximately 90 % of water was resolved leaving a concentrated layer of oil droplets on top. Dodecane-in-water emulsions showed slightly better stability to creaming after one week. This is believed to be due to dodecane-in-water emulsions having smaller droplets than HOSO-in-water emulsions, as will be shown later.

Immediately after preparation dodecane-in-water emulsions with less than 0.1 mM SSL (cac of SSL in water) showed a small degree of coalescence and those above 0.1 mM were completely stable to coalescence. HOSO-in-water emulsions, however, were found to be stable against coalescence immediately after homogenisation and no resolved oil was observed for all SSL concentrations. Both set of emulsions showed similar stability towards coalescence one week after preparation. The emulsions were unstable to coalescence, to varying degrees, up to 0.1 mM (cac of SSL) and were completely stable above that point. As shown in Chapter 3, SSL molecules aggregate into multi-layer vesicles and bilayer aggregates instead of forming micelles in water. The stability of the emulsions towards coalescence above the cac of SSL suggests that once the SSL aggregates are formed and adsorbed around oil droplets they create an effective protective layer, which protects the oil droplets from coalescence and Ostwald ripening. The increase in the stability of emulsions droplets towards coalescence and Ostwald ripening upon adsorption of lamellar phase forming surfactants such as SSL has been reported Krog.³²

Figure 6.2. Appearance of dodecane-in-water emulsions imaged immediately (upper) and one week (lower) after emulsification. The emulsions were prepared at 23 °C and were left to stand at room temperature (23 °C). Numbers below each emulsion refer to the concentration of SSL / mM in each emulsion, $\phi_o = 0.2$.

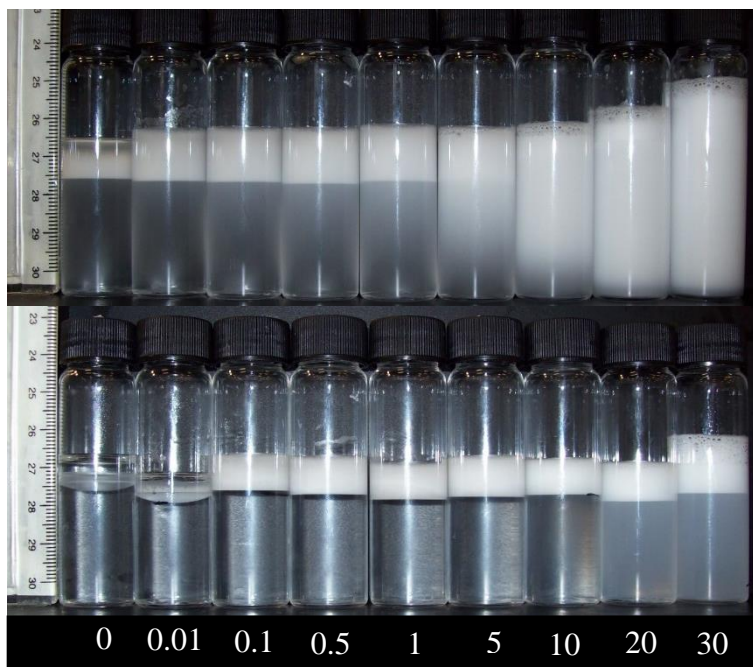


Figure 6.3. Appearance of HOSO-in-water emulsions imaged immediately (upper) and one week (lower) after emulsification. The emulsions were prepared at 23 °C and were left to stand at room temperature (23 °C). Numbers below each emulsion refer to the concentration of SSL / mM in each emulsion, $\phi_o = 0.2$.

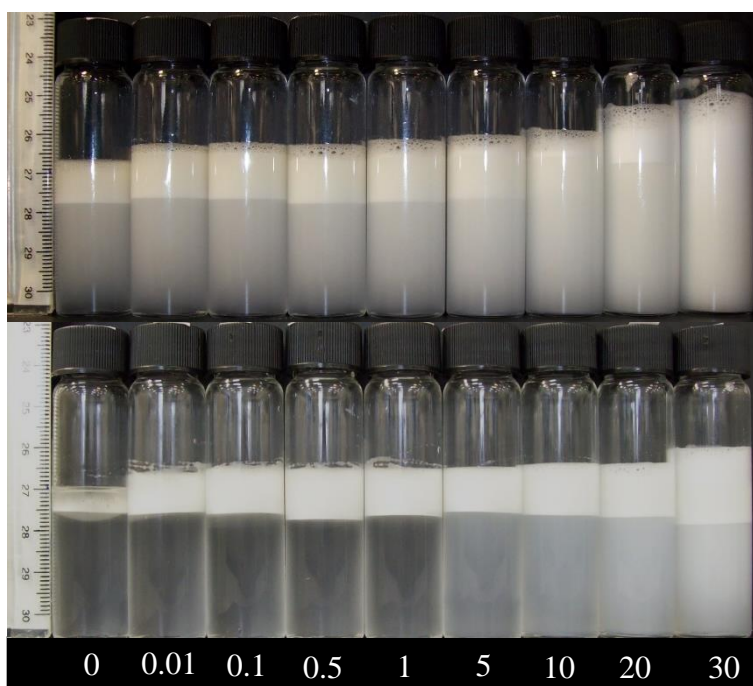


Figure 6.4. Stability of dodecane-in-water emulsions towards coalescence and creaming measured in terms of the fraction of dodecane (dashed line) and water (solid line) resolved as a function of SSL concentration immediately (empty points) and one week (filled points) after preparation. SSL concentration is with respect to total emulsion volume, $\phi_o = 0.2$.

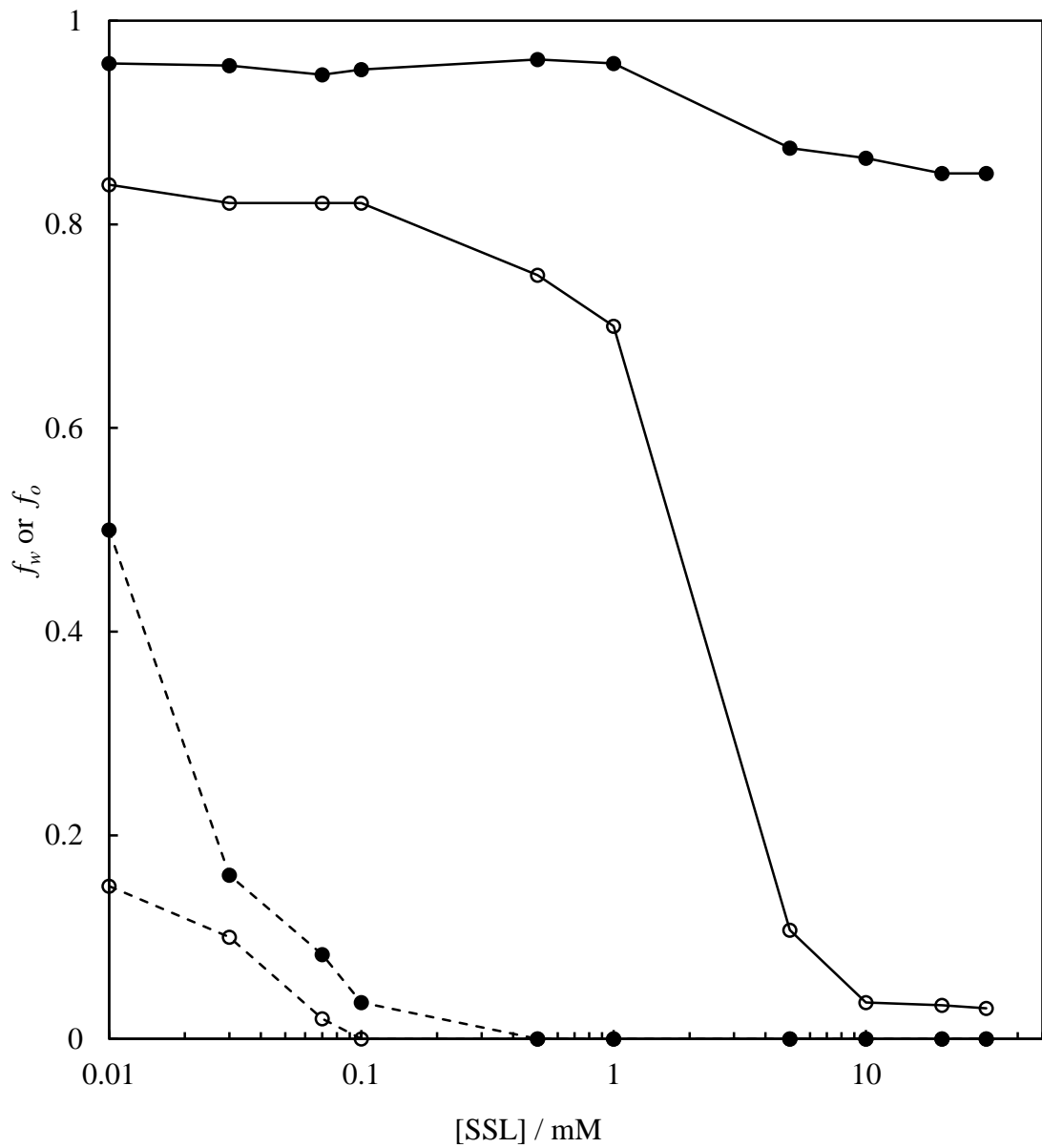
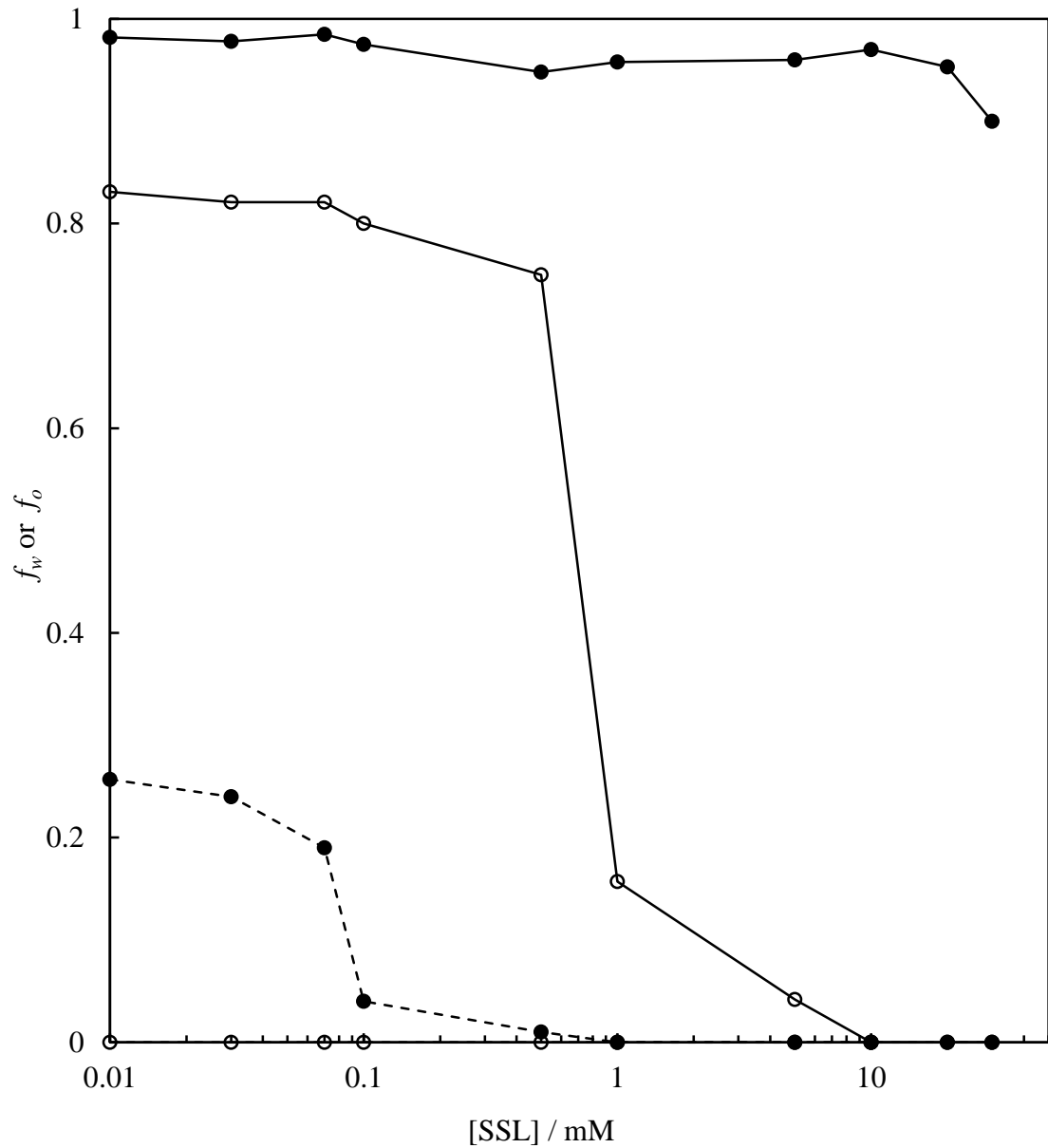
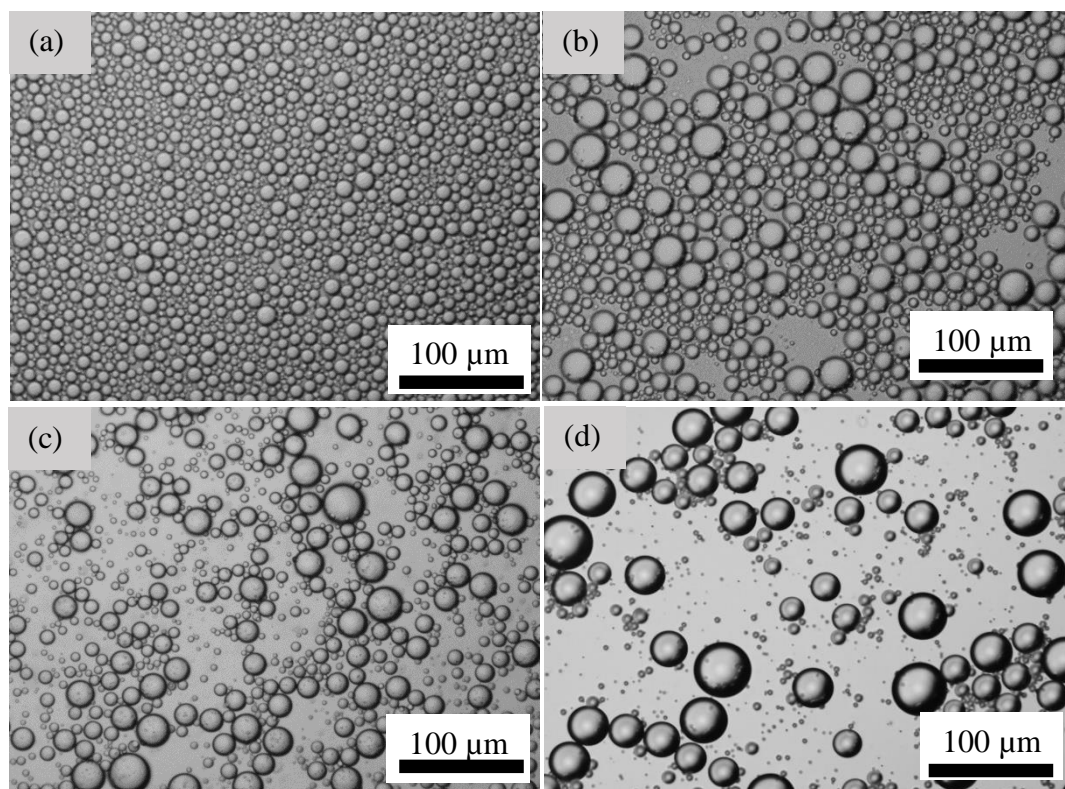


Figure 6.5. Stability of HOSO-in-water emulsions towards coalescence and creaming measured in terms of the fraction of HOSO (dashed line) and water (solid line) resolved as a function of SSL concentration immediately (empty points) and one week (filled points) after preparation. SSL concentration is with respect to total emulsion volume, $\phi_o = 0.2$.



The emulsions were observed using optical microscopy immediately and one week after preparation in order to study their droplet shape and size. The images are shown in Figure 6.6 for both dodecane-in-water and HOSO-in-water emulsions stabilised by 30 mM. It is clear from the images that droplets are all spherical in both emulsions. In images taken immediately, (a) and (c), one can see that dodecane droplets were slightly smaller and more uniform compared to HOSO droplets. One week after emulsification one can see the increase in droplet size due to coalescence and/or Ostwald ripening in the emulsions for both oils used.

Figure 6.6. Optical micrographs of dodecane-in-water emulsions (upper) and HOSO-in-water emulsions (lower) observed immediately (left) and one week (right) after preparation. The emulsions were stabilised with 30 mM SSL (with respect to total emulsion volume). Emulsion droplets were smaller and more uniform when dodecane was used as the dispersed phase, $\phi_o = 0.2$.



The size of oil droplets in the prepared emulsions was measured using both light scattering and optical microscopy. Image J software was used to measure the size of the droplets from optical microscopy images and the sizes of at least 100 droplets were measured. The size measurement data from both methods were in agreement for both set of emulsions. The median droplet diameters $d(0.5)$ of dodecane droplets and HOSO droplets in the oil-in-water emulsions, measured *via* light scattering, are shown in Figure 6.7 and Figure 6.8, respectively. It is clear that the size of droplets decreases with increasing surfactant concentration for both oils. The decrease in the size of oil droplets upon increasing surfactant concentration has been reported previously.³³ Surfactant molecules facilitate the droplet breakdown, during homogenisation, by lowering the interfacial tension associated with the interface.^{34, 35} The higher the surfactant concentration the larger the interfacial area between oil-water that can be stabilised by surfactant and smaller droplets are formed. This is in contrast with the findings of Kurukji *et al.*³⁶ who found no variation in the size of oil droplets ($d(3.2) = 2 \mu\text{m}$) in sunflower oil-in-water emulsions stabilised by SSL. It should be mentioned that they used a High Pressure Homogeniser (HPH) for emulsification, whereas an Ultra Turrax rotor-stator homogeniser was used in this study.

The average size of dodecane and HOSO droplets were increased in the emulsions one week after quiescent storage at room temperature due to coalescence and/or Ostwald ripening. Kurukji *et al.*³⁶ however reported no change in the size of sun flower oil droplets in emulsions stabilised by SSL after two month storage at 3 °C. These dissimilar observations could be related to the effect of temperature on the viscosity of the emulsions. It is believed that the viscosity of emulsions decreases with increasing temperature.³⁷ It has been suggested by Kundu *et al.*³⁸ that a decrease in the emulsion viscosity promotes emulsion destabilisation. They studied a series of diesel oil-in-water emulsions stabilised by sodium dodecylbenzenesulphonate (SDBS). In addition, a decrease in the viscosity of the emulsion increases the frequency of collision between oil droplets, which eventually increases the possibility of coalescence as suggested by Ghannam.³⁹

Comparing the size of oil droplets in the emulsions shows that dodecane-in-water emulsions contained smaller droplets than HOSO-in-water emulsions. This could be explained in terms of interfacial tensions. The interfacial tensions associated with SSL aqueous dispersions, dodecane and HOSO were determined using the du Noüy ring

method, as detailed in Chapter 2. At 25 °C a dodecane-water (30 mM SSL) interface was found to have a tension value of 14.8 mN m⁻¹ whereas the tension was 24.3 mN m⁻¹ for the HOSO-water (30 mM SSL) interface. The lower interfacial tension associated with the dodecane-water interface suggests that creating new interfacial area between dodecane-water requires less energy compared to the HOSO-water interface. This is therefore an important factor causing the breakdown of dodecane into smaller droplets than HOSO when equal shear is applied during emulsification. The viscosity of the dispersed phase is also known to affect the droplet size formed in emulsions.⁴⁰ The lower size of dodecane droplets may be linked to the lower viscosity of dodecane (1.36 mPa s)⁴¹ compared to that of HOSO (62.8 mPa s)⁴² at 25 °C . A less viscous liquid would breakdown into smaller droplets compared to a more viscous liquid when equal shear is applied.⁴³

Figure 6.7. Evolution of median droplet diameter $d(0.5)$ in dodecane-in-water emulsions as a function of SSL concentration measured immediately (solid line) and one week (dashed line) after preparation. SSL concentration is with respect to total emulsion volume, $\phi_o = 0.2$.

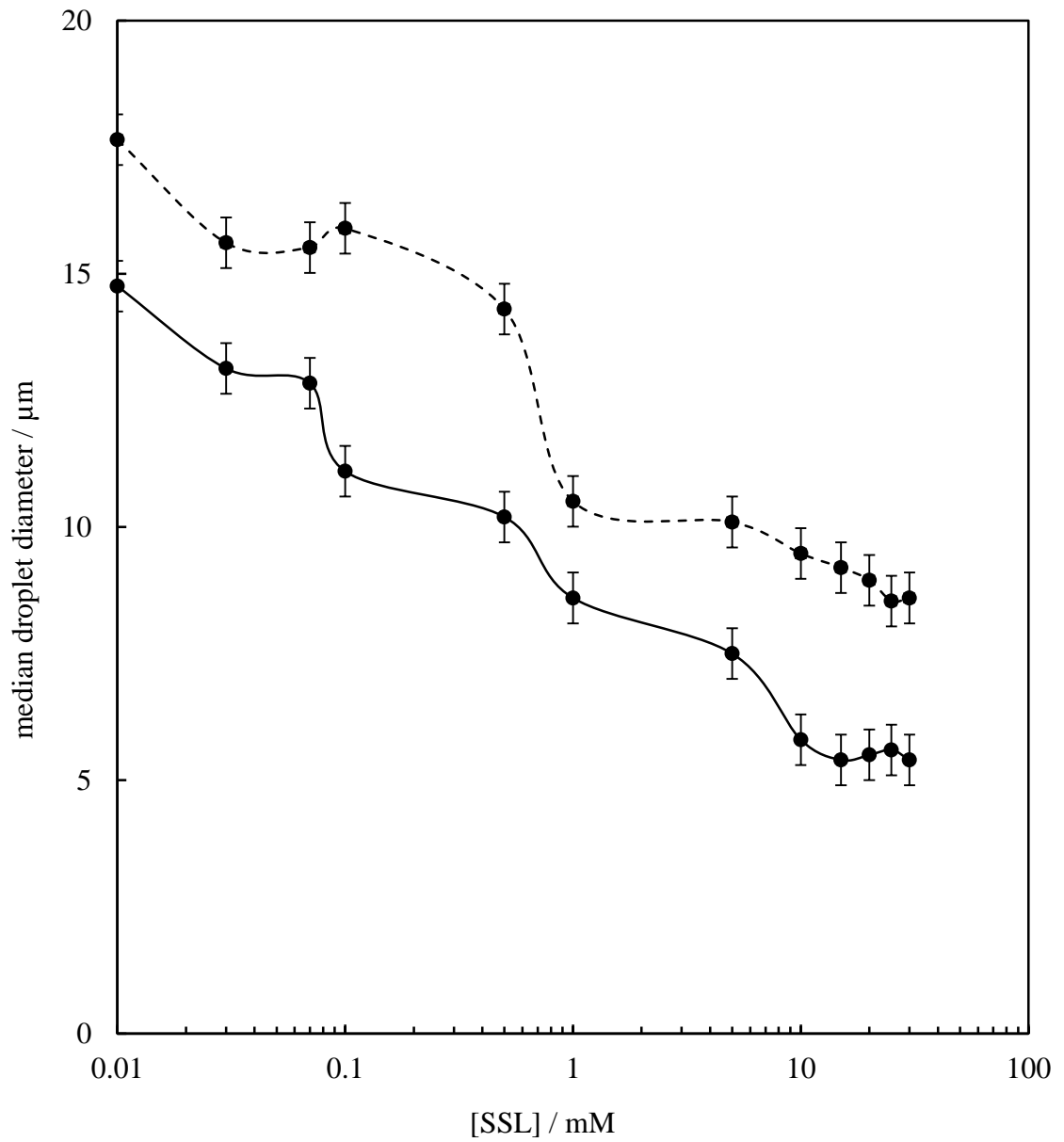
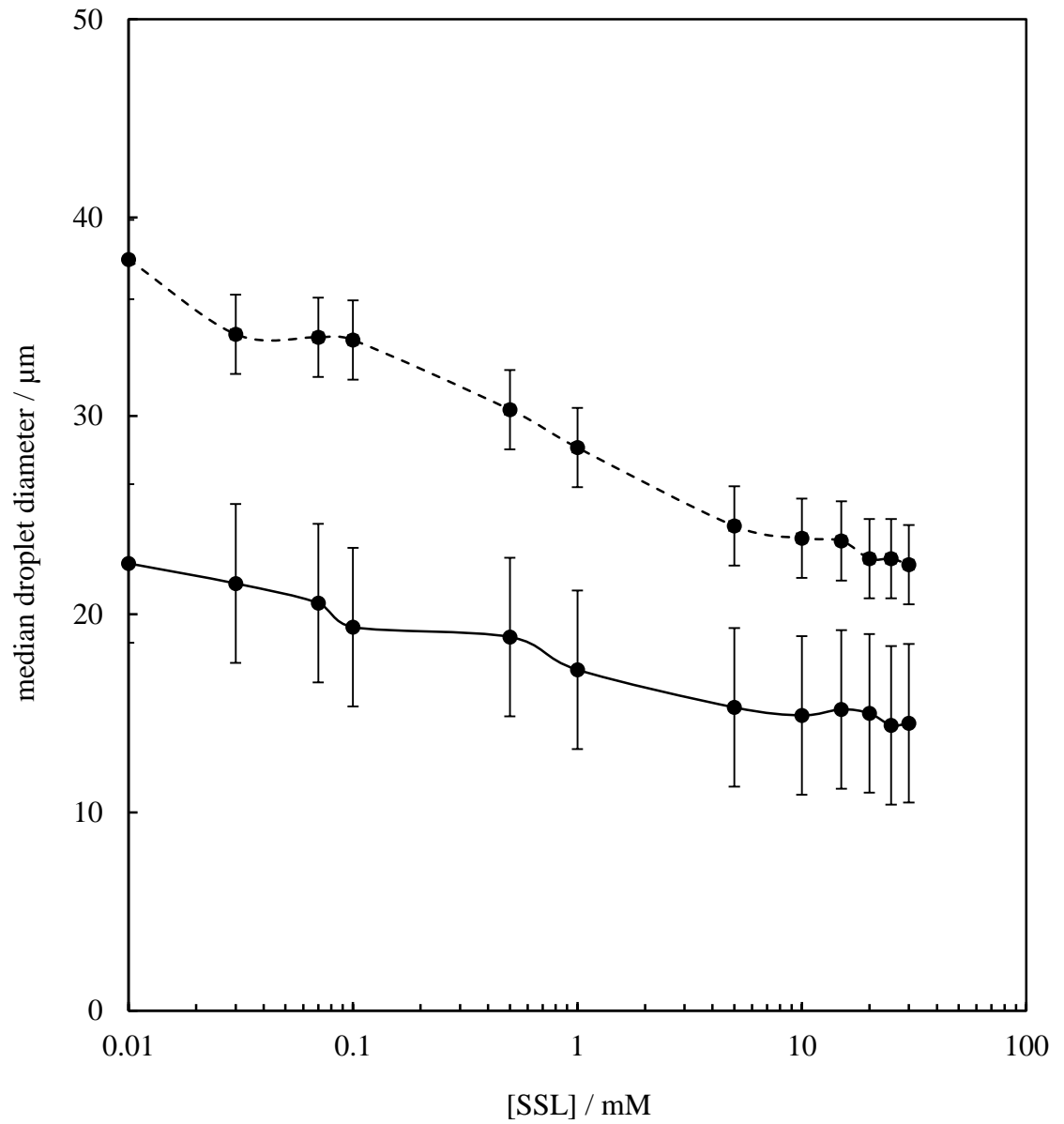


Figure 6.8. Evolution of median droplet diameter $d(0.5)$ in HOSO-in-water emulsions as a function of SSL concentration measured immediately (solid line) and one week (dashed line) after preparation. SSL concentration is with respect to total emulsion volume, $\phi_o = 0.2$.



6.2.2 *Effect of oil volume fraction*

The effect of dodecane and HOSO volume fraction on the preferred emulsion type and on the stability of the emulsions was investigated. All emulsions were stabilised by 30 mM SSL and the oil volume fraction was varied between 0.1 and 0.9. The appearance of the emulsions immediately and one week after preparation are shown in Figure 6.9 and Figure 6.10 for dodecane-water and HOSO-water emulsions, respectively. It is clear from both figures that up to 0.6 oil volume fraction the emulsions behave as expected and the height of the emulsified layer increases as there is more oil to emulsify. Emulsions were found to be oil-in-water determined using the drop test and by conductivity. An emulsion with 0.65 oil volume fraction was also prepared for both oils and was found to be oil-in-water. Above 0.65 oil volume fraction phase inversion occurs and homogenisation results in the formation of unstable water-in-oil emulsions in both cases. The electrical conductivity of both dodecane-water and HOSO-water emulsions was measured immediately after emulsification and the data are shown in Figure 6.11. The switch between emulsions of high and low conductivity occurs between 0.65 and 0.7 oil volume fraction for both oils. This is known as catastrophic phase inversion since it has the characteristics of a catastrophe, meaning a sudden change in behaviour of the system as a result of gradually changing conditions (oil volume fraction).⁴⁴ It was noticed that no foam was produced during emulsification of emulsions with $\phi_o \geq 0.7$, which further confirms the preparation of oil continuous emulsions. It worth mentioning that the phase inversion occurs close to the volume fraction of droplets for close packing of equal sized spheres ($\phi_o = 0.74$).⁴⁵ For both oils a white layer was visible between resolved oil and resolved water phases for the emulsions with $\phi_o = 0.7$ after one week. Samples of this layer was taken to observe with optical microscopy, however they contained very unstable droplets which broke during sampling.

Figure 6.9. Appearance of dodecane-water emulsions immediately (upper) and one week (lower) after their preparation. The emulsions were left to stand at room temperature (23 °C). Numbers below each emulsion refer to volume fraction of oil in each emulsion. [SSL] was constant and was 30 mM (with respect to total emulsion volume) for all emulsions.

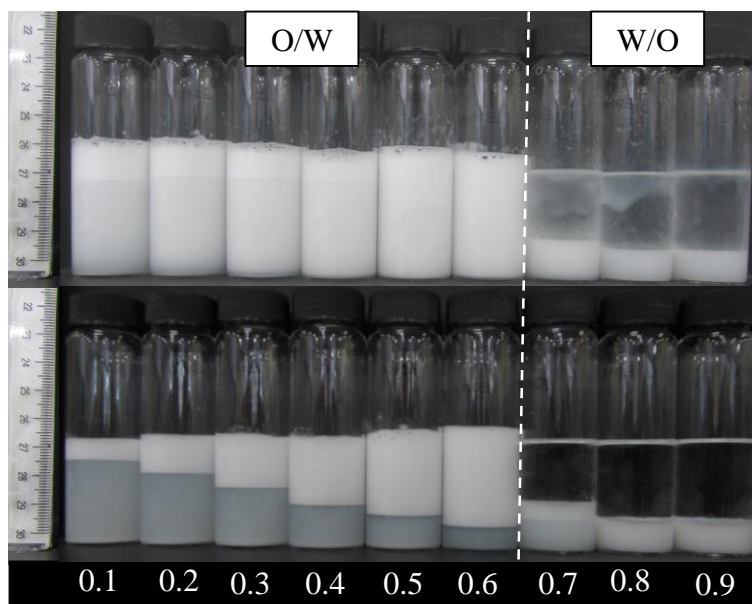


Figure 6.10. Appearance of HOSO-water emulsions immediately (upper) and one week (lower) after their preparation. The emulsions were left to stand at room temperature (23 °C). Numbers below each emulsion refer to volume fraction of oil in each emulsion. [SSL] was constant and was 30 mM (with respect to total emulsion volume) for all emulsions.

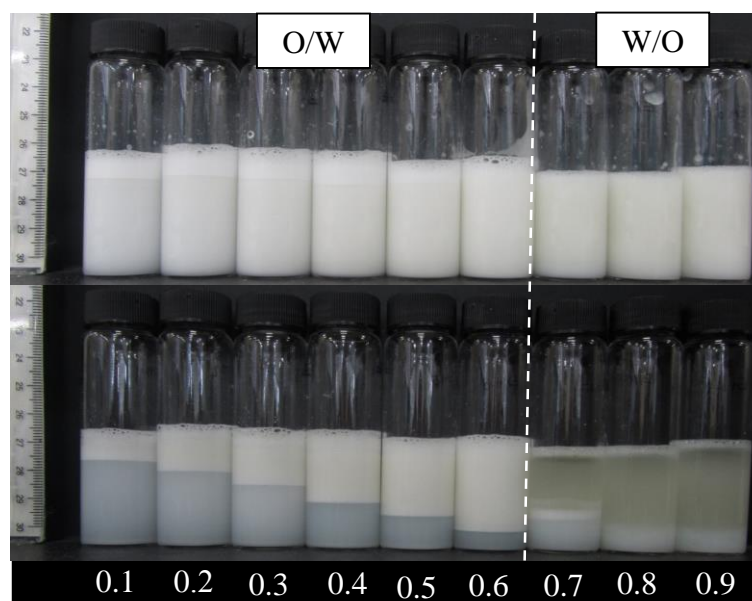
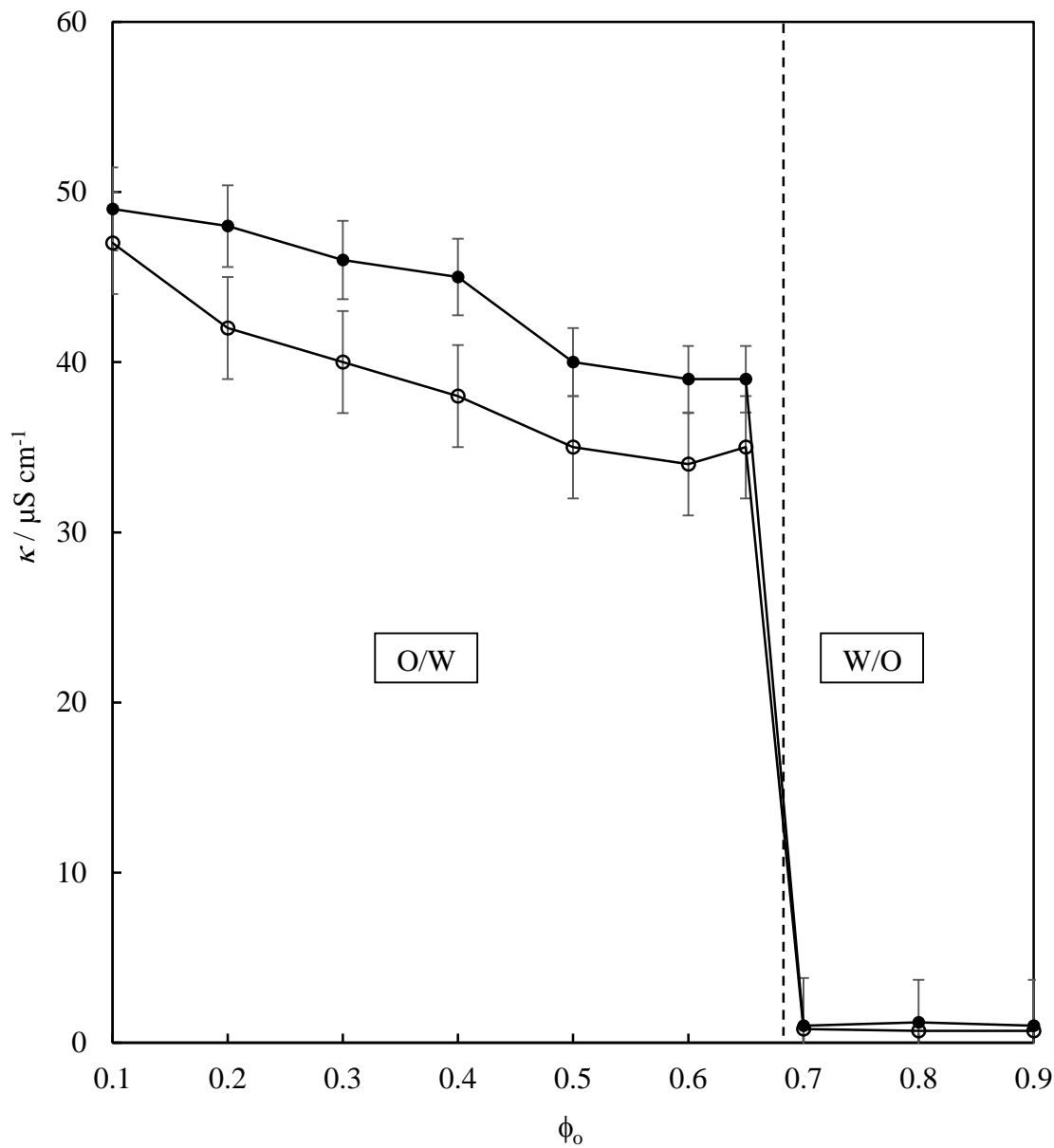


Figure 6.11. The change in conductivity of dodecane-water emulsions (filled points) and HOSO-water emulsions (empty points) stabilised by 30 mM SSL as a function of oil volume fraction (ϕ_o). All measurements were taken immediately after emulsification.



The stability of the emulsions against creaming and coalescence with changing oil volume fraction is presented by the fractions of water and oil resolved from the emulsions in Figure 6.12 and Figure 6.13. Dodecane-water emulsions above 0.65 dodecane volume fraction, destabilised immediately after homogenisation into water and oil phases. The similar phenomena occurred for HOSO-water emulsions for $\phi_o > 0.65$, however the rate of destabilisation was slower and total phase separation occurred after three minutes. Therefore, all emulsions with $\phi_o > 0.65$ were completely phase separated one week after preparation, as can be seen in the graphs. The extent of creaming one week after emulsification in the water continuous emulsions is least just before the catastrophic phase inversion. No resolved oil was observed for any of the oil-in-water emulsions one week after emulsification. However it was shown earlier that coalescence and/or Ostwald ripening occurred to varying degrees in these emulsions since the size of oil droplets increased with time for both oils used. It is believed that the extent of coalescence and/or Ostwald ripening was not enough to liberate sufficient free oil which appears above the emulsions in the vessel.

Figure 6.12. Stability of dodecane-water emulsions towards coalescence and creaming/sedimentation measured in terms of the fraction of dodecane (red) and water (blue) resolved for varying dodecane volume fractions. Circles and crosses represent the stability data determined immediately and one week after emulsification, respectively. [SSL] was constant and was 30 mM (with respect to total emulsion volume).

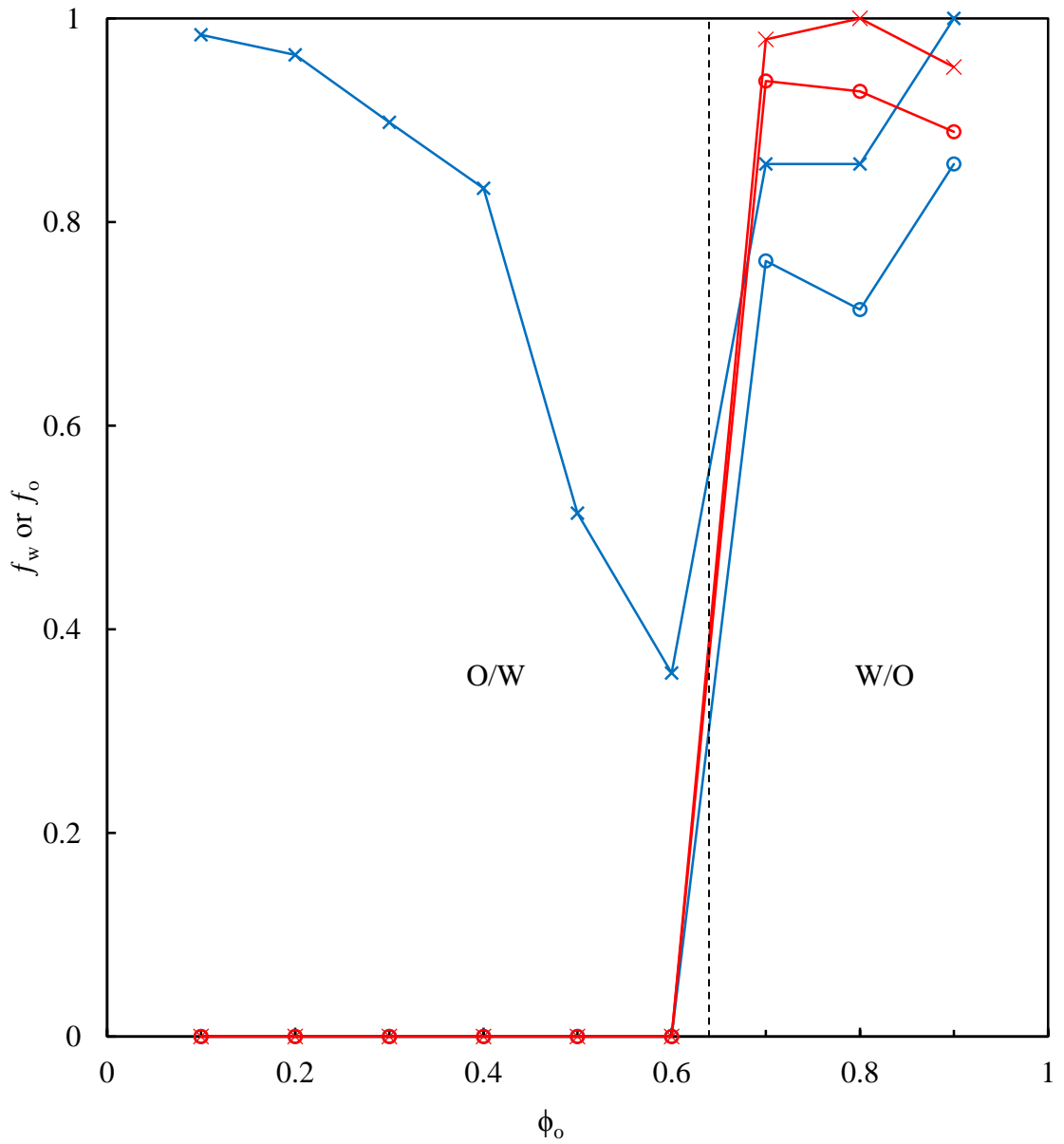
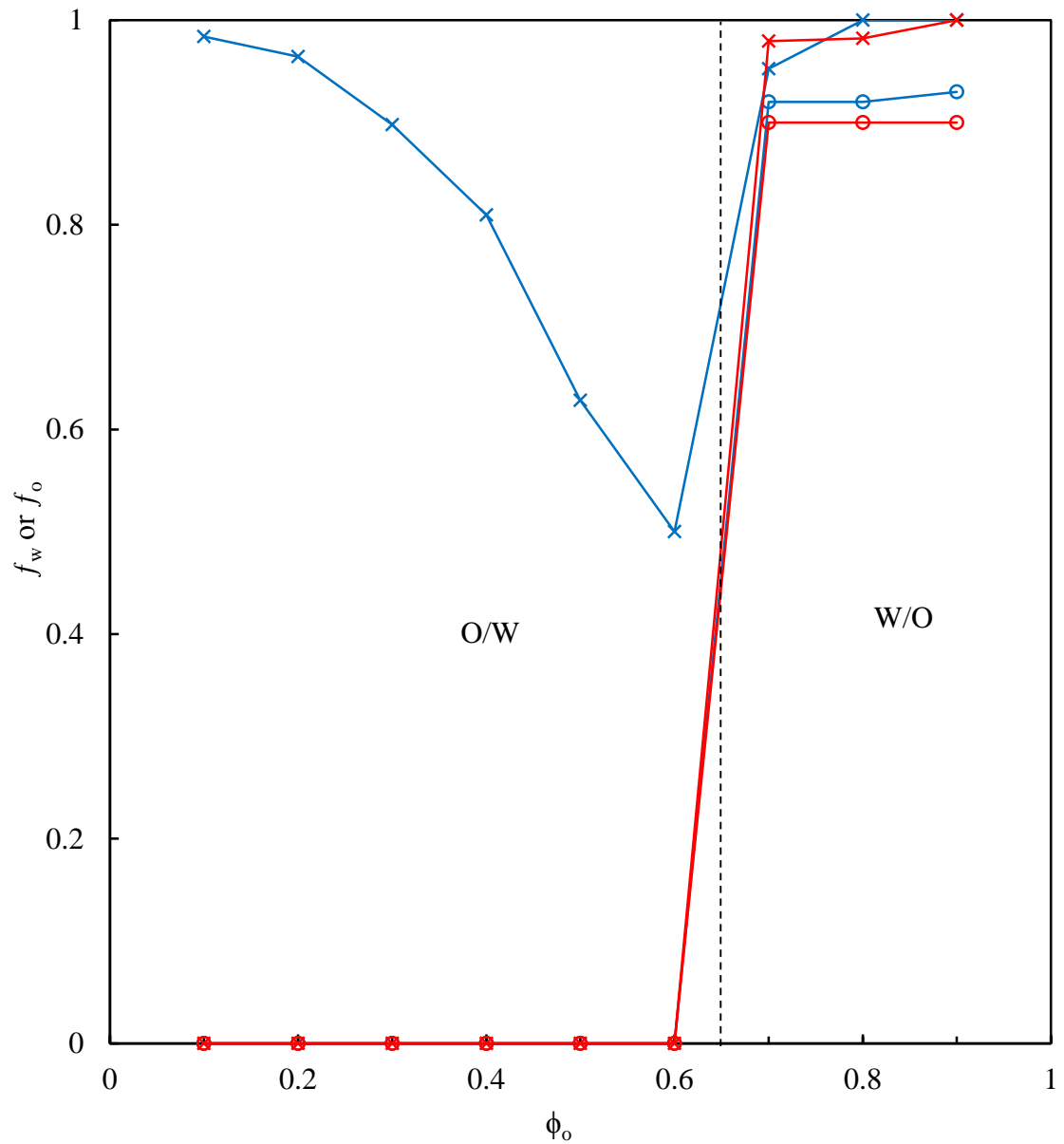


Figure 6.13. Stability of HOSO-water emulsions towards coalescence and creaming/sedimentation measured in terms of the fraction of HOSO (red) and water (blue) resolved for varying HOSO volume fractions. Circles and crosses represent the stability data determined immediately and one week after emulsification, respectively. [SSL] was constant and was 30 mM (with respect to total emulsion volume).



6.3 Aerated oil-in-water emulsions

6.3.1 Effect of surfactant concentration

Aeration properties of SSL aqueous dispersions were studied in detail in Chapter 3. It was shown that aqueous foams of SSL (a bilayer and vesicle-forming surfactant) were of higher stability compared to SDS (a micelle-forming surfactant). The high stability of the SSL aqueous foams was linked to the adsorption of SSL aggregates at the air-water interface and also to the accumulation of SSL vesicles within the Plateau borders of the foams. The former enhances the stability of the thin film against rupturing and the latter decreases the rate of water drainage from the foam.

Oil-in-water emulsions, at fixed oil volume fraction of 0.2 and varying SSL concentration were aerated immediately after homogenisation. As detailed in Section 2.2.16, 200 mL of the emulsions were aerated using a hand mixer equipped with a whisk in 1 L glass jars at room temperature of 23 ± 1 °C for 2 minutes at 1100 rpm. As shown previously production of foam during homogenisation of the emulsions was unavoidable, however it was attempted to keep it to a minimum. Figure 6.14 shows the appearance of aerated dodecane-in-water and HOSO-in-water emulsions immediately after aeration. As can be seen the total foam produced increased with SSL concentration. The foams had a turbid appearance and the interface between the foam layer and drained liquid was not clear due to turbidity caused by oil droplets and air bubbles dispersed in the water phase.

Figure 6.15 shows the initial foam volume produced from 200 mL of both SSL aqueous dispersion and oil-in-water emulsions. The trend showed that for oil-in-water emulsions, no foam was produced below the critical aggregation concentration (cac) of SSL similar to SSL aqueous dispersions. For emulsions, the initial foam volume produced increased with SSL concentration since the concentration of free SSL available to create air-water interface was higher.

Comparing the foamability of SSL aqueous dispersions with oil-in-water emulsions one can see that less foam was produced from the emulsions. The presence of oil droplets could affect the foamability *via* two mechanisms. Firstly, emulsification of oil droplets reduces the SSL concentration available for foaming since molecules adsorb around oil droplets and leave less surfactant available in the continuous phase for

foaming. In addition, the oil droplets may act as anti-foaming agents during aeration and break the stabilising film between air bubbles and reduce foamability. These effects will be discussed in the next section with regards to foam stability. The lower foamability of surfactant solutions in the presence of oil droplets was also mentioned by Salonen *et al.*¹⁷ for aerated dodecane-in-water emulsions stabilised by SDS. The lower foamability in their systems has been suggested to be due to adsorption of SDS molecules around dodecane droplets, leaving less for foaming.

It can also be seen from the graph that dodecane-in-water emulsions produced less foam compared to HOSO-in-water emulsions. This could be linked to the smaller droplets of dodecane compared with HOSO. The smaller the droplets in the emulsions, the larger the total surface area of the droplets and hence more surfactant is required around droplets and so less is available for foaming.

Figure 6.14. Appearance of aerated dodecane-in-water (upper) and HOSO-in-water (lower) emulsions immediately after aeration. The concentration of SSL (with respect to total emulsion volume) in each sample is highlighted. Total liquid volume before aeration = 200 mL, scale bar represents 3 cm, $\phi_o = 0.2$.

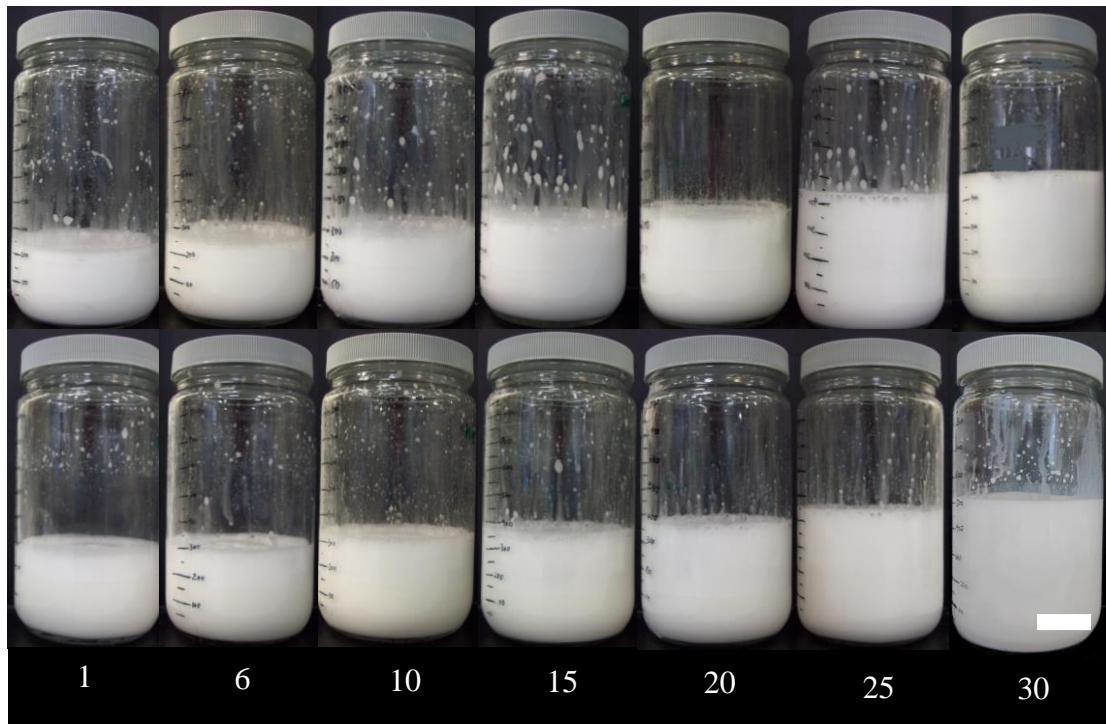
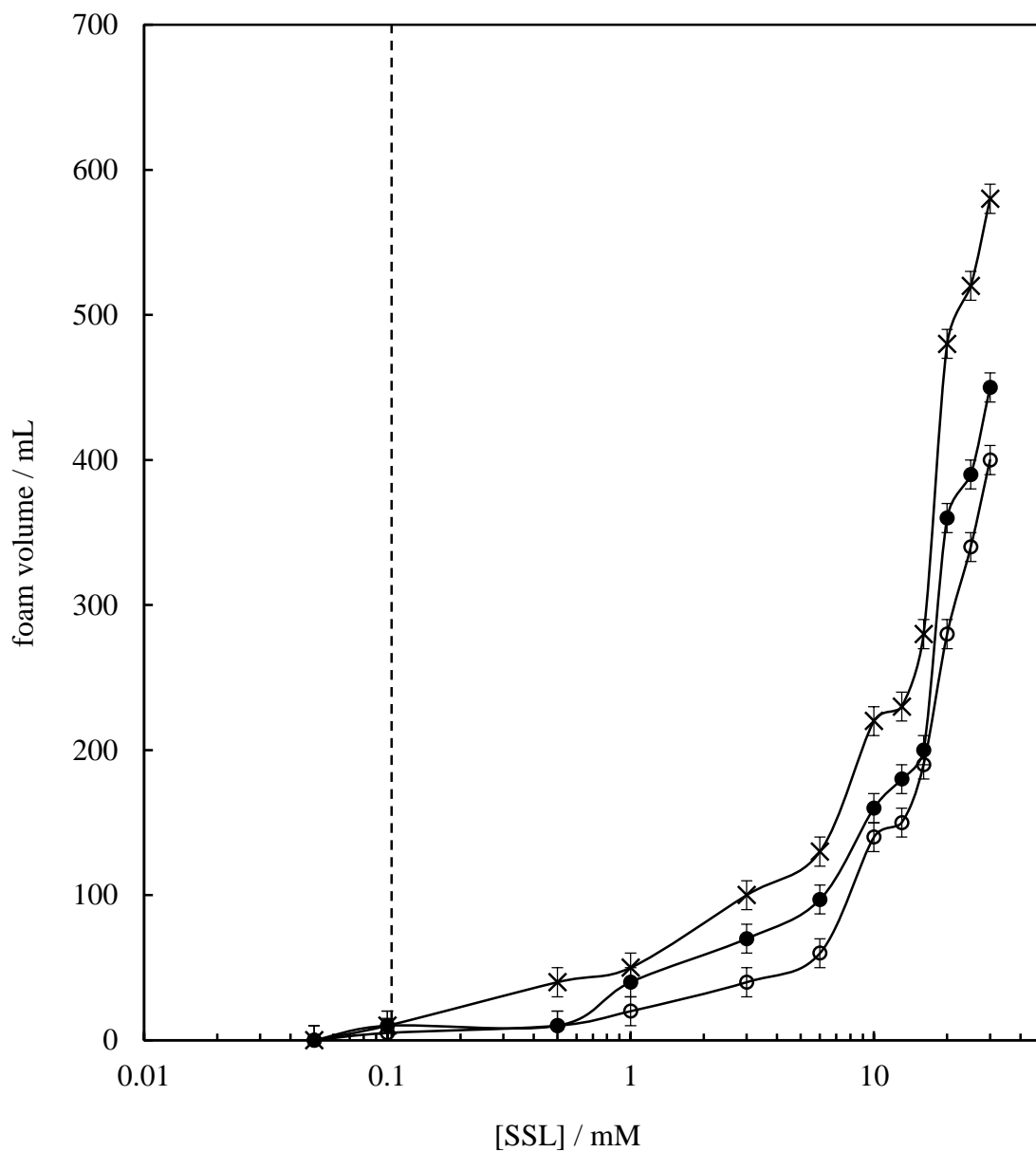


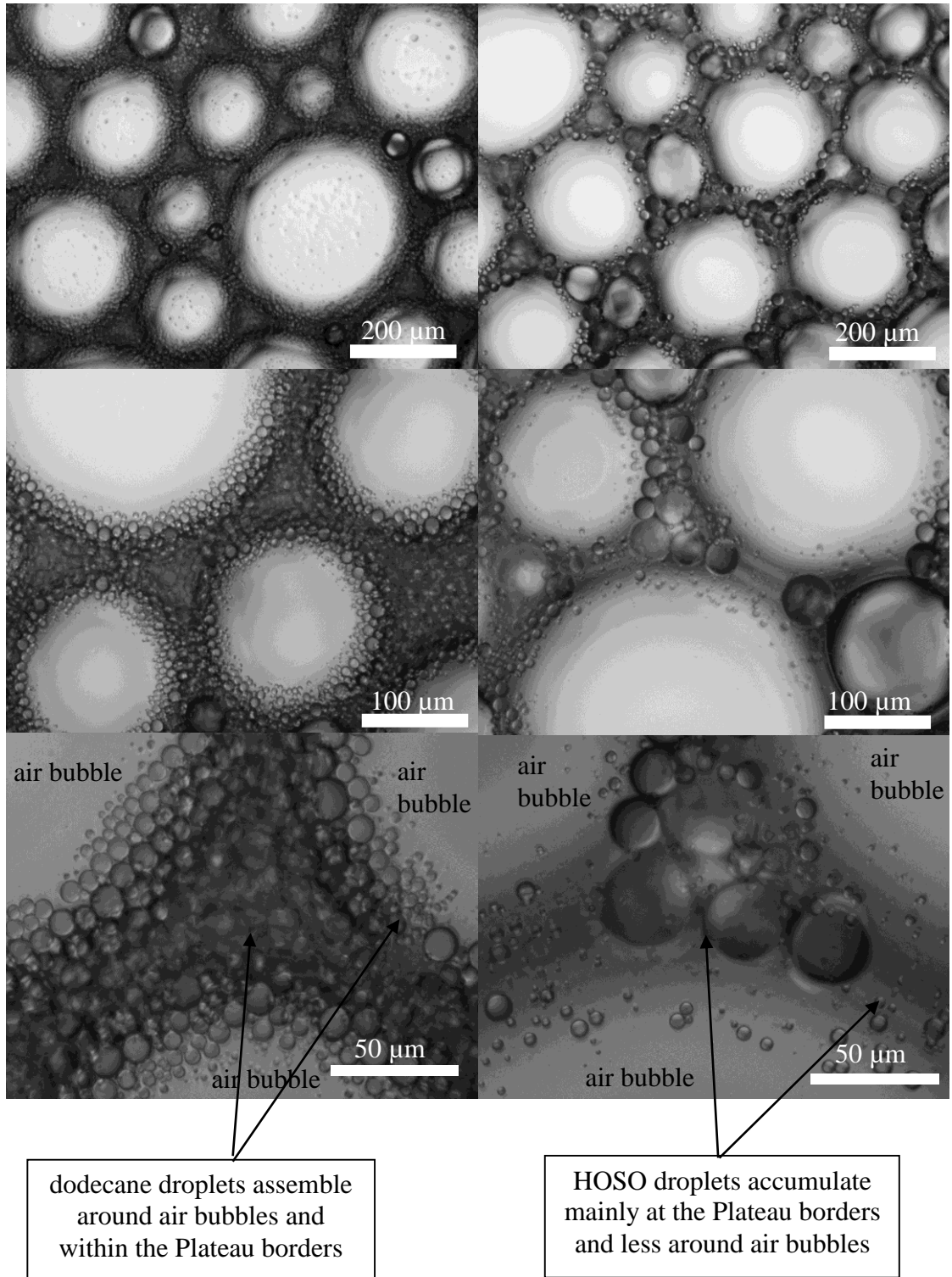
Figure 6.15. Initial foam volume produced from aeration of SSL aqueous dispersions (crosses), dodecane-in-water emulsions (empty points) and HOSO-in-water emulsions (filled points) as a function of SSL concentration. SSL concentration is with respect to total emulsion/dispersion volume. Total liquid volume before aeration = 200 mL, $\phi_o = 0.2$. Dashed line shows the cac of SSL in water at 25 °C.



The aerated emulsions were characterised by optical microscopy to assess the size and shape of air bubbles. In addition, the positioning of the oil droplets within the foam layer of the aerated emulsions was carefully studied to link this to the stability of the foams. Figure 6.16 shows optical micrographs of aerated dodecane-in-water and aerated HOSO-in-water emulsions with $\phi_o = 0.2$ stabilised by 30 mM SSL observed shortly after their aeration. Both samples have similar air bubble sizes. Aerated dodecane-in-water and HOSO-in-water emulsions had an average bubble size of $109 \pm 15 \mu\text{m}$ and $115 \pm 20 \mu\text{m}$, respectively. The average bubble sizes were determined by measuring the size of at least 100 air bubbles using optical micrographs for each oil. An average bubble size of $90 \pm 15 \mu\text{m}$ was measured for 30 mM SSL aqueous foam (no oil). The size of air bubbles in aqueous foams and aerated emulsions was not affected significantly by SSL concentration.

As can be seen in the figure, the two aerated emulsions had different oil droplet sizes. It was shown earlier that at 30 mM SSL and $\phi_o = 0.2$, the median droplet diameters were $6 \pm 1 \mu\text{m}$ and $15 \pm 2 \mu\text{m}$ for dodecane and HOSO, respectively. The arrangement of oil droplets around air bubbles and within the Plateau borders of the foams shows that dodecane and HOSO droplets display different behaviour. Smaller dodecane droplets appear to assemble around air bubbles and within the Plateau borders, but larger HOSO droplets were mainly accumulated within the Plateau borders. This observation will be linked to the foam stability data later in this chapter.

Figure 6.16. Optical micrographs of aerated dodecane-in-water emulsions (left) and aerated HOSO-in-water emulsions (right) stabilised with 30 mM SSL observed shortly after their aeration. Dodecane droplets adsorb around and on the surface of the air bubbles but HOSO droplets accumulate within the Plateau borders of the air bubbles. $\phi_o = 0.2$.



6.3.2 Foamability-experimental vs. calculated

It was shown in Figure 6.15 that aerated oil-in-water emulsions produced less foam compared to SSL aqueous dispersions of equal SSL concentration, due to loss of SSL molecules around oil droplets upon emulsification. The concentration of SSL adsorbed around oil droplets was calculated to determine the concentration of free SSL and to assess the effect of oil droplets on the foamability of the emulsions. In the calculations it was assumed that the area per molecule of SSL at the oil-water interface was equal to that at the air-water interface given in Chapter 3 and equal to $1.1 \pm 0.1 \text{ nm}^2 \text{ molecule}^{-1}$ at $25 \text{ }^\circ\text{C}$. The concentration of free surfactant in water after emulsification is:

$$[\text{SSL}]_{\text{free}} = [\text{SSL}]_{\text{initial}} - [\text{SSL}]_{\text{adsorbed}} \quad (6.3)$$

The concentration of SSL adsorbed around oil droplets was calculated using the equation below:¹⁷

$$[\text{SSL}]_{\text{adsorbed}} = \frac{3 * \phi_{\text{oil}}}{R} * \frac{M_w}{A_s * N_A} \quad (6.4)$$

where R is average droplet radius, M_w is the molecular weight of SSL (450 g mole^{-1}), A_s is surface area per molecule of surfactant ($1.1 \text{ nm}^2 \text{ molecule}^{-1}$) and N_A is Avogadro's number. The concentration of SSL left in the emulsions, available for foaming, was then used to predict the volume of foam expected from that specific concentration. This was done by using the data from foaming SSL aqueous dispersions ($\phi_o = 0$). For example for $[\text{SSL}]_{\text{free}} = 29.5 \text{ mM}$, the volume of foam expected was deducted from the foamability curve of SSL aqueous dispersions at that concentration. The data are shown in Figure 6.17 and Figure 6.18 for aerated dodecane-in-water and aerated HOSO-in-water emulsions, respectively. The figures compare the foam volume expected from the emulsions, based on the calculations above, and the experimental foam volume generated upon aeration. For dodecane-in-water emulsions, the experimental foam volume was found to be less than that calculated by an average 15 %, but for HOSO-in-water emulsions the volumes of foams produced were in agreement with those calculated. It can be concluded that HOSO droplets had no influence on the foamability of the emulsions whereas dodecane droplets possess some degree of anti-foaming behaviour as suggested by Salonen *et al.*¹⁷ for SDS aqueous foams.

Figure 6.17. Calculated foam volume (points) *versus* experimental foam volume (crosses) for a series of aerated dodecane-in-water emulsions as a function of SSL concentration. SSL concentration is with respect to total emulsion volume, $\phi_o = 0.2$.

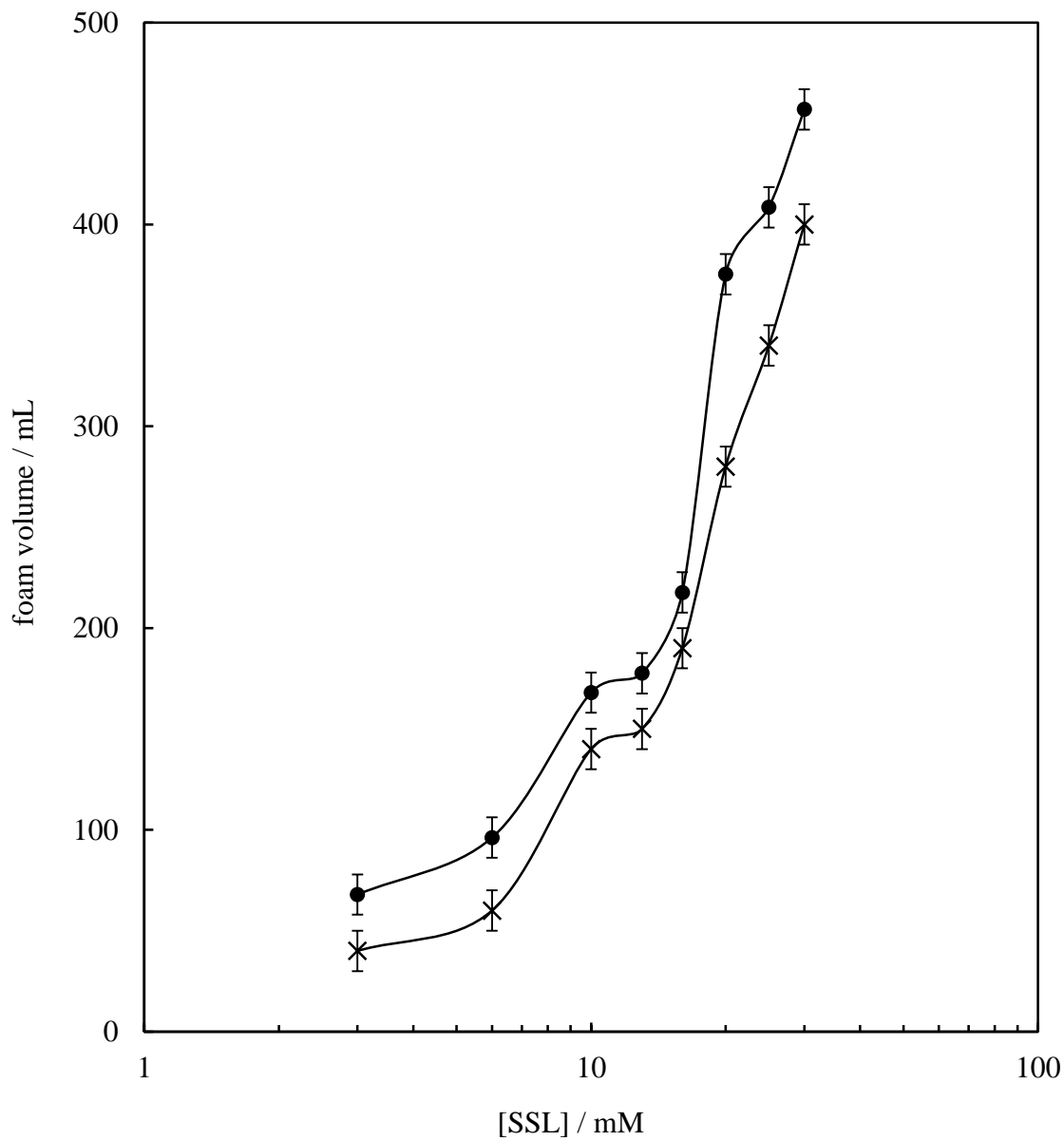
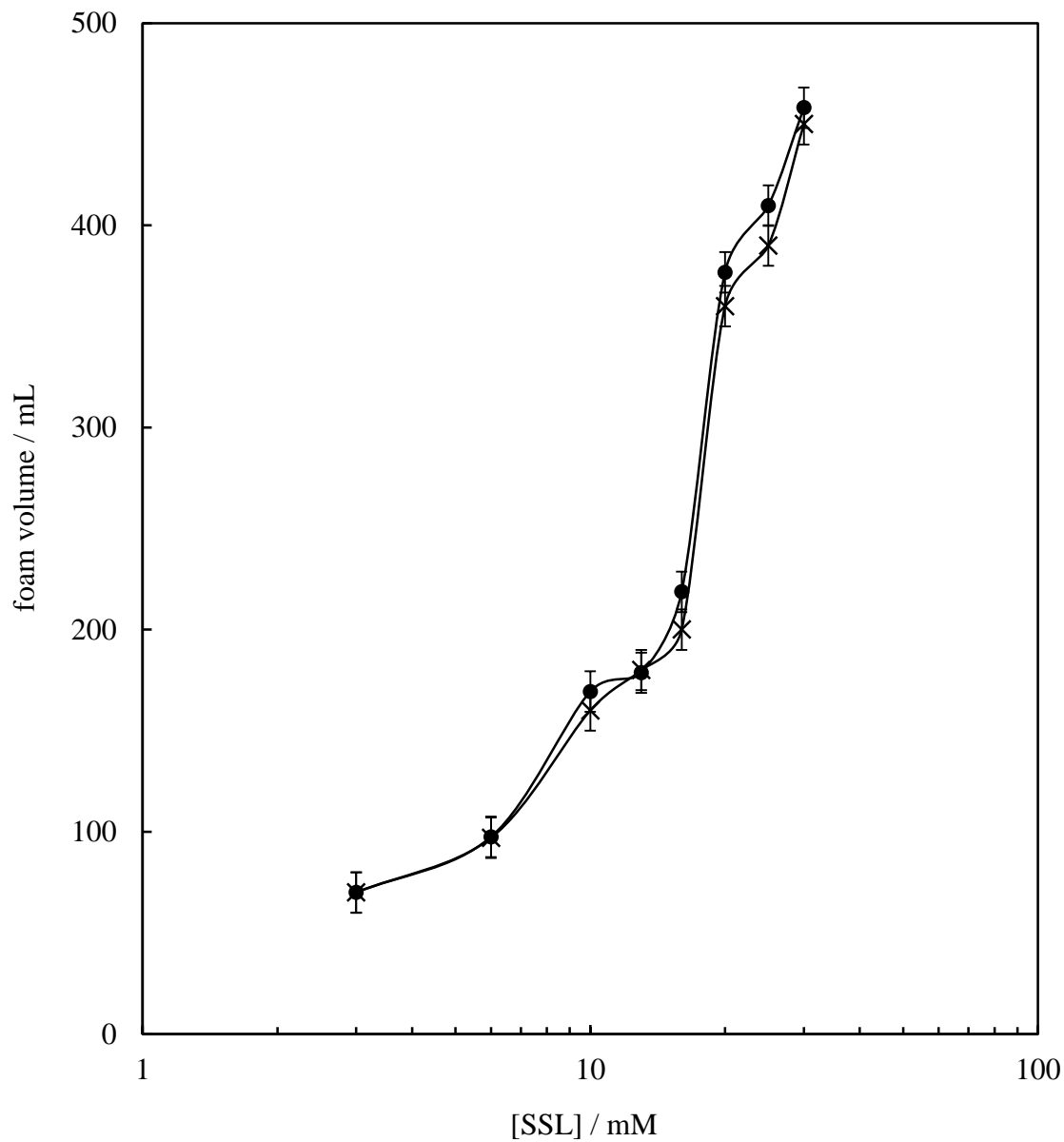


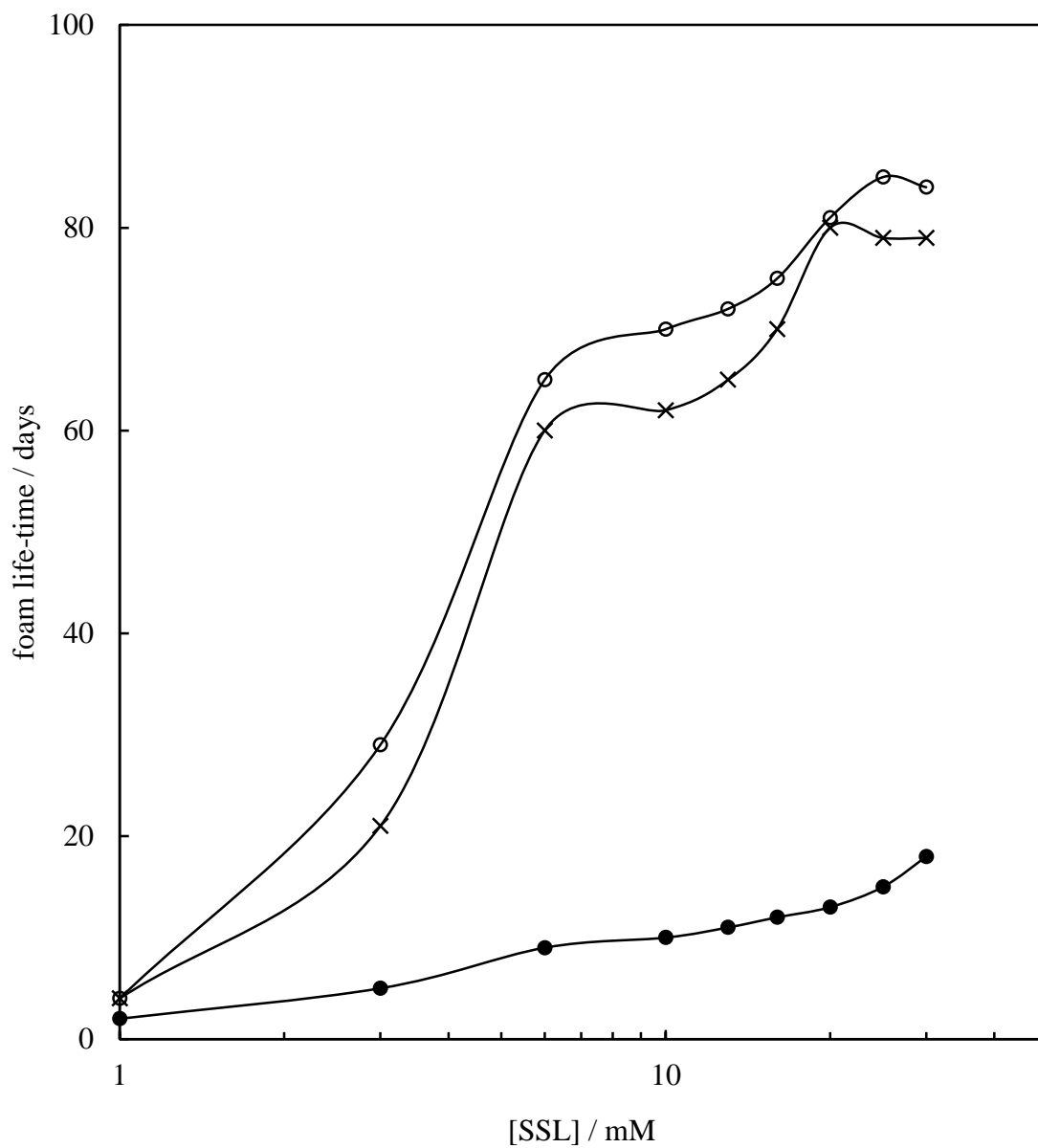
Figure 6.18. Calculated foam volume (points) *versus* experimental foam volume (crosses) for a series of aerated HOSO-in-water emulsions as a function of SSL concentration. SSL concentration is with respect to water phase in the emulsions, $\phi_o = 0.2$.



6.3.3 Stability of the foams

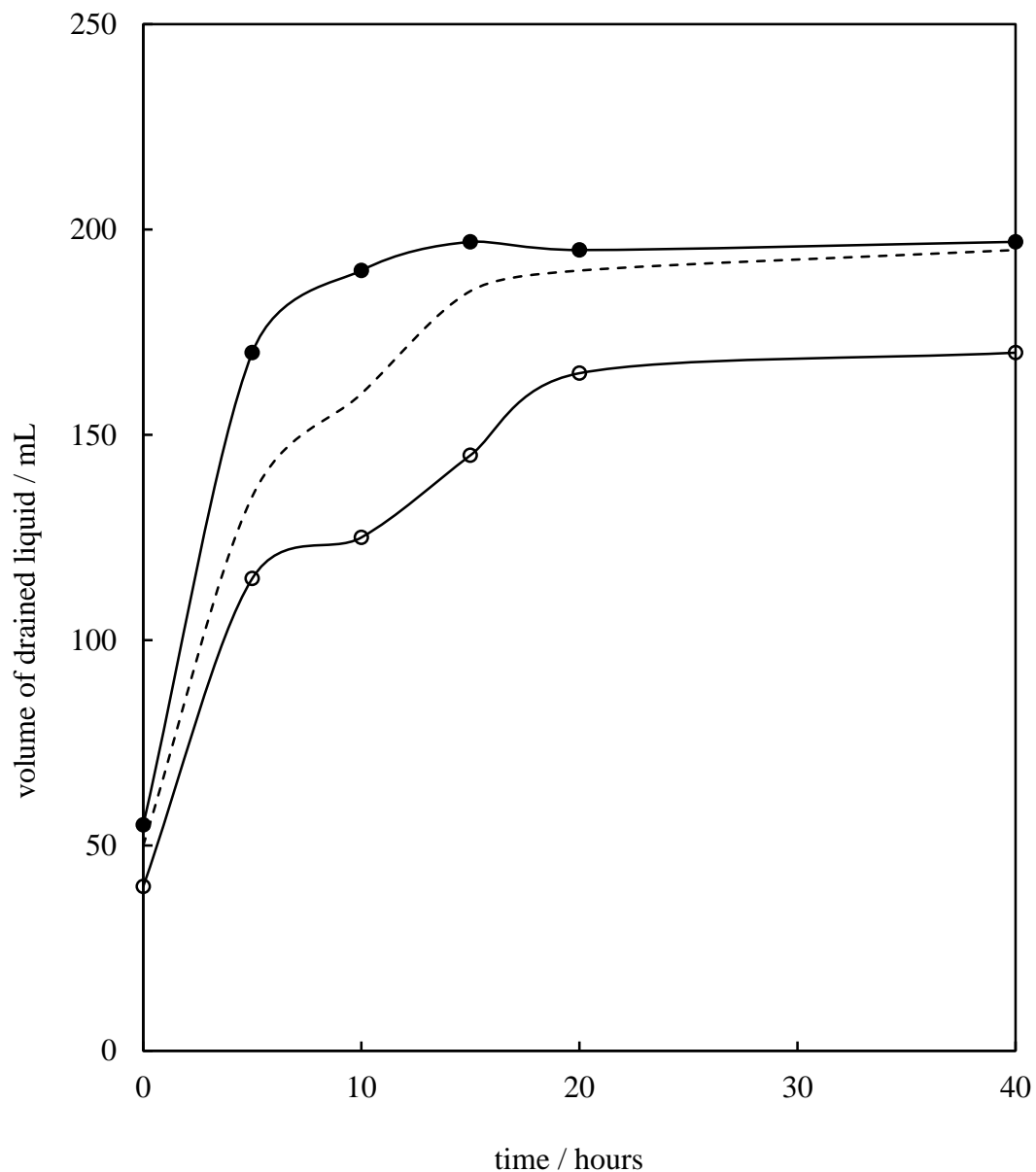
The presence of oil droplets in dodecane-in-water emulsions was found to reduce the foamability. The effect was different in the case of HOSO-in-water emulsions as HOSO droplets were found to have no anti-foaming effect. Monitoring the appearance of the aerated emulsions after their preparation however, showed that the type of oil and the size of oil droplets influenced the stability of the aerated emulsions. The height of the foam layer in the aerated emulsions was monitored over time to assess the stability of them against drainage and coalescence. Figure 6.19 shows the foam life-time (time taken for complete foam collapse) for aerated SSL aqueous dispersions, dodecane-in-water emulsions and HOSO-in-water emulsions at different SSL concentrations. Similar to the observations in Chapter 3, the stability of SSL aqueous foams increases as the surfactant concentration increased. As can be seen, aerated dodecane-in-water emulsions had significantly shorter life-times than SSL aqueous foams. On the other hand, aerated HOSO-in-water emulsions showed longer life-times compared to SSL foams. According to the data presented in the figure the most stable aerated dodecane-in-water emulsion collapses after only 18 days, which is much shorter compared to the most stable aerated HOSO-in-water emulsion with a life-time of over 80 days. The decrease in the stability of foams due to the presence of dodecane droplets was also observed by Salonen *et al.*¹⁷ They found that for aerated dodecane-in-water emulsions stabilised by SDS, the foams become less stable upon increasing the dodecane volume fraction up to 0.5, due to the anti-foaming effect of dodecane droplets.

Figure 6.19. Foam life-time for aerated SSL aqueous dispersions (crosses), dodecane-in-water emulsions (filled points) and HOSO-in-water emulsions (empty points) as a function of SSL concentration. SSL concentration is with respect to total dispersion/emulsion volume, $\phi_o = 0.2$.



The volume of drained liquid from the aerated emulsions was also measured at various times after their aeration and the data are shown in Figure 6.20 for the foams with $\phi_o = 0.2$ and stabilised by 30 mM SSL. The results for 30 mM SSL aqueous foams are also included for comparison. A steep rise in the volume of the liquid drained from the foams within the initial 20 hours of storage was observed for all three systems. It was noted that for SSL aqueous foams and aerated dodecane-in-water emulsions almost 95% of the initial liquid volume was drained after 20 hours. On the other hand, the volume of drained liquid for aerated HOSO-in-water emulsions was only around 75 % after 20 hours of storage and remained unchanged by 40 hours. The accumulation of large HOSO droplets primarily in the Plateau borders of foams is believed to prevent the liquid drainage after 20 hours and reduced the rate of lamella film thinning. This eventually increased the life-time of the aerated HOSO-in-water emulsions.

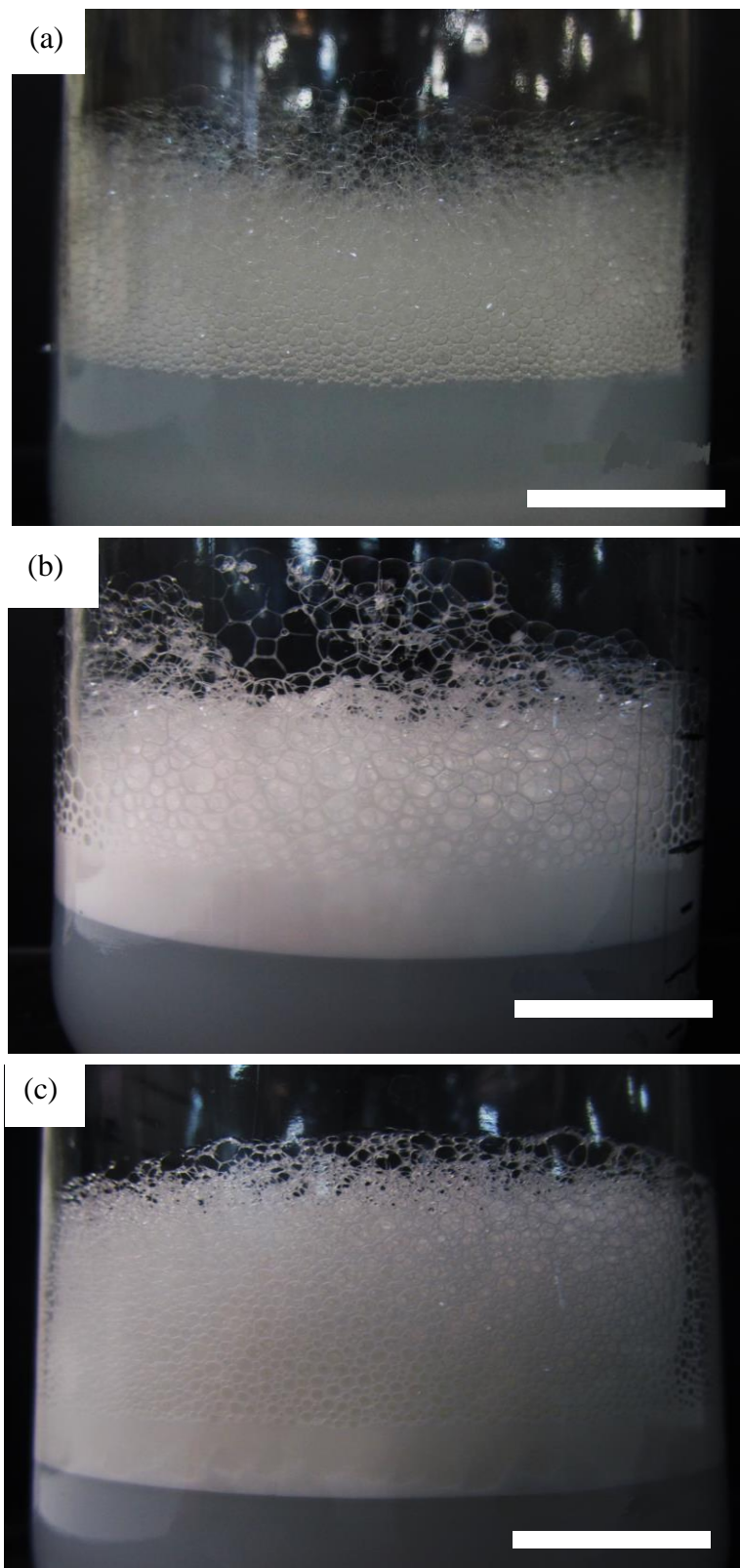
Figure 6.20. The volume of drained liquid from aerated SSL aqueous dispersion (dashed line), dodecane-in-water emulsion (filled points) and HOSO-in-water emulsion (empty points) as a function of time. Foams were stabilised by 30 mM SSL with respect to total dispersion/emulsion volumes and were left at rest at room temperature of 23 ± 2 °C. Total liquid volume before aeration = 200 mL, $\phi_o = 0.2$.



The appearance of the foam layer in the aerated emulsions and SSL aqueous foams was monitored using a digital camera one week after their aeration. The photos are shown in Figure 6.21 and were used to study the air bubble shape and size and to assess the thickness of the lamella film between the air bubbles. As can be seen in the figure aerated HOSO-in-water emulsions had smaller air bubbles compared to aerated dodecane-in-water emulsions and SSL aqueous foams. Smaller air bubbles in the foams containing HOSO droplets highlights their higher stability to coalescence and/or disproportionation compared to the other two systems. As mentioned before, it is believed that HOSO oil droplets drain along with aqueous phase from the thin film into the Plateau borders. Once oil droplets are trapped they squeeze into each other due to the shrinking of the Plateau borders and hence they block the drainage of water from thin films through the Plateau borders. This then enhances the stability of air bubbles by preventing thin film rupture in the foams containing HOSO droplets. Dodecane droplets were smaller than HOSO droplets and accumulate in the Plateau borders to a lesser extent because a lower buoyancy force acts on them. Therefore, they have less resistance to get trapped within the Plateau borders due to their smaller size. The size of oil droplets in the emulsions is therefore a determining factor in the stability of the aerated emulsions. Similar behaviour was reported by Koczko *et al.*¹⁶ for a series of aerated decane-in-water emulsions stabilised by SDBS. They showed that the stability of the foams decreased as the size of the oil droplets decreased.

Close inspection of the digital images of the foams one week after preparation reveals that the shape of air bubbles in aerated dodecane-in-water emulsions were polyhedral (non-spherical) whereas those for aerated HOSO-in-water emulsions were mainly spherical as observed previously after their preparation (Figure 6.16). It is known that air bubbles are spherical in wet foams (*i.e.* those with gas volume fraction up to 0.74, which is the maximum volume fraction possible for an internal phase made up of uniform incompressible spheres). The air bubbles in drier foams such as those in aerated dodecane-in-water emulsions, have distorted shapes and the lamella between air bubbles become thinner than wet foams, which enhances the chance of film rupture and foam breakdown.⁴⁶

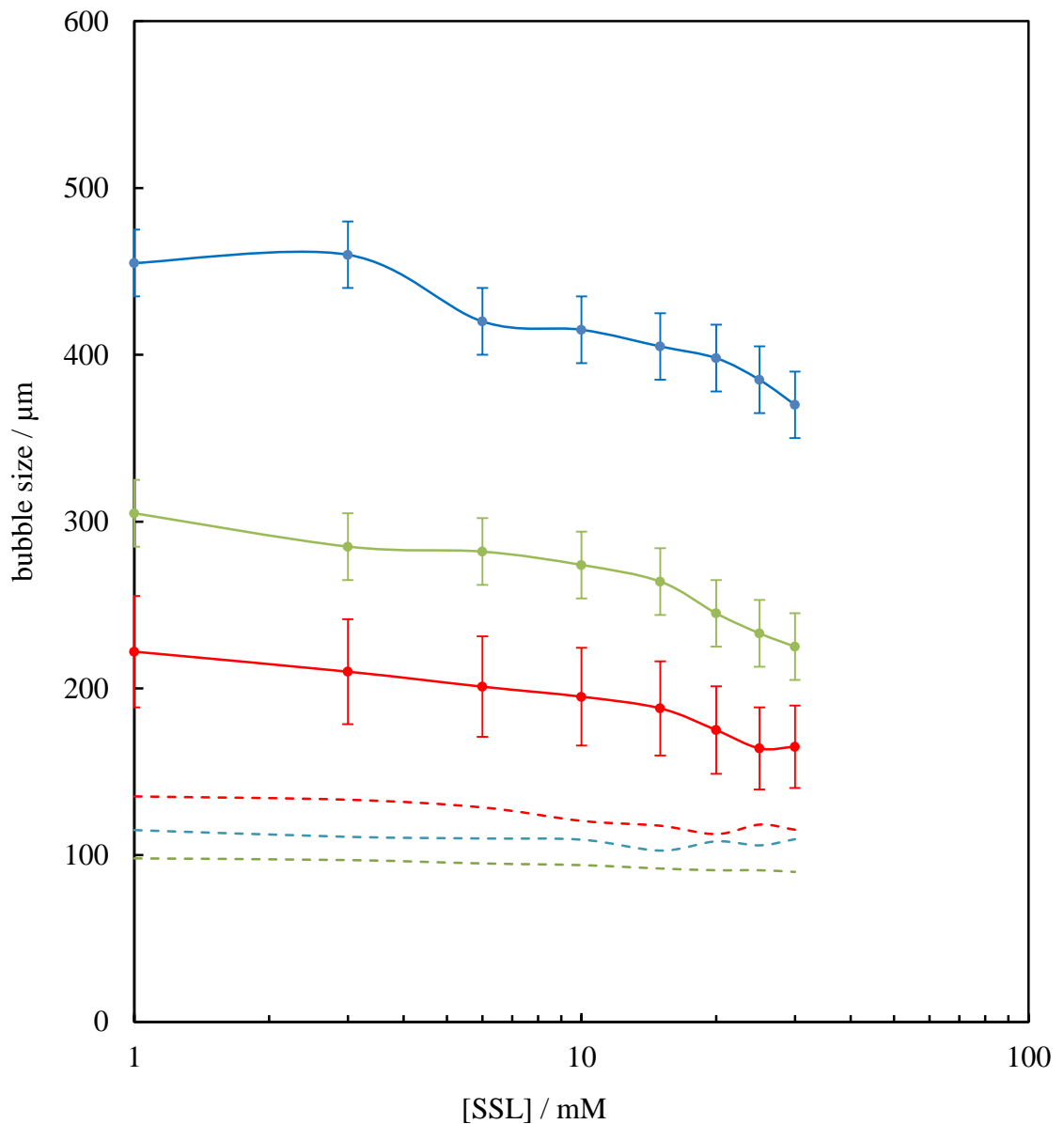
Figure 6.21. Appearance of (a) aerated SSL aqueous dispersions, (b) aerated dodecane-in-water emulsions and (c) aerated HOSO-in-water emulsions one week after their preparation. Concentration of SSL was 30 mM with respect to total emulsion/dispersion volume. Scale bar = 3 cm, $\phi_o = 0.2$.



The size of air bubbles in the foams was also measured one week after their aeration. The size of at least 100 air bubbles were measured for each sample. It should be noted that the initial size of air bubbles in the aerated emulsions ($\phi_o = 0.2$) and SSL aqueous foams was measured to be around $110 \pm 25 \mu\text{m}$ after preparation. Therefore the presence of oil droplets had no significant influence on the size of air bubbles. Figure 6.22 shows the size of air bubbles in SSL aqueous foams and aerated emulsions as a function of SSL concentration measured one week after preparation. It was found that the average size of air bubbles in the foams with 30 mM SSL after one week increased to around $370 \mu\text{m}$ for aerated dodecane-in-water emulsions, whereas it was 225 and $165 \mu\text{m}$ for SSL foams (no oil) and aerated HOSO-in-water emulsion, respectively. Therefore, one week after preparation aerated HOSO-in-water emulsions had the smallest air bubbles confirming their higher stability to coalescence and/or disproportionation. SSL concentration was found to slightly affect the size of air bubbles after one week and the average bubble size decreased slightly with increasing SSL concentration in the presence and absence of oil droplets, as shown in the graph.

So far, foamability of dodecane-in-water emulsions and HOSO-in-water emulsions were compared to those of SSL aqueous foams. It was shown that the emulsions had lower foamabilities due to the lower concentration of free surfactant available for foaming after emulsification. Aerated HOSO-in-water emulsions showed better stability compared to both SSL aqueous foams and aerated dodecane-in-water emulsions. This was linked to accumulation of HOSO droplets within the Plateau borders and the reduction in the rate of liquid drainage from the foams. It was also shown that the three foams studied in here had different bubble sizes one week after storage and this linked to the stability of the foams. In the next section, the effect of oil volume fraction on the foaming properties of the oil-in-water emulsions is presented.

Figure 6.22. Average diameter of air bubbles in SSL aqueous foams (green), aerated dodecane-in-water emulsions (blue) and HOSO-in-water emulsions (red) as a function of SSL concentration. Dashed lines show the data measured immediately after aeration and solid lines show those measured one week after aeration. Air bubbles in the presence of dodecane and HOSO droplets grow faster and slower in size, respectively, compared to SSL aqueous foams, $\phi_o = 0.2$.



6.3.4 Effect of oil volume fraction

Oil-in-water emulsions with varying oil volume fraction were aerated immediately after emulsification to assess the effect of oil droplet concentration on the initial foam produced and stability of the foams. Foamability of the emulsions was found to be dependent on oil volume fraction of the emulsions. The initial foam volume produced as a function of oil volume fraction from dodecane-in-water and HOSO-in-water emulsions stabilised by 30 mM SSL is shown in Figure 6.23. As expected emulsions with more oil produced less foam as more surfactant was used up to cover oil droplets in the emulsion and less was available for foaming. Similar to the results of foamability with varying SSL concentration, dodecane-in-water emulsions produced slightly less foam compared to HOSO-in-water emulsions. No foam was generated upon aeration of the emulsions with $\phi_o > 0.65$ as these were water-in-oil for both oils used.

The results of the foam stability for the aerated emulsions as a function of oil volume fraction are presented in Figure 6.24. As can be seen from the graph, and as was seen before, foams were more stable in the presence of HOSO droplets than in the presence of dodecane droplets. The effect of oil volume fraction on the stability of the foams showed different trends for the two oils used. The life-time of 30 mM SSL aqueous foam is also presented by the dashed line for comparison. Foams with dodecane were less stable with increasing dodecane volume fraction but the stability of the foams with HOSO increased with increasing HOSO volume fraction. The increase in the stability of foams in the presence of HOSO droplets is in line with previous explanations about their role as foam stabilisers. The higher the concentration of HOSO droplets the number of droplets accumulated at the Plateau borders increases, which prevents film thinning by reducing liquid drainage. This is believed not to be the case for the foams in the presence of dodecane droplets and the reduction in the stability of foams with increasing dodecane volume fraction is believed to be due to other mechanisms such as anti-foaming effect of dodecane droplets during their storage and that they may act as slow anti-foaming agents. This was also mentioned by Salonen *et al.*¹⁷ as a reason for lower stability of SDS foams in the presence of dodecane droplets. To further investigate the anti-foaming effect of dodecane droplets, the entering coefficient (E) and spreading coefficient (S) of oil droplets at air-water interfaces were calculated using equilibrium interfacial tension values as discussed in the next section.

Figure 6.23. Initial foam volume produced from aeration of dodecane-water emulsions (circles) and HOSO-water emulsions (crosses) as a function of oil volume fraction in the emulsions. [SSL] was constant and was 30 mM (with respect to total emulsion volume). Total liquid volume before aeration = 200 mL. For $\phi_o > 0.65$, emulsions were water-in-oil hence no foam was produced.

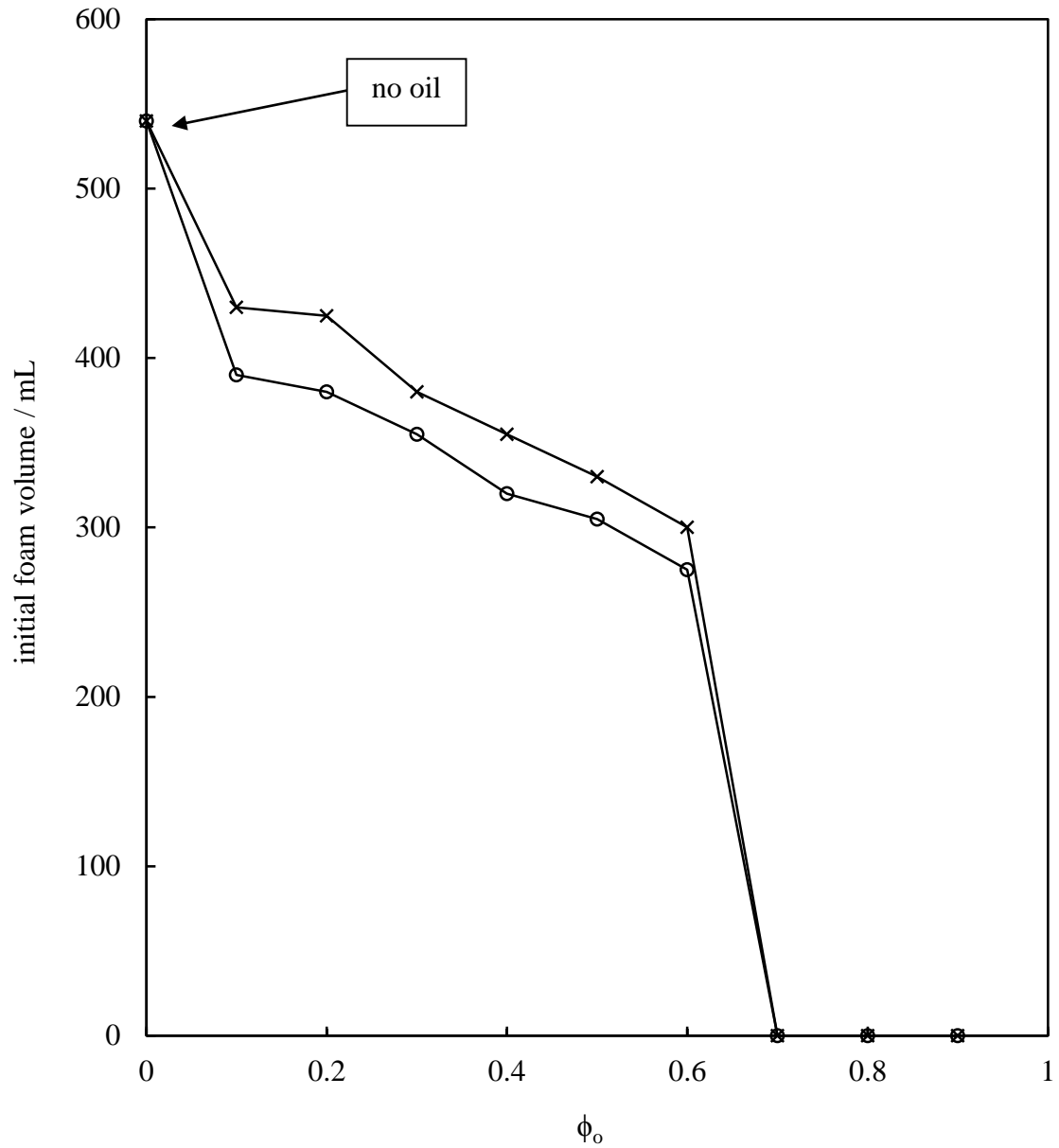
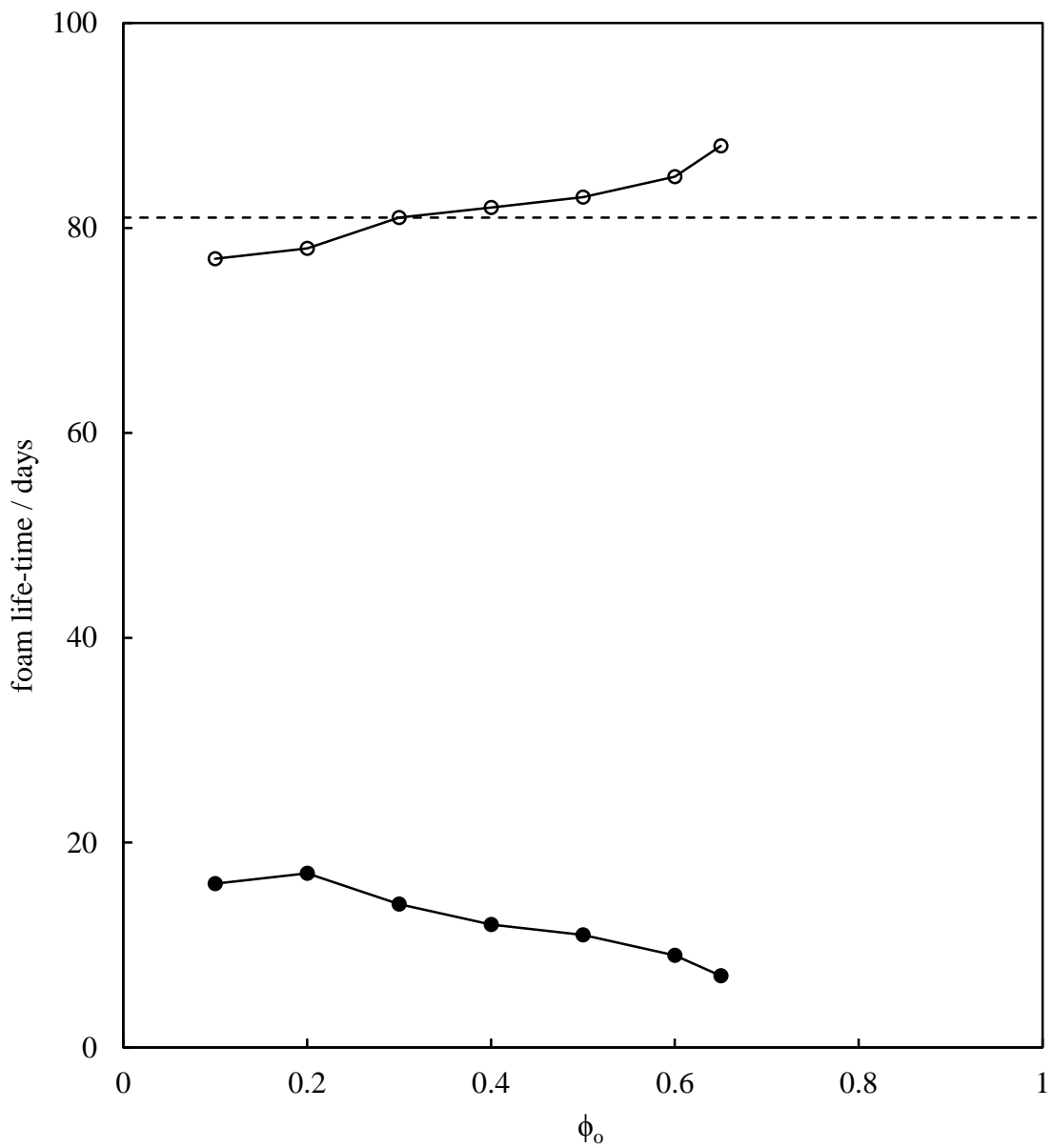


Figure 6.24. Foam life-time for aerated dodecane-in-water emulsions (filled points) and HOSO-in-water emulsions (empty points) as a function of oil volume fraction in the emulsions at fixed SSL concentration. [SSL] was 30 mM (with respect to total emulsion volume). Dashed line shows the life-time of 30 mM SSL aqueous foam. For $\phi_o > 0.65$, emulsions were water-in-oil and did not foam.



6.4 Entering and spreading coefficients *via* surface and interfacial tensions

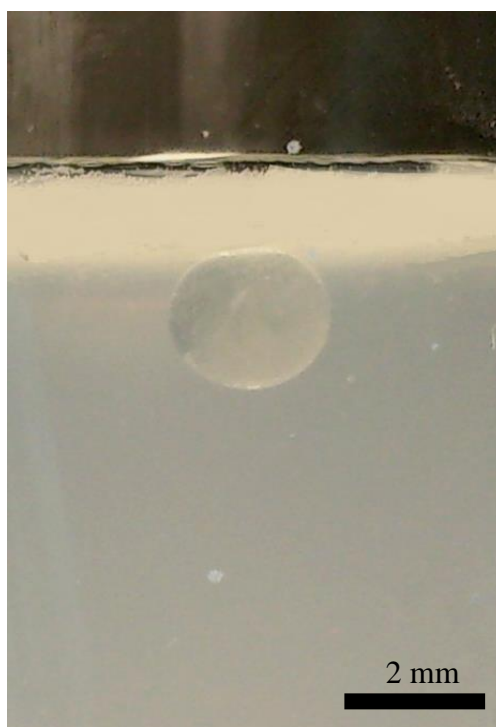
It is known that oil droplets present in a foaming solution may influence the foamability of the solution and stability of the foams produced.⁴⁷ Oil droplets may enter the lamella between two adjacent air bubbles within the foam and the liquid bridge so formed can lead to film rupture. In another scenario the droplet may spread as a film, which may cause film thinning and breakdown. The possibility of oil droplet entry into the air-solution interface and whether or not it will spread or make a lens after entry, might be assessed from appropriate surface and interfacial tensions. Table 6.1 shows the surface tensions, interfacial tensions, entering coefficient (E) and spreading coefficient (S) of the studied systems. The surface tension of dodecane at 25 °C was in agreement with that reported elsewhere.⁴⁸ As presented, E coefficients are positive for both oils. According to the theory, entering of oil droplets is thus thermodynamically favourable. Macroscopic observations from the measurements of the life-time of single oil droplets at air-aqueous SSL dispersion interface were not in agreement with this and both oil droplets did not merge into the interface within experiment time scale (12 hours, see Figure 6.25) possibly due to the high stability of the thin oil-water-air pseudofilm. A possible explanation for this was mentioned by Koczó *et al.*¹⁶ that E and S coefficients are thermodynamic properties, which determine the favourable configuration of the oil droplet, however they cannot predict the behaviour of the oil droplet in dynamic conditions which exists within the draining foam film and during aeration. Formation of a thin film between an approaching oil droplet and the air-water interface due to adsorption of surfactant molecules, can act as a kinetic barrier to droplet entering resulting in a metastable state.⁴⁹

As explained at the introduction of this chapter if an oil droplet merges at an air-water interface it may form a lens or spread at air-water interface, determined by the spreading coefficient. The spreading coefficients of dodecane droplets at air-30 mM aqueous SSL dispersion ($+2.8 \text{ mN m}^{-1}$) suggests that dodecane droplets would spread at the interface due to having a positive S coefficient. On the other hand, a negative S coefficient (-17.4 mN m^{-1}) was calculated for a HOSO droplet at air-30 mM aqueous SSL dispersion, suggesting the oil droplet would form a lens if enters the interface. However, as mentioned earlier due to the high stability of the oil-water-air pseudofilm, caused by adsorption of SSL aggregates, the droplets did not merge at the interface even though positive E coefficients were calculated for both oils.

Table 6.1. Equilibrium interfacial tensions, equilibrium surface tensions, entry coefficients (for oil into air-30 mM SSL solution) and spreading coefficients of the studied systems at 25 °C.

System	$\gamma_{\text{air-30 mM SSL}} / \text{mN m}^{-1}$	$\gamma_{\text{air-oil}} / \text{mN m}^{-1}$	$\gamma_{\text{oil-30 mM SSL}} / \text{mN m}^{-1}$	E / mN m^{-1}	S / mN m^{-1}
aq. SSL / dodecane	42.7	25.1	14.8	+32.4	+2.8
aq. SSL / HOSO	42.7	35.8	24.3	+31.2	-17.4

Figure 6.25. Appearance of a dodecane droplet under the air-aqueous SSL dispersion interface resting for 12 hours. [SSL] = 30 mM.



6.5 Conclusions

SSL, a vesicle-forming surfactant with a HLB number of 21 was used as the emulsion and foam stabiliser in a series of oil-in-water emulsions and aerated emulsions. The effects of oil type, surfactant concentration and oil volume fraction on the preferred emulsion type and the stability of the prepared emulsions prior to their aeration were studied. The data from the SSL concentration scan revealed the formation of oil-in-water type emulsions for both dodecane and HOSO at 0.2 oil volume fraction. Dodecane-in-water emulsions were found to have smaller droplets and were less polydispersed compared to HOSO-in-water emulsions. Both sets of emulsions were stable against coalescence at SSL concentrations of ≥ 0.1 mM, however most of the water resolved due to creaming one week after storage. At 30 mM SSL, emulsions phase inverted catastrophically between 0.65 and 0.7 oil volume fraction for both dodecane and HOSO. The water-in-oil emulsions completely phase separated immediately after preparation.

Emulsions were aerated shortly after emulsification and it was found that no foam was produced below the cac of SSL. The initial foam volume produced increased with SSL concentration. As expected, the prepared emulsions were found to produce less foam compared to pure SSL aqueous solutions, as less surfactant was available in the continuous phase for foaming to occur. The concentration of free SSL in the continuous phase after emulsification was calculated for both sets of emulsions and the data were used to predict the volume of foam expected from them upon aeration. It was shown that the presence of dodecane droplets during aeration decreased the volume of foam produced but HOSO droplets had no influence on the initial foam volume. Studying the optical micrographs of the aerated emulsions after their preparation revealed that dodecane droplets dispersed evenly around air bubbles but HOSO droplets were mainly accumulated within the Plateau borders of the foams. The difference in the size of the droplets produced from homogenisation of the two oils, at equal applied shear, was believed to be the major determining factor in their effect on the stability of foams. The stability of the foams in the presence of HOSO droplets was enhanced compared to those with no oil, but aerated emulsions with dodecane droplets had shorter life-times compared to pure SSL foams. For aerated HOSO-in-water emulsions, it is likely that HOSO droplets drain slower than the aqueous phase and accumulate within the Plateau borders. This was believed to block the drainage of water from thin films through the Plateau borders and enhanced the stability of air bubbles by preventing thin film rupture.

Dodecane droplets were found to be smaller than HOSO droplets and less of them accumulate in the Plateau borders because a lower buoyancy force acts on them. Therefore, the liquid drains from the thin films of the foams and the bubbles eventually collapse. It was also concluded that dodecane droplets may act as slow anti-foaming agents since the stability of the foams decreased with increasing dodecane volume fractions. On the other hand, the aerated emulsions with higher HOSO volume fractions showed better stability, further confirming the mechanism of their accumulation within the Plateau borders to reduce liquid drainage and increase the foam life-time.

Finally, the entry and spreading coefficients at the air-water interface for a single oil droplet when introduced into an aqueous SSL dispersion were calculated using equilibrium surface and interfacial tension values at the associated interfaces. E coefficients were calculated to be positive for both oils, suggesting that the entry of oil droplets at the air-water interface was thermodynamically favourable. However, macroscopic observations of the life-time of single oil droplets at the air-liquid interface for SSL dispersions, in the model setup, were not in agreement with this and oil droplets did not merge into the interface for both oils. This was believed to be due to the fact that the air-liquid films stabilised by SSL are very stable, meaning that oil droplets cannot break the film at rest but may do under agitation (as during aeration). The spreading coefficients of the oil droplets at the air-30 mM aqueous SSL dispersion was also calculated and was found to be different for dodecane and HOSO oils. For dodecane the S value was calculated to be $+2.8 \text{ mN m}^{-1}$ suggesting the droplet spreads at the interface but a negative S coefficient (-17.4 mN m^{-1}) was calculated for HOSO suggesting the formation of lens after entry. The spreading behaviour of the oil droplets at the interface however could not be assessed experimentally due to the stability of the interface.

6.6 References

1. *The Physics of Foams*, D. Weaire and S. Hutzler, Clarendon Press, Oxford, 2001.
2. *Modern Aspects of Emulsion Science*, ed. B.P. Binks, The Royal Society of Chemistry, Cambridge, 1998.
3. K.E. Allen, B.S. Murray and E. Dickinson, *Food Hydrocoll.*, **22**, 690 (2008).
4. M. Simjoo, T. Rezaei, A. Andrianov and P.L.J. Zitha, *Colloids Surf. A*, **438**, 148 (2013).
5. *Dairy chemistry and physics*, P. Walstra, R. Jenness and H.T. Badings, Wiley, Madison, 1984.
6. D. Rousseau, *Food Res. Int.*, **33**, 3 (2000).
7. K. Boode and P. Walstra, *Colloids Surf. A*, **81**, 121 (1993).
8. K. Boode, P. Walstra and A.E.A. de Groot-Mostert, *Colloids Surf. A*, **81**, 139 (1993).
9. H.D. Goff, *J. Dairy Sci.*, **80**, 2620 (1997).
10. F. Leal-Calderon, F. Thivilliers and V. Schmitt, *Curr. Opin. Colloid Interface Sci.*, **12**, 206 (2007).
11. K. Shamsi, Y. Che Man, M. Yusoff and S. Jinap, *J. Am. Oil Chem. Soc.*, **79**, 583 (2002).
12. N.E. Hotrum, M.A. Cohen Stuart, T. Van Vliet, S.F. Avino and G.A. Van Aken, *Colloids Surf. A*, **260**, 71 (2005).
13. P. Relkin and S. Sourdet, *Food Hydrocoll.*, **19**, 503 (2005).
14. E. Fredrick, P. Walstra and K. Dewettinck, *Adv. Colloid Interface Sci.*, **153**, 30 (2010).
15. M.D. Eisner, S.A.K. Jeelani, L. Bernhard and E.J. Windhab, *Chem. Eng. Sci.*, **62**, 1974 (2007).
16. K. Koczko, L.A. Lobo and D.T. Wasan, *J. Colloid Interface Sci.*, **150**, 492 (1992).
17. A. Salonen, R. Lhermerout, E. Rio, D. Langevin and A. Saint-Jalmes, *Soft Matter*, **8**, 699 (2012).
18. K.E. Allen, E. Dickinson and B. Murray, *LWT - Food Sci. Technol.*, **39**, 225 (2006).
19. N.D. Denkov, *Langmuir*, **20**, 9463 (2004).
20. C.A. Miller, *Curr. Opin. Colloid Interface Sci.*, **13**, 177 (2008).

21. R. Aveyard, P. Cooper, P.D.I. Fletcher and C.E. Rutherford, *Langmuir*, **9**, 604 (1993).
22. J.V. Robinson and W.W. Woods, *J. Chem. Technol. Biotechnol.*, **67**, 361 (1948).
23. E. Dickinson, B.S. Murray and G. Stainsby, *Journal of the Chemical Society, Faraday Transactions 1: Physical Chemistry in Condensed Phases*, **84**, 871 (1988).
24. A. Hadjiiski, R. Dimova, N.D. Denkov, I.B. Ivanov and R. Borwankar, *Langmuir*, **12**, 6665 (1996).
25. W.D. Harkins and A. Feldman, *J. Am. Chem. Soc.*, **44**, 2665 (1922).
26. *Emulsions, Foams, and Thin Films*, K.L. Mittal and P. Kumar, Marcel Dekker Inc., New York, 2000.
27. E. Armero and C. Collar, *J. Cereal Sci.*, **28**, 165 (1998).
28. M. Gómez, S. del Real, C.M. Rosell, F. Ronda, C.A. Blanco and P.A. Caballero, *Eur. Food Res. Technol.*, **219**, 145 (2004).
29. R.S. Manohar and P.H. Rao, *J. Sci. Food Agric.*, **79**, 1223 (1999).
30. *Nutraceutical and Specialty Lipids and their Co-Products*, F. Shahidi, CRC Press, Boca Raton, 2006.
31. *Food: The Chemistry of Its Components*, T.P. Coultate, Royal Society of Chemistry, Cambridge, 2009.
32. N. Krog, *Cereal Chem.*, **58**, 158 (1981).
33. S. Tcholakova, N.D. Denkov and T. Danner, *Langmuir*, **20**, 7444 (2004).
34. R. Aveyard, B.P. Binks and J.H. Clint, *Adv. Colloid Interface Sci.*, **100**, 503 (2003).
35. B.P. Binks, *Curr. Opin. Colloid Interface Sci.*, **7**, 21 (2002).
36. D. Kurukji, R. Pichot, F. Spyropoulos and I.T. Norton, *J. Colloid Interface Sci.*, **409**, 88 (2013).
37. *Emulsions, Foams, and Suspensions: Fundamentals and Applications*, L.L. Schramm, Wiley, Weinheim, 2006.
38. P. Kundu, A. Agrawal, H. Mateen and I.M. Mishra, *Chem. Eng. Sci.*, **102**, 176 (2013).
39. M.T. Ghannam, *Pet. Sci. Technol.*, **23**, 649 (2005).
40. H. Chung, T. Kim, I. Kwon and S. Jeong, *Biotechnol. Bioprocess Eng.*, **6**, 284 (2001).

41. Y. Liu, R. Difoggio, K. Sanderlin, L. Perez and J. Zhao, *Sensor. Actuat. A-Phys.*, **167**, 347 (2011).
42. L.A. García-Zapateiro, J.M. Franco, C. Valencia, M.A. Delgado, C. Gallegos and M.V. Ruiz-Méndez, *Grasas Aceites*, **64**, 497 (2013).
43. *Food Emulsions: Principles, Practice and Techniques*, D.J. McClements, CRC Press, Boca Raton, 1999.
44. *Colloid Science: Principles, Methods and Applications*, T. Cosgrove, John Wiley & Sons, Chippenham, 2010.
45. *Emulsion Formation and Stability*, T.F. Tadros, Wiley-VCH, Weinheim, 2013.
46. *Colloid and Interface Science*, P. Ghosh, Prentice-Hall of India Pvt. Ltd., New Delhi, 2009.
47. R. Aveyard, B.P. Binks, P.D.I. Fletcher, T.G. Peck and P.R. Garrett, *J. Chem. Soc. Faraday Trans.*, **89**, 4313 (1993).
48. G.S. Parks, *J. Am. Chem. Soc.*, **76**, 2032 (1954).
49. L. Lobo and D.T. Wasan, *Langmuir*, **9**, 1668 (1993).

CHAPTER 7 FINAL CONCLUSIONS AND FUTURE WORK

7.1 Conclusions

This thesis has investigated the application of calcium carbonate particles as potential stabilisers in food emulsions and foams. The poor stability and complexity of surfactant-stabilised materials has resulted in the need to investigate other emulsifiers, hence materials stabilised solely by particles have become of great interest. Whipped cream is an example of an aerated emulsion in which a three-phase partially crystallised oil-in-water emulsion (cream) is transformed into a four-phase system (whipped cream) upon the incorporation of air bubbles. In a whipped cream sample the air bubbles are surrounded and stabilised by partially-coalesced fat droplets. The stability of a whipped cream sample is therefore strongly dependent on the properties of the components stabilising the air bubbles. This project was set out to deepen the knowledge concerning the stabilisation of the air bubbles in whipped cream using solid particles; this was the main subject of investigation in Chapters 3 and 4. Moreover, understanding the differences in the stability of surfactant-stabilised oil-in-water emulsions to those stabilised by solid particles was of importance and was addressed in Chapter 5. In Chapter 6 oil-in-water emulsions and aerated emulsions, containing non-crystallisable oils, stabilised by surfactant were studied in order to understand the behaviour of fluid oil droplets around air bubbles.

In Chapter 3, fat-free aqueous foams stabilised by SSL alone and those stabilised by mixtures of Calofort U PCC particles and SSL at their natural pH have been studied systematically. It was shown that, particles alone were ineffective foamers due to their extreme hydrophilicity, aggregation state and charge. On the other hand, aqueous foams of SSL found to be stable due to the adsorption of the open-ended planar lamellar aggregates that cover the air cells as well as micron-sized vesicles that block the thin films and Plateau borders. These processes found to increase the stability of the foams towards coalescence, disproportionation and drainage. The adsorption of negatively charged SSL molecules on positively charged PCC particles were presented in aqueous dispersions. This promoted the adsorption of particles at air-water interfaces upon aeration. It was shown that aqueous foams produced from mixtures of SSL-PCC were significantly more stable than surfactant-stabilised foams. The interactions between solid particles and micelle forming surfactants have been investigated in different studies.^{1, 2}

The results presented in this chapter created a deeper understanding of the interactions between PCC particles and a vesicles forming surfactant, SSL.

Whipping properties of model whipping cream emulsions, partially-stabilised by PCC particles, were investigated in Chapter 4. The PKO droplets in the model emulsions were shown to have similar size to those in a commercial whipping cream. The emulsions were stabilised by SSL and were aerated in the presence of PCC particles. Addition of PCC particles was shown to significantly affect both the overrun and the structural properties of the model whipped cream foams. Studying the effect of oil volume fraction was shown that increasing the oil content of the emulsions increased the stiffness of the produced foams, however there was no significant effect on the overrun values. This was linked to the formation of the three-dimensional network of partially coalesced PKO droplets in the continuous phase of the foams. In addition, the effect of whipping duration was studied and found to affect both the overrun and the extent of partial coalescence between PKO droplets in the whipped sample. Application of solid particles in stabilising aqueous foams has been explored in several studies.^{3,4} However, the application of such particles as air bubble stabilisers in aerated oil-in-water emulsions has been less studied. Using Cryo-SEM images and rheology measurements the data from this chapter clearly presented that surface modified PCC particles can significantly improve the stability and structural properties of aerated emulsions. This suggests that these particles are suitable alternatives to oil droplets as air bubble stabilisers in whipped cream.

It is known that one of the main factors controlling the stability of emulsions is the type of stabiliser. Gelation properties of the PKO-in-water emulsions stabilised by PCC particles and those stabilised by SSL were compared in Chapter 5. It was presented that the mechanism by which gelation occurred in the emulsions was dependent on the nature of the stabiliser used. The gelation in particle-stabilised emulsions was found to occur due to jamming of the PKO droplets. The gelation in these emulsions was found to be reversible and the PKO droplets were re-dispersed back into the continuous phase. It was suggested that when PCC particles coat PKO droplets, they act as a mechanical barrier and stop the extension of crystals out through the droplet surface into the continuous phase, which is the main cause of partial coalescence in crystallised droplets. Surfactant-stabilised emulsions showed different behaviour and the gelation was found to occur by partial coalescence of the oil droplets. The gelation was therefore not

reversible due to the formation of large clumps of partially coalesced PKO droplets. Oil-in-water emulsions stabilised by solid particles have been studied extensively in past.⁵⁻⁷ However, the data reported here is believed to present for the first time, oil-in-water emulsions containing crystallisable oil can be stabilised by solid particles and how this differs them from those stabilised by surfactant.

Finally, in Chapter 6, aeration properties of oil-in-water emulsions containing non-crystallisable oil and stabilised by SSL were studied in order to understand the interactions of fluid oil droplets with an air-water interface. Upon aeration, the oil-in-water emulsions were found to produce less foam compared to pure SSL aqueous solutions, as less surfactant was available in the continuous phase for foaming to occur. Comparing the foam volume produced from the emulsions experimentally and that calculated, revealed that presence of dodecane droplets during aeration decreased the volume of foam produced but HOSO droplets had no influence on the initial foamability. In addition, HOSO droplets were found to enhance the stability of emulsions by accumulating at the Plateau borders of the foams, hence reducing the rate of drainage and film thinning. On the other hand, aerated dodecane-in-water emulsions presented much lower stability compared to oil-free foams and this was linked to their behaviour as slow anti-foaming agents in foams. The investigations regarding the entry coefficient of oil droplets at the air-SSL aqueous dispersion interface showed that neither of the oils were capable of entering into the interface even though a positive entering coefficient was calculated for them. This is believed to be due to the fact that the air-liquid films stabilised by SSL are very stable due to the adsorption of SSL aggregates to the interface. The results from this chapter further enhanced the understanding of the interactions between oil droplets and air bubbles in aerated emulsions with an interest in food applications.

7.2 Future work

The following ideas are suggested from the work described in this thesis:

Surface modified precipitated calcium carbonate particles were shown to significantly enhance the stability of aqueous foams by creating a rigid barrier around air bubbles. These particles are available with different specifications and surface properties.⁸ Studying the effect of calcium carbonate particles, pre-coated by amphiphilic molecules, is suggested. In addition to calcium carbonate particles, other

edible solid particles such as starch particles⁹ are recommended to study as foam stabilisers.

Model whipped cream foams partly-stabilised by calcium carbonate particles were shown to have great stability compared to those stabilised by surfactants in Chapter 4. The incorporation of other ingredients such as sugar, protein and flavour in the formulation of such systems is proposed in order to shift their composition closer to that of the commercial whipping cream studied (VBC). In addition, studying the stability of the model whipped cream foams as a function of temperature is suggested. This will enhance the understanding the mechanisms by which such foams are stabilised.

Furthermore, there are various performance evaluation tests, which are essential to evaluate the quality of the final whipped cream. The following tests are suggested to investigate: flavour characterisation (taste), mouth feel characterisation (firmness, viscosity, density and mouth coating), spreading characterisation (firmness, ease of spread and adhesiveness to the spatula) and cake applications.

Finally, aerated oil-in-water emulsions containing non-crystallisable oil were studied in terms of their foamability and foam stability. The incorporation of solid particles into such systems are recommended in order to investigate the foamability and the foam stability of the emulsions in the presence of solid particles.

7.3 References

1. Z.G. Cui, Y.Z. Cui, C.F. Cui, Z. Chen and B.P. Binks, *Langmuir*, **26**, 12567 (2010).
2. B.P. Binks, M. Kirkland and J.A. Rodrigues, *Soft Matter*, **4**, 2373 (2008).
3. L.R. Arriaga, W. Drenckhan, A. Salonen, J.A. Rodrigues, R. Íñiguez-Palomares, E. Rio and D. Langevin, *Soft Matter*, **8**, 11085 (2012).
4. S. Zhang, D. Sun, X. Dong, C. Li and J. Xu, *Colloids Surf. A*, **324**, 1 (2008).
5. N.P. Ashby and B.P. Binks, *Phys. Chem. Chem. Phys.*, **2**, 5640 (2000).
6. R. Aveyard, B.P. Binks and J.H. Clint, *Adv. Colloid Interface Sci.*, **100**, 503 (2003).
7. Z.G. Cui, K.Z. Shi, Y.Z. Cui and B.P. Binks, *Colloids Surf. A*, **329**, 67 (2008).
8. [http://www.mineralstech.com/Pages/SMI/Precipitated-Calcium-Carbonate-\(PCC\).aspx](http://www.mineralstech.com/Pages/SMI/Precipitated-Calcium-Carbonate-(PCC).aspx), Accessed 01/06/2014.
9. X.Z. Mo, J.B. Jiang, X.M. Huang, F.N. Yu, J.Y. Wu and S.F. Huang, *Appl. Mech. Mater.*, **513-517**, 193 (2014).